Studies on the Regulation of Genome Maintenance Factors by Non-Covalent Interaction with Poly(ADP-Ribose) with a Focus on RECQL Helicases

Dissertation zur Erlangung des
akademischen Grades eines Doktors der Naturwissenschaften
(Dr. rer. nat.)

vorgelegt von Sebastian Veith

an der

Universität Konstanz

Mathematisch-Naturwissenschaftliche Sektion
Fachbereich Biologie

Tag der mündlichen Prüfung: 12.02.2016
1. Referent: Prof. Dr. Alexander Bürkle
2. Referent: Prof. Dr. Mathias Ziegler

O you possessed of sturdy intellect,
observe the teaching that is hidden here
beneath the veil of verses so obscure.

Dante, Divine Comedy, Inferno, Canto IX

Acknowledgements

First of all, I would like to express my gratitude to Prof. Alexander Bürkle, who aroused my interest to the fields of DNA repair and aging and offered me the opportunity to do my PhD studies in this extremely interesting and fast-developing field.
I also like to thank Prof. Mathias Ziegler for serving as second evaluator of my dissertation. Furthermore, I thank the members of my thesis committee, Prof. Elisa May and Prof. Thomas Brunner, for vivid and fertile discussions.
My sincere thanks go to Dr. Aswin Mangerich for his resourcefulness and contribution to this thesis and the stimulating scientific discussions. Many thanks for all your help and support over the years and for your friendship.
Special thanks goes to my friends and colleagues Jan Fischer and Benjamin Hanf for all the great times, the uncountable cinema visits and the crazy things we did. I will miss Benni's daily question "What's for lunch" and the countless philosophical coffee breaks with Jan. I also like to thank my fellow PhD students Rita Martello, Arthur Fischbach, Jennifer Baur, Philipp Palombo, Katharina Hilger, Tabea Zubel and Lisa Rank for their help in the lab and the fun we had in and out of the lab. I thank Waltraud Burckhardt-Boer for her helpfulness and Claudia Hoffmann for her help with the bureaucratic jungle that is the university.
Furthermore, I would like to express my thanks to our cooperation partner Prof. Vilhelm A. Bohr, for the opportunity to come to his lab in Baltimore to learn the mastery of protein purification and its various pitfalls, and Drs. Tomasz Kulicowicz, Morten Scheibye-Knudsen, Evandro Fei Fang, Jennifer Illuzzi and Raghavendra Shamanna for their friendly welcome at the NIA, their help and the very productive time there.
Here, I also want to thank all my students, who contributed to this thesis: Christopher Vogel, Janine Demgenski, Lisa Rank and Andrea Schink (master students), Lisanne Luks, Johannes Delp, Valentin Schoop and Ernestine Treimer (VTK students), Janina Huber (HiWi) and Bokun Yin (bachelor student). I thank the rest of the Bürkle group for their assistance and technical support. Their friendly behavior created a convenient and collaborative atmosphere in the laboratory.
I would like to thank my family, Siegrid, Christina and Ulrich Veith and my friends, who are always there for me and support me and on whom I can always count. This thesis would not exist if it were not for their help and motivation. Thank you for all the good, the bad and the weird times.
Last but not least, I want to thank my wonderful girlfriend Heinke: thank you for being there for me, for all your help and support, for coping with my quirks and for your love.

Abstract

Both RecQL helicases and poly(ADP-ribose)ylation (PARylation), *i.e.* poly(ADP-ribose) polymerases (PARPs) and their product poly(ADP-ribose) (PAR), represent important quality control systems in DNA metabolism and are implicated in the aging process (Veith and Mangerich, ARR, 2015). Additionally to their name-giving helicase activity RecQL helicases also comprise strand-annealing and ATPase activities and, in case of WRN, also exonuclease activity. PARPs on the other hand catalyze the synthesis of the signaling molecule PAR, which is formed in large quantities upon DNA damage and which can be covalently or non-covalently attached to target proteins. PARPs and RecQL helicases have a considerable overlap in their cellular functions, such as DNA repair, telomere maintenance, DNA replication and transcription, and thus they have both been aptly nicknamed "guardians of the genome". Consequently, it is not surprising that over the last two decades increasing evidence of a thriving cooperation between RecQL helicases and PARPs/PARylation emerged. However, it remained largely unclear what role the non-covalent interaction of PAR with RecQL helicases plays in that regard.

Therefore, the objective of this thesis was to improve our understanding about the role of non-covalent PAR-interaction in the DNA damage response, with a focus on the RecQL helicases WRN and RECQL5.

Firstly, a novel, LC-MS/MS based method to quantify exonuclease activity was established by utilizing WRN as exemplary exonuclease (Mangerich/Veith *et al.,* MAD, 2012). Instead of analyzing the ladder-pattern of the digested strand as in the standard gel-based exonuclease assays, it measures the single nucleosides that are released by the exonuclease digest. These can be unequivocally identified and quantified by liquid chromatography coupled mass spectrometry. Employing this method allows a more detailed analysis of the regulation of WRN's exonuclease activity and it has the potential to facilitate the search for WRN exonuclease inhibitors.

Secondly, it could be demonstrated that all RecQL helicases interact non-covalently with PAR and that this interaction is, at least in case of WRN and RECQL5, mediated by several loosely conserved PAR-binding motifs (PBMs) (Popp/Veith *et al.,* ACS Chem Biol, 2013; Khadka/Hsu, Veith, *et al.,* Mol Cell Biol, 2015). Furthermore, amino acid exchange studies provided evidence that the conserved basic amino acids in the PBMs are crucial for PAR-binding. The interaction with PARP1, PARylated PARP1 or PAR differentially regulates the

functions of WRN and RECQL5. While all of WRN's enzymatic activities are inhibited to some degree by non-covalent interaction with free PAR or PARylated PARP1, *i.e.* its helicase, exonuclease, strand-annealing and ATPase activity, it increases RECQL5's strand-annealing activity. Interaction with unmodified PARP1, however, had inhibitory effects on all catalytic functions of both proteins, with the exception of ATPase activity.

Thirdly, it could be demonstrated that the well-documented relocalization of WRN from nucleoli to sites of DNA damage is, at least in case of oxidative damage, entirely dependent on the presence of PARP1, but only weakly on PARP activity (Veith/Schink *et al.,* in preparation).

Fourthly, a newly developed HeLa *PARP1* KO cell system allows to dissect the functions of human PARP1 and its crosstalk with other repair factors in more detail and in a cellular setting. In the context of this project, the non-covalent interaction between PARP1 and its product PAR could be characterized in more detail (Rank/Veith *et al.,* in preparation). This interaction, which could be assigned to two newly identified PBMs in PARP1, led to the formation of higher-molecular complexes, thereby indicating a PAR-dependent multimerization of PARP1. However, non-covalent PAR-binding abrogated PARP1's DNA-binding. Combined, the results indicate that non-covalent interaction of PAR with PARP1 regulates PARP1's recruitment and retention dynamics at sites of DNA damage.

Finally, CSB was established as a novel PAR-binding protein, with considerable consequences for its function in DNA repair (Scheibye-Knudsen, […], Veith, *et al.,* Cell Metabolism, 2014). Non-covalent PAR-interaction is necessary for CSB retention at DNA damage sites but also for displacement of activated PARP1 from the damage by CSB. The prolonged activation of PARP1 in case of CSB loss (*i.e.* Cockayne syndrome) and the resulting NAD^+ depletion might contribute to the detrimental effects of Cockayne syndrome.

In conclusion, this thesis provides novel insight into the role of non-covalent PAR-interaction in the regulation of DNA repair. The combined results presented in this thesis allow well-founded speculations about the regulation of DNA repair by reciprocal regulation of PARP1 and other repair factors: PARP activity is required for the efficient recruitment of PARP1 to, and activation of PARP1 at, DNA damage sites. Other repair factors such as RecQL helicases or CSB are recruited more efficiently by non-covalent PAR interaction to DNA damage sites and seem to be important for displacement of PARP1 from the damage and the termination of the PARylation reaction.

Zusammenfassung

Sowohl RecQL Helikasen als auch Poly(ADP-Ribosyl)ierung (PARylierung), d.h. Poly(ADP-Ribose) Polymerasen (PARPs) und ihr Produkt Poly(ADP-Ribose) (PAR), stellen wichtige Kontrollsysteme des DNA-Metabolismus dar und werden mit dem Alterungsprozess in Verbindung gebracht (Veith and Mangerich, ARR, 2015). Zusätzlich zu ihrer namensgebenden Helikase-Aktivität besitzen RecQL Helikasen auch ATPase-Aktivität und Einzelstrang-annealing-Aktivität und, im Falle von WRN, auch Exonuklease-Aktivität. PARPs hingegen katalysieren die Synthese des Signalmoleküls PAR, welches nach DNA-Schäden in großen Mengen produziert wird und kovalent oder nicht-kovalent an Zielproteine binden kann. PARPs und RecQL Helikasen weisen erhebliche Überschneidungen in ihren zellulären Funktionen auf, wozu DNA-Reparatur, Telomer-Instandhaltung, DNA-Replikation und Transkription zählen, und wurden daher beide passenderweise „Wächter des Genoms“ getauft. Infolgedessen ist es wenig überraschend, dass während der letzten zwei Jahrzehnte vermehrt Belege für eine florierende Zusammenarbeit von RecQL Helikasen und PARPs/PARylierung aufkamen. Allerdings blieb dabei weitestgehend unklar, welche Rolle die nicht-kovalente Interaktion von PAR und RecQL Helikasen in diesem Zusammenhang spielt.

Das Ziel der vorliegenden Arbeit war es daher, unser Verständnis von der Rolle der nicht-kovalenten PAR-Interaktion innerhalb der DNA-Schadensantwort zu verbessern, mit dem Schwerpunkt auf den beiden RecQL Helikasen WRN und RECQL5.

Dazu wurde erstens eine neue, LC-MS/MS-basierte Methode etabliert um Exonuklease-Aktivität zu quantifizieren, mit WRN als beispielhafter Exonuklease (Mangerich/Veith *et al.,* MAD, 2012). Anstatt, wie in den standardmäßig Gel-basierten Exonuklease-Versuchen, das Leitermuster des abgebauten DNA-Strangs zu analysieren werden hier die einzelnen Nukleoside gemessen, die bei dem Exonuklease-Verdau freigesetzt werden. Diese können mittels Flüssigchromatografie-gekoppelter Massenspektrometrie eindeutig identifiziert und quantifiziert werden. Die Benutzung dieser Methode erlaubt eine detailliertere Untersuchung der Regulierung von WRN’s Exonuklease-Aktivität und hat das Potential, die Suche nach Exonuklease-Inhibitoren für WRN zu vereinfachen.

Zweitens konnte gezeigt werden, dass alle RecQL Helikasen nicht-kovalent mit PAR interagieren und dass diese Interaktion, zumindest im Fall von WRN und RECQL5, durch mehrere schwach konservierte PAR-Bindemotive (PBM) vermittelt wird (Popp/Veith *et al.,*

ACS Chem Biol, 2013; Khadka/Hsu, Veith, *et al.,* Mol Cell Biol, 2015). Des Weiteren erbrachten Versuche, bei denen einzelne Aminosäuren ausgetauscht wurden, den Nachweis, dass die konservierten basischen Aminosäuren des PBM essentiell für die PAR-Bindung sind. Das Zusammenspiel mit PARP1, PARyliertem PARP1 oder PAR reguliert die Funktionen von WRN und RECQL5 unterschiedlich. Während sämtliche enzymatischen Aktivitäten von WRN, d.h. Helikase-, Exonuklease-, ATPase- und annealing-Aktivität, bis zu einem gewissen Grad durch die nicht-kovalente Interaktion mit freier PAR oder PARyliertem PARP1 gehemmt werden, wird die annealing-Aktivität von RECQL5 dadurch verstärkt. Interaktion mit nicht-modifiziertem PARP1 hatte dagegen eine hemmenden Wirkung auf alle katalytischen Aktivitäten beider Proteine, mit Ausnahme der ATPase-Aktivität.

Drittens konnte gezeigt werden, dass die gut beschriebene Translokation von WRN aus den Nukleoli zu DNA-Schäden vollständig von der Präsenz von PARP1, aber nur wenig von der PARP-Aktivität abhängig ist, zumindest im Fall oxidativer Schäden (Veith/Schink *et al.,* in Vorbereitung).

Viertens erlaubt es ein neu entwickeltes HeLa *PARP1* Knock-Out Zellsystem, die Funktionen humaner PARP1 und seine Wechselwirkungen mit anderen Reparaturproteinen mit größerer Genauigkeit und in einem zellulären Kontext zu analysieren. In Verbindung mit diesem Projekt konnte die nicht-kovalente Interaktion von PARP1 und seinem Produkt PAR mit größerer Präzision charakterisiert werden (Rank/Veith *et al.,* in Vorbereitung). Diese Interaktion, welche zwei neu identifizierten PBM zugeordnet werden konnte, führte zu der Bildung von höhermolekularen Komplexen und deutet damit auf eine PAR-abhängige Multimerisierung von PARP1 hin. Andererseits wurde die DNA-Bindung von PARP1 durch die nicht-kovalente Interaktion mit PAR unterbrochen. Zusammengenommen deuten die Ergebnisse darauf hin, dass die nicht-kovalente Interaktion von PARP1 mit PAR sowohl die Dynamik der Rekrutierung als auch des Verweilens von PARP1 an DNA-Schäden reguliert.

Zu guter Letzt konnte CSB als neues PAR-Bindeprotein etabliert werden, eine Eigenschaft die erhebliche Konsequenzen für seine zellulären Funktionen hat (Scheibye-Knudsen, […], Veith, *et al.,* Cell Metabolism, 2014). Die nicht-kovalente Interaktion ist einerseits notwendig für das Verweilen von CSB an DNA-Schäden, aber andererseits auch für das Entfernen von aktiviertem PARP1 vom DNA-Schaden durch CSB. Die anhaltende Aktivierung von PARP1 im Falle des Verlustes von CSB (wie z.B. beim Cockayne Syndrom) und die daraus resultierende Erschöpfung der NAD^+-Speicher könnten zu den schädlichen Auswirkungen des Cockayne Syndroms beitragen.

Zusammengenommen bietet die vorliegende Arbeit neue Einblicke in die Rolle der nicht-kovalenten PAR-Interaktion in der Regulation der DNA-Reparatur. Die kombinierten Ergebnisse die in dieser Arbeit vorgestellt werden erlauben wohlfundierte Spekulationen über die Steuerung der DNA-Reparatur durch die wechselseitige Regulierung von PARP1 und anderen Reparaturfaktoren: PARP-Aktivität ist nötig für die effiziente Rekrutierung und vollständige Aktivierung von PARP1 an DNA-Schäden. Andere Reparaturfaktoren, wie zum Beispiel RecQL Helikasen oder CSB, werden durch die nicht-kovalente Interaktion mit PAR effizienter zu den DNA-Schäden rekrutiert und scheinen wichtig für das Entfernen von PARP1 vom Schaden und die Beendigung der PARylierungs-Reaktion zu sein.

Table of Contents

ACKNOWLEDGEMENTS **5**

ABSTRACT **7**

ZUSAMMENFASSUNG **9**

TABLE OF CONTENTS **13**

INTRODUCTION **17**

GENERAL INTRODUCTION 17

Aging *18*

DNA repair *19*

Direct damage reversal 20

Base excision repair (BER) 21

Nucleotide excision repair (NER) 21

DNA double-strand break repair (DSBR) 22

Homologous recombination (HR) 22

Non-homologous end-joining (NHEJ) 23

Mismatch repair (MMR) 23

Translesion synthesis (TLS) 24

CHAPTER I: RECQ HELICASES AND PARP1 TEAM UP IN MAINTAINING GENOME INTEGRITY 25

Abstract *26*

Introduction *26*

RecQ helicases *27*

Poly(ADP-ribose) polymerases and poly(ADP-ribosyl)ation *29*

Interplay of RecQL helicases and PARP1 ..... *34*

RECQL1 34

DNA replication: 35

DNA repair: 36

Telomere maintenance: 37

WRN (RECQL2) 38

Replication: 41

DNA repair: 42

Telomere maintenance: 44

BLM (RECQL3) 45

RECQL4 47

DNA repair and genotoxic stress response: 48

Telomere maintenance: 50

RECQL5 51

Concluding remarks and future directions 53

Acknowledgments: 57

PREMATURE AGING SYNDROMES 59

Werner Syndrome (WS) *59*

Bloom Syndrome (BS) *60*

RecQL4-related diseases *61*

Rothmund-Thomson Syndrome (RTS) 62

RAPADILINO 62

Baller-Gerold Syndrome (BGS) 62

Cockayne Syndrome (CS) *62*

Cockayne syndrome complementation group B protein (CSB) 63

PARP1 polymorphisms *64*

OBJECTIVE 65

REGULATION OF RECQL HELICASES BY PARYLATION **67**

CHAPTER II: QUANTITATIVE ANALYSIS OF WRN EXONUCLEASE ACTIVITY BY ISOTOPE DILUTION MASS SPECTROMETRY 67

Abstract *68*

Introduction *68*
Results *69*
Discussion *74*
Acknowledgements *75*
Experimental Procedures *75*
Purification of recombinant proteins 75
Exonuclease reaction 76
Detection of WRN exonuclease activity via biotin detection of the digested strand 76
Preparation of samples for LC-MS/MS analysis 77
LC-MS/MS analysis 77
Statistical analysis 78
Supplementary Data *79*
CHAPTER III: SITE-SPECIFIC NON-COVALENT INTERACTION OF THE BIOPOLYMER POLY(ADP-RIBOSE) WITH THE WERNER SYNDROME PROTEIN REGULATES PROTEIN FUNCTIONS 83
Abstract *84*
Introduction *85*
Results and Discussion *88*
PAR binds to WRN in a non-covalent manner 88
Identification of a PAR-binding motif in the WRN exonuclease domain 90
Basic and hydrophobic amino acids in the PBM contribute to PAR binding 92
PAR inhibits WRN-DNA interaction 93
PAR inhibits WRN's helicase and exonuclease activities 95
Material and Methods *99*
Sequence alignment of PAR-binding motifs 99
Expression and purification of human His-WRN 99
Synthesis and purification of PAR 99
Biotinylation of PAR and HPLC fractionation 99
Binding of immobilized proteins and peptides to PAR (PAR-overlay blot) 100
Oligonucleotides 100
Electrophoretic mobility shift assay (EMSA) 100
WRN helicase assay 101
WRN exonuclease assay 101
Acknowledgements *102*
Supplementary Data *103*
CHAPTER IV: DIFFERENTIAL AND CONCORDANT ROLES FOR PARP1 AND POLY(ADP-RIBOSE) IN REGULATING WRN AND RECQL5 ACTIVITIES 105
Abstract *106*
Introduction *106*
Results *108*
RECQL5 interacts with PAR and PARP1 108
RECQL5 helicase is inhibited regardless of the modification status of PARP1 111
ATPase is inhibited by PARP1 activation 113
Strand-annealing activities of RECQL5 are stimulated by PAR 115
PARP activation mediates the early recruitment of RECQL5-GFP to DSBs 115
Loss of RECQL5 or WRN is associated with high sensitivity to PARP inhibitor 119
PAR formation regulates the recruitment of RECQL5-GFP domains to DSB sites 120
RECQL5's role in homologous recombination DSB repair depends on PARP1 122
Discussion *125*
Acknowledgements *128*
Materials and Methods *129*
Cell lines and transfection 129
Recombinant proteins 129
Far western with PAR (PAR-overlay) 129
PAR overlay blot assay 130
Peptide binding study 130
Electrophoretic mobility shift assay with end-biotinylated PAR (PAR-EMSA) 130
Co-immunoprecipitation and immunoblotting 131
Biotin PAR pull-down 131
In vitro poly(ADP-ribosyl)ation assay 132
Helicase assay 132
Strand annealing 132
ATPase assay 133

Laser micro-irradiation and confocal microscopy....133
Cell survival assay....134
Immunofluorescence....134
In vivo DSB repair assays....134
In vitro end joining....135
Data and statistical analysis....135
Supplementary Data....*136*
CHAPTER V: PARP1 IS ESSENTIAL FOR OXIDATIVE STRESS-INDUCED RELOCALIZATION OF WRN FROM NUCLEOLI TO SITES OF DNA DAMAGE....141
Abstract....*142*
Introduction....*142*
Results....*144*
WRN interacts non-covalently with PAR via at least 4 different PBMs....144
WRN translocates from the nucleoli upon genotoxic stress....146
PFA fixation can trigger artificial PAR formation....148
WRN's translocation from the nucleoli is almost exclusively PARP1-dependent....150
PARP activity plays a minor role in WRN translocation from the nucleoli....150
PARP1 translocates from nucleoli to nucleoplasm upon oxidative stress....154
Discussion....*157*
Material and Methods....*162*
Cell culture and treatment conditions....162
Immunofluorescence microscopy....162
Plasmids....163
Transfections....163
In silico search for PAR binding motifs....164
Far-western blot with PAR (PAR-overlay blot)....164
Generation and purification of recombinant WRN fragments....164
Supplementary Data....*166*

PARP1 AND PARYLATION....169
CHAPTER VI: ANALYZING STRUCTURE-FUNCTION RELATIONSHIPS OF PARP1 BY RECONSTITUTING HELA *PARP1* KNOCK-OUT CELLS WITH ARTIFICIAL AND NATURAL PARP1 VARIANTS....169
Abstract....*170*
Introduction....*171*
Results....*174*
Generation and characterization of HeLa PARP1 knock-out cells....174
Reconstitution of HeLa PARP1 knock-out cells with PARP1 variants....178
Reconstitution of HeLa PARP1 knock-out cells with wild-type and artificial PARP1 variants....179
Cellular PAR and NAD^+ metabolism of artificial PARP1 mutants....180
DNA recruitment and dissociation dynamics of artificial PARP1 mutants....182
Non-covalent PARP1-PAR interaction....183
Cellular consequences of PARP1 reconstitution....185
Reconstitution of HeLa PARP1 knock-out cells with natural PARP1 variants....190
Discussion....*194*
Material and Methods....*199*
Generation of HeLa PARP1 KO cells by TALEN-mediated gene targeting....199
Orthologous expression and purification of recombinant PARP1....199
PARP1 activity assay....200
In silico search for PAR binding motifs....200
Far-western PAR binding assay....201
Biotinylation and size-fractionation of poly(ADP-ribose)....201
Electrophoretic mobility shift assays (EMSAs)....202
Identification of F304L variant in a patient with pediatric colorectal carcinoma....203
Generation of PARP1-GFP expression constructs and cell transfection....203
Immuno-chemical detection of PARP1 and PAR by fluorescence microscopy....204
Western blot analysis....205
LC-MS/MS quantification of cellular PAR....205
NAD^+ cycling assay....206
Cytotoxicity analysis....207
Cell cycle analysis....207
Clonogenic survival assay....208
Recruitment studies....208
Deconvolution microscopy....208
Statistical analysis....209

Acknowledgements ... *209*
Funding ... *209*
Supplementary Data ... *210*

ADDITIONAL DATA ... **215**
RECIPROCAL REGULATION OF CSB AND PARYLATION ... 215
Results ... *215*
Discussion ... *219*
Material and Methods ... *222*
Western, far-western and slot-blotting ... 222
Biochemistry and recombinant proteins ... 222
Site-directed mutagenesis for substitutions K292A, K297A, K334A and K337A in CSB-GFP plasmid ... 223
Protein recruitment and retention experiments ... 223

DISCUSSION ... **225**
NON-COVALENT PAR INTERACTION AS A REGULATOR OF PROTEIN FUNCTIONS ... 225
WRN is regulated by PARPs and PARylation ... *225*
RECQL5 is differentially regulated by PARylation ... *228*
Non-covalent PAR-binding might regulate PARP1 multimerization and displacement from damage sites ... *230*
WRN'S SPATIO-TEMPORAL DISTRIBUTION IN RESPONSE TO OXIDATIVE STRESS IS REGULATED BY PARP1 ... 232
PARYLATION AND NAD^+ METABOLISM PLAY PIVOTAL ROLE IN COCKAYNE SYNDROME ... 234
SUMMARY ... 236
OUTLOOK ... 237

RECORD OF CONTRIBUTIONS ... **241**

APPENDIX ... **243**
ABBREVIATIONS ... 243
TABLE OF FIGURES ... 247
TABLE OF TABLES ... 248
TABLE OF SUPPLEMENTARY FIGURES ... 249
TABLE OF SUPPLEMENTARY TABLES ... 249
REFERENCES ... 250

Introduction

General introduction

Poly(ADP-ribose) polymerases (PARPs) and their product poly(ADP-ribose) (PAR), as well as RecQL helicases, are extremely important for proper cellular function. They are implicated in virtually every aspect of DNA metabolism and other cellular functions beyond that as well. By now it is evident that there is extensive interaction between PARPs and some of the RecQL helicases, *i.e.* PARP1 and RecQL helicases interact directly, non-covalently via PAR or RecQL helicases are covalently modified with PAR. From these interwoven connections it is especially the non-covalent PAR-protein interaction that acts as the common denominator that connects the work presented in this thesis.

The introduction starts with a brief overview of the bio-medical aspect of aging, followed by an introduction into DNA damage response, *i.e.* DNA repair and its various pathways. Poly(ADP-ribosyl)ation (PARylation) and RecQL helicases, and the various ways they interact, are covered by a comprehensive review that was prepared during the work on this thesis (Chapter I). The introduction is completed by a short overview of the various diseases associated with RecQL helicases, CSB and PARP1.

Chapter II describes a novel, LC-MS based method to assess the exonuclease activity of the Werner syndrome protein (WRN; RECQL2). The chapters II-V (RecQL helicases and PARylation) cover the work performed on the interaction of PARP, PAR and RecQL helicases, with a focus on WRN.

Chapter VI is dedicated to PARP1 and its PARylation capacity, as well as its recently described non-covalent interaction with PAR, and the characterization of novel *PARP1* knock-out (KO) cells and PARP1 variants.

The chapter Additional Data covers work done on the non-covalent interaction of the CSB protein with PAR, which is the result of a cooperation with the Laboratory of Molecular Gerontology (LMG) at the National Institute on Aging (NIA). Only experiments performed by myself or with my participation are shown and discussed here. The broader implications of these results are then discussed in the general Discussion.

Lastly, the thesis is concluded by a general Discussion, bringing together and discussing the different aspects of non-covalent PAR interaction and PARP1-protein interaction described in this thesis.

Aging

The process of human aging is inevitable and irreversible. It is defined by decreasing mental and physical abilities with increasing age after maturation. Aging is characterized by: *i*) increased mortality after maturation, *ii*) changes in biochemical composition in tissues with age, *iii*) progressive decrease in physiological capacity with age, *iv*) reduced ability to respond adaptively to environmental stimuli with age, and *v*) increased susceptibility and vulnerability to disease (Troen, 2003). Among these aging-associated diseases are for example cataracts, atherosclerosis, osteoporosis, Type II diabetes mellitus, and different types of dementia and cancer. More recently, nine hallmarks of aging were postulated, defining aging more comprehensively: genomic instability, telomere attrition, epigenetic alterations, loss of proteostasis, deregulated nutrient sensing, mitochondrial dysfunction, cellular senescence, stem cell exhaustion and an altered intercellular communication (López-Otín et al., 2013).

On a molecular level, aging is characterized by an accumulation of damage in the cells (to proteins, fatty acids, nucleic acids, and other biomolecules) that eventually leads to either senescence, cell death or escape of the two former conditions and subsequent carcinogenesis (Poele et al., 2002; van Steeg, 2001). Senescence is the irreversible stop of cell division and can be further divided into cellular senescence and replicative senescence, however, they are not mutually exclusive (Zglinicki et al., 1995). Although their ability to further divide is deactivated, senescent cells can still fulfill their physiological functions (Campisi and d'Adda di Fagagna, 2007). Cellular senescence is caused by extensive DNA damage or cellular stress in general (Poele et al., 2002). Replicative senescence is defined as the inability to further progress through the cell cycle after a certain number of cell divisions. This is called the Hayflick limit and it is determined by the length of the telomeres (Hayflick, 1965; Zglinicki et al., 1995). The telomeres that cap the ends of the chromosomes erode with each cell division and stop the cell proliferation when critically shortened (Harley et al., 1990). However, cells that express telomerase, an RNA/enzyme complex capable of elongating the telomeres, are able to escape replicative senescence (Bodnar et al., 1998). Consequently, a lot of tumor cells express telomerase in order to escape senescence or cell death (Shay and Bacchetti, 1997). Likewise, cells can overcome replicative senescence by employing a process known as alternative lengthening of telomeres (ALT). It is assumed that they elongate their telomeres by employing a recombinational mechanism. Accordingly, this leads to strong heterogeneity in telomere length within single cells and the formation of ALT-associated PML bodies

(APBs), which consist of extra-chromosomal telomeric DNA and mostly telomeric and recombination-associated proteins (Henson et al., 2002).

The NAD^+ metabolism plays a fundamental role in the aging process, since two of its main pathways, namely PARylation by PARPs and NAD^+-dependent deacetylation by sirtuins, are both very important in DNA repair, cell death and aging (Fouquerel and Sobol, 2014; Lin et al., 2000; Mangerich and Bürkle, 2012). It has been shown that the catalytic activity of PARP1 is linked to the life span in different species (Beneke et al., 2010; Grube and Burkle, 1992). In support of this it has been found that extremely long lived humans, so called centenarians, display a significantly higher PARylation capacity than the average population (Muiras et al., 1998). Mouse studies suggest that this beneficial role of PARylation in aging is attributed to its role in various DNA repair pathways and genomic maintenance (Mangerich and Bürkle, 2012). Likewise, sirtuins have been first described as aging regulating factors and since then evidence emerged that they also participate in DNA repair and energy metabolism (Guarente, 2013). Both sirtuins and PARPs can interact directly, as well as indirectly via competition for their shared substrate NAD^+ (Fouquerel and Sobol, 2014).

In essence, DNA damage is a strong driver of the aging process since it accumulates over time if left unrepaired and can induce senescence, cell death and carcinogenesis.

DNA repair

One mechanism to cope with the increasing detrimental effects of the aging process is the repair of DNA damage. Cells are constantly exposed to a variety of DNA damage-inducing factors, both endogenous and exogenous ones. This results in approximately 50,000 single-strand breaks (SSBs), 8,000 alkylations, 2,000 oxidative lesions and ten double-strand breaks (DSBs) on average per cell and per day (Bernstein and Bernstein, 1991; Lindahl, 1993; Lindahl and Nyberg, 1972; Richter et al., 1988). Endogenous factors include oxidative stress caused by radical formation, *i.e*. reactive oxygen/nitrogen species (ROS and RNS, respectively), spontaneous hydrolysis of nucleotides and deamination of bases. Exogenous factors include various types of radiation (*e.g.* gamma, X-ray, UV and heat), industrial compounds and chemotherapeutics (*e.g.* H_2O_2, tobacco smoke and cisplatin), toxins, viruses and chemical warfare agents (*e.g.* sulfur mustard) (Hoeijmakers, 2001; Mangerich et al., 2015). For cells suffering from DNA damage too heavy to be repaired there are three possible outcomes: cell death, senescence or immortalization and subsequent carcinogenesis (van Steeg, 2001). In order to avoid the formation of cancer, cells have developed an efficient and

extensive DNA repair machinery to cope with the constant strain of damage. What types of damage exist and by which repair mechanisms they are dealt with is briefly described in the sections below and references for more detailed descriptions are provided (Figure 1).

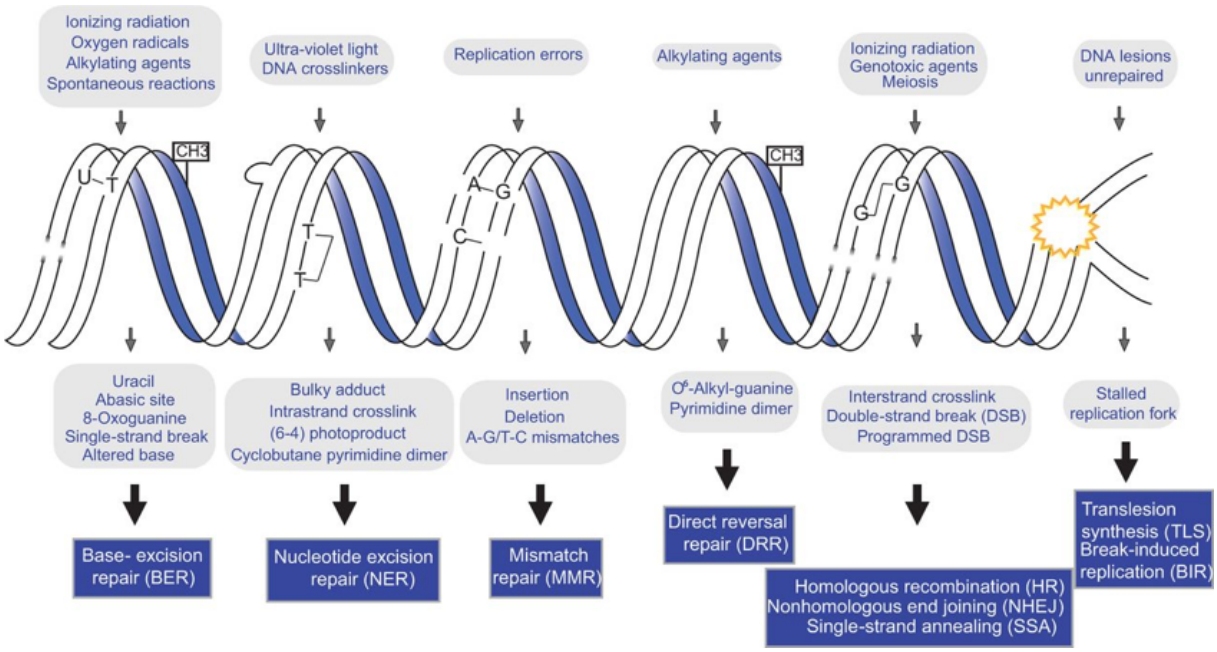

Figure 1: Overview of the different DNA damage lesions, their possible causes and their respective repair pathways. Each cell is constantly exposed to a variety of damaging agents, *e.g.* irradiation, radicals or chemical compounds. The various resulting types of damage must be repaired swiftly and efficiently to avoid mutagenesis and/or cell death. Therefore, cells have developed different repair pathways to cope with these different types of damage. Adapted from (Genois et al., 2014).

Direct damage reversal

Some types of damage can be directly reverted. This includes 6-4 photoproducts (6-4PP) and cyclobutane pyrimidine dimers (CPD), both caused by UV light, and O^6-methylguanine, which are removed by photolyases or O^6-methylguanine methyl transferase (MGMT), respectively (Essen and Klar, 2006; Hoeijmakers, 2001). However, photolyases, which use blue light to catalyze the separation of the bases, are not active in mammals and therefore CPDs and 6-4PPs are repaired by nucleotide excision repair (NER) (Essen and Klar, 2006; Sancar, 2003; Weber, 2005). MGMT is a "suicide-enzyme" since it transfers the methyl-group permanently onto itself and is degraded afterwards. This limits the repair capacity for this type of damage, as new MGMT has to be re-synthesized (Hoeijmakers, 2001).

Base excision repair (BER)

BER repairs small, non helix-distorting lesions, *e.g.* caused by oxidation, methylation, alkylation or deamination of bases. If left unrepaired, these lesions could cause mutations by mispairing or formation of DSBs during replication. Therefore, they are repaired by either short-patch BER (SP-BER, replacement of one base) or long-patch BER (LP-BER, replacement of up to 8 bases). The damaged base is excised by one of several specialized, lesions-specific glycosylases (*e.g.* OGG1, NEIL1) and the resulting abasic site (apurinic/apyrimidinic site (AP-site)) in the DNA is opened by APE1, thus generating a SSB site. The SSB is then either repaired by SP-BER or LP-BER, depending on the lesion type, protein interactions and the cell cycle phase (Fortini and Dogliotti, 2007). A direct SSB (*e.g.* caused by irradiation) can also be recognized by PARP1 and XRCC1. They recruit PNK, which removes the blocking 3'-phosphate. The resulting SSB site is then repaired via one of the BER pathways.

In SP-BER, the missing nucleotide is inserted by Pol β and XRCC1 and the nick in the sugar-phosphate backbone is sealed by DNA Ligase III. Up to 90% of the respective types of damage are repaired by SP-BER. In LP-BER, Pol δ or ε, in concert with PCNA, synthesize a short stretch of DNA starting at the damage site, thereby displacing the original strand. This flap is then cut off by FEN1 and the resulting nick in the backbone is sealed by DNA Ligase I. Spontaneous AP-sites, generated by spontaneous hydrolysis, are also recognized by APE1 and thus fed into the BER pathway (Boiteux and Guillet, 2004).

This is only a simplified synopsis about the BER pathway, introducing the main mechanism and the most important proteins involved therein. Of course, there are several other proteins involved, which are described elsewhere (Fortini and Dogliotti, 2007; Zharkov, 2008).

Nucleotide excision repair (NER)

NER recognizes and repairs bulky adducts (*e.g.* benzo(a)pyrene-induced DNA adducts) and helix-distorting lesions, such as interstrand (*e.g.* induced by cisplatin derivatives, sulfur mustard or mitomcyin C) and intrastrand (*e.g.* CPD, 6-4PP) crosslinks. NER can be subdivided into two pathways, the global genome NER (GG-NER) that is active on the whole genome and the transcription-coupled NER (TC-NER), where only transcriptionally active sites are repaired. The two sub-pathways differ only in their mode of damage recognition while sharing the actual repair process. During transcription, RNA Pol II is stalled at sites of damage, leading to the recruitment of CSB and CSA (TC-NER). In GG-NER, the damage is

recognized by a complex consisting of XPC, HR23B and CEN2 (and in case of UV lesions also UV-DDB). Subsequently, in both sub-pathways, the TFIIH complex is recruited and its two helicases XPB and XPD unwind the DNA, forming a ~30 nt long bubble. XPA and RPA are recruited and the damage-containing strand-fragment is excised by the nucleases XPG and XPF/ERCC1. Lastly, the resulting gap is closed by polymerases δ or ε and the nick is sealed by DNA Ligase I. The importance of this repair pathway is illustrated by the severe diseases caused by mutations in key proteins of this pathway: Xeroderma pigmentosum (XP), caused by mutations in either one of the above mentioned XP proteins, and Cockayne syndrome (CS), caused by mutations in either CSA or CSB (Cockayne syndrome complementation group A and B, respectively). For more detailed information on the NER pathway please refer to (Nouspikel, 2009; 2008; Shuck et al., 2008).

DNA double-strand break repair (DSBR)

DNA double-strand breaks can arise from several sources: they can either directly be generated by irradiation, chemicals or enzymes or they can arise during replication, when the replication machinery runs into a SSB or into a blocked replication fork. DSBs are the severest type of DNA damage and must be dealt with immediately as they can lead to massive genomic rearrangements, deletions, mutations, carcinogenesis, and cell death. They can be repaired by either homologous recombination (HR, error-free, during cell replication) or by non-homologous end-joining repair (NHEJ, error-prone) (Dexheimer, 2013). The free DNA ends are recognized by protein kinases ATM and ATR, leading to phosphorylation of histone H2A (γH2A.X) and subsequent recruitment of repair factors, as described below.

Homologous recombination (HR)

The free DNA double-strand ends, covered by γH2A.X, are recognized by the MRN complex (MRE11, Rad50, NBS1), which resects the 5'- ends. This 5' to 3' resection is then further extended by the BLM/EXO 1 complex (or WRN/DNA 2), thereby generating a short 3' overhang. This overhang is coated by RPA, thus protecting the single strand (Sturzenegger et al., 2014). RPA is then replaced by the RAD51-nucleoprotein complex (RAD51, RAD52, RAD54, BRCA2), which mediates the homology search and strand invasion of the homologous strand. Next, DNA synthesis from the 3' end is started by Pol η and the nick is sealed by DNA Ligase I, resulting in a 4-way junction termed Holliday Junction (HJ). This HJ

can then be resolved by several different ways, resulting in two intact double strands (Dexheimer, 2013; Li and Heyer, 2008).

Non-homologous end-joining (NHEJ)

The DNA ends are recognized by the Ku heterodimer (Ku78/80), which serves as a "loading platform" for the other proteins that are required for efficient NHEJ. Protein kinase DNA-PKcs binds to Ku and orchestrates the subsequent processes by phosphorylation of itself and other proteins. The DNA ends are further processed depending on their appearance, *i.e.* blunt ended, 3'-overhang or 5'-overhang. In case of an overhang, the protruding DNA end is resected by the Artemis nuclease, which has intrinsic 5'-3' exonuclease activity as well as DNA-PKcs-dependent endonuclease activity. Although Artemis is thought to be the most important NHEJ nuclease other nucleases have been implicated as well to participate in NHEJ, *e.g.* WRN, EXO 1 and APLF. Alternatively, sticky ends can be filled by DNA polymerases μ and λ. The blunt ends are then joined by the Ku/DNA-PKcs complex and ligation is mediated by DNA Ligase IV, in conjunction with XRCC4 and XLF (Lieber, 2010). It is worth mentioning that NHEJ is also employed to re-ligate the deliberately induced DSBs during V(D)J recombination in some immune cells.

Mismatch repair (MMR)

Sometimes, a polymerase can slip, especially on repetitive sequences. Thus, a wrong base is introduced opposite of the template or even more than one base, thereby generating either a missense mutation or, worse, a frameshift. This can happen sporadically with replicative DNA polymerases but more likely by translesion polymerases (see next section). To prevent this, MMR is employed. In the recognition step, single base pair mismatches are recognized by the MutSα heterodimer (Msh2 & 6), whereas base insertions or deletions are recognized by the MutSβ heterodimer (Msh2 & 3). The damage-containing strand is then incised by the MutLα heterodimer (Mlh1 & PMS2), followed by strand-degradation through EXO 1. The ssDNA is protected by RPA binding. Finally, the resulting gap is filled by DNA Pol δ in conjunction with PCNA and the nick is sealed by DNA Ligase I.
This is a highly simplified summary of MMR, describing just the core functionality. A thorough description can be found at (Fukui, 2010; Li, 2008).

Translesion synthesis (TLS)

A stalled replication fork, *e.g.* caused by a small adduct, a SSB or an AP site, can also be dealt with by TLS, whereby the replication polymerases ε and δ (leading and lagging strand, respectively) are replaced by special TLS polymerases (Pol η, ι, κ and ζ). These polymerases have a higher tolerance on small adducts or slightly distorting lesions and are able to drive DNA synthesis across these lesions, *i.e.* they have less fidelity and specificity. This is not a repair in the traditional sense but more a damage tolerance, as the damage is not repaired but rather bypassed to allow replication to continue and to avoid severer damage by strand breaks. Other repair pathways can then later deal with the bypassed damage, although some damages might not be recognized and ultimately lead to mutagenesis. However, the TLS is highly conserved across species and, since it increases genetic variability by promoting mutagenesis, it is considered as a driver of evolution (Waters et al., 2009).

Chapter I: RecQ helicases and PARP1 team up in maintaining genome integrity

Sebastian Veith and Aswin Mangerich

Aging Research Reviews, 2015 Sep; 23(Pt A): 12-28

Abstract

Genome instability represents a primary hallmark of aging and cancer. RecQL helicases (*i.e.*, RECQL1, WRN, BLM, RECQL4, RECQL5) as well as poly(ADP-ribose) polymerases (PARPs, in particular PARP1) represent two central quality control systems to preserve genome integrity in mammalian cells. Consistently, both enzymatic families have been linked to mechanisms of aging and carcinogenesis in mice and humans. This is in accordance with clinical and epidemiological findings demonstrating that defects in three RecQL helicases, *i.e.*, WRN, BLM, and RECQL4, are related to human progeroid and cancer predisposition syndromes, *i.e.*, Werner, Bloom, and Rothmund Thomson syndrome, respectively. Moreover, PARP1 hypomorphy is associated with a higher risk for certain types of cancer. On a molecular level, RecQL helicases and PARP1 are involved in the control of DNA repair, telomere maintenance, and replicative stress. Notably, over the last decade, it became apparent that all five RecQL helicases physically or functionally interact with PARP1 and/or its enzymatic product poly(ADP-ribose) (PAR). Furthermore, a profound body of evidence revealed that the cooperative function of RecQLs and PARP1 represents an important factor for maintaining genome integrity. In this review, we summarize the status quo of this molecular cooperation and discuss open questions that provide a basis for future studies to dissect the cooperative functions of RecQL helicases and PARP1 in aging and carcinogenesis.

Introduction

Genome instability, telomere attrition, epigenetic alterations, and loss of proteostasis have been recently defined as four primary hallmarks of aging (López-Otín et al., 2013). Among those, in particular, genome instability and telomere attrition are considered important causative factors of human aging, which is impressively underscored by the fact that all known human progeroid syndromes are a result of mutations in genes involved in DNA metabolism [reviewed in (Vijg and Suh, 2013)]. To date, four categories of human segmental progeroid syndromes have been identified. Those are caused by hereditary defects in genes that are involved in nucleotide excision repair (*e.g.*, xeroderma pigmentosum and Cockayne syndrome), nuclear organization (*e.g.*, Hutchinson Gilford progeria), DNA damage signaling (*e.g.*, ataxia telangiectasia), and RecQL helicase function (see below) [reviewed in (Ghosh and Zhou, 2014)]. To ensure integrity of the genome a multifaceted network of maintenance mechanisms has evolved relying on the concerted action of nucleases, ligases,

topoisomerases, polymerases and helicases [reviewed in (Ciccia and Elledge, 2010)]. This review addresses the intriguing connection between two major players in genome maintenance and mammalian aging biology: RecQL helicases and poly(ADP-ribose) polymerase 1 (PARP1).

RecQ helicases

Helicases, in general, are molecular motors that unwind double- or multi-stranded DNA or RNA structures in a 3' to 5' or a 5' to 3' directionality by using ATP as an energy source. They participate in many aspects of DNA metabolism, such as replication and transcription [reviewed in (Brosh, 2013; Singleton et al., 2007)]. In particular, the members of the RecQ helicase family act as guardians of the genome to assure proper DNA metabolism in response to genotoxic stress, such as replicative, transcriptional, and telomeric stress. The family of RecQ helicases is highly conserved across species, with members identified in bacteria (*E. coli*), fungi (*e.g. S. cerevisiae, S. pombe*), plants (*A. thaliana*), and animals (*e.g. C. elegans*, *D. melanogaster*, *X. laevis*, *M. musculus*) (Karow et al., 2000). In mammals five RecQ-like (RECQL) helicases exist, *i.e.*, RECQL1, WRN, BLM, RECQL4, RECQL5 [reviewed in (Croteau et al., 2014)] (Figure 2). To date, monogenic diseases have been associated with defects in three out of five RecQL helicases. Thus, mutations in *WRN*, *BLM*, and *RECQL4*, cause Werner syndrome (WS), Bloom syndrome (BS), and Rothmund Thomson syndrome (RTS), respectively [reviewed in (Hanada and Hickson, 2007)]. [*N.B*. Two additional diseases were linked to mutations in *RECQL4*, *i.e.*, RAPADILINO and Baller-Gerold syndrome (Croteau et al., 2014)]. All three diseases are characterized by growth and skin abnormalities, cancer predisposition, a reduced life expectancy, and signs of premature aging; however, they are clearly distinguishable in their precise clinical features. In particular, WS patients recapitulate many (but not all) aspects of normal human aging with life expectancies of ~50 years of age. WS patients develop normally until adolescence, thereafter evolving symptoms, such as cataracts, osteoporosis, atherosclerosis, hair graying, type II diabetes, and cancer predisposition [reviewed in (Bernstein et al., 2010; Chu and Hickson, 2009; Hanada and Hickson, 2007)]. In contrast to *WRN*, *BLM*, *RECQL4*, so far no genetic diseases have been linked to *RECQL1* and *RECQL5* mutations, however, there is convincing evidence that all RecQL helicases work as tumor suppressive factors in mice and humans [reviewed in (Brosh, 2013; Chu and Hickson, 2009)]. Evidently, clinical findings from RecQL helicase disorders

raised considerable interest in the underlying biochemical and cellular mechanisms of how these enzymes are involved in normal human aging.

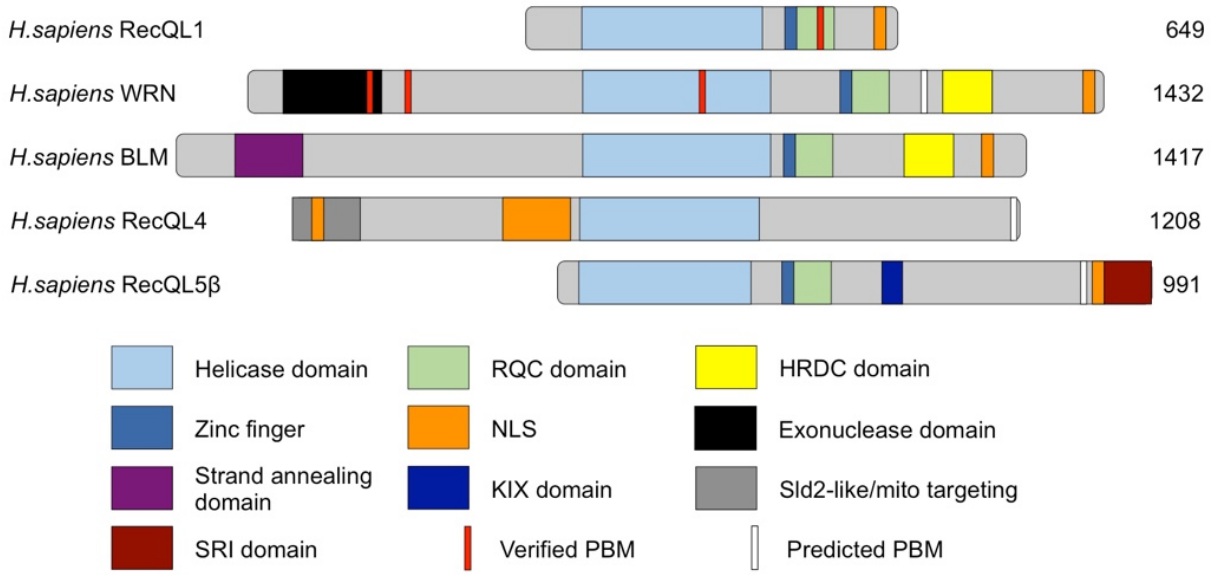

Figure 2: Overview of the domain structures of RecQL helicases.
HRDC indicates helicase and RNase D-like C-terminal domain; NLS, nuclear localization signal; PBM, PAR binding motif; RQC, RecQ C-terminal domain; SRI, set2 Rpb1 interacting; KIX, interactor of kinase inducible domain.

Specifically, RecQL helicases are involved in the replicative stress response, DNA repair, telomere maintenance, and transcription. Thus, many substrates of RecQL helicases resemble DNA repair intermediates and unusual DNA structures, such as 3' overhangs, forked and bubbled structures, D-loops, Holliday junctions (HJ), four-way junctions, and G-quadruplex DNA [reviewed in (Bernstein et al., 2010; Chu and Hickson, 2009; Croteau et al., 2014)]. In addition to their 3' to 5' helicase function, all five RecQL helicases exhibit ATP-independent single-strand DNA annealing (SSA) activities. ATP binding induces conformational changes in RecQL structures, switching their activity from SSA to DNA helicase activity (Sami and Sharma, 2013; Sharma et al., 2005). Structurally, RecQL helicases share three highly conserved domains: a core helicase domain, the RecQ C-terminal (RQC) domain, and the helicase and RNase D-like conserved (HRDC) domain, however RECQL1/4/5 lack the HRDC domain (Figure 2). Furthermore, each helicase comprises specific domains that confer unique functional characteristics to each homolog, being responsible for subcellular localization, specific protein-protein interactions, oligomerization, or further enzymatic activities [reviewed in (Croteau et al., 2014)]. For example, unlike all other RecQLs, WRN possesses an N-terminal exonuclease domain (Croteau et al., 2014). It is interesting to note that RecQL helicases themselves interact with each other, and redundant (RECQL5-BLM), synergistic (RECQL4-BLM, WRN-RECQL5, WRN-BLM), complimentary (RECQL5-

WRN), as well as distinct functions have been described [reviewed in (Croteau et al., 2014)]. For the proper function of RecQL helicases, it is important that their action is orchestrated in a spatio-temporal manner with other DNA metabolizing factors (Croteau et al., 2014). Furthermore, their action needs to be tightly controlled until it is needed, because uncontrolled unwinding of the DNA (or nuclease activity in case of WRN) can cause genome instability, leading to catastrophic consequences for cells (Singleton et al., 2007). Consistent with this view, a variety of stimulating and inhibiting binding partners as well as post-translational modifications (PTMs) regulate the activities of the individual RecQL helicases [reviewed in (Böhm and Bernstein, 2014; Croteau et al., 2014)]. Besides phosphorylation, ubiquitination, and SUMOylation, poly(ADP-ribosyl)ation plays an important role in the regulation of RecQL helicases, as it will be discussed in this review. For a more detailed discourse on general RecQL biochemistry and biology the reader is referred to several excellent reviews on this topic (Bernstein et al., 2010; Bohr, 2008; Brosh, 2013; Chu and Hickson, 2009; Croteau et al., 2014; Mason and Cox, 2012).

Poly(ADP-ribose) polymerases and poly(ADP-ribosyl)ation

Poly(ADP-ribosyl)ation (PARylation) is an ubiquitous and reversible post-translational modification that takes place in the nucleus and to a lesser extent also in the cytoplasm [reviewed in (Gibson and Kraus, 2012; Rouleau et al., 2010; Vyas and Chang, 2014)]. The reaction is carried out by poly(ADP-ribose) polymerases (PARPs, also named ARTDs (Hottiger et al., 2010)) that use NAD^+ as a substrate to synthesize the nucleic-acid-like biopolymer poly(ADP-ribose) (PAR) with variable branching and chain length of up to 200 ADP-ribose units (Figure 3) [reviewed in (Mangerich and Bürkle, 2012).

The human *PARP* gene family consists of 17 members, however so far only six of them, *i.e.*, PARPs 1-3, vaultPARP (PARP4), and tankyrases 1 and 2 (TNKS1/2), have been reported to synthesize PAR. Other family members exhibit mono(ADP-ribosyl)ation activity or are catalytically inactive [reviewed in (Hottiger et al., 2010)]. PARP1 is the founding member of the family and upon induction of DNA damage, in particular DNA strand breaks, PARP1 is responsible for the bulk of cellular PAR synthesis leading to a rise in PAR levels of up to ~100-fold with >100,000 PAR chains present in each cell (Martello et al., 2013; Robert et al., 2013).

The finding that *Parp1*$^{-/-}$ mice still synthesize PAR led to the identification of other DNA-damage dependent PARPs, such as PARP2 and later on PARP3 (Shieh et al., 1998). Recently

it was shown that PARP1, PARP2 and PARP3 differentially recognize specific types of DNA lesions and DNA repair intermediates (Langelier et al., 2014). All three PARPs exhibit overlapping as well as homolog-specific functions in numerous genome maintenance pathways [reviewed in (Robert et al., 2013)]. Apart from DNA damage-dependent activation, PARP activity is also regulated by PTMs, such as phosphorylation, acetylation, and SUMOylation (Cohen-Armon et al., 2007; Hassa et al., 2005; Kauppinen et al., 2006; Messner et al., 2009; Walker et al., 2006), as well as by direct protein-protein interactions (Berger et al., 2007; Guastafierro et al., 2008; Krukenberg et al., 2014; Midorikawa et al., 2006).

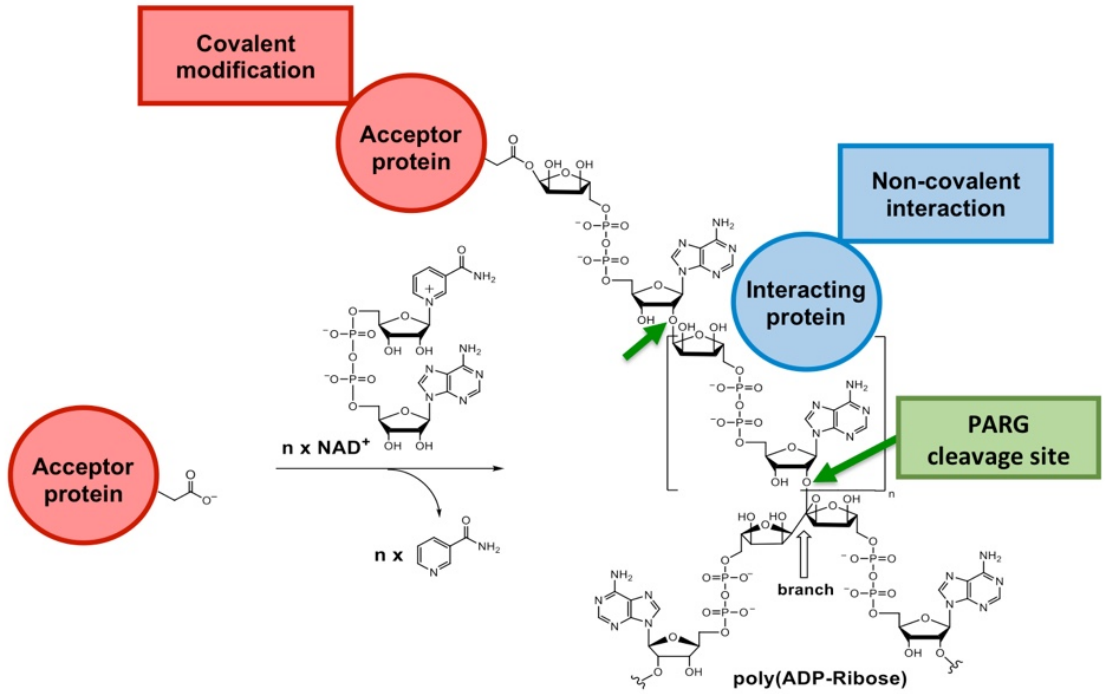

Figure 3: Biochemistry of poly(ADP-ribosyl)ation.
PARPs cleave the glycosidic bond of NAD^+ between nicotinamide and ribose followed by the covalent modification of acceptor proteins with an ADP-ribosyl unit. PARPs also catalyze an adduct elongation, giving rise to linear polymers with chain lengths of up to 200 ADP-ribosyl units, characterized by their unique ribose (1''→2') ribose phosphate–phosphate backbone. At least some of the PARP family members also catalyze a branching reaction by forming ribose (1'''→2'') ribose linkages. Poly(ADP-ribose) glycohydrolase (PARG) degrades the polymer by its endo- and exoglycosidic activity. The macrodomain-containing proteins MacroD1, MacroD2 and TARG1/C6orf130 act as mono(ADP-ribosyl) hydrolases to remove the most proximal ADP-ribose residue from acidic amino acids of target proteins. Modified from (Mangerich and Bürkle, 2012).

Upon catalytic activation, PARPs covalently modify various proteins with PAR at glutamate, aspartate or lysine residues. Target proteins include PARPs themselves (*i.e.,* automodification), as well as hundreds of other proteins that are involved in DNA metabolism, transcription, chromatin organization, and mRNA processing (Jungmichel et al., 2013; Zhang et al., 2013). Besides covalent modification, numerous proteins interact with PAR non-covalently (Figure 3). The non-covalent PAR-protein interaction is mediated via at

least six different PAR binding modules, all of which fulfill diverse cellular functions [reviewed in (Krietsch et al., 2012)]. Those include (*i*) a weakly conserved ~20-amino-acid PAR binding motif (PBM) (Gagné et al., 2008; Pleschke et al., 2000), (*ii*) distinct macrodomains (Ahel et al., 2009; Gottschalk et al., 2009), (*iii*) a PAR-binding zinc finger (Ahel et al., 2008), (*iv*) a WWE domain (Zhang et al., 2011), (*v*) a PAR-binding regulatory motif (PbR) (Min et al., 2013), and (*vi*) an oligonucleotide/oligosaccharide-binding fold (OB fold) (Zhang et al., 2014). Interaction and covalent modification with PAR regulate physico-chemical properties of target proteins, thereby modifying their enzymatic activities or interactions with other macromolecules such as DNA, RNA, or proteins (Figure 4). In consequence, PARylation controls and fine-tunes the dynamic localization and activity of target proteins within the cell [reviewed in (Beneke, 2012; Gibson and Kraus, 2012)]. Essential for such a spatio-temporal control of protein function is the fact that DNA-damage-dependent PAR formation is highly dynamic, because shortly after being synthesized, it is rapidly hydrolyzed by PARPs catabolic counterpart, poly(ADP-ribose) glycohydrolase (PARG) in an exo- and endoglycosidic manner (Figure 3) (Barkauskaite et al., 2013a; Meyer-Ficca et al., 2004; Min et al., 2010; Niere et al., 2008). Additionally, a second enzyme exerts PAR-degrading activity, *i.e.*, ARH3, with evidence that this enzyme is associated with PAR degradation in mitochondria (Niere et al., 2012; Oka et al., 2006). While both enzymes, PARG and ARH3, are not able to remove the last ADP-ribose moiety from acceptor proteins, macrodomain-containing proteins, such as MacroD1 and MacroD2, fulfill this task, leaving behind an unmodified amino acid that is readily available for the next round of PARylation (Jankevicius et al., 2013; Rosenthal et al., 2013).

Proteins that are targeted by PARylation are involved to a wide spectrum of cellular mechanisms such as (*i*) genome maintenance, (*ii*) epigenetics and transcriptions, (*iii*) proteostasis, (*iv)* cell death and senescence, (*v*) energy metabolism, and (*vi*) inflammation and immunity, all of which have profound functions in aging and cancer development (Figure 5) [reviewed in (Mangerich and Bürkle, 2012)]. With regards to cancer biology, *e.g.*, a hypomorphic PARP1 polymorphism (V762A) has been associated with a higher risk for several types of cancers (Cottet et al., 2000; Hua et al., 2014; Qin et al., 2014). Furthermore, inhibitors of PARylation are currently tested in clinical cancer therapy, either in combination with classical chemo- or radiotherapy, or as stand-alone drugs following the concept of synthetic lethality (Bryant et al., 2005; Farmer et al., 2005; Lord et al., 2015; Mangerich and Bürkle, 2012; Sonnenblick et al., 2015). With regards to aging biology, a large body of evidence demonstrates a positive correlation of PARylation capacity and mammalian

longevity [reviewed in (Beneke and Bürkle, 2007; Mangerich and Bürkle, 2012; Shilovsky et al., 2013)]. For example, PARylation capacity in peripheral blood mononuclear cells (PBMCs) of 13 mammalian species strongly correlates with their maximum lifespan (Grube and Burkle, 1992). Moreover, PARylation capacity in PBMCs declines with age in humans and rodents (Grube and Burkle, 1992; Kunzmann et al., 2008).

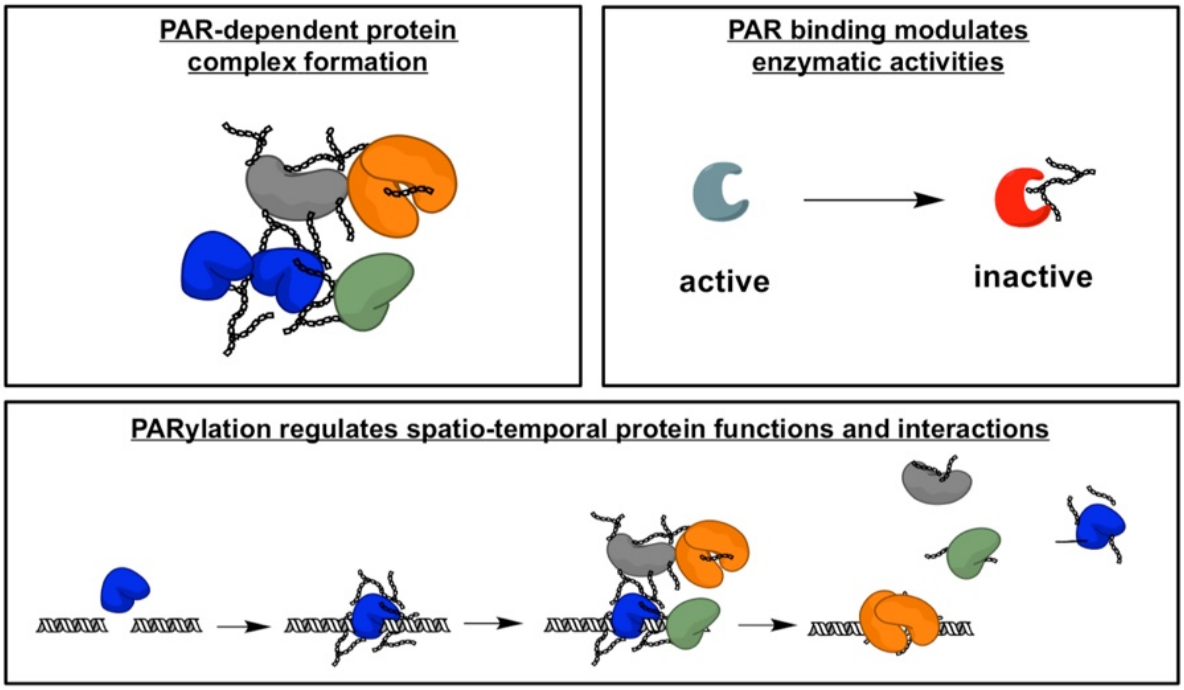

Figure 4: Biochemical consequences of poly(ADP-ribosyl)ation (PARylation).
It is important to note that PARylation can regulate protein function and localization in both directions. Thus, depending on the specific target protein and the cellular condition; on the one hand, PARylation can mediate protein complex assembly and recruitment of proteins to other macromolecules such as DNA (*e.g.*, DNA repair factors); however, on the other hand PARylation can also induce disassembly of protein complexes and repulsion of proteins from DNA (*e.g.* during transcriptional regulation and chromatin remodeling). The same holds true for the regulation of enzymatic activities, as inhibiting as well as stimulatory effects of PAR have been described. In consequence, it is thought that PARylation regulates protein dynamics in a spatio-temporal manner, *e.g.*, regulating the time-dependent coordinated action of DNA repair factors at the site of the damage.

Interestingly, humans exhibiting an exceptional long lifespan, *i.e.,* centenarians, display a significantly higher PARylation capacity than the average population (Muiras et al., 1998), which is comparable to those of young subjects (Chevanne et al., 2007). Moreover, in support of the view that PARP1 acts as a longevity assurance factor is the finding that *Parp1*$^{-/-}$ mice age moderately faster compared to wild-type animals, which is associated with a higher frequency of malignant tumors at advanced age (Piskunova et al., 2008). On the other hand, PARP1 may act as an aging-promoting factor, due to its regulation of NF-κB signaling, its severe effects on NAD^+ metabolism, and its potential to induce cell death. Consistently, PARylation is associated with many age-related inflammatory and degenerative diseases, which is supported by numerous studies demonstrating that pharmacological PARP inhibition as well as a genetic knock out of *Parp1* in mice protect from such diseases. It is tempting to

speculate that the opposing effects of PARylation in cellular homeostasis on the one hand, and inflammation and cell death on the other hand, at least in part, explain the rather mild premature aging phenotype of *Parp1*$^{-/-}$ mice [reviewed in (Mangerich and Bürkle, 2012)].

With regards to genome maintenance, PARylation is involved in DNA repair (Robert et al., 2013; Rouleau et al., 2010), telomere maintenance (Beneke et al., 2008; d'Adda di Fagagna et al., 1999), and replicative stress response (Ray Chaudhuri et al., 2012). Strikingly, as outlined above, these processes are also in the center of RecQL functions, and therefore, it is not surprising that accumulating evidence demonstrates an intimate interplay between RecQL helicases and PARPs, both of which act as important quality control systems to maintain genome integrity during the aging process. In each of the following sections, we will shortly discuss functions of individual RecQL helicases and then focus on current evidence of how those interact with PARP1 and PARylation on a molecular level to safeguard mammalian longevity.

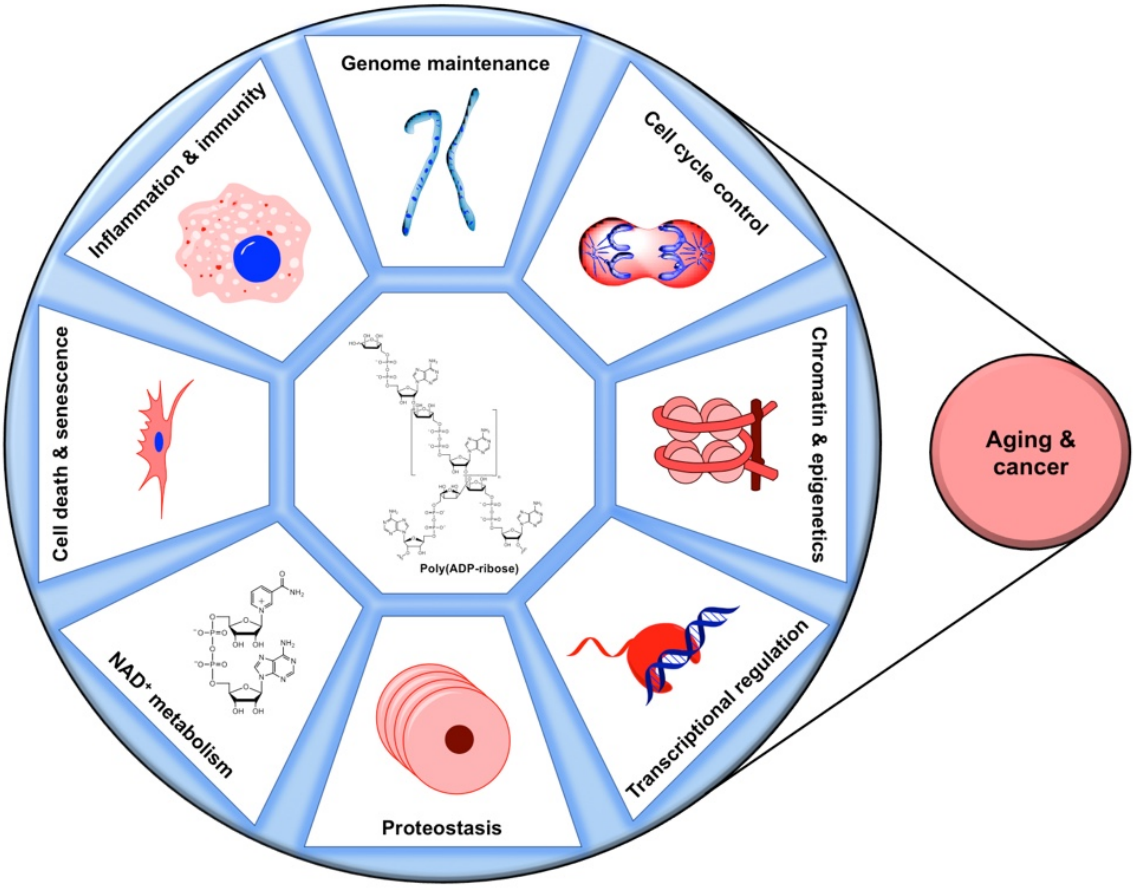

Figure 5: The role of PARylatio in aging and cancer.
PARylation exerts pleiotropic functions in many cellular processes, which have been linked to aging and cancer biology.

Interplay of RecQL helicases and PARP1

RECQL1

RECQL1 was the first of the five RecQL helicases that was discovered, owing to its strong ATPase activity and its high abundance in cells (Seki et al., 1994). At present, no genetic disease has been associated with RECQL1 deficiency and *Recql1* knock-out (KO) mice are phenotypically normal, at least under unstressed conditions. On the other hand, RECQL1-deficient cells exhibit various features of chromosomal instability and are hypersensitive to ionizing radiation (Sharma and Brosh, 2007), suggesting important functions in genome maintenance. Furthermore, RECQL1 has been associated with human cancer biology. Thus, RECQL1 expression was found to be dysregulated in various types of cancers (Brosh, 2013; Lao et al., 2013) and *RECQL1* polymorphisms are associated with reduced survival rates of patients with pancreatic cancer (Li et al., 2006a; 2006b). On the cellular level, RECQL1 is involved in DNA replication, repair, and telomere maintenance, thus providing several potential functional overlaps with PARP1 and other RecQL helicases [reviewed in (Croteau et al., 2014)]. Yet, so far, no direct interaction with other RecQL helicases has been demonstrated and RECQL1 shows some unique substrate specificities, pointing to distinctive, non-redundant functions (Sharma et al., 2012).

With respect to a RECQL1-PARP1 interplay, there is strong evidence that PARP1 and RECQL1 physically interact via the C-terminal domain of RECQL1 and the C-terminus and the BRCT domain of PARP1 (Berti et al., 2013; Sharma et al., 2012) (Figure 6). Interestingly, in contrast to WRN (see below), RECQL1 is also able to interact with PARylated PARP1 and this interaction appears to be even stronger than with unmodified PARP1 (Berti et al., 2013; Kobbe et al., 2003a). Furthermore, Berti *et al.* reported that RECQL1 interacts non-covalently with PAR via a putative PBM in the C-terminus (Berti et al., 2013). Consistent with these findings, when using a modified search algorithm that is based on the consensus sequence previously published by Pleschke *et al.* (Pleschke et al., 2000; Popp et al., 2012), we identified a putative PBM at aa 544-551 in the C-terminus of RECQL1 (own observation). The same region of RECQL1 is possibly also covalently PARylated (Berti et al., 2013; Jungmichel et al., 2013), however this was not found by others (Sharma et al., 2012).

DNA replication:

Even though, so far there is no direct biochemical evidence that PARP1 and PARylation influence RECQL1 helicase activity, cellular studies strongly indicate that PARylated PARP1 and PAR themselves inhibit RECQL1 activity during the replicative stress response. Upon treatment with clinically relevant doses of the topoisomerase (TOPO1) inhibitor camptothecin (CPT), replication forks slow down and undergo fork reversal, which prevents replication fork run-off and DSB formation (Ray Chaudhuri et al., 2012). RECQL1 plays a central role in restarting replication forks after CPT-induced TOPO1 inhibition. However, before doing so, activated PARP1 transiently suppresses RECQL1-dependent replication fork restart and stabilizes regressed forks to provide sufficient time for the repair of the blocking lesion. After DNA repair is completed, RECQL1 is then allowed to restart the fork, presumably after PARG-dependent PAR degradation (Illuzzi et al., 2014). This hypothesis is supported by the findings that PARP inhibition leads to accumulation of DSBs, while the combination of PARP inhibition and RECQL1 depletion leads to damage-free fork restart, potentially by employing HR for fork restart (Berti et al., 2013). If and how a reported direct interaction of PARP1 and PAR with TOPO1 (Bauer et al., 2001; Malanga and Althaus, 2004; Yung et al., 2004) may contribute to this mechanism awaits further analysis.

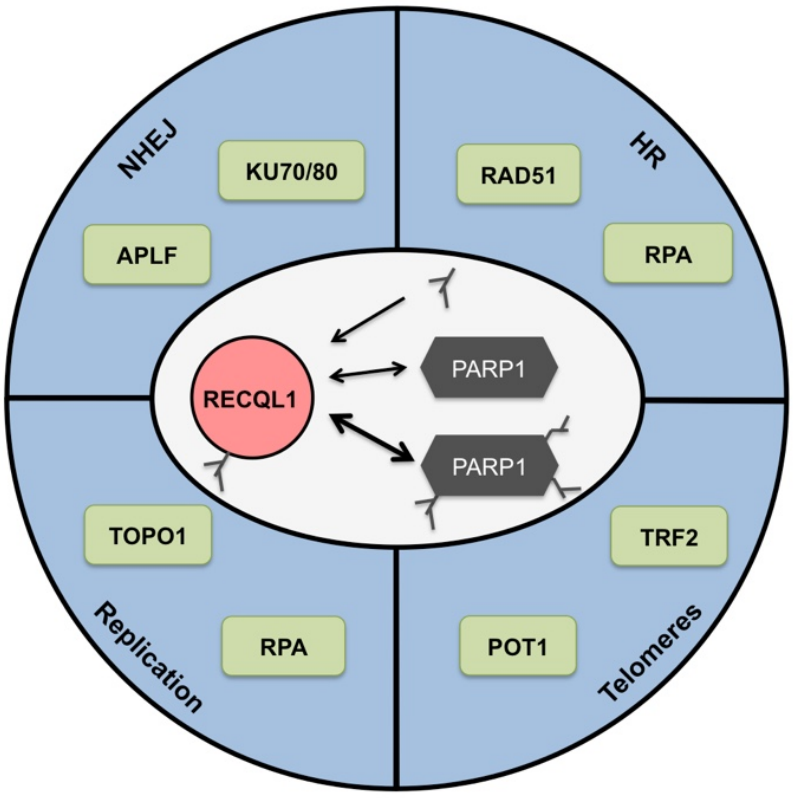

Figure 6: Interplay of RECQL1, PARP1, and PARylation.
Overlapping functions are indicated in blue; shared interaction partners in green. Thickness of arrows indicates strength of interaction.

DNA repair:

Replicative stress is intimately connected to the repair of DNA double strand breaks (DSBs), since the collapse of stalled replication forks can cause DSB formation (Zeman and Cimprich, 2014). DSBs present a major problem for cells, as they are (*i*) difficult to repair, lead to (*ii*) genomic instability and mutagenesis, and (*iii*) ultimately to cell death or carcinogenesis. To combat these lesions several repair pathways evolved, such as the largely error-free homologous recombination repair (HR) and canonical non-homologous end-joining pathway (cNHEJ) as well as the error-prone alternative NHEJ (alt-NHEJ) (Boboila et al., 2012; Ciccia and Elledge, 2010). RECQL1 participates in the repair of DSBs, which is evident by the fact that cells deficient in RECQL1 display defects in DSB repair (Sharma and Brosh, 2007; Sharma et al., 2007). Such cells exhibit elevated levels of sister chromatid exchanges, γH2A.X foci, are sensitive to DSB formation, and show reduced DNA end-joining activity (Parvathaneni et al., 2013). On a molecular level, RECQL1 interacts with factors involved in HR and NHEJ, such as RAD51, RPA, and Ku70/80 (Parvathaneni et al., 2013; Sharma et al., 2007), and RECQL1, similar to WRN and BLM, is able to resolve or branch migrate Holliday junctions (HJ) and other HR intermediates (Bugreev et al., 2008; LeRoy et al., 2005). Notably, PARP1 and PARylation play important, yet complex and not fully understood roles in HR and NHEJ (Pines et al., 2013), suggesting a functional collaboration between RECQL1 and PARylation in DSB repair. This notion is supported from proteomics studies, revealing that RECQL1 and PARP1 form an intracellular complex together with Ku70/80 and APLF (APTX-PNK-Like Factor), which are key components in NHEJ repair (Berti et al., 2013; Parvathaneni et al., 2013). Furthermore, RECQL1 and PARP1 form a complex with replication protein A (RPA) (Sharma et al., 2012), which may stimulate RECQL1's helicase activity during HR (Cui et al., 2004; Sami and Sharma, 2013). Interestingly, RPA is a direct target for covalent PARylation as well as non-covalent PAR interaction during genotoxic and replicative stress, thereby modulating the binding of RPA onto ssDNA (Illuzzi et al., 2014; Jungmichel et al., 2013). Together, these results argue for a significant interplay between RECQL1, RPA and PARP1 during DSB repair and replicative stress response.

Besides DSB repair, there is evidence that RECQL1 participates in the repair of oxidative DNA damage by base excision repair (BER), because RECQL1-depleted cells are moderately sensitive to H_2O_2 treatment and such a treatment leads to a rapid association of RECQL1 to the chromatin fraction (Sharma et al., 2012). In contrast to WRN and BLM, RECQL1 depletion does not sensitize cells to PARP inhibition and basal levels of PARP activity are not elevated. Remarkably, however, RECQL1 depletion leads to a strong hyper-activation of

PARP activity upon H_2O_2 treatment (Sharma et al., 2012). The finding that the recruitment of RECQL1 to chromatin after oxidative stress is independent of PARP activity, suggests that RECQL1 depletion leads to persistence of H_2O_2-induced DNA damage that triggers PARP activation and possibly leads to repair by PARP-dependent alternative mechanisms. Despite this initial evidence for a cooperative function of RECQL1 and PARP1 in BER, the exact molecular details of such an interplay await to be established.

Telomere maintenance:

Telomeres are repetitive sequences at the end of the chromosomes and function as buffers to prevent loss of coding sequences during DNA replication. They are capped by a protein complex known as shelterin, which tightly regulates the telomeric structure by interaction with several DNA repair proteins and the telomere-elongating reverse transcriptase, *i.e.*, telomerase. Deterioration of telomeres can be seen as a specific sub-form of genomic instability, as uncapped telomeres trigger a sustained DNA damage response. Telomere shortening has been described as an important factor during normal human aging [reviewed in (Blasco, 2007)]. Recent evidence suggests that RECQL1 plays a significant role in telomere maintenance, especially in the alternative lengthening of telomeres pathway (ALT), which is independent of telomerase activity (Popuri et al., 2014). Specifically, RECQL1 resolves telomeric D-loop and HJ substrates and interacts with telomere repeat binding factor 2 (TRF2), which regulates RECQL1's activity at telomeric substrates. Consistently, loss of RECQL1 results in dysfunctional telomeres and telomere shortening. Intriguingly, PARP1 was reported to be crucial for telomere maintenance and interacts with TRF2 as well, whose activity is negatively regulated by PARP activity (Beneke et al., 2008; d'Adda di Fagagna et al., 1999; Dantzer et al., 2004; O'Connor et al., 2004). Therefore, it is tempting to speculate that in addition to their physically interaction, PARP1, RECQL1, and TRF2 functionally cooperate during telomere maintenance.

In conclusion, these studies provide a basis that clearly demonstrates overlapping and collaborative functions of RECQL1 and PARP1 in maintaining genome integrity (Figure 6), however, in particular with respect to DNA repair and telomere maintenance mechanisms our understanding is incomplete and calls for further investigations.

WRN (RECQL2)

WRN was first identified by positional cloning in 1996 as the gene responsible for WS and is by now probably the best studied RecQL helicases member (Yu et al., 1996). Of all known segmental premature aging disorders, features of WS resemble closest normal human aging, and therefore functions of WRN may play a significant role during the normal aging process. Surprisingly, mice lacking functional WRN have no phenotype similar to WS, although they display a slight increase in cancer incidence (Lebel and Leder, 1998; Lombard et al., 2000). In contrast, a strong premature aging phenotype was observed, when *Wrn* mutants were crossed with late-generation *Terc* KO mice (Chang et al., 2004). *Terc* encodes for the telomerase RNA component and *Terc* KO mice display progressively shortened telomeres with every new generation. In terms of telomere biology, late-generation *Terc* KO mice resemble more the human situation, because, in contrast to humans, WT mice exhibit considerably longer telomeres than humans and normal mouse aging does not depend to the same extent to telomere shortening (Rudolph et al., 1999). The fact that the *Wrn*/*Terc* double deficient animals display a premature aging phenotype similar to the one observed in humans indicates the importance of telomeres on the phenotype of WS (Chang et al., 2004). On the cellular level, WRN interacts with multiple factors linking it to numerous DNA metabolic processes, such as replication, DNA repair, telomere maintenance and transcription [reviewed in (Croteau et al., 2014; Rossi et al., 2010a)]. Interestingly, WRN interacts with all other RecQL helicases except RECQL1, indicating it may also act as a backup factor for other helicases (Croteau et al., 2014). Recently, such a complimentary role has been shown for WRN and RECQL5 in the repair and restart of stalled replication forks, with cells deficient in both proteins displaying synthetic lethality (Popuri et al., 2013). In addition, WRN and BLM interact with each other and have overlapping functions in replication, recombination and telomere processing, suggesting some level of redundancy as well. Nevertheless, the intensity of the individual collaborations between WRN and other RecQL helicases is strongly pathway specific [reviewed in (Croteau et al., 2014)].

Meanwhile, a rich body of evidence reveals a close interaction between WRN, PARP1 and PARylation on a molecular and organismic level (Figure 7). First *in vivo* evidence for an interplay between WRN and PARylation came from the analysis of $Wrn^{\Delta hel/\Delta hel}$ mice, which display increased genome instability (Lebel, 2002). When interbreeding these mice into a $Parp1^{-/-}$ background, $Parp1^{-/-}/Wrn^{\Delta hel/\Delta hel}$ mice display enhanced oxidative damage and develop more neoplasms at younger age than WT or single KO animals (Lebel et al., 2003). Consistently, mouse embryonic fibroblasts (MEFs) generated from these mice show genome

and telomere instability and stop dividing already after two to three population doublings. In addition, gene expression is differentially regulated in the *Wrn*/*Parp1* double KO mice as compared to the single KO mice, with the most affected genes being involved in apoptosis, cell cycle control, metabolism and signal transduction (Deschênes et al., 2005). Interestingly, $Parp1^{-/-}/Wrn^{\Delta hel/\Delta hel}$ mice show a reduced lifespan, yet the aging phenotype of these mice has never been reported in detail (Lebel et al., 2003).

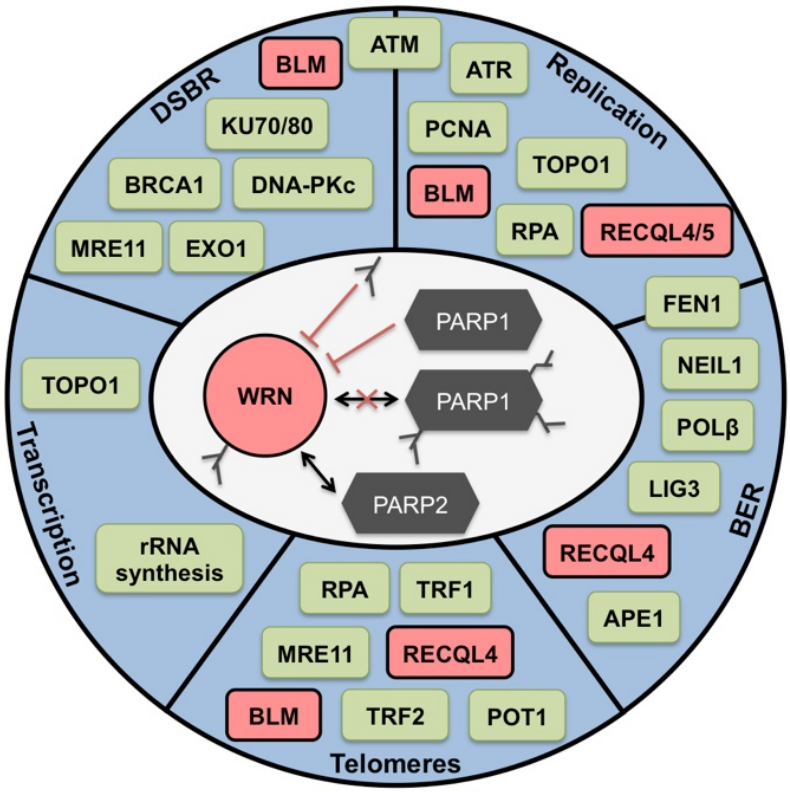

Figure 7: Interplay of WRN, PARP1, and PARylation.
Overlapping functions are indicated in blue; shared interaction partners in green. RecQL helicases are indicated in red.

On the biochemical level, Adelfalk *et al.* were the first to report a molecular interaction between PARP1 and WRN. They suggested that PARP1 covalently modifies WRN at its N-terminus (Adelfalk et al., 2003). Although other groups could not confirm this covalent modification (Li et al., 2004), recent proteomics studies also suggest covalent PARylation of WRN (Gagné et al., 2012; Jungmichel et al., 2013). Strikingly, within a set of representative DNA repair factors, WRN was among the most heavily PARylated proteins upon induction of alkylating DNA damage (Gagné et al., 2012). In addition, more recently, we revealed a high-affinity non-covalent interaction of PAR with WRN via at least one PBM located in the WRN exonuclease domain. Importantly, PAR binding to WRN inhibits its DNA binding abilities as well as its helicase and exonuclease functions (Popp et al., 2012). Furthermore, our data

indicates that the inhibitory effect of PAR binding to WRN is stronger on the helicase than on the exonuclease activity (Popp et al., 2012). This is on the one hand startling, since the PBM is located in the exonuclease domain, but on the other hand may imply a differential regulation of WRN's catalytic activities and thus favoring some pathways over others.

Apart from PAR modification and interaction, WRN and PARP1 themselves physically interact via the BRCT domain in PARP1 and the N-terminus/RQC domain in WRN (Kobbe et al., 2003a; 2004a; Lachapelle et al., 2011; Lebel et al., 2003). Interestingly, PARylated PARP1 interacts with WRN less efficiently, suggesting a dynamic interaction of WRN dependent on the PARylation status of PARP1 (Kobbe et al., 2004a). Importantly, the binding of PARP1 to WRN has functional consequences on WRN, since both exonuclease and helicase activities are inhibited upon PARP1 binding (Kobbe et al., 2004a; Mangerich et al., 2012; Popp et al., 2012). Consistent with the finding of reduced binding of PARylated PARP1 to WRN, PARylated PARP1 inhibits WRN's enzymatic functions less efficiently. How these findings can be reconciled with the ones showing that 'free' PAR efficiently inhibits WRN's biochemical functions (Popp et al., 2012) remains an open question, however a hypothetical model depicts a negative feedback of PARP1 activation. Thus, when PARP1 is activated by DNA damage, it is automodified, and WRN is free to act on the damage site, but the PAR chains released by PARG soon start to inhibit WRN activity until PARP1 is restored and can exert its inhibitory function again. This would limit WRN's activity to a specific time window and prevent it from inducing genome instability in phases, when its action would be detrimental.

As observed with other RecQL helicases and PARylation target proteins (Fischer et al., 2014), the WRN-PARP1 interaction is not unidirectional, but rather appears to happen in a reciprocal manner. This becomes evident by the finding that overexpression of WRN's PARP1 binding domain severely impairs PARylation activity in cells exposed to oxidative stress (Kobbe et al., 2003a). On the other hand, depletion of WRN leads to PARP1 hyperactivation and co-treatment of cells with WRN and PARP1 inhibitors synergistically inhibit cell proliferation (Aggarwal et al., 2011; Gottipati et al., 2010). In terms of a cellular interaction of WRN and PARP1, it is interesting to note that considerable amounts of PARP1 and WRN reside in the nucleoli (Gray et al., 1998; Meder et al., 2005; Woo et al., 2006). Upon genotoxic stress both proteins leave the nucleolus and accumulate at sites of DNA damage (Woo et al., 2006). It is tempting to speculate that nucleoli serve as a storage place for WRN, PARP1 and other DNA repair factors under non-stress condition and that upon DNA damage, those translocate to sites of DNA damage. Although this may occur in a PARylation dependent manner, at present

it is unknown, whether PARP1 and WRN require each other during this synchronous spatial redistribution. On the other hand, it is possible that PARP1 and WRN directly cooperate in nucleolar functions. While in general the role of PARP1 in nucleolar biology is not very well understood, it has been shown that nucleolar structure disintegrates in *Parp1* mutants. Furthermore, PARP1 localization seems to be dependent on nucleolar activity, since PARP1 translocates from the nucleolus to the nucleoplasm, when ribosomal DNA (rDNA) transcription is inhibited (Boamah et al., 2012; Desnoyers et al., 1996; Meder et al., 2005). Consistently, PARP1 has been associated with rRNA processing and pre-ribosome assembly in nucleoli (Boamah et al., 2012). Similarly, the role of WRN in nucleoli is still unclear, but the findings that rRNA transcription is significantly decreased in WS fibroblasts and that WRN is able to unwind DNA/RNA heteroduplexes suggest that WRN is involved in nucleolar transcription by resolving transcription intermediates (Shiratori et al., 2002; Suzuki et al., 1997). It will be interesting to find out how PARP1 and WRN cooperate in these processes.

Replication:

Each of the RecQL helicases participates in DNA replication at some point, but probably their most important function is to deal with and to resolve replicative stress. WS cells are highly sensitive to replicative stress (Lebel and Leder, 1998). Fork progression, and thus replication, lasts longer in these cells, indicating that WRN removes or resolves DNA structures blocking fork movement (Poot et al., 1992; Sidorova, 2008; Sidorova et al., 2013). Specifically, WRN is involved in replication fork stabilization and prevents erroneous recombination events at stalled forks (Popuri et al., 2013). WRN also interacts with several DNA polymerases, acting as a proofreader or stimulating translesion synthesis during replication (Kamath-Loeb et al., 2007; 2012; Maddukuri et al., 2014; 2012). The importance of RecQL helicases in replication is demonstrated by the synthetic lethality of WRN/RECQL5 double deficient cells, indicating that the two proteins complement each other in the repair and restart of replication forks (Popuri et al., 2013).

Similar to the situation for RECQL1, it is likely that WRN and PARP1 cooperate during the replicative stress response. Thus, MEFs isolated from *Parp1*/*Wrn* KO mice rapidly stop dividing in culture and exhibit replication-related signs of chromosomal instability such as multi-radial chromosomes (Lavoie et al., 2005). Furthermore, cells treated with both PARP and WRN inhibitors displayed a strong reduction in cell proliferation, further strengthening a

putative cooperation during replication (Aggarwal et al., 2011). In addition, recent evidence demonstrates that both WRN and PARP1 are crucial for proper checkpoint signaling upon fork stalling (Min et al., 2013; Patro et al., 2011). Thus, on the one hand, PARP1 binds to DSB formed at stalled replication forks, leading to retention and activation of CHK1 in a PAR- and ATR-dependent manner (Min et al., 2013). On the other hand, WRN is important for recruiting ATR to sites of stalled forks and subsequent phosphorylation of CHK1 (Patro et al., 2011). Although, at present, it is not clear whether PARP1 and WRN directly collaborate to mediate correct checkpoint signaling, it is tempting to speculate that PARylation regulates the time-dependent concerted action of WRN-ATR-CHK1 during this process (Patro et al., 2011; Popp et al., 2012).

Taken together, it appears as if both, WRN and PARP1, join forces to resolve replicative stress, however the exact mechanistic details of this cooperation are currently unknown. In particular, it will be interesting to see to what extent WRN participates in the cooperative function of RECQL1 and PARP1 to resolve fork stalling after TOPO1 inhibition as reported by Berti *et al.* (Berti et al., 2013).

DNA repair:

WRN and PARP1 play a significant role in DSB repair and seem to participate in all three sub-pathways, *i.e.*, HR, cNHEJ, and alt-NHEJ. For example, both WRN and PARP1 are recruited to DSBs (Haince et al., 2008; Lan et al., 2005). Although WRN is recruited to DSBs autonomously via its HRDC domain (Lan et al., 2005), it is likely that active PARylation modulates WRN recruitment kinetics. Furthermore, PARP1 and WRN cooperate in the processing of DSBs at the site of the damage. Most strikingly, both proteins are part of a multi-protein complex together with the core cNHEJ factors Ku70/80 and DNA-PKcs, (Cooper et al., 2000; Kusumoto et al., 2008; Li et al., 2004; Spagnolo et al., 2012). Specifically, the Ku70/80 proteins strongly stimulate WRN exonuclease activity, but this effect is abolished when Ku70/80 are covalently PARylated by PARP1, which also decreases their affinity for DNA (Cooper et al., 2000; Li et al., 2004). This indicates that under certain conditions PARP1 inhibits cNHEJ in favor of HR. In support of this idea, *PARP1* and *WRN* KO cells are sensitive to CPT treatment, while deficiencies of Ku70/80 and DNA-PKcs lead to resistance against CPT. This suggests that cNHEJ can be toxic in the repair of CPT-induced DSBs and WRN and PARP1 act in directing the repair in favor of HR (Otsuki et al., 2007). In agreement with this notion, PARP1 promotes HR at stalled replication forks by directly

suppressing the activity of Ku70/80 and LIGIV (Hochegger et al., 2006; Sugimura et al., 2008). Moreover, both WRN and PARP1 actively participate in HR directly and share several interaction partners therein such as EXO1, RPA, MRE11, BRCA1, and ATM (Aguilar-Quesada et al., 2007; Bryant et al., 2009; Cheng et al., 2006; Croteau et al., 2012b; Gottipati et al., 2010; Hu et al., 2014; Illuzzi et al., 2014; Liu et al., 2011). Nevertheless, it should be mentioned that the role of PARP1 in HR is still not fully understood, since under certain conditions PARP1 can also exert anti-recombinogenic effects, suggesting an inhibitory role in HR [reviewed in (Pines et al., 2013)].

In the absence of functional Ku70/80, alt-NHEJ can mediate the repair of DSBs in a PARP1-dependent fashion, which additionally requires XRCC1-LIGIII. The biological relevance of the alt-NHEJ pathway is still unclear, but there is evidence that both WRN and PARP1 participate therein (Aggarwal et al., 2010; Audebert et al., 2004; Boboila et al., 2012; Sallmyr et al., 2008; Wang et al., 2006).

In summary, these results reveal a central and biologically relevant interplay between WRN and PARP1 in DSBR. In the future, it will be interesting to test the hypothesis that the WRN/PARP1 complex may act as a dynamic switch between the different sub-pathways. In this context another layer of complexity is added by recent findings that PARP3 also acts as a critical determinant in this decision (Beck et al., 2014). However, a potential cooperative function of WRN and PARP3 has so far not been addressed.

Base excision repair (BER) removes small DNA lesions, such as oxidized or methylated bases or abasic sites by either short-patch (SP-BER, replacement of one base) or long-patch BER (LP-BER, replacement of up to 8 bases). WRN is involved in both sub-pathways and interacts with several key BER factors, such as NEIL1, APE1, DNA polymerase β (POL β), and FEN1 (Ahn et al., 2004; Brosh et al., 2001b; Das et al., 2007; Harrigan and Bohr, 2003). On a functional level, WRN is blocked by certain lesions like apurinic sites, 8oxodG and 8oxodA (Machwe et al., 2000). Therefore, WRN may act as a damage sensor for BER lesions (Das et al., 2007). While WRN is unable to pass by 8oxodG lesions, WRN can be stimulated by the interaction with Ku70/80 to remove them (Orren et al., 2001). Furthermore, WRN supports the excision of oxidative DNA lesions by stimulating the activity of the NEIL1 glycosylase (Das et al., 2007). Taken together with the finding that WS cells accumulate oxidative lesions after H_2O_2 treatment, this suggests a role of WRN in the repair of oxidative DNA damage (Das et al., 2007; Kobbe et al., 2004b). Although, the precise role of PARP1 in BER is still not fully understood, physical and functional interactions with numerous BER factors have been established during the last decades [reviewed in (Robert et al., 2013)], rendering a

cooperation with WRN in BER possible. This hypothesis is supported by the fact that WS cells show an impaired PARylation response upon oxidative stress (Kobbe et al., 2003a). Furthermore, PARP1 directly interacts with WRN, but also with APE1, NEIL1, OGG1, XRCC1, LIG3, and POLβ during LP-BER (De Vos et al., 2012; Leppard et al., 2003; Noren Hooten et al., 2012; Sukhanova et al., 2005). This extremely high overlap in protein interaction partners, as well as the fact that WS and *Parp1* mutant cells show deficiencies in BER, strongly reinforces the idea of a vital interaction of WRN and PARP1 in this repair pathway (De Vos et al., 2012; Harrigan et al., 2003; 2006). Along this line, Ren *et al.* speculate that WRN may act as a kind of sentinel for oxidative lesions and signals these lesions to PARP1. PARP1 may then verify the damage and recruit other repair factors to initiate and orchestrate subsequent DNA repair steps (Ren et al., 2009).

Recently, we and others established a role for PARylation in nucleotide excision repair (NER) (Fischer et al., 2014; Pines et al., 2013). For example, PARylation shows a biphasic response upon UV irradiation (Vodenicharov et al., 2005), suggesting a role in the early as well as late phase of NER. Moreover, XPA, which represents a central factor in NER, interacts both with PARP1 and PAR, which leads to reciprocal regulation of protein function (Fischer et al., 2014; King et al., 2012). To date there is very limited evidence for a role of RecQL helicases in NER, but WRN has been shown to interact with XPG, a structure-specific endonuclease that acts during NER (Trego et al., 2011). Yet, at present, it is not clear if the WRN-XPG interaction is relevant for NER, since this complex may also be involved in the repair of damaged replication forks in S-phase (Trego et al., 2011). If PARP1 and PARylation participate in the cooperative function of WRN and XPG is unknown.

Telomere maintenance:

WRN has a strong preference for several unique DNA structures like G-quadruplexes and telomeric D-loops that can be preferentially found at telomeres (Mohaghegh et al., 2001; Opresko et al., 2004). WRN also plays an important role in the replication of difficult and repetitive DNA sequences like telomeres, where it can resolve stalled replication forks (Croteau et al., 2014; Fouché et al., 2006). Striking evidence for a role of WRN in telomere biology stems from the fact that only *Wrn*/*Terc* double KO mice reproduce the phenotype of WS in mice, while *Wrn* single KO mice show only a slight increase in cancer incidence (Chang et al., 2004) (see above). Altogether, these findings indicate an important role of WRN in telomere maintenance. WRN and PARPs (*i.e.*, PARP1 and tankyrase1) share several

important interaction partners at telomeres like the shelterin components TRF1, TRF2 and POT1 (Gomez et al., 2006; Machwe et al., 2004; Opresko et al., 2002; 2005; Smith et al., 1998). Also, both PARP1 and WRN are crucial for maintaining telomere length, which is evident by the findings that *Parp1* and *Wrn* KO mice exhibit shorter telomeres (d'Adda di Fagagna et al., 1999; Gomez et al., 2006; Lebel et al., 2003; Opresko et al., 2002; 2005). Moreover, both proteins are recruited to laser-induced telomere damage, where PARP1 persists longer at telomeric damage than at non-telomeric damage, while WRN is exclusively recruited to telomeric damage (Silva et al., 2014). Nevertheless, despite these interesting functional correlations, the exact mechanistic details of how WRN and PARP1 may cooperate during telomere maintenance remain to be elucidated. In particular, it would be very interesting to investigate the phenotype of *Wrn*/*Parp1* double KO mice as well as *Wrn*/*Terc*/*Parp1* triple KO mice in terms of telomere biology.

In conclusion, there is strong experimental support for a functional and biological relevant interaction between WRN and PARP1 on a biochemical, cellular, and organismal level (Figure 7), but in most cases, the exact mechanistic details remain to be established. In particular, it needs to be clarified to which extent covalent or the non-covalent interaction with PAR as well as protein-protein interactions control individual cellular functions.

BLM (RECQL3)

Defects in *BLM* cause a rare autosomal recessive disorder that was first described by David Bloom in 1954 (Bloom, 1954) and which is associated with growth retardation, premature cancer development and diabetes (German et al., 2007; Manthei and Keck, 2013). In contrast to WS, BS patients develop a broader cancer spectrum, which is similar to the one observed in the normal population, however at an earlier time point in life (Croteau et al., 2014). Correspondingly, *Blm*-deficient mice show increased apoptosis during embryogenesis, chromosomal instability, and a high incidence of cancer in adult animals (Chester et al., 1998; Goss et al., 2002; Luo et al., 2000). On the cellular level, BLM is involved in many DNA metabolic pathways, including replication, DNA repair, telomere maintenance, and transcription. It plays important roles in HR, where it is involved in DNA end-resection as well as in the subsequent branch migration and resolution of HJs or double HJs (dHJs). Thereby, it is thought to ensure HR fidelity and suppress crossover reactions (Manthei and Keck, 2013; Wu and Hickson, 2003). Similarly, during replicative stress, it facilitates the dissolution of potential recombinogenic substrates at stalled replication forks (Kohzaki et al.,

2012; Manthei and Keck, 2013). BLM also physically and/or functionally interacts with other RecQL helicases, *i.e.*, WRN, RECQL4, and RECQL5 [reviewed in (Croteau et al., 2014; Lu et al., 2011)], which, for example, causes an inhibition of WRN's exonuclease activity (Kobbe et al., 2002).

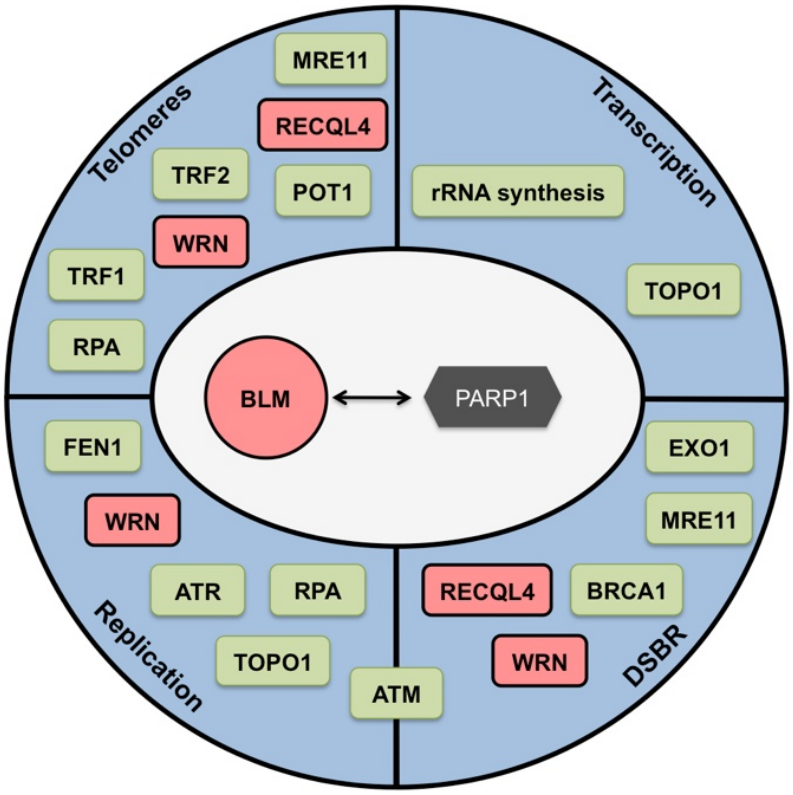

Figure 8: Interplay of BLM, PARP1, and PARylation.
Overlapping functions are indicated in blue; shared interaction partners in green. RecQL helicases are indicated in red.

First evidence for a possible crosstalk between BLM and PARP1 came from Gottipati *et al.*, who demonstrated that BLM depletion leads to PARP1 hyperactivation in U2OS cells, similar to WRN and RECQL5 depletion (Gottipati et al., 2010; Sharma et al., 2012; Tadokoro et al., 2012a) (Figure 8). In support of a molecular collaboration between BLM and PARP1, a proteomics approach identified PARP1 as a cellular interaction partner of BLM, though up to now this finding has not been further evaluated (Wang et al., 2013). Yet, the interaction with PARP1 does not come as a surprise, since PARP1 activity is necessary for the recruitment of MRE11 to sites of DSB and BLM is a major player in the control of end-resection process (Haince et al., 2008; Nimonkar et al., 2008; Sturzenegger et al., 2014). Apart from this, BLM and PARP1 share numerous physical and functional interaction partners involved in DNA repair and DNA replication. For example, like other RecQL helicases and PARP1, BLM interacts with RPA, which strongly stimulates its DNA unwinding activity (Brosh et al., 2000). Therefore, it is tempting to speculate that BLM, PARP1, and RPA functionally

collaborate during DNA replication. Moreover, BLM and topoisomerases work together during replication [reviewed in (Manthei and Keck, 2013)]. As mentioned above, PARP1 and PAR also physically and functionally interact with TOPO1 in response to DNA damage (Malanga and Althaus, 2004; Yung et al., 2004).

Also with respect to DSB repair, cooperative functions of BLM and PARP1 are expected to exist, since, *e.g.*, both proteins act together with BRCA1 during HR (Hu et al., 2014; Manthei and Keck, 2013). Furthermore, BLM stimulates FEN1 activity by resolving DNA secondary structures, suggesting an active role for BLM during BER (Wang and Bambara, 2005). As outlined above, PARP1 plays important roles during BER and SSB repair, and similar to the situation with WRN, it shares many physical and functional interaction partners with BLM in these processes, including FEN1 (Robert et al., 2013).

Recent data indicates that BLM contributes to telomere maintenance (Acharya et al., 2014; Barefield and Karlseder, 2012). Specifically, loss of BLM leads to increased telomeric defects like telomere fragility and elevated sister telomere loss (Barefield and Karlseder, 2012). Moreover, BLM is capable to efficiently unwind G-quadruplexes and D-loops, DNA structures that are most prominent at telomeres (Mohaghegh et al., 2001). As mentioned above, PARP1 also plays significant roles in telomere maintenance, thus representing another possible area of interaction. This notion is supported by the finding that both BLM and PARP1 physically and functionally interact with shelterin component TRF2 (Gomez et al., 2006; Opresko et al., 2002).

In conclusion, these studies suggest that a significant crosstalk between BLM, PARP1 and PARylation exists (Figure 8), however additional work is necessary to obtain more insight into the details of these putative collaborative functions.

RECQL4

Deficiencies in RECQL4 are associated with three different diseases, *i.e.*, Rothmund-Thomson syndrome (RTS), RAPADILINO syndrome, and Baller-Gerold syndrome (BGS), all of which increase the risk for various cancer types, thus rendering RECQL4 an important determinant for genome integrity (Dietschy et al., 2007). So far, three different *Recql4* mutant mouse models have been reported [reviewed in (Croteau et al., 2014; 2012a)]. Depending on the exact genetic mutation, phenotypes of these mice vary from complete embryonic lethality to normal lifespan, but none of them recapitulate the phenotype of the human diseases very accurately. Interestingly, mice that escape embryonic lethality in a model with a genetic

deletion of exon 13 show clear signs of premature aging, such as skin atrophy, hair graying and loss, growth defects, cataracts and immunological abnormalities (Hoki et al., 2003). Similar to other RecQL helicases, RECQL4 is involved in replication, DNA repair and telomere maintenance, but in addition, at present, it is the only RecQL helicase that has been reported to be present in mitochondria. Compared to other RecQL helicases, RECQL4 shows very low DNA unwinding activity, but preferentially anneals single-stranded DNA (Croteau et al., 2012a). RECQL4 physically interacts with BLM (Singh et al., 2012b), WRN (Ghosh et al., 2012), and RECQL5 (Zheng et al., 2009). For example RECQL4 stimulates BLM's helicase activity *in vitro*, and depletion of RECQL4 and BLM potentiates the frequency of sister chromatid exchanges (Singh et al., 2012b). Interestingly, distinct roles of RECQL4 and RECQL1 were reported during initiation and progression of DNA replication, during which RECQL4 is recruited to replication origins at late G1 phase, while both helicases are loaded at origins at the onset of S-phase (Thangavel et al., 2010).

It was found in several prostate cancer cell lines that of all RecQL helicases only RECQL4 levels were consistently elevated (Su et al., 2010). Experimentally induced RECQL4 depletion increases spontaneous DNA strand break accumulation in metastatic prostate cancer cells, leading to an increase in PARP1 and 53BP1 focalization as well as an increase in H2A.X phosphorylation. Furthermore, cellular depletion of RECQL4 leads to an increase in PARP1 protein levels and PARP1-dependent apoptosis specifically in prostate cancer cells (Su et al., 2010), suggesting a link between RECQL4 and PARP1 functions. This notion is consistent with the finding that RECQL4 interacts with PARP1 *in vitro* and *in vivo* (Woo et al., 2006) (Figure 9). This interaction is mediated by the C-terminus of RECQL4 and the BRCT domain of PARP1. Additionally, RECQL4 is covalently PARylated by PARP1 at the C-terminus (Woo et al., 2006). Interestingly, the C-terminus of RECQL4 has been related to the response to IR (Kohzaki et al., 2012), and therefore it has been hypothesized that the RECQL4-PARP1 interaction may be important in this context (Croteau et al., 2012b). So far, there is no experimental evidence for a non-covalent interaction of RECQL4 and PAR, although a homology search using the PBM consensus sequence suggests a PBM in the C-terminus of RECQL4 (Gagné et al., 2008).

DNA repair and genotoxic stress response:

Several studies revealed that RECQL4 dynamically associates with foci produced by DNA damaging agents including H_2O_2, IR, TOPO inhibitors and UV, however, the present

literature on this is inconsistent, which may be related with the genetic heterogeneity of RTS patient cells. Moreover, cells depleted in RECQL4 are sensitive to such genotoxic agents (Croteau et al., 2012b; Jin et al., 2008; Werner et al., 2006). In contrast to WRN, upon oxidative stress, RECQL4 relocates from the nucleoplasm to the nucleoli. Intriguingly, pretreatment with PARP inhibitors can prevent this relocalization (Woo et al., 2006). This may suggest that PARP activity rather than PARP1 binding to RECQL4 is relevant for this relocalization. It is tempting to speculate that PAR modification initiates a conformational change that exposes the nucleolar targeting signal (Boamah et al., 2012; Léger et al., 2014; Rancourt and Satoh, 2009).

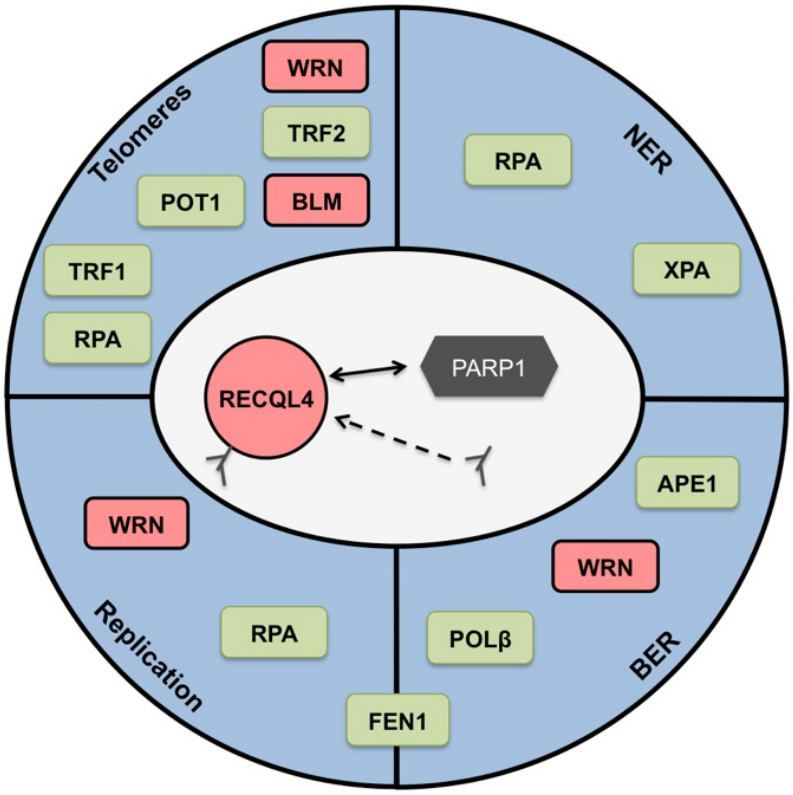

Figure 9: Interplay of RECQL4, PARP1, and PARylation.
Overlapping functions are indicated in blue; shared interaction partners in green. RecQL helicases are indicated in red.

A role of RECQL4 in BER is supported by the fact that RECQL4-depleted cells accumulated more H_2O_2-induced DNA strand breaks and XRCC1 foci than control cells (Schurman et al., 2009). In addition, after H_2O_2 treatment RECQL4 co-localizes with APE1 and FEN1, two central players in BER. RECQL4 stimulates endonuclease activity of APE1, strand displacement activity of DNA POLβ, and incision activity of FEN1 (Schurman et al., 2009). The fact that APE1, POLβ, and FEN1 are also PARP1 interaction partners (Robert et al.,

2013) points to a possible functional crosstalk between PARP1 and RECQL4 during BER, however, the precise role of the PARP1-RECQL4 cooperation awaits further investigations.
While some RTS cells are not hypersensitive to UV irradiation, others are (Croteau et al., 2012b). Specifically in a study by Fan and Luo, RECQL4 formed distinct nuclear foci in response to UV irradiation and supported the repair of such lesions in human cells (Fan and Luo, 2008). Moreover, upon UV irradiation RECQL4 colocalized with NER factor XPA, and consistent with this, interacts with XPA on a molecular level. This interaction was stimulated upon UV irradiation (Fan and Luo, 2008). Taken together, these results suggest that RECQL4 participates in the late stage of NER, potentially to resynthesize DNA after excision of the lesion (Fan and Luo, 2008). As mentioned above, recent evidence links PARP1 and PARylation to XPA and NER [reviewed in (Pines et al., 2013)]. To which extent the participation of PARP1 and RECQL4 in NER coincide is unknown.

Telomere maintenance:

Besides RECQL1, WRN and BLM, RECQL4 acts on telomeres as well (Croteau et al., 2012b). Thus, RECQL4 depleted cells or cells from RTS patients show dysfunctional telomeres. RECQL4 can act synergistically with WRN, but not BLM, to resolve telomeric D-loop substrates, by stimulating WRN's helicase activity (Croteau et al., 2012b). Furthermore, RECQL4 interacts with TRF2, which, in turn, can stimulate RECQL4's helicase activity on a telomeric DNA substrate (Ghosh et al., 2012). It is well possible that PARylation of TRF2 (Gomez et al., 2006) serves as a signal to attract PAR binding proteins, such as RecQL helicases to telomeres.
In conclusion, a physical and functional interaction between RECQL4 and PARP1 has been established (Figure 9), however, knowledge about the detailed molecular mechanisms is much in its infancy. Apart from sharing a host of overlapping interaction partners, it appears as if PARP1 is regulating RECQL4's spatial distribution upon oxidative stress. On the other hand, there is also evidence that RECQL4 regulates PARP1 either directly or indirectly (Su et al., 2010). In this context, it would be interesting to analyze the PARP and PARylation status in cells derived from RTS, BG or RAPADILLINO patients. That is, if they have decreased levels in PARP1 and PARylation, as reported for WS cells (Kobbe et al., 2003a), or if they display an overexpression of PARP1 as shown for the prostate cancer cells (Su et al., 2010).

RECQL5

Even though RECQL5 has so far not been associated with any human disease, *Recql5* KO mice are cancer prone and cells derived from these mice display signs of genome instability (Hu et al., 2007). For this reason, it is likely that RECQL5 functions as a tumor suppressor in mammals, such as the other RecQL helicases (Hu et al., 2010; Popuri et al., 2013). However, unlike other RecQL helicases, RECQL5 exists in three different splice variants. Two of these are located in the cytoplasm (RecQL5α and γ), while isoform β (the most abundant form, from now on referred to as RECQL5) is located in the nucleus (Shimamoto et al., 2000). RECQL5 can unwind forked and partial duplex DNA substrates, however it does not efficiently unwind D-Loop, G-quadruplex and HJ substrates [reviewed in (Popuri et al., 2013)]. So far a direct physical interaction of RECQL5 has been established with WRN (but not BLM) and this interaction is most prominent during S-phase upon the induction of replicative stress (Popuri et al., 2012a). Like other RecQL helicases, RECQL5 plays important roles in replication and DNA repair and may provide essential backup functions for other RecQL helicases [reviewed in (Popuri et al., 2013)]. For example, cooperative as well as complementary functions with WRN and BLM have been established (Hu et al., 2005; Popuri et al., 2012a; 2013). Specifically, RECQL5 stays longer at DSB in the absence of BLM and WRN, but not in the absence of RECQL4 (Popuri et al., 2012a). Furthermore, these results reveal a close physical and functional interaction between RECQL5 and WRN during replicative stress and WRN/RECQL5 deficiency results in synthetic lethality (Popuri et al., 2012a) (see above section on WRN).

A physical interaction between PARP1 and RECQL5 has been suggested, but awaits further characterization (Croteau et al., 2014; Popuri et al., 2013; Tadokoro et al., 2012b) (Figure 10). Furthermore, there is a considerable body of evidence on a functional level that links RECQL5 and PARylation. Tadokoro *et al.* show that depletion of RECQL5 results in increased DNA damage and PAR formation, similar to the effects observed with RECQL1. However, RECQL5 depletion results in decreased PARP1 expression levels, which may be linked to a possible role of RECQL5 as a transcriptional modulator of DNA repair genes (see below) (Popuri et al., 2013; Tadokoro et al., 2012b).

A role for RECQL5 in replication is evident by the fact that *Recql5* deficient cells are hypersensitive to CPT-induced replication-dependent cell death (Hu et al., 2009). Mechanistically, RECQL5 synergistically cooperates with WRN during replication (Popuri et al., 2012a) and may contribute to the strand exchange on RPA-coated forked structures at stalled replication forks to facilitate the bypass of replication-blocking lesions by template-

switching (Kanagaraj et al., 2006). Given the overlap in interaction partners and participation of RECQL5 and PARP1 in the replicative stress response, a cooperative function of both factors during DNA replication is likely, but so far unexplored.

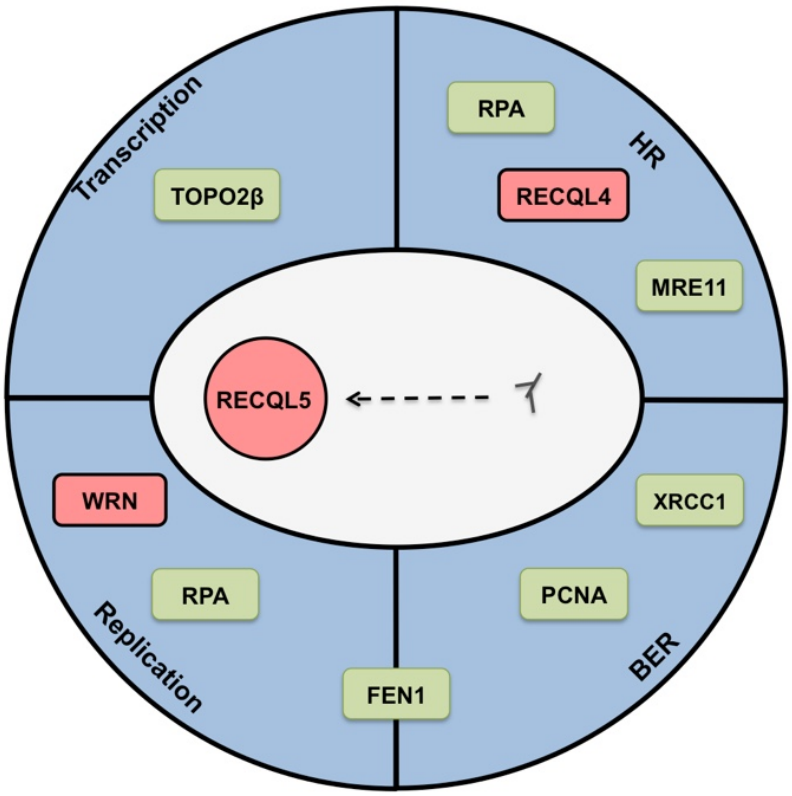

Figure 10: Interplay of RECQL5, PARP1 and PAR.
Overlapping functions are indicated in blue; shared interaction partners in green. RecQL helicases are indicated in red.

A possible role for RECQL5 in DSB repair is supported by the finding that it is recruited to DSBs in an autonomous manner (Popuri et al., 2012b). Furthermore, RECQL5 interacts with MRE11 in cells (Zheng et al., 2009). On the other hand, as mentioned earlier the recruitment of MRE11 to DSBs is supported by PARP activity (Bryant et al., 2009; Haince et al., 2008). Interestingly, both PARP1 and RECQL5 control MRE11 exonuclease activity, which may restrict MRE11 action to a tight and well-controlled time-window during end-resection of free DNA ends in preparation of subsequent DNA repair steps (Ying et al., 2012; Zheng et al., 2009).

Like other RecQL helicases, RECQL5 participates in BER/SSBR, as it is evident by the fact that depletion of RECQL5 leads to an accumulation of oxidative DNA damage and sensitizes cells to oxidative stress (Tadokoro et al., 2012b). Notably, RECQL5, unlike other RecQL helicases, is recruited to DNA SSBs (Tadokoro et al., 2012b), suggesting a unique non-redundant role of RECQL5 in SSB repair. Interestingly, the depletion of RECQL5 leads to

delayed dissociation kinetics of XRCC1 from the site of the damage. On the other hand, recruitment of XRCC1 to damage sites is very much dependent on PARP activity (Mortusewicz et al., 2007), suggesting that RECQL5 and PARP1 collaboratively control the spatio-temporal function of XRCC1 at DNA damage sites. In addition, this might explain the elevated PAR levels under conditions of RECQL5 depletion, which may be caused by persistent DNA damage and subsequent, prolonged PARP activity due to delayed repair kinetics. Furthermore RECQL5 and PARP1 share a number of other interaction partners with key roles during BER, such as PCNA and FEN1 (Speina et al., 2010) (see above). These findings imply a connection between PARylation and RECQL5 in the repair of endogenous DNA lesions and cellular response to oxidative stress.

Recent evidence points to a unique role of RECQL5 in transcription, as it is the only RecQL helicase member associated with RNA polymerase II (Aygün et al., 2008; 2009). Specifically it may act as a general elongation factor that preserves genome stability during transcription (Saponaro et al., 2014). Interestingly, PARP1 is involved in transcription on many levels as well [reviewed in (Kraus and Hottiger, 2013)]. Specifically, PARP1 is attracted to TOPO2β-mediated dsDNA breaks, where it is activated and mediates transcriptional initiation by inducing local changes in the chromatin structure (Ju et al., 2006). Although RECQL5 has been shown to interact with TOPO2β in the context of replication only, it is tempting to speculate that RECQL5 interacts with TOPO2β during transcription as well (Ramamoorthy et al., 2012). This suggests a yet to be established cooperative function of RECQL5, PARP1 and TOPO2β in the regulation of gene expression.

In conclusion, an initial connection of RECQL5, PARP1 and PARylation has been revealed. However, similar to the situation observed with all other RecQL helicases, the mechanistic details are often of hypothetical nature and need to be verified by experimental studies.

Concluding remarks and future directions

Both, RecQL helicases and PARPs act as independent quality assurance systems to maintain integrity of the genome to ensure mammalian longevity (Chu and Hickson, 2009; Croteau et al., 2014; Mangerich and Bürkle, 2012). As summarized in this review, apart from their independent roles, both show a vibrant interplay on a molecular and functional level, which is manifested by several findings: (*i*) all five RecQL helicases interact with PARP1 and/or its enzymatic product PAR. (*ii*) RecQL helicases and PARP1 show a striking overlap in the cellular pathways and mechanisms they participate in, such as DNA replication, repair of

oxidative DNA damage and DNA strand breaks, telomere maintenance, and transcription. (*iii*) Within these processes, RecQLs and PARP1 share a remarkable number of protein interaction partners. (*iv*) Deficiencies in RecQL helicases in many cases induce alterations in basal or stress-induced PARylation metabolism. (*v*) PARP1 deficiency or inhibition of cellular PARylation modify the intracellular localization of many RecQL helicases, or their redistribution upon different genotoxic stimuli.

Despite the profound body of evidence that documents the physical and functional RecQL-PARP1 interactions, much of our current knowledge about this interplay is rather correlative and descriptive and studies that uncover mechanistic details and a biological relevance of these interactions are limited by now. Challenges that arise from studying independent as well as cooperative functions of RecQL helicases and PARP1 arise from the fact that both are involved in pleiotropic molecular mechanisms affecting multiple levels of cellular physiology. Thus, when interfering with RecQL or PARP1 function, this leads to a multitude of cellular effects, for which it is difficult to disentangle individual molecular mechanisms. Nevertheless, several studies, in particular on RECQL1 and WRN, provide proof of principle that it is feasible to unravel mechanistic details and the functional significance of the RecQL and PARP1 interactions (Berti et al., 2013; Deschênes et al., 2005; Kobbe et al., 2003a; 2004a; Lavoie et al., 2005; Lebel et al., 2003; Li et al., 2004; Popp et al., 2012).

Based on our current knowledge on the RecQL-PARP1 interactions, several key questions arise that need to be addressed in future studies:

To what extent does PARylation regulate the spatio-temporal functions of RecQL helicases and contribute to the division of labor between the individual RecQL helicases?

To dismantle combined and distinct functions of the five RecQL homologs in time and space represents a key question in RecQL biology [reviewed in (Croteau et al., 2014)]. In this respect, it is interesting to note that PARP1 can regulate RecQL functions differentially. For example, while PARylated PARP1 strongly binds to RECQL1, this seems not to be the case for WRN (Berti et al., 2013; Kobbe et al., 2004a). Consequently, it can be speculated that PARylation serves as signal to differentially modulate RecQL activities in order to “choose” the most appropriate RecQL helicase at the right time to fulfill the relevant task. Since PARylation is often induced in a dose-dependent manner with increasing levels of genotoxic stress, it is conceivable that this leads to a step-wise control of the functions of different RecQL helicases dependent on the type and level of cellular DNA damage load. For example,

it is tempting to speculate that PARP1 and PARylation play significant roles to regulate the coordinative action of the different RecQL helicases during the replicative stress response.

Does PARylation control oligomerization status and the interaction of RecQL helicases?

The oligomerization status of RecQL helicases is critical for RecQL function and may represent a mechanism of how RecQL helicases could be differentially regulated [reviewed in (Croteau et al., 2014)]. Depending on the specific target proteins, PARylation and non-covalent PAR binding can mediate protein complex dissociation or association (Gibson and Kraus, 2012). For example, non-covalent PAR binding mediates p53 homo-oligomerization (Fahrer et al., 2007). In this context, if PAR serves as a regulatory factor of RecQL homo- as well as hetero-oligomerization, and if this may be important to control their cellular functions, it represents an important area of future research.

Do other DNA damage-dependent PARPs interact with RecQL helicases?

As summarized in this work, various physical and/or functional interactions have been reported of RecQLs with PARP1. On the other hand, it would be very interesting to see if other nuclear PARPs such as PARP2/3 also interact with RecQL helicases. In this respect, it has been shown that WRN interacts with PARP2 with similar affinities as PARP1 (Kobbe et al., 2004a), however, at present, the functional relevance of this interaction is completely unknown.

What is the interplay of PARylation and other PTMs to control RecQL helicases function?

RecQL helicases are modified and controlled by several other PTMs. For example, WRN is phosphorylated, SUMOylated, and acetylated at various positions [reviewed in (Croteau et al., 2014)]. It will be interesting to define how the different PTMs work together to modulate RecQL's enzymatic activities, cellular localizations, and protein-protein interactions. For example, a crosstalk between PARylation and acetylation is particularly likely. In this context, it has been shown that MMS-treatment leads to p300-dependent acetylation of WRN, and this acetylation stimulates WRN's catalytic functions and LP-BER (Muftuoglu et al., 2008a). Interestingly, MMS / PARP inhibitor co-treatment, but not PARP inhibitor treatment alone, further increases WRN acetylation, suggesting a crosstalk of WRN acetylation and PARylation during the repair of MMS-induced DNA damage (Lozada et al., 2014). Furthermore, BLM and WRN functionally interact with the histone deacetylase SIRT1 (Vaitiekunaite et al., 2007). SIRT1, on the other hand, maintains a close interplay with PARP1 on many levels, starting from the fact that both enzymes share the same substrate, *i.e.*, NAD^+ (Cantó et al., 2013).

Can combined inhibition of RecQL helicases and PARPs be a useful approach to target tumor cells?

Interestingly, the RecQL-PARP1 interaction can be of high clinical relevance. Several PARP inhibitors are currently being tested in clinical trials, including phase III trials, as potential cancer therapeutics [reviewed in (Lord et al., 2015; Mangerich and Bürkle, 2011; Sonnenblick et al., 2015)]. The mechanistic basis for their use in cancer therapy is two-fold: (i) either PARP inhibitors are used in combination therapy with classical radio- or chemotherapy in order to sensitize cancer cells for such DNA-damaging agents. Or (ii), they are used as stand-alone drugs in HR-deficient tumors following the concept of synthetic lethality. Considering individual and cooperative functions of PARP1 and RecQL helicases, it is tempting to speculate that deficiency in both factors may result in synthetic lethality. In this regard, it is important to note that epigenetic inactivation of WRN is a common event in human cancer cells (Agrelo et al., 2006), suggesting that such tumors may represent a good target for PARP inhibitor treatment. Furthermore, recently pharmacological WRN and BLM inhibitors have been identified and co-treatment of cells with WRN and PARP1 inhibitors led to a strong reduction in cell proliferation (Aggarwal et al., 2011; 2013; Nguyen et al., 2013). Future studies need to test if tumor cells can be targeted with this kind of combination treatment.

Does the interplay of RecQL helicases and PARP1 affect the aging process?

The limited data that is available studying the combined role of RecQLs (*i.e.*, WRN) and PARP1 during mammalian aging on an organismic level, suggests a close interplay between the two systems during the aging process. Thus, results from *Parp1*$^{-/-}$/*Wrn*$^{\Delta hel/\Delta hel}$ mice indicate features of premature aging compared to single mutant and WT mice, including development of cancer at a younger age. At present, the mechanistic basis for this phenotype has not been evaluated. Furthermore, it is also not clear, whether RecQL-PARP interactions play a mechanistic role in the phenotypes associated with RecQL-derived genetic diseases.

As we summarized here, both RecQL helicases and PARPs represent two central quality control systems of genome integrity. There is now a profound body of evidence indicating that they do this in a cooperative manner, which in the end ensures genome integrity and safeguards mammalian longevity. Although, at present, much of our knowledge about the RecQL-PARP interactions is still elementary, the intensive and dynamic crosstalk between the two systems stresses the importance of analyzing interactive networks on many levels in order to understand the big puzzle of aging biology.

Acknowledgments:

The authors thank Alexander Bürkle (University of Konstanz) for constant support and critical reading of the manuscript. Our experimental work is supported by the University of Konstanz (AFF and *Zukunftskolleg*) and the DFG through the Research Training Group (RTG) 1331, the Graduate School Chemical Biology (KoRSCB), and the Collaborative Research Center (CRC) 969.

Premature aging syndromes

Most proteins covered in this thesis are associated with certain genetic diseases and almost all of them are to a certain degree accompanied by an accelerated aging phenotype. However, they display only some aging features at a younger age and hence they are called segmental progerias. The exception here are RECQL1 and RECQL5, which, so far, have no known disease associated (Croteau et al., 2014). This can have three possible reasons: *i*) the phenotype is extremely severe and thus embryonically lethal or *ii*) the loss of RECQL1/5 has no phenotype and has therefore not been recorded yet, and/or *iii*) the phenotype is rescued by backup functions of the other RecQL helicases. PARP1 also has no disease associated with it, however, a polymorphism in PARP1 can lead to reduced PARP1 function and higher cancer incidence as will be discussed below.

Werner Syndrome (WS)

The Werner syndrome, an autosomal recessive disorder, was first described by Dr. Otto Werner in 1904 in Kiel as part of his doctoral thesis (Werner, 1904). The underlying reason though, mutations in the *WRN* gene, was not discovered until 1996 (Yu et al., 1996). Since 1904, approximately 1500 cases world-wide have been described, with ~75% of them recorded in Japan, thus being an extremely rare disease (Goto et al., 2013). The reason for the high incidence of WS in Japan is the much higher percentage of heterozygosity in the general population (1:100) (Goto et al., 1981; Satoh et al., 1999). Also, most Japanese WS patients have the same mutation in the *WRN* gene (mutation type 4), indicating a founder effect (Goto et al., 2013).

Persons suffering from WS are usually displaying the following four cardinal symptoms: premature hair graying/thinning, bilateral cataracts, characteristic dermatological pathology and short stature. Furthermore, most patients display a bird-like appearance and thin limbs and suffer from osteoporosis, atherosclerosis, hypogonadism, Type II diabetes mellitus, soft tissue calcifications and neoplasms (Friedrich et al., 2010; Huang et al., 2006; Muftuoglu et al., 2008b). Recently, also neuropathological effects have been described in some of the WS patients (Goto et al., 2013). Due to these symptoms and their earlier onset compared to the general population WS has been classified as an premature aging syndrome or segmental progeroid syndrome (Figure 11 A&B) (Epstein et al., 1966; Goto, 1997). These characteristics render it an ideal model system to study the aging process (Goto, 1997).

The onset is usually around the age of 30 while the median age of death shifted from 38.2 years in 1966 to 52.8 and 55 years in 2004 and 2008, respectively. The onset of malignancy also shifted from 38.8 to 48.8 years in the same time, with cancer and heart disease being the most prevalent causes of death (Goto and Matsuura, 2008). This shift in median life span corresponds well with the increased life span of the general population in the same time and is a hint that other factors besides genetic factors influence the life span of WS patients, namely environmental factors as well as better medical accommodation. Interestingly, heterozygote carriers of *WRN* mutations, related to WS patients, have been reported to become rather old (90+ years). This might be related to WRN's reported role in modulating ROS levels by repressing HIF-1 (hypoxia inducible factor 1). The 50% decrease in WRN levels might have beneficial effects on mitochondrial ROS and therefore promote longevity (Goto et al., 2013; Labbé et al., 2012). However, so far this is mostly speculation and warrants further investigations.

Besides the classical WS described above there is also an atypical WS. The underlying cause for this are mutations in the *lamin A/C* gene (*LMNA*). The patients display the same clinical features as WS patients while possessing a WT *WRN* gene (Cheng et al., 2003; Doh et al., 2009; Huang et al., 2005). Interestingly, defects in *LMNA* are also the cause for another disease, Hutchinson-Gilford progeria syndrome (HGPS) or childhood progeria, underlining the importance of the lamin A/C (De Sandre-Giovannoli et al., 2003; Eriksson et al., 2003). Similar to WS, patients age faster than usual. In contrast to WRN however, patients with HGPS display these symptoms almost from birth on and die at very young age, with a median life expectancy of ~13 years (Merideth et al., 2008).

Bloom Syndrome (BS)

Like WS, Bloom Syndrome is an autosomal recessive genetic disorder and it has been first described by Dr. David Bloom in 1954 (Arora et al., 2014; Bloom, 1954). It is most prevalent in the Ashkenazi Jewish population where a founder mutation has been identified (Ellis et al., 1998). The underlying cause for BS are mutations in the *BLM* gene, coding for the RecQL helicase BLM (RECQL3) (Ellis et al., 1995).

Similar to WS patients BS patients die at an early age but they don't display an obvious premature aging phenotype. They also have bird-like features, short stature or dwarfism, hypogonadism and Type II diabetes mellitus. However, they are 150-300 times more prone to certain malignancies than the general population, which is also their leading cause of death

(Arora et al., 2014). On a molecular level, BS is characterized by a 10-fold increase in sister-chromatid exchanges (SCE) (Chaganti et al., 1974).

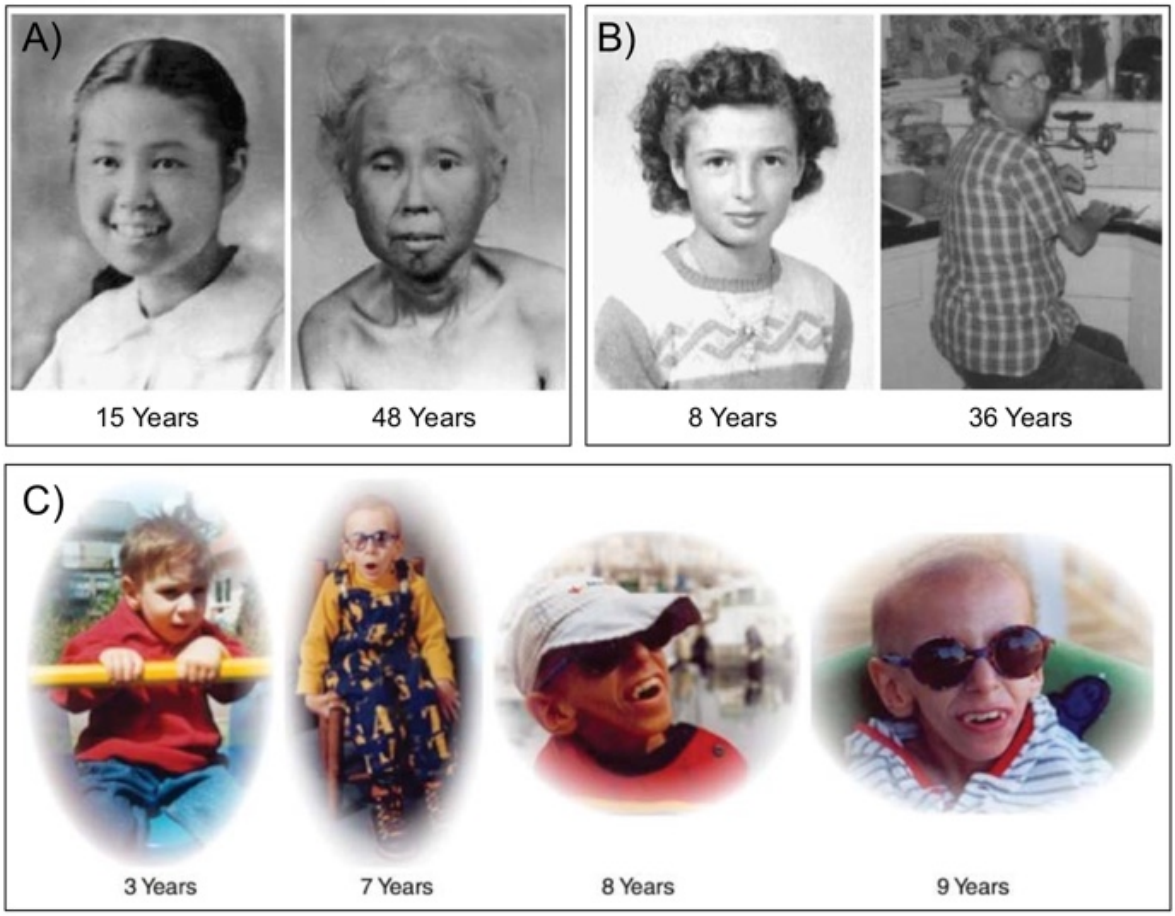

Figure 11: Patients suffering from WS and CS at different ages.
A. Female WS patient of Japanese-American heritage at ages 15 and 48. **B.** Female WS patient at ages 8 and 36. **C.** Male CS patient with a severe form of CS. The patient died at the age of 10. Pictures taken from (Muftuoglu et al., 2008a; Vermeulen and Fousteri, 2013).

RecQL4-related diseases

The *RecQL4* gene was identified in 1998 by Kitao and colleagues and mutations therein were found to be responsible for the Rothmund-Thomson Syndrome (RTS) (Kitao et al., 1999; 1998). This gene codes for the RECQL4 helicase and mutations therein cause two other diseases besides RTS, which will be covered in the following section (Hanada and Hickson, 2007).

Rothmund-Thomson Syndrome (RTS)

RTS is, like WS and BS, an autosomal recessive disorder, which is characterized by similar aging features as WS: premature hair graying and loss, cataracts and the small stature. Furthermore, the patients have skeletal and dental abnormalities, poikiloderma and a predisposition for cancer (Hanada and Hickson, 2007).

RAPADILINO

RAPADILINO is also an autosomal recessive disorder caused by mutations in *RecQL4* and its name is an acronym for its most prevalent clinical features: RAdial hypoplasia or aplasia (RA), PAtellar hypoplasia or aplasia and cleft or high arched PAlate (PA), DIarrhoea and DIslocated joints (DI), LIttle size and LImb malformation (LI), and NOse slender and NOrmal intelligence (NO) (Kääriäinen et al., 1989). In contrast to RTS, patients have no higher incidence for malignancies. RAPADILINO is most prevalent in Finland but cases elsewhere have also been reported. However, it is an extremely rare disease with only about two dozen reported cases (Siitonen et al., 2003).

Baller-Gerold Syndrome (BGS)

BGS is named after the two German physicians F. Baller and M. Gerold who first described this syndrome (Gerold, 1959). Its symptoms include short stature, craniosynostosis, radial ray hypoplasia and skeletal dysplasia (dwarfism) (Hanada and Hickson, 2007). The noticeable overlap in clinical features between BGS, RTS and RAPADILINO led to the finding that mutations in *RecQL4* also cause BGS (Van Maldergem et al., 2006).

Cockayne Syndrome (CS)

Cockayne Syndrome is a rare autosomal recessive disease caused by mutations in the genes of either CSA (20% of the cases) or CSB (80%) and has been first described by Dr. Edward Cockayne with the symptoms dwarfism, retinal atrophy and deafness (Cockayne, 1936). A follow-up examination of the two siblings ten years later added cataracts, mental retardation and an unusual facies and body habitus to the hallmarks of CS (Cockayne, 1946). CS can be divided into four groups of severity: juvenile CS, which can be mild, moderate or severe with

a median life expectancy of 5, 16 and 30.9 years, respectively (Figure 11 C). Additionally, there is a mild form of adult CS, which is characterized by sensitivity to UV exposure during youth and young adulthood and a late onset of the more severe hallmarks (> 45 years) (Natale, 2011).

Recently, CS has been categorized as a mitochondrial disease, which is supported by the finding that it shares most of its symptoms with other mitochondrial diseases. Furthermore, CSB-negative cells were found to be impaired in mitophagy (Scheibye-Knudsen et al., 2013a; 2013b).

Cockayne syndrome complementation group B protein (CSB)

ERCC6, the gene coding for the Cockayne syndrome complementation group B protein (CSB or ERCC6) has been identified 1992 by Troelstra and colleagues (Troelstra et al., 1992). It encodes for a 1493 aa and 168 kDa protein belonging to the SWI2/SNF helicase superfamily. CSB comprises ATPase and ss-annealing activity but no helicase activity (Muftuoglu et al., 2006; Selby and Sancar, 1997). While the ss-annealing activity is ATP independent and can anneal RNA and DNA double-strands as well as RNA/DNA heteroduplexes, CSB's ATPase activity seems to be important for chromatin remodeling and may be involved in the backtracking function of RNA polymerase (Beerens et al., 2005; Citterio et al., 2000). CSB is the first protein to be recruited to the stalled RNA polymerase in TC-NER, which then leads to the recruitment of the CSA-containing E3 ubiquitin ligase complex, as well as the NER core proteins (see chapter NER) (Fousteri et al., 2006; Groisman et al., 2003). The ubiquitination of CSB seems to be important to release CSB from the damage site and allow continuation of repair (Groisman et al., 2003). CSB is localized in the nucleus and the nucleoli, as well as the mitochondria where it participates in mitochondrial BER (Aamann et al., 2010; Thorslund et al., 2005). It interacts with several proteins in DNA repair, most prominently other NER factors such as CSA (ERCC8), XPA, XPB, XPD, XPF and XPG (Anindya et al., 2010; Fousteri et al., 2006; Selby and Sancar, 1997). Furthermore, it seems to play a role in BER, since it interacts with important BER factors like NEIL1, NEIL2, APE1 and PARP1 (Aamann et al., 2014; Muftuoglu et al., 2009; Thorslund et al., 2005; Wong et al., 2007). It has been demonstrated that CSB interacts physically with PARP1 and that it may be covalently modified by PARP1. However, to date there is no conclusive explanation for this interaction and its implication for BER or for CSB's role in BER in general (Stevnsner et al.,

2008; Thorslund et al., 2005). In addition, more recently CSB has also been implicated in the regulation of DSBR (Batenburg et al., 2015; Sakai et al., 2012).

PARP1 polymorphisms

To date, there is no monogenic disease known to be linked to mutations/deletions of *PARP1*, potentially because such a mutation would be embryonically lethal, as it has been shown for a *PARP1* knock-out in *Drosophila* and a *PARP1/2* double KO in mice (both embryonically lethal) (Ménissier-de Murcia et al., 2003; Miwa et al., 1999). However, there is evidence that at least one *PARP1* polymorphism is linked to increased cancer risk, the Val762Ala polymorphism (Hua et al., 2014; Lockett et al., 2004; Qin et al., 2014). The effects, however, seem to be highly specific regarding the types of cancer affected and the ethnic background of the patients, *i.e.* middle eastern and Asian populations seem to be more prone to this effect (Alshammari et al., 2014; Hua et al., 2014; Qin et al., 2014; Wang et al., 2014). The relevance of the Val762Ala polymorphism is in concordance with *in vitro* data, showing that PARP1 V762A has less catalytic activity than WT PARP1 (Beneke et al., 2010).

Objective

Both RecQL helicases and PARylation, *i.e*. PARPs and their product PAR, play crucial roles in DNA metabolism, especially in the response to DNA damage and genotoxic stress. Hence, they were aptly nicknamed guardians of the genome (Bohr, 2008; Croteau et al., 2014; Jeggo, 1998; Mangerich and Bürkle, 2012). Knowledge about the interplay between PARylation and RecQL helicases has been scarce for a long time, but in the last decade significant work has been done to shed more light on this interaction (as discussed in Chapter I). As a result of these efforts, it is now known that several RecQL helicases interact directly with PARP1, some are covalently modified with PAR and some interact non-covalently with PAR (Veith and Mangerich, 2014). Unfortunately, most knowledge that has been gained so far about PAR(P)-RecQL interaction is on a biochemical level and the relevance of these interactions for cellular processes is still largely unclear. It is known though, that WS cells are impaired in PARylation, indicating a reciprocal regulation of WRN and PARP1 (Kobbe et al., 2003a). Additionally, studies on $WRN^{\Delta hel/\Delta hel}/PARP1^{-/-}$ mice revealed that they are suffering from enhanced oxidative damage, develop more neoplasms and display a shorter life span compared to single KO or WT mice. Strikingly, this decrease in life span has never been investigated in detail (Lebel et al., 2003).

This thesis aimed to investigate the interplay between RecQL helicases and PARylation in more detail, with a special focus on the RecQL helicases WRN and RECQL5. We wanted to further characterize the biochemical interaction between PARP1 and WRN, but also the newly identified non-covalent interaction of PAR and the RecQL helicases (Berti et al., 2013; Khadka et al., 2015; Popp et al., 2012; Veith and Mangerich, 2014) (Chapters I, III, IV and V). Moreover, we wanted to investigate which cellular processes are affected by these interactions. Specifically, we wanted to know what effect the PAR(P)-WRN interaction has on the different DNA repair pathways in which they both are involved. The same question was asked for the interaction of PAR(P) and RECQL5, a RecQL member that, until recently, has largely been neglected by the research community.

Another question of importance that we aimed to answer, and which is tightly linked to the first part, is how PARylation and the interaction with PARP1 regulate the spatio-temporal distribution and activation of RecQL helicases in the nucleus. Both WRN and PARP1 are localized partly in the nucleolus and in both cases it is unknown why they are localized there (Gray et al., 1997; Kanagaraj et al., 2012; Lan et al., 2005; Meder et al., 2005). However, both translocate from the nucleoli into the nucleoplasm as a response to genotoxic stress. We

wanted to investigate whether this translocation of WRN out of the nucleoli and the recruitment and retention at sites of DNA damage is dependent on PARP and/or PAR. Moreover, we were interested in the process of PARP1 translocation out of the nucleoli, since this process has never been described in detail.

A discovery that received scant attention so far is the finding that PARP1 can interact non-covalently with its product PAR, too (Huambachano et al., 2011). The authors describe a non-covalent PAR-binding to ZnII, ZnIII, the WGR domain and the DsDB domain, however only the interaction with ZnII seems to have a relevant function. Although the authors suggest a hypothetical model in which the PAR polymers bind to the DNA interaction sites of PARP1 and thus displace it from the DNA, they did not further elaborate their findings. Also, so far, no follow-up study on this report appeared. We therefore aimed to map this non-covalent interaction in more detail and could verify it independently. Consequently, this finding was further investigated with regards to its consequences on a biochemical and a cellular level. Additionally, we wanted to analyze a novel, cancer-associated PARP1 mutation, identified by cooperation partners in Leiden, Netherlands. To achieve these goals we established a novel *PARP1* KO cell line with the genetic background of the excellently characterized HeLa Kyoto cells.

Regulation of RecQL helicases by PARylation

Chapter II: Quantitative analysis of WRN exonuclease activity by isotope dilution mass spectrometry

Aswin Mangerich, Sebastian Veith*, Oliver Popp, Jörg Fahrer,*
Rita Martello, Vilhelm A. Bohr, and Alexander Bürkle

Mechanisms of Aging and Development, 2012 Aug; 133(8): 575-9

* Equal contribution

Abstract

Werner syndrome is a disorder characterized by a premature aging phenotype. The disease is caused by mutations in the *WRN* gene, which encodes a DNA helicase/exonuclease, which is involved in multiple aspects of DNA metabolism. Current methods mostly rely on radiometric techniques to assess WRN exonuclease activity. Here we present an alternative, quantitative approach based on non-radioactive isotope dilution mass spectrometry (LC-MS/MS). An oligoduplex substrate mimicking the telomeric sequence was used for method development. Released nucleotides, which correlate with the degree of oligoduplex degradation, were dephosphorylated, purified, and quantified by LC-MS/MS. Heavy-isotope-labeled internal standards were used to account for technical variability. The method was validated in terms of reproducibility, time-course and concentration-dependency of the reaction. As shown in this study, the LC-MS/MS method can assess exonuclease activity of WRN mutants, WRN's substrate and strand specificity, and modulatory effects of WRN interaction partners and posttranslational modifications. Moreover, it can be used to analyze the selectivity and processivity of WRN exonuclease and allows the screening of small molecules for WRN exonuclease inhibitors. Importantly, this approach can easily be adapted to study nucleases other than WRN. This is of general interest, because exonucleases are key players in DNA metabolism and aging mechanisms.

Introduction

Werner syndrome (WS) is a rare autosomal recessive disorder characterized by a segmental premature aging phenotype, including early onset of atherosclerosis, osteoporosis, and a high cancer incidence. The disease is caused by loss-of-function mutations in the *WRN* gene, which encodes the WRN protein, a member of the RecQL helicase family. On the cellular level, fibroblasts derived from WS patients display genomic instability and a reduced replicative life span (Kudlow et al., 2007). This phenotype is in accordance with experimental data demonstrating that WRN is involved in multiple aspects of DNA metabolism, such as DNA replication, genomic maintenance, and telomere regulation (Bohr, 2008; Reddy et al., 2010; Rossi et al., 2010a). In contrast to the other five members of the human RecQL helicase family, WRN also possesses a unique 3' to 5' exonuclease activity (Huang et al., 1998).

The WRN exonuclease cleaves the DNA phosphodiester bond and releases free 5'-dNMPs from the DNA strand (Kamath-Loeb et al., 1998). To elicit its exonuclease activity, WRN

requires a 3'-recessed end (5'-overhang) substrate. WRN does not degrade duplex DNA with blunt ends, unless the substrate also contains a junction or alternate DNA structures such as a fork (Brosh et al., 2006; Shen and Loeb, 2000). It is largely inactive on short single-stranded DNA substrates (Kamath-Loeb et al., 1998), but longer ssDNA substrates are efficiently degraded (Machwe et al., 2006). Its activity is regulated by posttranslational modifications and protein interactions. For instance, phosphorylation of WRN by DNA-PK inhibits its exonuclease activity (Karmakar et al., 2002; Yannone et al., 2001). In addition, p53, BLM, and PARP1 cause inhibitory effects (Brosh et al., 2001a; Kobbe et al., 2002; 2004a; Sommers et al., 2005), whereas the Ku70/80 complex stimulates exonuclease activity (Cooper et al., 2000; Kudlow et al., 2007; Li and Comai, 2000; 2001).

Standard methods to assess WRN's exonuclease activity utilize radioactively or fluorescently 5' end-labeled DNA substrates to detect the degradation of the full-length DNA molecules (Boubriak et al., 2009; Brosh et al., 2006). Here we present an alternative approach to assess WRN exonuclease activity based on isotope dilution mass spectrometry (LC-MS/MS). This method may be particularly useful in two situations: Firstly, for laboratories that wish to replace the common radioactive assays with a non-radioactive one and, secondly, the method can be incorporated into high throughput screening approaches for small molecules that affect exonuclease activity.

Results

We have validated our newly developed method and compared it to a modified version of an established protocol that uses a 5'-biotin-end-labelled DNA substrate to detect activity of recombinant WRN exonuclease (Brosh et al., 2006) (Suppl. Figure 1). Importantly, using a telomeric substrate mimics one of the key functions of WRN, which is to operate at the telomeres (Bohr, 2008). To assess if this oligoduplex indeed serves as a suitable substrate for WRN in our hands, an exonuclease reaction was carried out as published previously (Brosh et al., 2006). The reaction mixture contained 75 fmol of the oligoduplex and 0.1-1 pmol of recombinant WRN. Subsequently, digestion products were resolved by denaturing polyacrylamide gel electrophoresis (PAGE) and biotin was detected by streptavidin-POD (Suppl. Figure 2). In this method, loss of signal intensity of the full-length end-labeled DNA substrate was used as readout to assess exonuclease activity. As is evident from Suppl. Figure 2, WRN efficiently catalyzes the degradation of this oligoduplex to truncated DNA molecules of various lengths in a concentration-dependent manner. Initial degradation of the substrate is

visible at an enzyme to substrate ratio (E/S) of ~1 (10 nM WRN) and reached saturation at an E/S of ~8 (60 nM WRN) with a maximum efficiency of ~80%.

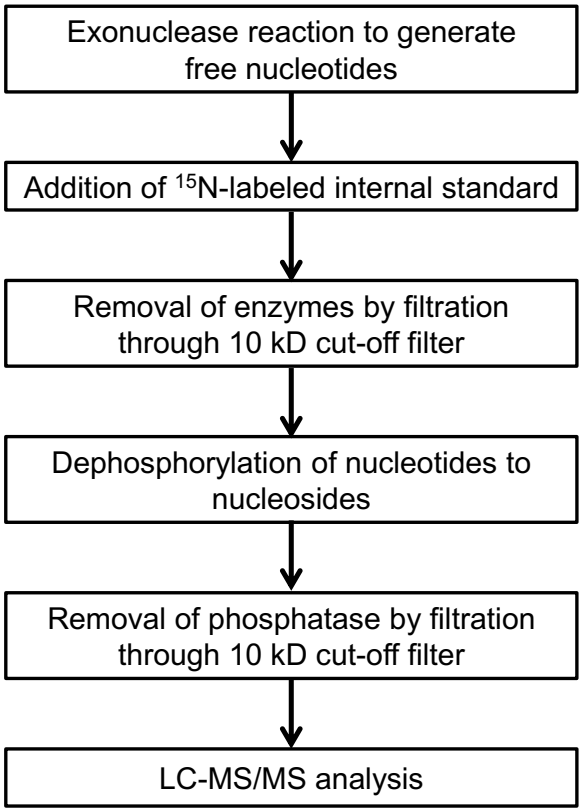

Figure 12: Flow chart for the LC-MS/MS quantification of WRN exonuclease activity.

Instead of detecting the shortened DNA substrate, the rationale of the LC-MS/MS-based method is to detect degradation end products, *i.e.,* free nucleosides, to assess WRN exonuclease activity. To allow comparability to the biotin-end-labeling technique, the same substrate and identical reaction conditions were chosen to develop the LC-MS/MS-based method. Since the oligoduplex contains a repetitive telomeric sequence $(TTAGGG)_4$, LC-MS/MS quantification of free 2'-deoxyguanosine (dG) was expected to be a suitable readout to assess WRN exonuclease activity. Figure 12 shows a flow chart of the experimental procedure; a detailed protocol is available in the supplementary information section. Briefly, after the exonuclease reaction was carried out, samples were placed on ice and ^{15}N-labeled dG was added as an internal standard to the reaction mixture to account for technical variability during sample work-up and mass spectrometric measurement. Thereafter, recombinant WRN was removed by spin column filtration, followed by dephosphorylation of the nucleotides to nucleosides using alkaline phosphatase (AP), removal of the phosphatase by spin column filtration, and subsequent LC-MS/MS analysis. The recovery rate of the internal standard was

usually ~70%. Typical LC-MS/MS chromatograms of unlabeled and ^{15}N-labeled dG as well as a calibration curve are shown in Suppl. Figure 3.

The method shows adequate assay-to-assay variability (Suppl. Figure 4 A) and can be performed in 1-2 days, depending on the time chosen for AP digestion (Suppl. Figure 4 B; *N.B.:* no significant differences in the quantities of dG were observed between 4-h and overnight AP digestion, indicating that an AP digestion time of 4 h is sufficient for complete dephosphorylation of dGMP).

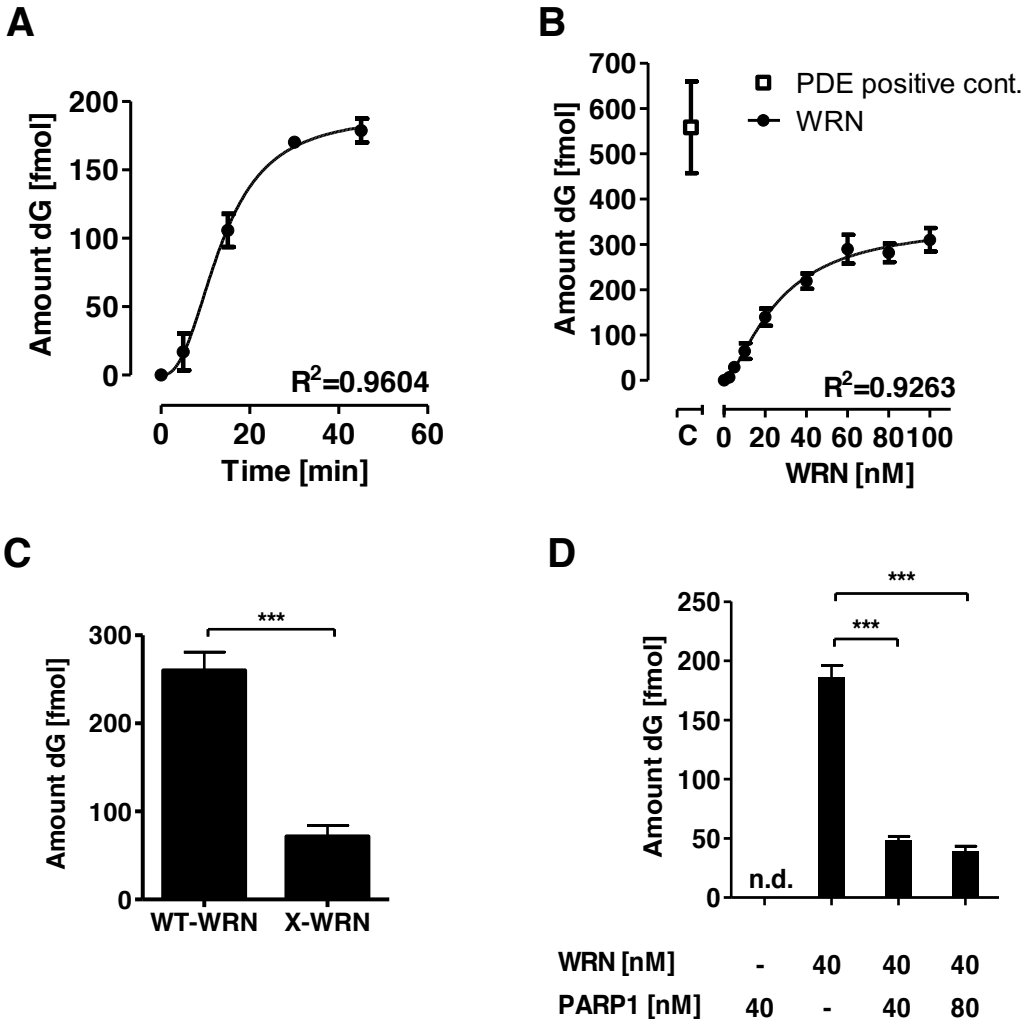

Figure 13: Analysis of WRN exonuclease activity by isotope dilution mass spectrometry.
WRN degrades an oligoduplex substrate mimicking the telomeric repeat sequence $(TTAGGG)_4$ to mononucleotides. Due to the repetitive sequence of the oligoduplex the amount of free 2'-deoxyguanosine (dG) correlates with the extent of oligoduplex degradation. Prior to LC-MS/MS analysis, nucleotides were dephosphorylated using alkaline phosphatase. Samples were subjected to LC-MS/MS analysis monitoring the transition m/z 268→152 (dG) in the multiple reaction monitoring (MRM) mode. ^{15}N-labeled dG was added as an internal standard directly after the reaction to account for technical variability during sample work-up and LC-MS/MS analysis; the ion transition m/z 273→157 was monitored in MRM mode. **A.** Time course analysis of WRN exonuclease activity using 40 nM WRN shows that the reaction reached a plateau after 30 min. **B.** WRN degrades the oligoduplex in a concentration dependent manner. After incubation with 60 to 100 nM WRN for 45 min, the reaction reached a plateau. Incubation of the oligoduplex with snake venom phosphodiesterase (PDE) served as a positive control. **C.** A mutation in the WRN exonuclease domain (WRN-E84A, X-WRN) led to a strongly diminished exonuclease activity (40 nM of WT-WRN and X-WRN, respectively; reactions were run for 45 min). **D.** Recombinant PARP1 inhibits WRN exonuclease activity. Concentrations of WRN and PARP1 were used as indicated; reactions were run for 45 min. Oligoduplex substrate was used in a concentration of 75 fmol (A, B, D) or 100 fmol (C) per reaction. Statistical analysis was performed using one-way ANOVA following Bonferroni's multiple comparison test. *** $p < 0.0001$. Data represent means ± SEM ($N \geq 3$); R represents the non-linear regression coefficient. n.d., not detectable.

As shown in Figure 13, free dG was detected in a time and concentration dependent manner. Since the reaction is still in its dynamic range after 15 min in terms of release of free dGMP (Figure 13 A), a reaction time of 45 min was chosen for the following experiments to achieve maximum oligoduplex degradation. In agreement with results obtained from biotin-end-labeling technique, WRN activity was already detected at an E/S of ~1 (5-10 nM WRN) and reached saturation at an E/S of ~8 (60 nM WRN) (Figure 13 B). A maximum of 32% of the expected total amount of dG was detected in WRN-digested samples. The lower efficiency of WRN compared to phosphodiesterase (PDE) may be related to incomplete annealing of the DNA strands and therefore to incomplete digestion by WRN. A WRN mutant with a mutation in the exonuclease domain (WRN-E84A or X-WRN) (Huang et al., 1998; Machwe et al., 2000) showed strongly diminished exonuclease activity compared to WT-WRN (Figure 13 C). The residual exonuclease activity observed in the X-WRN sample may be related to the sensitivity of the LC-MS/MS method, to some contamination with Zn^{2+} ions, which can trigger minimal exonuclease activity of X-WRN (Choudhary et al., 2004), or to contamination of the X-WRN protein with an unknown nuclease.

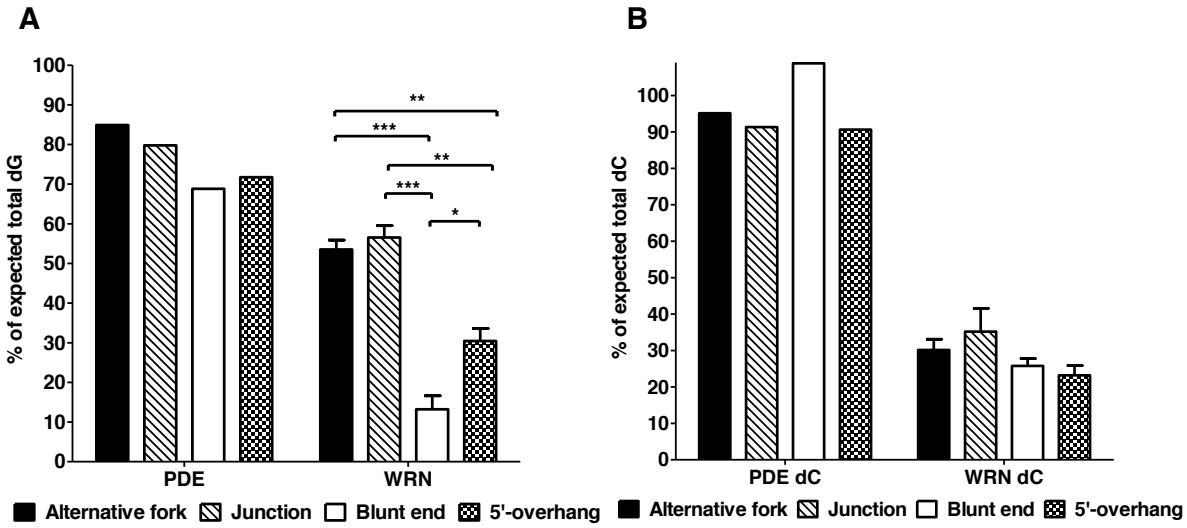

Figure 14: Analysis of WRN substrate and strand specificity.
WRN substrate specificity was tested with several oligoduplex substrates containing the repetitive sequence element $(XXXGGG)_6$ (X=A,T). Reaction mixtures contained 100 fmol of each oligoduplex, *i.e.*, an optimized fork ("alternative fork"), a 4-way junction containing oligoduplex, a blunt ended oligoduplex, and an oligoduplex with a 5' overhang (for sequence information see SI section). ^{15}N-dG and ^{15}N/^{13}C-dC were added as internal standards directly after the reaction to account for technical variability during sample work-up and LC-MS/MS analysis. Samples were analyzed in multiple reaction-monitoring (MRM) mode with the following transitions: ^{14}N-dG (m/z 268→152), ^{15}N-dG (m/z 273→157), ^{14}N/^{12}C-dC (m/z 228→112) and ^{15}N/^{13}C-dC (m/z 240→119). PDE digestion served as a positive control and led to the release of 70-100% of the expected total amount of dG **(A)** and dC **(B)** of each oligonucleotide. WRN exonuclease reaction was performed in the presence of 40 nM WRN for 45 min. **A.** Evaluation of the release of free dG of substrates as indicated. Whereas the blunt-ended oligoduplex served as a poor substrate for WRN exonuclease, the 5'-overhang led to the release of 30% of total dG, and the forked and 4-way-junction-containing substrates served as efficient substrates (> 50% release of expected total dG). **B.** WRN activity on the dG-complementary strand of the different substrates was tested by detecting the release of free dC. In contrast to the WRN-dependent degradation of the dG-strands, as expected the dC-strands served as poor substrates for WRN exonuclease showing a release of < 35% of the expected total amount of dC. WRN data represent mean ± SEM (*N* = 3). PDE data represent means from two independent experiments. WRN data was evaluated by Student's t-test for statistical significant differences. * $p < 0.05$, ** $p < 0.01$, *** $p < 0.001$.

Conceivable applications of the LC-MS/MS-based method include studying effects of factors that modulate WRN exonuclease activity, such as posttranslational modifications and protein interaction partners. For example, PARP1, which catalyzes the synthesis of the biopolymer poly(ADP-ribose) upon genotoxic stress, is an established interaction partner of WRN (Rossi et al., 2010a; Rouleau et al., 2010). Previously, it was shown that PARP1 inhibits both WRN's helicase and exonuclease activities (Kobbe et al., 2004a). In agreement with these results, PARP1 led to an inhibition of WRN exonuclease activity by up to 80% as detected by LC-MS/MS analysis (Figure 13 D).

Furthermore, the method can be applied to study WRN's substrate and strand specificity. To this end, we tested several newly designed WRN oligoduplex substrates, which are compatible with our assay, *i.e.* an optimized forked oligoduplex, a blunt-ended oligoduplex, and oligoduplexes containing a 4-way junction and a 5'-overhang (Suppl. Table 1 for full sequence details). All substrates comprised a strand that contains only dG within a repetitive sequence element $(XXXGGG)_6$ (X=A,T in alternating sequence to assure annealing specificity) and a complementary strand that only contains dC. Except for the blunt-ended substrate, the dG-strand was expected to be accessible for WRN exonuclease activity. In agreement with previous reports (Brosh et al., 2006; Kamath-Loeb et al., 1998), oligoduplexes containing the fork and 4-way junction served as efficient substrates for WRN exonuclease, whereas the blunt ended oligoduplex showed almost no release of free dG (Figure 14 A).

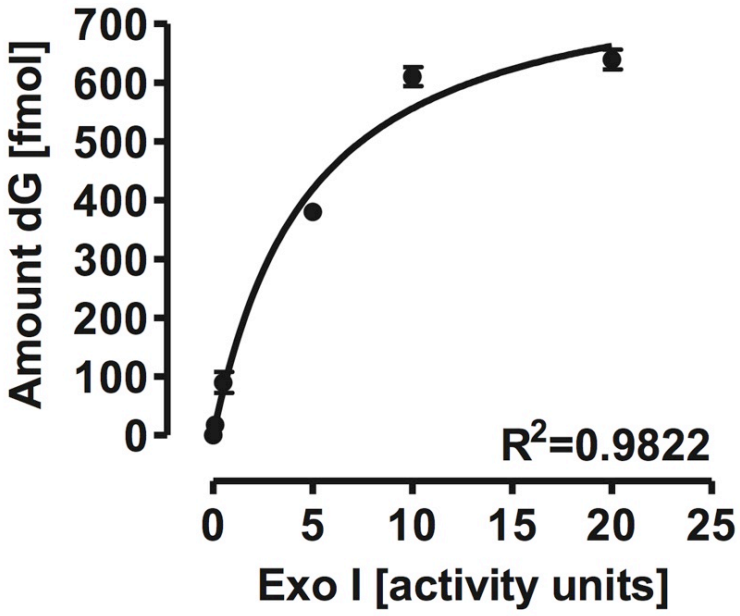

Figure 15: Analysis of Exo I activity.
LC-MS/MS quantification of Exo I activity. *E. coli* Exo I degrades a single-stranded oligonucleotide substrate (75 fmol), containing a repetitive element $(TTAGGG)_4$, to mononucleotides in a concentration dependent manner. Data are means ± SEM ($N = 3$). R represents the non-linear regression coefficient.

Moreover, significant WRN exonuclease activity was detected with the 5'overhang substrate, however to a lesser extent than with the fork and 4-way junction oligoduplexes. As expected, WRN wasn't able to degrade the complementary strand as efficiently as evaluated by analyzing the release of free dC (Figure 14 B). In summary, the method described herein opens up new possibilities to study substrate and strand specificity of WRN in particular and exonucleases in general.

Discussion

In conclusion, we have developed a novel, non-radioactive LC-MS/MS-based quantitative method to assess WRN's exonuclease function and activity with high sensitivity, accuracy, and precision. As mass spectrometry is a common tool in molecular bioscience, this method represents a reliable and easy-to-use alternative to existing techniques with 5' end-labeled oligonucleotides. Our method is comparable to existing radiometric techniques in terms of workload and economic aspects, but can be performed in higher throughput and enables mass spectrometric structural characterization and full quantification of the exonuclease digestion products. For this reasons this new method should be instrumental for several applications. As demonstrated in this study, the LC-MS/MS method can be used to study exonuclease activity of WRN mutants (Figure 13 C), modulatory effects of WRN interaction partners and posttranslational modifications on its exonuclease activity (Figure 13 D), and WRN's substrate and strand specificity (Figure 14). Moreover, the LC-MS/MS method can be employed to analyze the selectivity and processivity of WRN exonuclease with high specificity. For example, as shown by classical radiometric techniques, WRN exonuclease is selectively blocked by specific base modifications such as 8-oxo-guanine, 8-oxo-adenine, and cholesterol adducts, but is active on other lesions such as uracil or hypoxanthine (Bukowy et al., 2008; Machwe et al., 2000). Since released base adducts can be unequivocally identified, characterized, and quantified by mass spectrometry, the current method represents a promising approach to extend such studies. In addition, this method allows the screening of small molecule libraries for potential WRN exonuclease inhibitors. In analogy to a recently identified WRN helicase inhibitor (Aggarwal et al., 2011), such potentially existing exonuclease inhibitors could be useful tools to study the function of WRN in a cellular context and may also have therapeutic potential in cancer treatment. We are currently planning such screening approaches for finding inhibitors or stimulators of the WRN exonuclease activity at nanomolar levels. Finally, the LC-MS/MS-based method can be

extended and adapted to study the activity, specificity, and processivity of nucleases other than WRN. Experiments with *E. coli* Exo I show the feasibility of such extended applications (Figure 15).

A limitation of the assay includes that access to an LC-ESI-MS/MS system is a prerequisite for its use. Moreover, it is limited to study exonuclease activity in non-cellular systems and so far it is not applicable to study the exonuclease directionality.

In summary, the LC-MS/MS-based exonuclease activity assay adds to the armamentarium of methods to study DNA metabolism in general and, as demonstrated in this study, in particular in the field of molecular aging research.

Acknowledgements

This work was supported by the *Deutsche Forschungsgemeinschaft* (Konstanz Research School Chemical Biology, KoRS-CB) and the University of Konstanz (*Ausschuss für Forschungsfragen*). OP and RM were supported by fellowships of the KoRS-CB. The work was partially supported by the intramural Program of the National Institute on Aging, National Institutes of Health. We would like to thank Peter C. Dedon, Erin G. Prestwich, and Koli Taghizadeh from the MIT Center for Environmental Health Sciences for sharing their expertise in quantitative mass spectrometry.

Experimental Procedures

Purification of recombinant proteins

WRN was expressed in *Sf*9 insect cells and purified as described previously (Orren et al., 1999). Briefly, 1×10^7 cells were lysed in 1 ml Ni-NTA lysis buffer (150 mM Tris-HCl, pH 8.0; 10 mM NaCl; 10% glycerol, 0.5% NP40; 1 mM PMSF; 5 mM β-mercaptoethanol). The suspension was rotated for 20 min, followed by centrifugation at 10,000 *g* for 30 min. The Ni resin suspension (Qiagen) was centrifuged twice at 500 *g* for 5 min; each time the supernatant was discarded and the resin was resuspended in 6 ml MilliQ water. Thereafter, the suspension was centrifuged again at 500 *g* for 5 minutes, the supernatant was discarded, and the resin mixed with the cell lysate. This suspension was rotated for 1 h and was then loaded onto a polyprep column (Bio-Rad). The flow-through was once again loaded on the column to ensure maximum protein binding. Then the column was washed with 15 ml wash buffer I (50

mM Tris-HCl, pH 8.0; 0.5 mM LiCl; 10% glycerol; 1 mM PMSF; 5 mM β-mercaptoethanol), 10 ml wash buffer II (10 mM PIPES, pH 7.0; 50 mM NaCl; 10% glycerol; 1 mM PMSF; 5 mM β-mercaptoethanol), 10 ml wash buffer III (wash buffer II supplemented with 10 mM imidazole), and 15 ml wash buffer IV (wash buffer II supplemented with 25 mM imidazole). Then the WRN protein was eluted three times with 1 ml elution buffer, (10 mM PIPES, pH 7.0; 50 mM NaCl; 20% glycerol; 1 mM PMSF; 5 mM β-mercaptoethanol; 300 mM imidazole). The eluates were immediately supplemented with 100 ng/µl BSA and stored at -80°C until further usage.

hPARP1 was expressed in *Sf*9 insect cells and purified as described previously (Beneke et al., 2000; 2010). Briefly, 0.3 g DNA-cellulose (Sigma-Aldrich) was suspended in 5 ml of 50 mM Tris-HCl (pH 8.0), 100 mM KCl, 0.5 mM EDTA, 5 mM $MgCl_2$, 5% (v/v) glycerol, 1 mM PMSF, and 12 mM β-mercaptoethanol (Buffer A) and filled into a polyprep column (BioRad). The fractions containing PARP1 were loaded onto the column. Following washing the column with two bed volumes of buffer A, one bed volume buffer A (100 mM KCl) and one bed volume buffer A (200 mM KCl), PARP1 was eluted in two steps with 2 ml buffer A (400 mM KCl) and 2 ml buffer A (1 M KCl).

Exonuclease reaction

WRN exonuclease digestion was performed as described previously, with modifications (Brosh et al., 2006). Substrates (Sigma-Aldrich) were annealed in TE buffer (pH 7.4) supplemented with 50 mM NaCl by incubation for 5 min at 95°C and subsequent cooling to room temperature (Suppl. Table 1). Exonuclease reactions were performed in a total volume of 10 µl in the presence of 40 mM Tris-HCl (pH 8.0), 4 mM $MgCl_2$, 0.1 mg/ml BSA, 4 mM DTT, oligoduplex, and recombinant WRN in concentrations as indicated. Recombinant PARP1 was added to the reaction mixture at concentrations as indicated. *E. coli* Exo I (Fermentas) activity was tested with a single-stranded oligonucleotide.

Detection of WRN exonuclease activity via biotin detection of the digested strand

Samples were incubated at 37°C for 15 min and reactions were stopped with 10 µl of 'stop dye' (97.5% formamide; 10 mM EDTA, pH 7.5; 0.04% of each bromphenol blue, xylene cyanol and OrangeG), heat denatured at 95°C for 10 min, loaded on a denaturing 14% PAGE, and blotted onto a nylon membrane (GE Healthcare). Biotinylated oligonucleotides were

detected after incubation with streptavidin-POD (GE Healthcare) via chemiluminescence reaction.

Preparation of samples for LC-MS/MS analysis

After incubating samples at 37°C for periods as indicated, samples were placed on ice and 90 µl of 30 mM Na-acetate (pH 7.8) and 2 pmol of ^{15}N-dG (and ^{15}N/^{13}C-dC in the case of substrates B-E) were added to the reaction mixture. To remove recombinant enzymes, samples were filtered through a 10 kD cut-off filter (Pall). Then the samples were incubated with 34 U alkaline phosphatase (Sigma) [and 0.2 U phosphodiesterase I (US Biological) in the case of PDE samples] at 37°C overnight. To remove enzymes, samples were filtered again through a 10 kD cut-off filter and subjected to LC-MS/MS analysis. 'No-enzyme' controls, containing oligonucleotides but no nuclease to be tested, were run in parallel with every experiment.

LC-MS/MS analysis

Analyses were performed using a Waters LC-MS/MS system consisting of an HPLC 2695 Separations Module and a Micromass Quattro Micro mass spectrometer equipped with an electrospray ionization source. Samples were resolved using a Hypersil Gold column (150 mm x 2.1 mm; 3 µm particle size; Thermo Fisher) under isocratic conditions with a solvent composition of 97% of 0.1% acetic acid in water (A) and 3% of 0.1% acetic acid in acetonitrile (B) at a flow rate of 0.2 ml/min and a column temperature of 25°C. The MS was operated in positive ion mode. Multiple reaction-monitoring (MRM) mode was used for data acquisition with settings as listed in Suppl. Table 1. Calibration curves of ^{15}N-labeled and unlabeled dG and ^{15}N/^{13}C-labeled and unlabeled dC were acquired concomitantly with each set of samples (Suppl. Table 2). Response ratios were obtained by plotting the MRM area ratios between the labeled and unlabeled analytes against their corresponding concentration ratios. Squares of Pearson's correlation coefficients (R^2) were consistently > 0.99. Quantification of dG and dC in each sample was achieved using the MRM signal ratio between the analyte and its labeled internal standard and the response curve. Amounts of dG and dC detected were corrected for background levels detected in 'no-enzyme' controls.

Statistical analysis

Graphpad Prism software was used for statistical analyses of data as indicated. A sigmoidal model was used for curve fitting when appropriate.

Supplementary Data

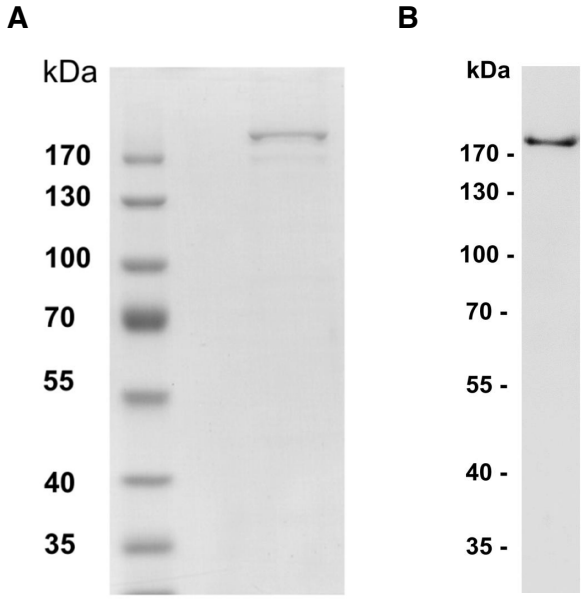

Supplementary Figure 1: Characterization of purified human His-tagged WRN.
A. Human His-tagged WRN was isolated from *Sf*9 insect cells after baculovirus infection and subjected to PAGE analysis. A prominent band was detected after Coomassie staining. **B.** Western blot analysis using a WRN-specific antibody confirmed the nature of the band as WRN.

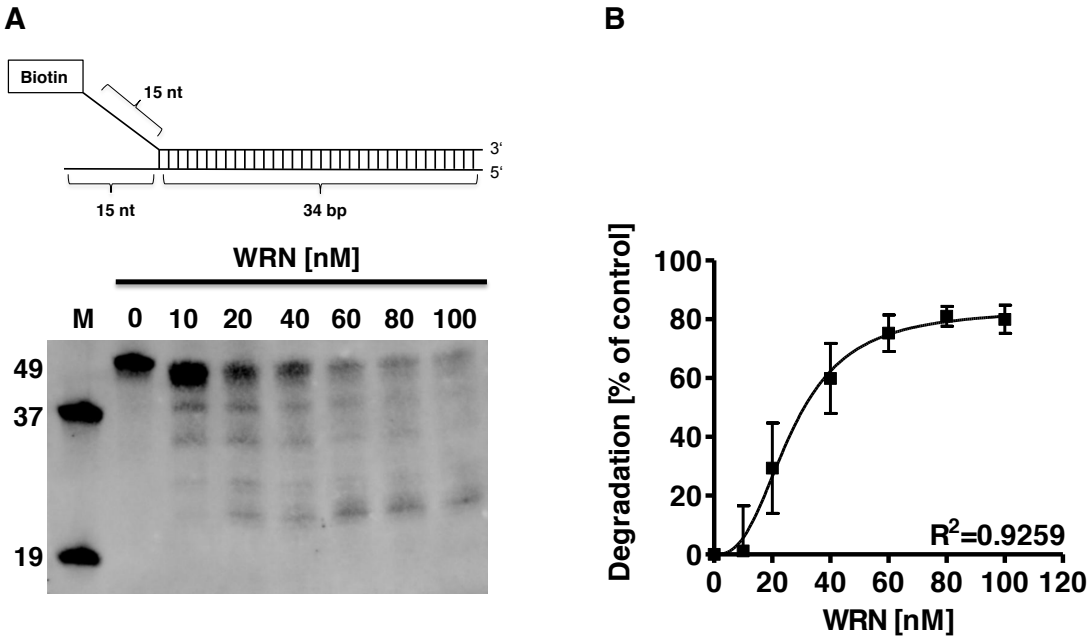

Supplementary Figure 2: Analyzing WRN exonuclease activity by detection of a biotin 5'-end-labeled oligonucleotide duplex via streptavidin-POD.
A. WRN degrades an oligoduplex substrate mimicking the telomeric repeat sequence in a concentration-dependent manner [sequence of the substrate is based on (Brosh et al., 2006)]. The reaction was incubated for 15 min. Samples were separated by PAGE under denaturing conditions and visualized after blotting by streptavidin-POD. **B.** Densitometric evaluation indicates that WRN degrades up to ~80% of the full-length oligoduplex to smaller degradation products. Data are means ± SEM (N = 3). R represents the non-linear regression coefficient.

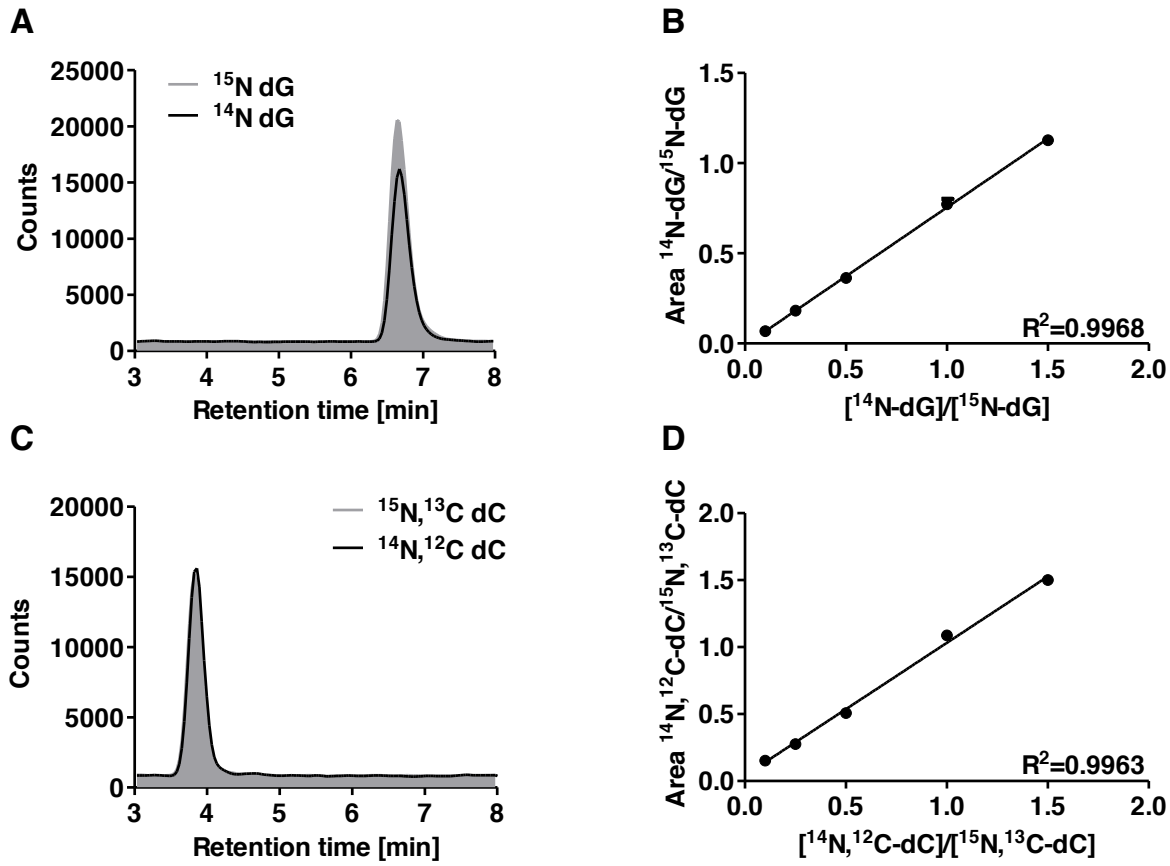

Supplementary Figure 3: LC-MS/MS quantification of WRN exonuclease activity.
A. LC-MS/MS chromatogram showing the quantitative detection of ^{15}N-labeled (grey shaded curve) and unlabeled (black line) dG (100 nM each). Samples were analyzed in multiple reaction-monitoring (MRM) mode with the following transitions: ^{14}N-dG (m/z 268→152) and ^{15}N-dG (m/z 273→157). **B.** Calibration curve for isotope dilution LC-MS/MS of dG. **C.** LC-MS/MS chromatogram showing the quantitative detection of ^{15}N/^{13}C-labeled (grey shaded) and unlabeled (black line) dC (100 nM each). Samples were analyzed in MRM mode with the following transitions: ^{14}N/^{12}C-dC (m/z 228→112) and ^{15}N/^{13}C-dC (m/z 240→119). **D.** Calibration curve for isotope dilution LC-MS/MS of dC. R represents the linear regression coefficient.

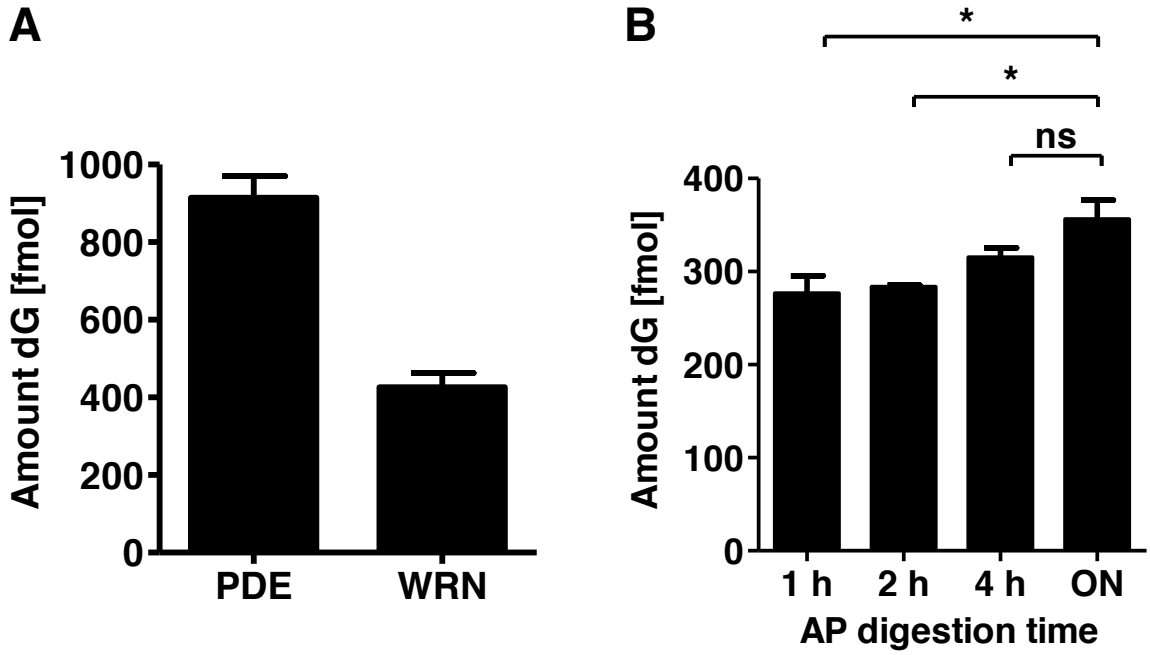

Supplementary Figure 4: Method validation.
A. forked oligoduplex substrate (100 fmol), containing a repetitive element, *i.e.* $(TTAGGG)_4$, served as a substrate for phosphodiesterase (PDE) and WRN digestion. A. Robustness test. Experiments were performed on four different days to evaluate assay-to-assay variability. Data represent means ± SEM (N = 4). **B.** Testing the influence of the alkaline phosphatase digestion time prior to the analysis of the LC-MS/MS analysis of WRN-digested samples (40 nM WRN). No significant difference was observed between 4-h and over-night (ON) digestion. Data represent means ± SEM (N = 3).

Supplementary Table 1: WRN substrates used in this study.

A	Fork based on Brosh et al. 2006	5'-Bio-TTTTTTTTTTTTTTTTTTAGGGTTAGGGTTAGGGTTAGGGCATGCACTAC XXXXXXXXXXXXXXXXX|||||||||||||||||||||||||||||||||| 3'-TTTTTTTTTTTTTTTTTTCCCAATCCCAATCCCAATCCCGTACGTGATG
B	Alternative Fork	5'-TTTTTTTTTTTTTTTAATGGGATAGGGTAAGGGTTAGGGTATGGGATTGGG XXXXXXXXXXXXXXX|||||||||||||||||||||||||||||||||| 3'-TTTTTTTTTTTTTTTTTACCCTATCCCATTCCCAATCCCATACCCTAACCC
C	Blunt ended	5'-AATGGGATAGGGTAAGGGTTAGGGTATGGGATTGGG |||||||||||||||||||||||||||||||||| 3'-TTACCCTATCCCATTCCCAATCCCATACCCTAACCC
D	5'-overhang	5'-AATGGGATAGGGTAAGGGTTAGGGTATGGGATTGGG |||||||||||||||||||||||||||||||||| 3'-TTACCCTATCCCATTCCCAATCCCATACCCTAACCCAATCCCAATCCCTATA
E	4-way junction	5'-AATGGGAAAATTTTAATGGGATAGGGTAAGGGTTAGGGTATGGGATTGGG ||||||XXXXXXXX|||||||||||||||||||||||||||||||||| 3'-TTACCCAAAATTTTTTACCCTATCCCATTCCCAATCCCATACCCTAACCC

Supplementary Table 2: Optimized settings for mass spectrometric analysis.

Parameter	Value
Capillary	2.70 kV
Cone	11.00 V
Extractor	0.00 V
RF lens	0.2 V
Source temperature	80°C
Desolvation temperature	270°C
Cone gas flow	Off
Desolvation gas flow	600 L/min
LM 1 resolution	11.0
HM 1 resolution	4.0
Ion energy 1	0.5
Entrance	1
Collision	15
Exit	1
LM 2 resolution	13
HM 2 resolution	10
Ion energy 2	2.0
Dwell time	500 msec
Ion pairs used for MRM analysis	$^{14}N_5$-dG: 268→152 (m/z) $^{15}N_5$-dG: 273→157 (m/z) $^{14}N/^{12}C$-dC: 228→112 (m/z) $^{15}N/^{13}C$-dC 240→119 (m/z)

Supplementary Table 3: Concentrations of ^{14}N-dG, ^{15}N-dG and $^{14}N/^{12}C$-dC, $^{15}N/^{13}C$-dC used for acquisition of calibration curves.

[^{14}N-dG, $^{14}N/^{12}C$-dC]	[^{15}N dG, $^{15}N/^{13}C$-dC]
10 nM	100 nM
25 nM	100 nM
50 nM	100 nM
100 nM	100 nM
150 nM	100 nM

Chapter III: Site-specific non-covalent interaction of the biopolymer poly(ADP-ribose) with the Werner syndrome protein regulates protein functions

Oliver Popp, Sebastian Veith*, Jörg Fahrer, Vilhelm A. Bohr,*

Alexander Bürkle and Aswin Mangerich

ACS Chemical Biology, 2013 Jan 18; 8(1): 179-88

* Equal contribution

Abstract

Werner syndrome is a premature aging disorder that is caused by defects in the Werner protein (WRN). WRN is a member of the RecQL helicase family and possesses helicase and exonuclease activities. It is involved in various aspects of DNA metabolism such as DNA repair, telomere maintenance, and replication. Poly(ADP-ribose) polymerase 1 (PARP1) is also involved in these processes by catalyzing the formation of the nucleic-acid-like biopolymer poly(ADP-ribose) (PAR). It was previously shown that WRN interacts with PARP1 and that WRN activity is inhibited by PARP1. Using several bioanalytical approaches, we demonstrate here that the enzymatic product of PARP1, *i.e.*, PAR, directly interacts with WRN physically and functionally. First, WRN binds HPLC-size-fractionated short and long PAR in a non-covalent manner. Second, we identified and characterized a PAR-binding motif (PBM) within the WRN sequence and showed that several basic and hydrophobic amino acids are of critical importance for mediating the PAR binding. Third, PAR-binding inhibits the DNA-binding, the helicase and the exonuclease activities of WRN in a concentration-dependent manner (Figure 16). Based on our results we propose that the transient nature of PAR produced by living cells would provide a versatile and swiftly reacting control system for WRN's functions. More generally, our work underscores the important role of non-covalent PAR-protein interactions as a regulatory mechanism of protein function.

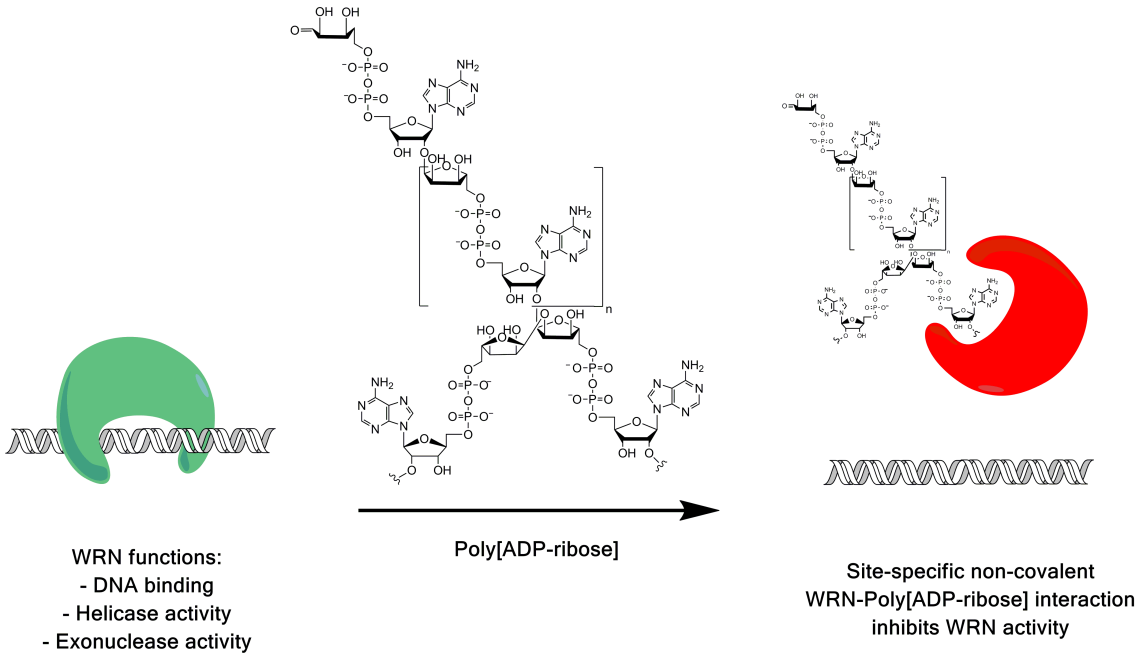

Figure 16: Graphical abstract, summarizing the main findings: PAR can bind to WRN non-covalently and thus inhibit WRN's ability to bind DNA and its enzymatic functions.

Introduction

Poly(ADP-ribosyl)ation (PARylation) is a post-translational modification catalyzed by poly(ADP-ribose) polymerases (PARPs). PARP1 accounts for the bulk of the cellular PARylation capacity and is involved in various cellular processes, such as DNA repair, telomere regulation, transcription, and the regulation of cell death (Hottiger et al., 2010; Rouleau et al., 2010). It is catalytically activated by DNA strand breaks and forms linear and branched chains of poly(ADP-ribose) (PAR) consisting of up to 200 ADP-ribose units, which are covalently bound to acceptor proteins, such as PARP1 itself (automodification) and histones (Figure 17) (Hottiger et al., 2010; Rouleau et al., 2010). Poly(ADP-ribose) glycohydrolase (PARG), on the other hand, hydrolyzes PAR both in an endo- and exoglycosidic manner, which leads to rapid turnover of PAR in the cell and to the formation of free PAR. In addition to covalent modification, free PAR can bind to proteins in a non-covalent manner, which may alter their functions or subcellular localization. Although PAR and DNA are structurally related, non-covalent PAR-protein interactions are not mediated via common DNA binding domains, since general DNA binding enzymes such as polymerases, ligases, and DNase1 do not bind PAR (Althaus et al., 1995; Malanga et al., 1998a). Instead the PAR-protein interaction is mediated by at least three specific PAR binding motifs: *(i)* distinct macrodomains, *(ii)* a PAR-binding zinc finger motif, and *(iii)* a weakly conserved ~20 amino acid (aa) PAR binding motif (PBM) (Ahel et al., 2008; Gagné et al., 2008; 2003; Pleschke et al., 2000; Timinszky et al., 2009). Whereas the first two binding motifs are present in a limited number of human proteins (<50), the 20 aa PBM has been identified in several hundred human protein sequences (Gagné et al., 2008; Pleschke et al., 2000). This motif consists of (i) a cluster rich in basic aa and (ii) a pattern of hydrophobic aa interspersed with basic residues (Gagné et al., 2008; Pleschke et al., 2000). Most of the PAR interaction partners identified so far are involved in genomic maintenance and cell-cycle control. For example, the recruitment of the base-excision repair (BER) protein XRCC1 to sites of DNA damage is completely dependent on efficient PAR formation (El-Khamisy et al., 2003). Moreover, the binding of PAR to the DEK oncoprotein promotes the formation of DEK multimers with potential impact on gene transcription and maintenance of genomic stability (Fahrer et al., 2010). Also, the ability of p53 to bind to DNA is decreased upon non-covalent interaction with PAR, suggesting a PAR-dependent regulation of transactivation functions of p53 (Malanga et al., 1998b).

Another factor involved in many aspects of DNA metabolism such as replication, DNA repair, and telomere maintenance is the Werner syndrome protein (WRN) (Rossi et al., 2010a). In the hereditary disease Werner syndrome (WS), the *WRN* gene is mutated and dysfunctional.

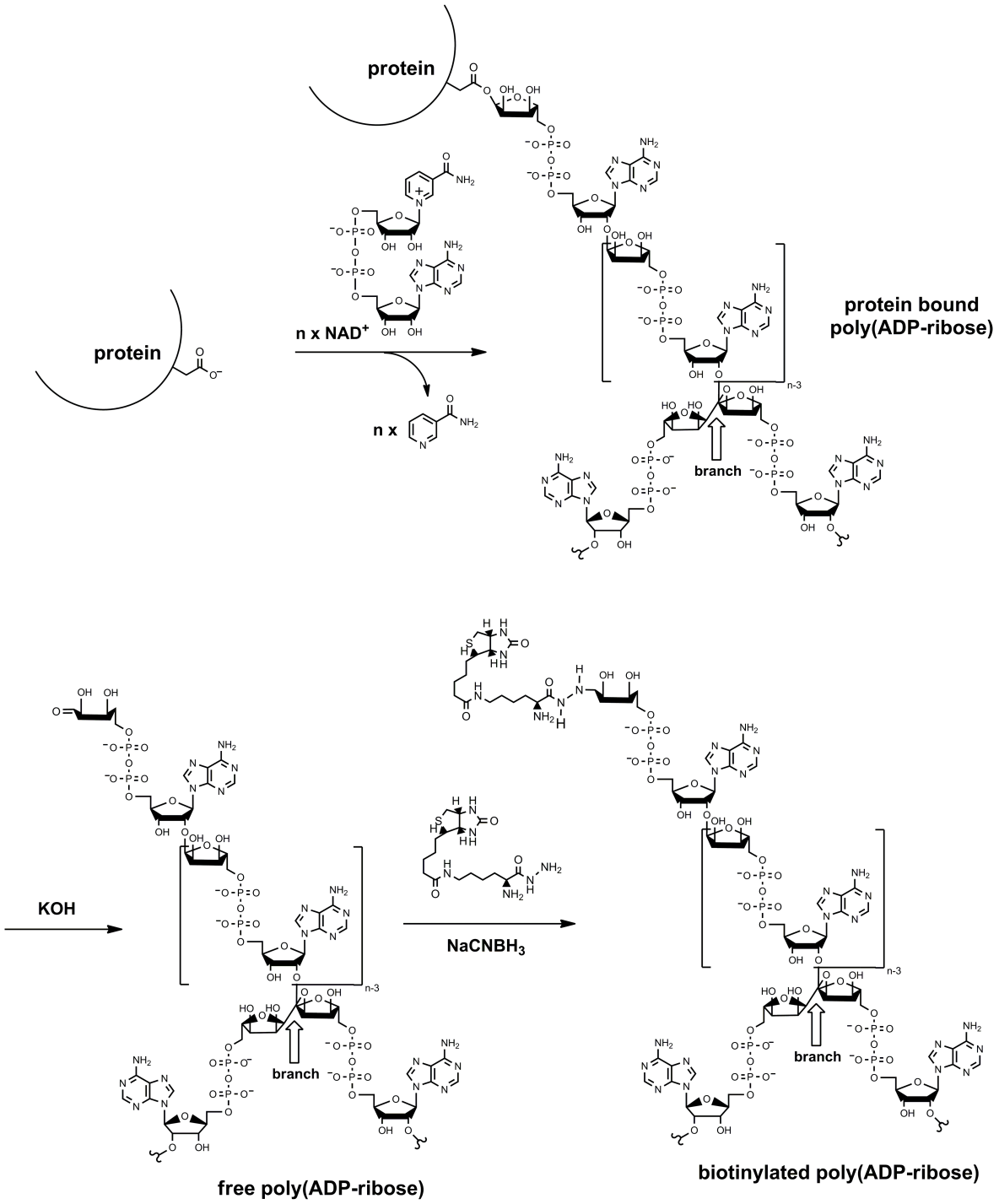

Figure 17: *In vitro* production and biotinylation of poly(ADP-ribose).
PARPs cleave the glycosidic bond of NAD^+ between nicotinamide and ribose followed by the covalent modification of acceptor proteins with an ADP-ribosyl unit. PARPs also catalyze adduct elongation, giving rise to linear polymers with chain lengths of up to 200 ADP-ribosyl units, characterized by their unique ribose (1''→2') ribose phosphate-phosphate backbone. Some of the PARP family members also catalyze a branching reaction by creating ribose (1'''→2'') ribose linkages. *In vitro*-synthesized poly(ADP-ribose) (PAR) was detached from proteins by KOH treatment, purified by phenol-chloroform extraction, and for some experiments HPLC-size-fractionated and labeled with biotin via a carbonyl-reactive biotin analog (biocytin hydrazide) for detection purposes.

Patients show premature aging starting after puberty, with age-associated characteristics such as osteoporosis, atherosclerosis and high cancer incidence, which is paralleled and probably caused by a high susceptibility to genotoxic stress at a cellular level (Muftuoglu et al., 2008b). WRN is a RecQL helicase with additional exonuclease and ATPase activities (Rossi et al., 2010a). It binds to various DNA substrates such as forked structures, DNA/RNA duplexes, and repair intermediates including Holliday junctions, bubbles, recessed ends, and telomeric substrates (Kobbe et al., 2003b). Both WRN's helicase and exonuclease activities work in 3' to 5' direction and can act independently of each other (Ahn and Bohr, 2011; Huang et al., 2000). Enzymatic properties of WRN can be altered by post-translational modifications such as acetylation, which regulates WRN function in BER (Muftuoglu et al., 2008a), and phosphorylation, which inhibits WRN's enzymatic activities (Cheng et al., 2003). A potential covalent PARylation of WRN by PARP1 has been reported (Adelfalk et al., 2003). Furthermore, a physical and functional interaction between PARP1 and WRN has been discovered. First, cells derived from WS patients carrying a mutant form of WRN are severely deficient in their PARylation activity under conditions of genotoxic stress. Furthermore, WRN directly interacts with PARP1 physically in human cells (Kobbe et al., 2003a; Lachapelle et al., 2011). The WRN-PARP1 interaction is mediated via three WRN regions, *i.e.*, the N-terminus, the helicase domain and a C-terminal region containing the RecQ-conserved (RQC) domain; and via two PARP1 regions, *i.e.*, the DNA-binding and the BRCT domain (Kobbe et al., 2004a). Interestingly, the WRN-PARP1 interaction seems to be dependent on the PARylation state of PARP1, because PARylated PARP1 binds WRN less efficiently than unmodified PARP1 (Kobbe et al., 2003a). Also dependent on its PARylation state, PARP1 inhibits both exonuclease and helicase activities of WRN (Kobbe et al., 2004a). Thus, unmodified PARP1 has a stronger inhibitory effect on WRN activity than PARylated PARP1 (Kobbe et al., 2004a). *In vivo*, $Parp1^{-/-}/Wrn^{\Delta hel/\Delta hel}$ mice develop cancer at higher incidence and exhibit a shorter lifespan than corresponding single knock-outs. Furthermore, cells derived from those mice display major signs of genomic instability (Lebel et al., 2003) as well as a pronounced dysregulation of gene transcription, including genes involved in apoptosis, cell cycle control and metabolism (Deschênes et al., 2005).

The present work highlights the role of non-covalent PAR-protein interactions as a regulatory mechanism of protein function. WRN is considered an important factor in genome maintenance, with implications in aging and cancer biology (Rossi et al., 2010a). The cellular functions of WRN and PARP1 are highly overlapping and the interplay between both factors leads to an inhibition of WRN's catalytic activities (Kobbe et al., 2004a). Here we are using a

series of bioanalytical approaches, *e.g.*, HPLC size-fractionation of PAR, PAR-protein interaction assays with biotin end-labeled PAR, and quantitative isotope dilution mass spectrometry to reveal that WRN directly and specifically interacts with free PAR in a non-covalent manner and that this interaction regulates WRN activity. We demonstrate that the PAR-protein interaction is mediated via at least one PBM located in WRN's exonuclease domain. In addition, binding of PAR to WRN decreases WRN's ability to bind to a physiologically relevant DNA substrate and also inhibits its exonuclease and helicase activities. We propose that the production of PAR provides a versatile, swiftly reacting and highly efficient system to control WRN's function in a spatio-temporal manner.

Results and Discussion

PAR binds to WRN in a non-covalent manner

A direct physical and functional interaction of WRN with PARP1 was reported previously (Kobbe et al., 2003a; 2004a). To test the hypothesis that WRN is capable of binding the enzymatic product of PARP1, *i.e.*, PAR, we performed interaction studies using purified recombinant WRN. Increasing amounts of WRN were separated by SDS-PAGE, immobilized on a nitrocellulose membrane and incubated with *in-vitro*-synthesized, purified PAR (see Figure 17 for synthesis). After high-stringency salt washes, protein-bound PAR was detected using the PAR-specific antibody 10H (Figure 18 A). As expected, no detectable levels of PAR bound to negative controls, such as bovine serum albumin, cytochrome C or lysozyme, whereas strong binding was observed to histone H1, which served as a positive control. Importantly, a PAR-specific signal was associated with WRN demonstrating that the latter is capable of specific non-covalent interaction with free PAR (Figure 18 A).

The finding that WRN is potentially modified covalently with PAR on the one hand (Adelfalk et al., 2003) and that it interacts with PAR in a non-covalent fashion on the other hand fits with data on other proteins such as histone H1 and DEK, where dual regulation by PAR has been shown (Fahrer et al., 2010; Kappes et al., 2008; Ogata et al., 1980; Panzeter et al., 1992). This highlights the complex regulation of proteins by PAR on multiple levels.

As we have shown previously, non-covalent binding of PAR to some proteins, *e.g.*, DEK and XPA, depends on the chain length of the polymer (Fahrer et al., 2007). We therefore investigated the ability of WRN to bind to PAR of different, well-defined chain length. As is shown in Suppl. Figure 5, PAR of a chain length ranging from 5 to >65 units was size-

fractionated using a previously established anion exchange HPLC protocol (Fahrer et al., 2007; Kiehlbauch et al., 1993). In a PAR-overlay assay equal amounts of membrane-immobilized WRN were incubated with equal amounts of PAR of defined chain length. Binding of PAR to WRN was observed for all PAR fractions, with a slight tendency for stronger binding of WRN to longer PAR chains (Figure 18 B). Nonetheless, PAR chains smaller than 10 units could still bind strongly to WRN, with signal intensities similar to those of unfractionated PAR, indicating that WRN is able to bind even very short PAR chains with high affinity (Figure 18 B).

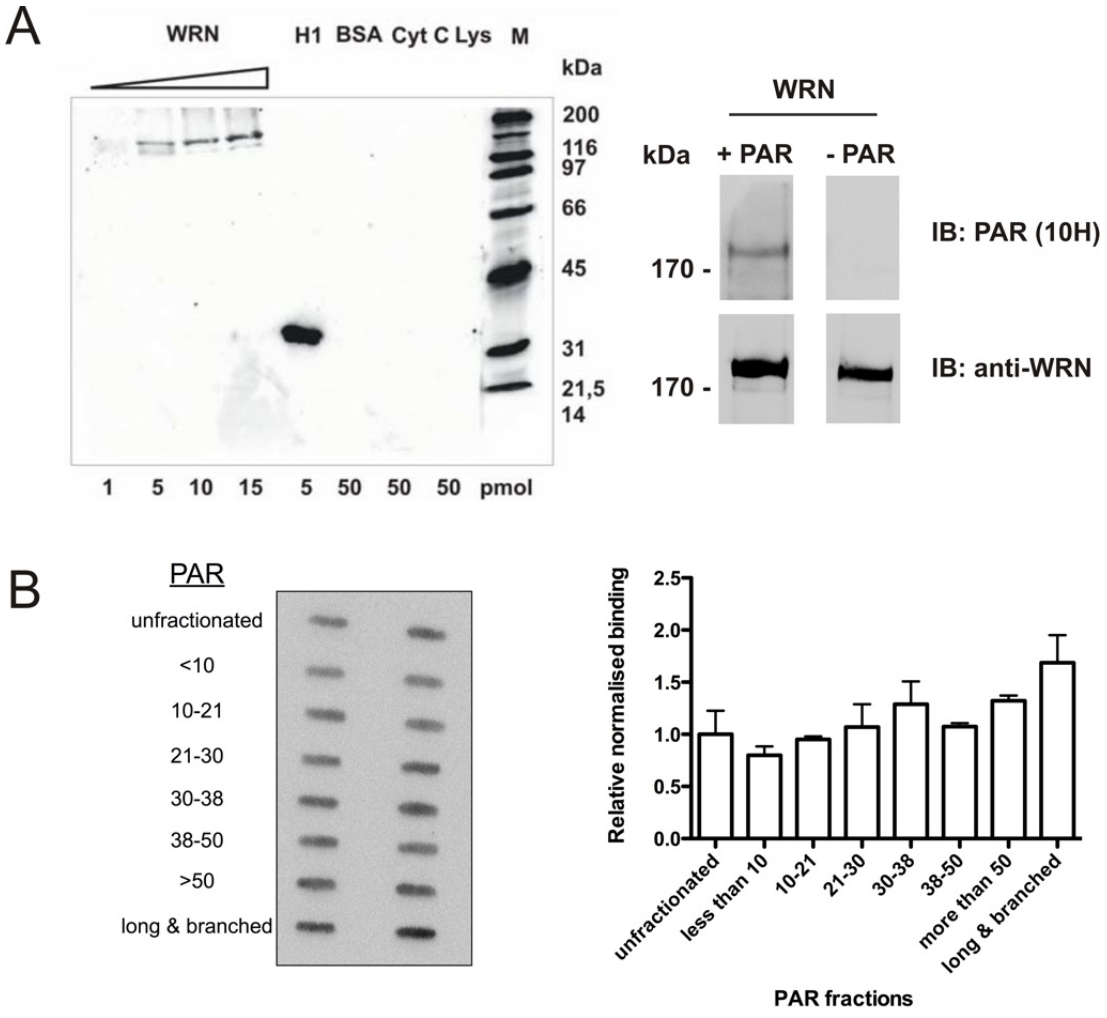

Figure 18: PAR binds to WRN in a non-covalent manner.
A. PAR-overlay blots demonstrating WRN-PAR interaction. Proteins were separated by SDS-PAGE, immobilized on a nitrocellulose membrane and incubated with 0.2 µM (referring to ADP-ribosyl units) of unfractionated PAR. Protein-bound PAR was detected using the anti-PAR monoclonal antibody 10H. **Left panel.** Histone H1 served as a positive control; bovine serum albumin (BSA), cytochrome C (Cyt C), lysozyme (Lys) served as negative controls. **Right panel.** Specificity control of the 10H antibody. 5 pmol of WRN were loaded per lane. After blotting, the membrane was cut and incubated with or without 0.2 µM PAR (+/- PAR), respectively. Apart from this, both membranes were processed identically. After probing with the 10H antibody, membranes were stripped and incubated with an anti-WRN antibody as loading control. WRN-PAR binding was only observed for the PAR-incubated membrane, whereas no signal was detected for the control membrane. **B. Left panel.** PAR overlay slot-blot evaluating the dependency of WRN-PAR binding on PAR chain length. WRN (15 pmol/slot) was immobilized on a nitrocellulose membrane (in duplicates) and incubated with 0.2 µM PAR of chain length as indicated. **Right panel.** Densitometric quantification of B, normalized to signals obtained from binding of unfractionated PAR.

A control experiment using XPA showed a strong dependency of PAR-XPA binding on PAR chain length, which confirmed our previous results (Suppl. Figure 6) (Fahrer et al., 2007). The finding that some PAR-interacting proteins, such as XPA and DEK, exhibit a strong preference for long PAR chain lengths (Fahrer et al., 2007; 2010), whereas others, such as WRN and H1, also efficiently bind to short polymer underscores the importance of PAR chain length and probably also branching complexity in the regulation of protein function.

Identification of a PAR-binding motif in the WRN exonuclease domain

The most frequent feature of proteins that associate with PAR non-covalently is the presence of a weakly conserved PBM (Pleschke et al., 2000). This PBM consensus sequence consists of a stretch of basic aa that are separated by hydrophobic aa from a further cluster of N-terminally located basic aa (Figure 19 A). A homology search based on the PBM consensus sequence reported by Pleschke *et al.* revealed a total of four potential PBMs within the WRN protein (Figure 19 A&B). The first PBM is located in the WRN exonuclease domain (aa 166-188), the second in between the exonuclease domain and the acidic region (aa 251-275), the third in the RecQ conserved (RQC) domain (aa 785-812), and the fourth in the helicase and RNase D C-terminal (HRDC) domain (aa 1032-1058) (Figure 19 B). These sequences were synthesized as oligopeptides and tested for their ability to bind PAR using a PAR overlay assay. Increasing amounts of each peptide were immobilized on a nitrocellulose membrane and incubated with biotin end-labeled PAR (Figure 17) to detect PAR with high specificity and sensitivity (Fahrer et al., 2007). Biotinylated PAR was detected after high-stringency salt washes using streptavidin-coupled horseradish peroxidase (HRP). Peptide ‘166-188’ at the N-terminus of WRN revealed strong PAR-binding (indicated by an asterisk, Figure 19 B), whereas weak PAR-binding was observed for peptides ‘251-275’ and ‘785-812’. No or very weak PAR-binding was detected for peptide ‘1032-1058’, further demonstrating the specificity of the PAR binding to peptide ‘166-188’ (Figure 19 C-E). The finding that peptide ‘166-188’ has been identified in an *in silico* search for putative PBMs in combination with the result that this peptide binds PAR with high affinity provides strong evidence for the existence of a PBM within aa 166-188 of the WRN protein.

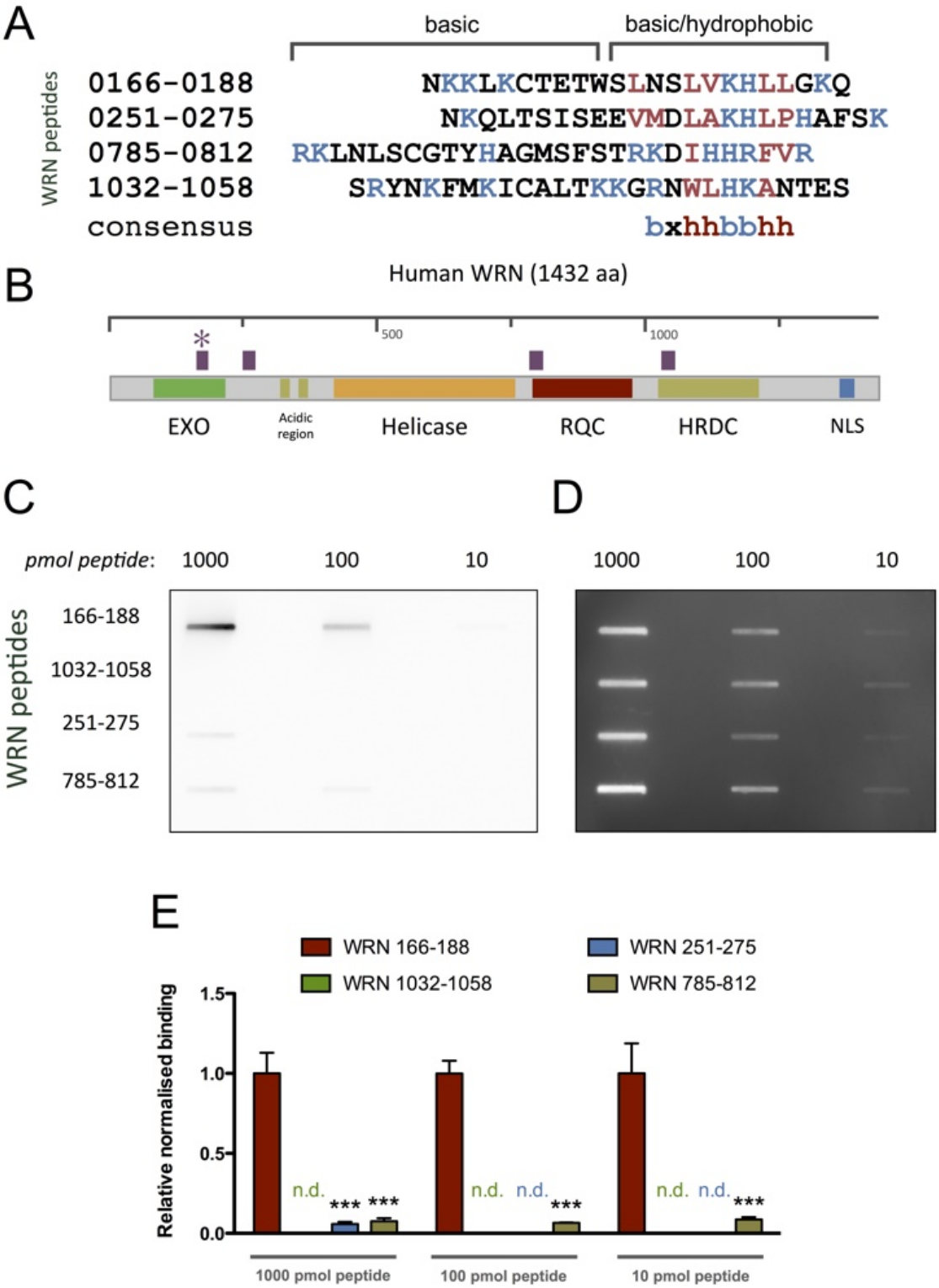

Figure 19: WRN exhibits a PAR-binding motif in its exonuclease domain.
A. Alignment of the PAR-binding motif (PBM) consensus sequence with the WRN polypeptide sequence revealed four putative candidates. Basic and hydrophobic aa are depicted in blue and red, respectively. **B.** Scheme of the WRN protein highlighting functional domains as well as the location of putative PBMs (in purple). Asterisk indicates the PBM that was confirmed experimentally. **C.** Experimental confirmation of the PBM. WRN peptides '166–188', '251–275', '785–812', and '1032–1058' were tested for their ability to bind PAR, by using a PAR-overlay assay. Peptides were immobilized on a nitrocellulose membrane and incubated with 3 nM biotinylated PAR. PAR was detected using streptavidin-HRP. Peptide '166–188' bound PAR strongly, whereas peptides '251–275' and '785–812' showed weak PAR-binding. No PAR-binding was detected with peptide '1032–1058'. **D.** Peptide loading control using SYPRO Ruby staining **E.** Densitometric quantification of C. Data represent means ± SEM from three independent experiments. Statistical analysis was performed using ANOVA and Dunnett's post-test. *** $p<0.001$; n.d., not detectable; EXO, exonuclease domain; RQC, RecQ C-terminal domain; HRDC, helicase and RNase D C-terminal domain; NLS, nuclear localization signal.

Basic and hydrophobic amino acids in the PBM contribute to PAR binding

To determine which aa residues within the PBM mediate PAR-binding, peptide '166-188' was subjected to an aa exchange analysis. Both hydrophobic and basic aa have been described to contribute to the specificity of PAR-binding within PBMs (Gagné et al., 2008; Pleschke et al., 2000). To this end, the PBM was mutated consecutively either by changing basic or hydrophobic aa in groups of two or three (Figure 20 A). A PAR-overlay assay was performed to test the interaction of the four peptides with PAR (Figure 20). As expected, the wild type (WT) peptide displayed the strongest PAR-binding affinity. PAR-binding was significantly weaker with peptide W-h1, carrying exchanges of three hydrophobic aa to alanine. Peptide W-h2 with exchanges of five hydrophobic aa as well as peptide W-b1 with exchanges of three basic aa displayed no detectable PAR-binding.

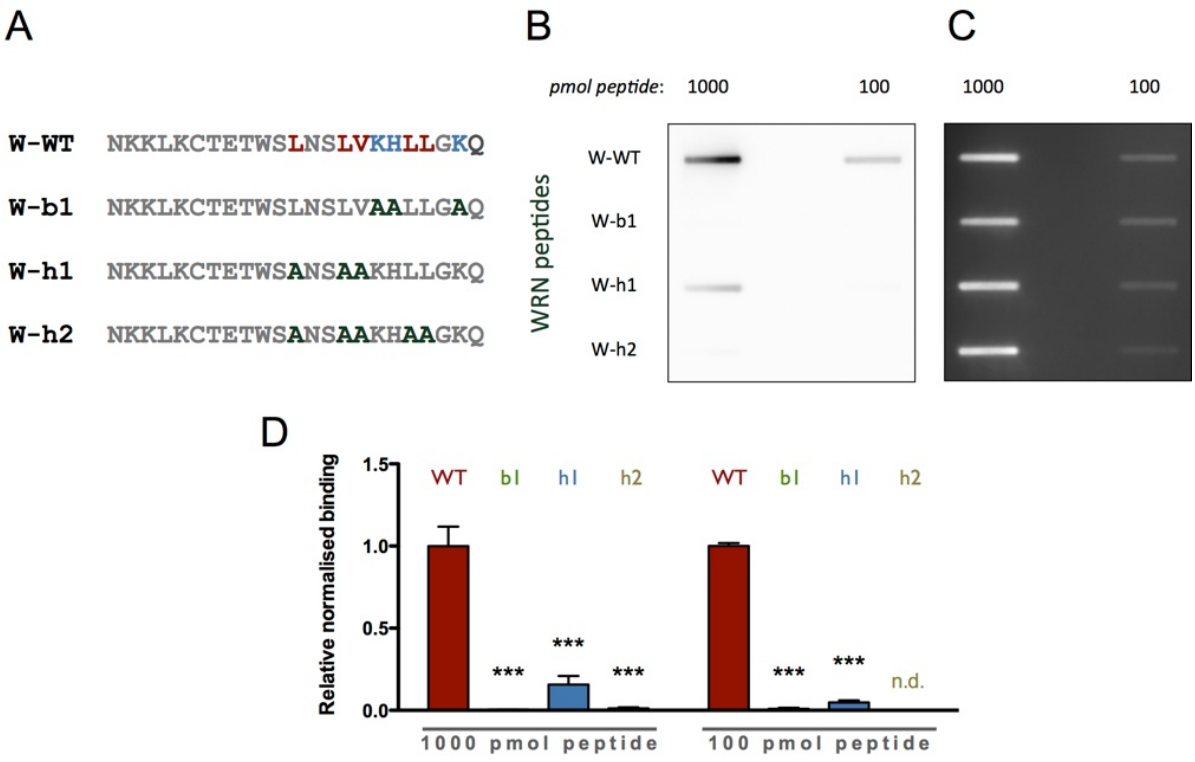

Figure 20: PAR-overlay blot with mutant WRN peptides derived from peptide '166-188'.
A. Peptide sequences used for PAR binding studies with amino acid exchanges highlighted in bold. **B.** Peptides were immobilized on a nitrocellulose membrane in concentrations as indicated and incubated with 3 nM biotinylated PAR. PAR was detected using streptavidin-HRP. The WT PAR binding motif displays the strongest binding to PAR followed by the peptide W-h1, which possesses only minor PAR-binding ability. For both W-h2 and W-b1 binding is strongly reduced. **C.** Peptide loading control using SYPRO Ruby staining. **D.** Densitometric quantification of B. Data represent means ± SEM of three independent experiments. Statistical analysis was performed as described in Figure 19. *** $p<0.001$; n.d.: not detectable.

In summary, we have identified a PBM at aa position 166-188 of the WRN protein. Within this motif, both basic and hydrophobic aa contribute to efficient binding of the polymer, although basic aa appeared to have a slightly greater impact on PAR-binding than hydrophobic ones. Next, we tested three different functional end points of WRN activity, *i.e.*, DNA binding properties as well as WRN's enzymatic activities to analyze potential functional consequences of the WRN-PAR interaction.

PAR inhibits WRN-DNA interaction

For WRN-DNA interaction studies, we chose a commonly used DNA oligoduplex substrate, which comprises a forked structure carrying a 5'-biotin end label to allow detection via streptavidin-HRP. As shown previously such a DNA structure can be potentially formed during processes such as transcription, replication and at telomeric ends and serves as a good substrate for WRN, because it can be recognized as ssDNA, dsDNA, a DSB, or a forked structure (Kobbe et al., 2003b). Binding of full-length WRN to this oligoduplex was analyzed using an electrophoretic mobility shift assay (EMSA). As it is evident from Figure 21 A, WRN efficiently bound to the oligoduplex in a concentration-dependent manner as expected. An almost complete and highly significant shift was observed at a molar ratio of WRN:oligoduplex of 2.5:1, where even residual single-stranded DNA (from incompletely annealed oligoduplexes) is bound by the protein (Figure 21 A). To analyze if the WRN-PAR interaction interferes with WRN-DNA binding, we pre-incubated WRN with increasing concentrations of PAR before adding the oligoduplex. As no major influence of PAR chain length on its WRN-binding affinity was observed, EMSA experiments were performed with unfractionated PAR representing a mixture of short and long chains ranging from 1 to over 200 units, with an estimated mean chain length of 100 ADP-ribosyl units (PAR_{100mer}). Figure 21 B demonstrates that with increasing concentrations of PAR fewer WRN-DNA complexes were formed. At a concentration of 10 µM PAR (PAR concentration refers to monomeric ADP-ribose if not stated otherwise) a highly significant reduction of the electrophoretic shift was observed to ~50% compared to control (2:1 molar ratio PAR_{100mer}:WRN). Maximum reduction of the electrophoretic shift by ~75% was observed at a PAR concentration of 20 µM (4:1 molar ratio of PAR_{100mer}:WRN) (Figure 21 B).

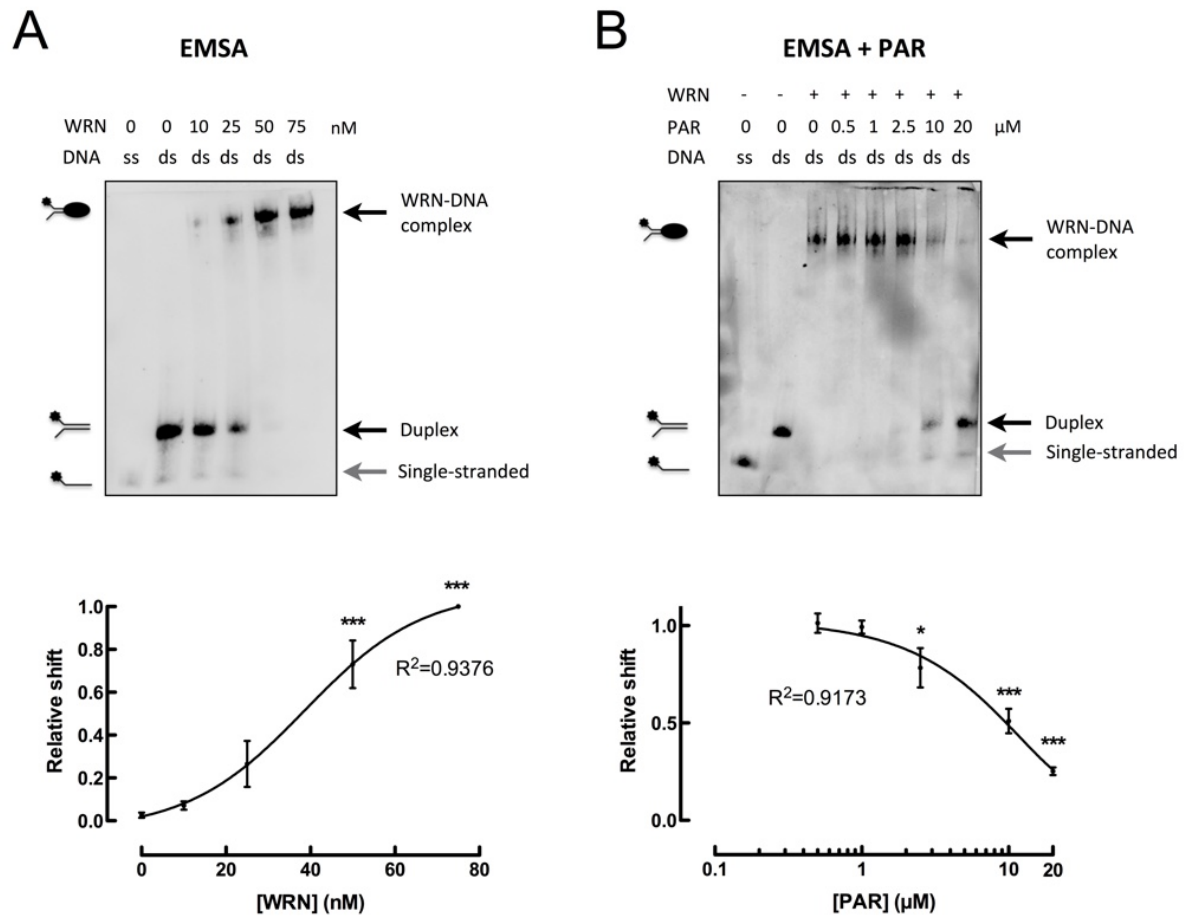

Figure 21: WRN-PAR interaction inhibits binding of WRN to DNA.
A. **Upper panel**: Increasing concentrations of WRN were incubated with 200 fmol of biotin-labeled forked oligoduplex. A WRN-dose-dependent shift of the oligoduplex is indicative of WRN-DNA binding. **Lower panel:** Densitometric quantification of three independent experiments (means ± SEM). **B. Upper panel:** Effect of PAR on the WRN-DNA interaction. WRN (50 nM) was pre-incubated with increasing concentrations of PAR. 10 µM PAR correspond to a 2:1 molar ratio of PAR_{100mer}:WRN. The presence of PAR inhibited the formation of the WRN-DNA complex in a dose-dependent manner. **Lower panel:** Densitometric quantification of three independent experiments (means ± SEM). Statistical analysis was performed using ANOVA and Dunnett's multiple comparison test, *** $p<0.001$. Curves were fitted using a sigmoidal dose-response curve with variable slope. Single-stranded oligonucleotide (grey arrow), duplex oligonucleotide and WRN-DNA complex (black arrow) are indicated. ds, double-stranded biotinylated oligonucleotide; ss, single-stranded biotinylated oligonucleotide.

These results demonstrate a direct functional effect of free PAR by interfering with WRN's DNA-binding ability. WRN harbors three DNA-binding domains with distinct substrate specificities (Kobbe et al., 2003b). One of these DNA-binding domains is located N-terminally within the exonuclease domain, the other two C-terminally, *i.e.*, within the RQC and helicase domains. Because all three of these DNA-binding domains bind to forked substrates, as used in this study, with high affinity, we speculate that steric and/or structural changes within the WRN protein are responsible for the reduced WRN-DNA interaction upon PAR-binding. Furthermore, PAR may compete with the DNA substrate for WRN-binding via WRN's N-terminal DNA-binding domain, which overlaps with the N-terminal PBM. Conversely, it is possible that DNA is able to dissociate PAR from WRN. In this respect, it

was shown previously that PAR and DNA compete for PAR binding sites in histone H1 at a high molar excess of DNA (Malanga et al., 1998a; Pleschke et al., 2000). Because WRN shows a weaker PAR binding compared to histone H1 (Figure 18 A), it is therefore likely that at high concentrations DNA is able to dissociate PAR from WRN as well. If this is of any physiological relevance remains to be elucidated.

PAR inhibits WRN's helicase and exonuclease activities

To study if the WRN-PAR interaction affects WRN's enzymatic functions, first a WRN helicase assay was developed based on a previously published protocol (Brosh et al., 2006). Instead of using a radioactively end-labeled substrate, a non-radioactive biotin-labeled forked DNA oligoduplex was used. The oligoduplex was incubated with increasing concentrations of WRN, separated by native PAGE, immobilized on a nylon membrane, and detected via streptavidin-HRP. As expected, a dose-dependent unwinding of the substrate was observed (Figure 22 A). At a molar ratio of WRN:oligoduplex of 0.75:1 significant formation of single-stranded DNA was observed that reached saturation at a molar ratio of WRN:oligoduplex of 1.25:1 (Figure 22 A). When WRN was preincubated with increasing concentrations of PAR before adding the oligoduplex substrate, WRN's unwinding activity was inhibited in a concentration-dependent manner (Figure 22 B). PAR significantly inhibited DNA unwinding by 62% at a concentration of 2.5 µM (1:1 molar ratio of PAR_{100mer}:WRN). A maximum inhibitory effect of 80% was observed at 10 µM PAR (4:1 molar ratio of PAR_{100mer}:WRN) (Figure 22 B).

As the WRN-PBM is located in the exonuclease domain, we examined a potential impact of PAR on WRN's exonuclease function using a recently developed method to quantify WRN's exonuclease activity (Mangerich et al., 2012). In this method WRN's exonuclease activity is analyzed by detecting the release of free deoxyguanosine (dG) via isotope dilution mass spectrometry (LC-MS/MS). A forked oligoduplex mimicking the telomeric repeat sequence was used as a substrate. A concentration-dependent reduction in WRN's exonuclease activity was observed in the presence of PAR (Figure 23). A significant inhibition of exonuclease activity by ~25% was observed at a PAR concentration of 10 µM (2.5:1 molar ratio of PAR_{100mer}:WRN). Maximum inhibition of exonuclease activity of ~45% was observed with PAR concentrations >50 µM. These results were confirmed using a classical WRN exonuclease activity assay by detection of a 5'-biotin-end-labeled oligonucleotide after electrophoretic separation under denaturing conditions (Suppl. Figure 7).

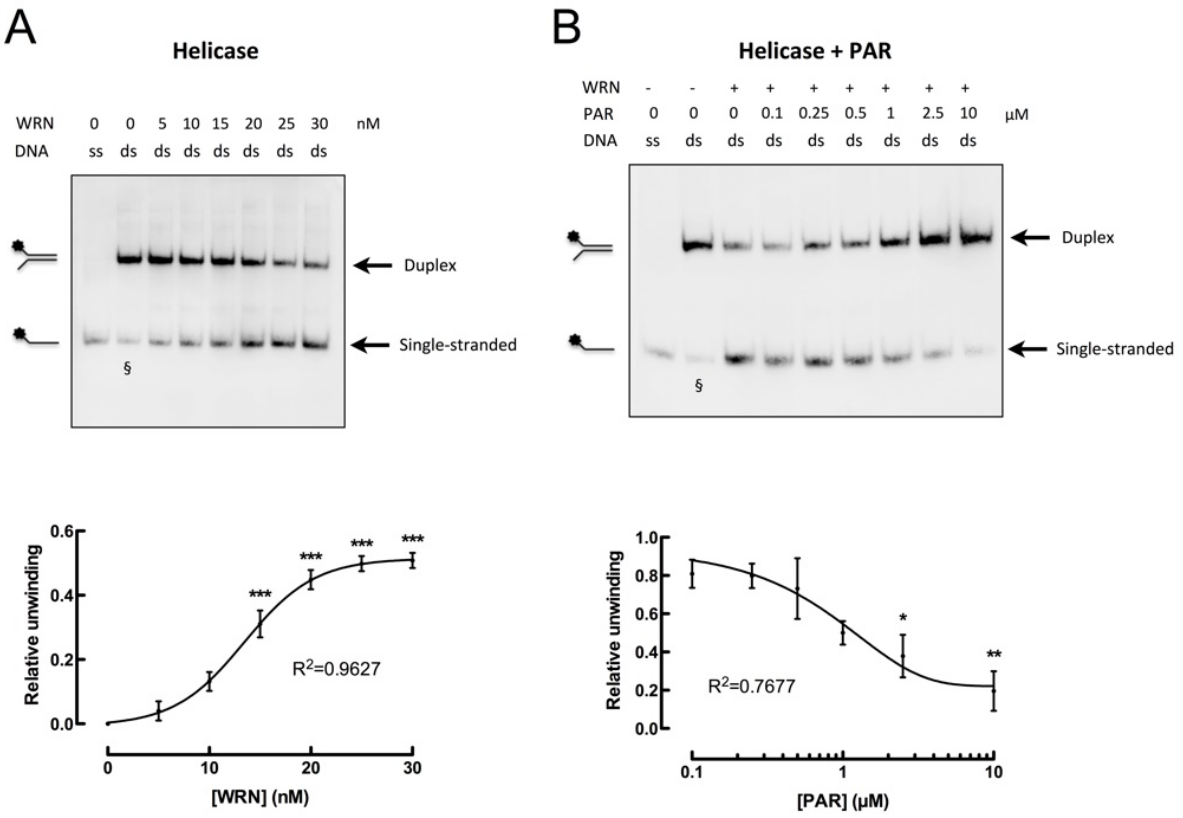

Figure 22: WRN-PAR interaction inhibits WRN's helicase activity.
A. WRN helicase assay. **Upper panel:** Unwinding of a forked oligoduplex in a WRN-concentration-dependent manner. **Lower panel:** Densitometric quantification from three independent experiments (means ± SEM). Reactions were performed at 37°C for 20 min. **B.** Impact of PAR binding on WRN's helicase activity. **Upper panel:** Recombinant WRN (25 nM) was pre-incubated with increasing concentrations of PAR as indicated. Helicase reaction was started by addition of the biotin-labeled oligoduplex. The presence of PAR inhibited WRN's helicase activity in a concentration-dependent manner. **Lower panel:** Densitometric quantification of three independent experiments (means ± SEM). 10 µM PAR correspond to a 4:1 molar ratio of PAR_{100mer}:WRN. § indicates single-stranded DNA due to incomplete annealing of oligonucleotides. This signal was background-subtracted in quantitative analyses. Statistical analysis and curve fitting were performed as described in Figure 21. * $p<0.05$; ** $p<0.01$; *** $p<0.001$.

In summary, our results demonstrate that WRN-PAR interaction significantly interferes with WRN's helicase and exonuclease functions *in vitro*. The effect of PAR on WRN's exonuclease and helicase activities may be induced by conformational changes upon PAR-binding leading to allosteric inhibition of the enzyme or by the reduced DNA-binding ability of WRN upon PAR-binding. The effect of PAR on WRN's exonuclease activity is conclusive, considering that the PBM as identified in this study is located in this domain. Notably, molar ratios of WRN and PAR as used in this study are in agreement with physiological ratios. Previous studies estimated that cells contain ~60,000 WRN and ~45,000 PAR_{100mer} molecules, respectively, under conditions of genotoxic stress (Juarez-Salinas et al., 1979; Moser et al., 2000). Furthermore, PAR production in cells is highly controlled in a spatio-temporal manner, *e.g.* at sites of DNA damage, potentially resulting in very high local concentrations.

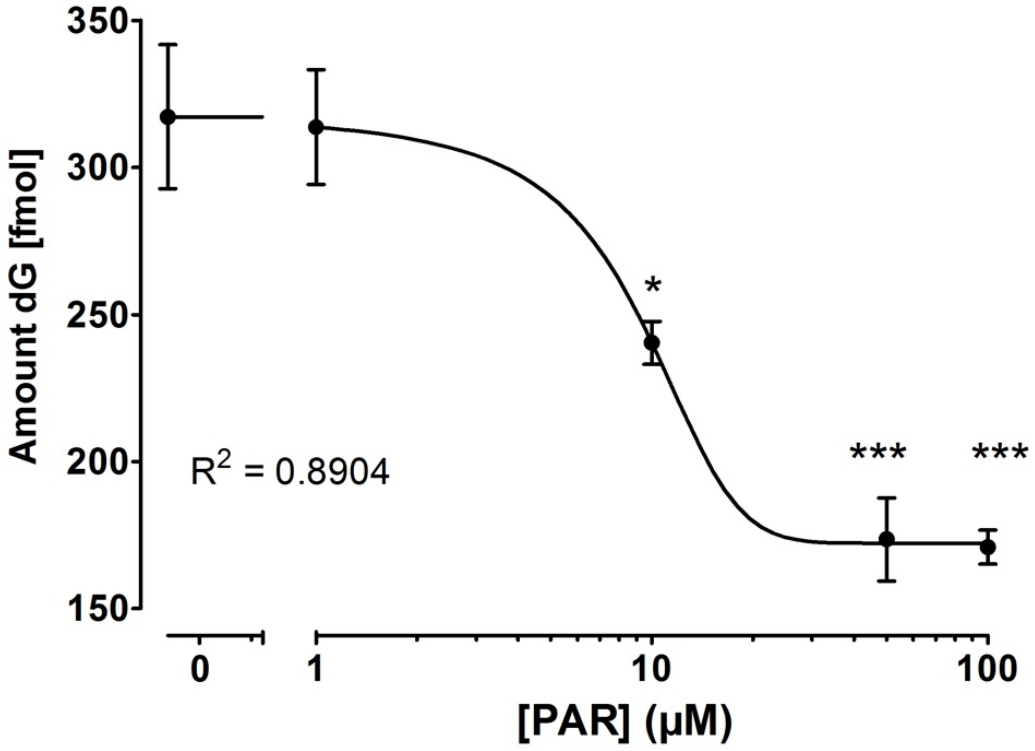

Figure 23: WRN-PAR interaction inhibits WRN's exonuclease activity.
WRN (40 nM) was pre-incubated with increasing concentrations of PAR. Exonuclease reaction was started by addition 75 fmol of a forked oligoduplex. Exonuclease reaction was carried out at 37°C for 45 min, subsequently the mixture was placed on ice, ^{15}N-labeled dG was added to samples as an internal standard to account for technical variability, and nucleotides were dephosphorylated by alkaline phosphatase. After removal of enzymes, free deoxyguanosine (dG), which directly correlates with WRN's exonuclease activity, was quantified via isotope dilution LC-MS/MS. 10 µM PAR correspond to a 2.5:1 molar ratio of PAR_{100mer}:WRN. Statistical analysis and curve fitting were performed as described in Figure 21. * $p<0.05$; *** $p<0.001$.

It is important to note that WRN activity needs to be tightly controlled *in vivo*, because uncontrolled WRN activity may cause genomic instability. Von Kobbe *et al.* showed that the unmodified PARP1 is able to inhibit both catalytic activities of WRN, while enzymatic activation of PARP1 released WRN from its enzymatic inhibition (Kobbe et al., 2004a). Considering our finding that PAR itself controls WRN activity, it is tempting to speculate that the transient nature of PAR produced by living cells in response to DNA strand breakage and specific DNA structures like four-way junctions would provide a versatile and swiftly reacting control system for WRN's function (Figure 24). In such a scenario, under physiological conditions unmodified PARP1 would inhibit WRN by 'taming' its exonuclease and helicase activities. Upon a genotoxic stimulus, *e.g.* a DNA strand break, PARP1 is PARylated and WRN is released from its repression, opening a time window during which WRN can take action on its DNA substrates. Shortly thereafter, PARG releases free PAR leading to a non-covalent WRN-PAR complex, which shuts down WRN activity, as we have shown in the present work.

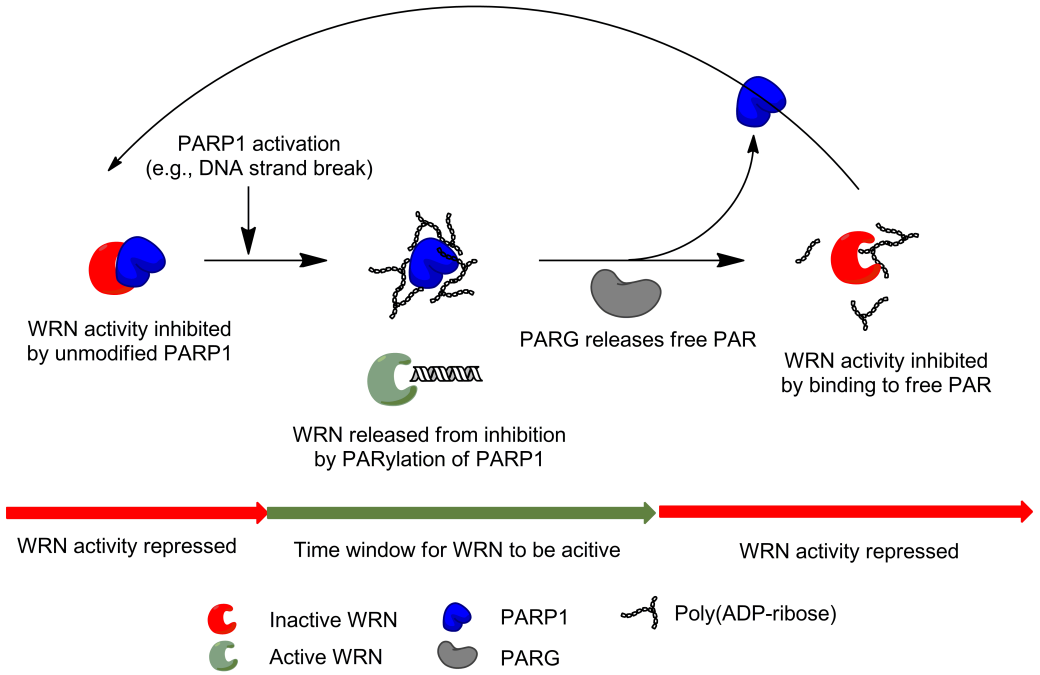

Figure 24: Potential molecular mechanism for temporally controlled regulation of WRN activity by PAR and PARP1. The model summarizes the results from the present study and (Kobbe et al., 2004a). For details see text.

Thus, the WRN-PAR complex may represent an intermediate state to control WRN activity until unmodified PARP1 is fully reconstituted and able to take over the function of repressing WRN activity. Because PARP1 and WRN are both multifunctional proteins, additional factors are presumably involved *in vivo*.

The physiological relevance of a functional regulation of WRN has impressively been demonstrated in a recent study which characterized the PAR-associated proteome in response to alkylating DNA-damage-mediated PARP activation (Gagné et al., 2012). This study identified WRN as factor that is strongly modified by PAR upon DNA damage. Whether this occurs in a covalent or non-covalent manner remains to be clarified.

In conclusion, by using an array of bioanalytical approaches we provide new insight into the regulation of the multifunctional WRN protein via non-covalent interaction with the nucleic-acid-like biopolymer PAR. Results from this study and other recent findings provide evidence that PARP1 and its enzymatic product PAR work cooperatively to modulate WRN activity in a spatio-temporal manner. This may have important implications in DNA metabolism and genomic maintenance, aging as well as cancer biology. Notably, inhibitors of PARP catalytic activity are currently being tested in cancer therapy either as radio- or chemosensitizers or as stand-alone drugs following the concept of synthetic lethality (Mangerich and Bürkle, 2011). Overall, this work exemplifies how the non-covalent interaction of a protein, *e.g.*, WRN with a scaffold and signaling molecule like PAR can mediate efficient regulation of protein functionality.

Material and Methods

Sequence alignment of PAR-binding motifs

In silico alignment was performed using the PattInProt motif search tool (http://npsa-pbil.ibcp.fr/cgi-bin/npsa_automat.pl?page=npsa_pattinprot.html) with the algorithm [HKR]-X-[AVILFWP]-[AVILFWP]-[HKR]-[HKR]-[AVILFWP]-[AVILFWP] allowing one mismatch, according to Pleschke *et al.* (Pleschke et al., 2000).

Expression and purification of human His-WRN

Human His-WRN was overexpressed in *Sf*9 cells and purified as described (Mangerich et al., 2012). WRN oligopeptides were custom-synthesized by Genscript.

Synthesis and purification of PAR

Human PARP1 was expressed in *Sf*9 cells and purified as described (Beneke et al., 2000; Fahrer et al., 2007). Synthesis of PAR was performed as described (Fahrer et al., 2007). Briefly, 75 nM of recombinant PARP1 was incubated in a mixture containing Tris-HCl pH 7.8 (100 mM), $MgCl_2$ (10 mM), DTT (1 mM), histone H1 (60 µg/ml), histone H2a (180 µg/ml), EcoRI linker [5'-GGAATTCC-3'] (50 µg/ml), βNAD^+ (1 mM) for 20 min at 37°C. The reaction was stopped by adding ice-cold trichloroacetic acid (TCA) to a final concentration of 10% (w/v). After precipitation and centrifugation at 9000 × *g* for 10 min at 4°C, the pellet was washed twice with ice-cold ethanol. PAR was detached from proteins by incubation in 0.5 M KOH and 50 mM EDTA for 10 min at 37°C. After adjustment of pH to 7.5, DNA and proteins were digested using DNase I [200 µg/ml] and proteinase K [100 µg/ml]. PAR was finally purified by phenol-chloroform extraction and ethanol precipitation.

Biotinylation of PAR and HPLC fractionation

Biotinylation and preparative anion-exchange HPLC fractionation was performed as described (Fahrer et al., 2007). Briefly, *in-vitro*-synthesized and purified PAR was incubated with 4 mM biocytin hydrazide under reductive amination conditions in sodium acetate buffer pH 5.5 for 8 h at RT. Samples were dialyzed and PAR was precipitated using ethanol.

Biotinylated PAR was size-fractionated using a Shimadzu LC-8A HPLC system with a semi-preparative DNA Pac PA100 column (Dionex). PAR fractions were eluted using a multistep NaCl gradient in 25 mM Tris-HCl pH 9.0 [modified from (Kiehlbauch et al., 1993)]. PAR fractions were ethanol-precipitated, dissolved in water, concentration determined via absorption at 258 nm, and characterized on a silver-stained sequencing gel (GELCODE Color silver stain, Pierce).

Binding of immobilized proteins and peptides to PAR (PAR-overlay blot)

Proteins were separated by 8% SDS-PAGE and immobilized on a nitrocellulose membrane (GE Healthcare). Peptides were immobilized directly by slot-blotting. Subsequently, membranes were incubated with PAR as indicated in TBST buffer for 1 h at RT before unspecific binding was removed by high-stringency washes using 1 M NaCl in TBST (3 times for 5 min at RT). Blots were blocked in 5% (w/v) milk powder and bound PAR was detected using 10H antibody or streptavidin-HRP (GE Healthcare).

Oligonucleotides

Oligonucleotides were purchased from Sigma-Aldrich. For WRN helicase assays and EMSAs 200 fmol of 5'-biotin-$(TTT)_5$-GAGTGTGGTGTACATGCACTAC-3' oligonucleotide was annealed with 400 fmol of 5'-GTAGTGCATGTACACCACACTC-$(TTT)_5$-3' complementary oligonucleotide by heating to 95°C for 5 min in TE buffer supplemented with 50 mM NaCl followed by cooling to RT. For exonuclease assays, 5'-biotin-$(TTT)_5$-$(TTAGGG)_4$-CATGCACTAC-3' oligonucleotide was annealed with 5'-GTAGTGCATG-$(CCCTAA)_4$-$(TTT)_5$-3' complementary oligonucleotide. Annealing of the oligonucleotides was confirmed via 20% TBE-PAGE followed by semi-dry TBE-blotting. After immobilizing on nylon membranes (GE Healthcare) biotin-labeled oligonucleotides were detected via streptavidin-HRP.

Electrophoretic mobility shift assay (EMSA)

WRN (in concentrations as indicated) was incubated with 200 fmol of the annealed oligoduplex in EMSA buffer containing 40 mM Tris-HCl pH 8.0, 4 mM $MgCl_2$ 0.1 mg/ml BSA, 5 mM DTT and 0.1% (v/v) Nonidet P-40 for 30 min at 4°C in a total reaction volume of

10 µl. To test the influence of PAR on WRN-DNA binding, PAR was added in concentrations as indicated and mixtures incubated for 20 min at RT prior to the addition of oligoduplex. After addition of 4 µl loading dye [40% (v/v) glycerol, 0.05% (w/v) Orange G and 0.05% (w/v) bromphenol blue], DNA and DNA-WRN complexes were separated via 4% TBE-PAGE and detected as described above.

WRN helicase assay

WRN was incubated (at concentrations as indicated) in helicase reaction buffer containing 30 mM HEPES-KOH pH 7.4, 5% (v/v) glycerol, 40 mM KCl, 0.1 mg/ml BSA, 1 mM $MgCl_2$, and 1 mM ATP in a total volume of 10 µl. To test the influence of PAR on the WRN helicase activity, PAR was added as indicated and mixtures were incubated for 20 min at RT prior to the addition of oligoduplex. Helicase reaction was carried out for 20 min at 37°C and was stopped by the addition of 4 µl stop dye [1% (w/v) SDS, 40% (v/v) glycerol, 50 mM EDTA, 0.05% (w/v) Orange G, 0.05% (w/v) bromphenol blue and 0.05% (w/v) xylene cyanol]. Afterwards oligonucleotides were separated by 12% TBE-PAGE and detected as described above.

WRN exonuclease assay

The assay was carried out as described recently (Mangerich et al., 2012). Briefly, 40 nM WRN was incubated in a reaction buffer containing 40 mM Tris-HCl pH 8.0, 4 mM $MgCl_2$, 0.1 mg/ml BSA and 4 mM DTT together with 75 fmol oligonucleotide substrate and concentrations of PAR as indicated for 45 min at 37°C in a total volume of 10 µl. After completion of the reaction, the mixture was immediately transferred on ice, and 90 µl of 30 mM sodium acetate (pH 7.8) and 2 pmol of ^{15}N-labeled-dG (internal standard) were added to the mixture before filtering through a 10-kDa cut-off spin column filter (Pall). Subsequently, nucleotides were dephosphorylated by incubation with 34 U alkaline phosphatase (Sigma-Aldrich) at 37°C overnight. Samples were filtered through a 10-kDa cut-off spin column filter and subjected to LC-MS/MS analysis using a Waters LC-MS/MS system consisting of an HPLC 2695 Separations Module and a Micromass Quattro Micro mass spectrometer equipped with an electrospray ionization source. Samples were resolved using a Hypersil Gold column (150 mm x 2.1 mm; 3 µm particle size; Thermo Fisher) under isocratic conditions with a solvent composition of 97% of 0.1% acetic acid in water and 3% of 0.1% acetic acid in

acetonitrile at a flow rate of 0.2 ml/min and a column temperature of 25°C. The MS was operated in positive ion mode. Multiple reaction-monitoring (MRM) mode was used for data acquisition. Response ratios were obtained by plotting the MRM area ratios between the labeled and unlabeled dG against their corresponding concentration ratios.

Acknowledgements

We thank M. Malanga for her initial help with *in silico* analysis. Furthermore we thank M. Miwa (Nagahama, Japan) and T. Sugimura (Tokyo, Japan) for the kind gift of 10H antibody and A. Marx (University of Konstanz) for sharing scientific equipment. This work was supported by the *Deutsche Forschungsgemeinschaft* (FOR434, Konstanz Research School Chemical Biology [KoRS-CB], and Research Training Group [RTG] 1331) and by the Intramural Program of the National Institute on Aging, National Institutes of Health. O. Popp and S. Veith were supported by fellowships of the KoRS-CB and the RTG 1331, respectively.

Supplementary Data

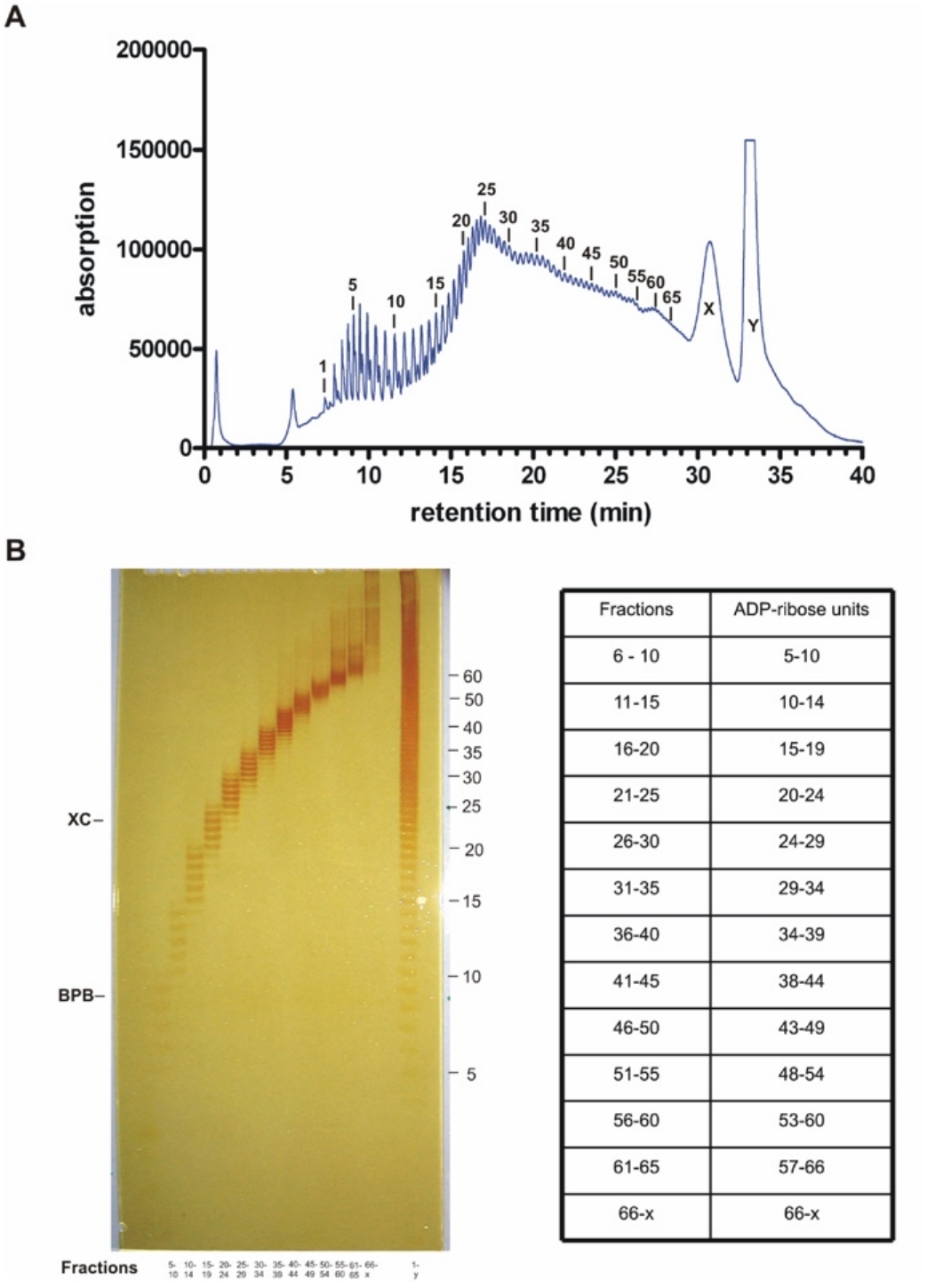

Fractions	ADP-ribose units
6 - 10	5-10
11-15	10-14
16-20	15-19
21-25	20-24
26-30	24-29
31-35	29-34
36-40	34-39
41-45	38-44
46-50	43-49
51-55	48-54
56-60	53-60
61-65	57-66
66-x	66-x

Supplementary Figure 5: Analytical HPLC fractionation of PAR and subsequent characterization of pooled fractions by sequencing gel analysis.
A. 100 nmol of PAR was separated by anion exchange HPLC using a complex salt gradient. Peaks 1-65 are indicated. Peaks X and Y represent long PAR with high branching frequency. **B.** Fractionated PAR was analyzed on modified sequencing gels and silver staining. 100 pmol of each pooled fraction as well as 2 nmol of unfractionated PAR (1-Y) were separated by 15% native PAGE followed by silver staining. Fraction numbers refer to the peak sequence obtained during HPLC. BPB migrates at the same position as an ADP-ribose octamer. BPB, bromphenol blue; XC, xylene cyanol.

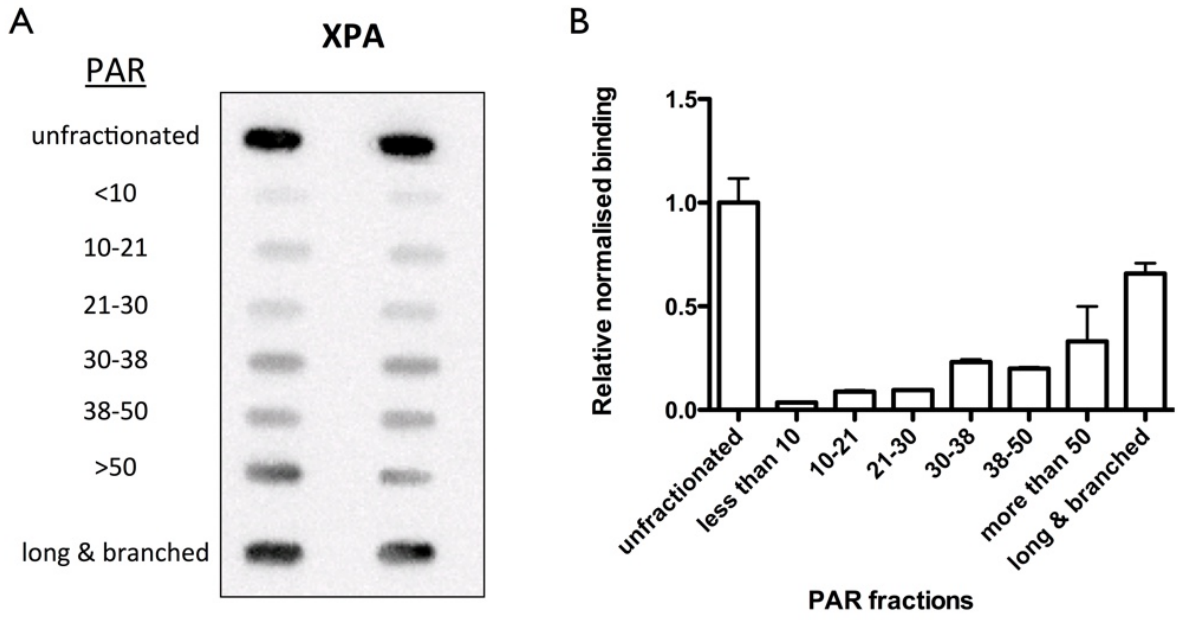

Supplementary Figure 6: XPA binds longer PAR chains with higher affinity than short ones.
A. PAR overlay slot-blot evaluating the dependency of XPA-PAR binding on PAR chain length. XPA (15 pmol/slot) was immobilized on a nitrocellulose membrane (in duplicates) and incubated with 0.2 µM PAR of chain lengths as indicated. Removal of unspecific binding was ensured by high-stringency washing. Protein-bound PAR was detected using the anti-PAR monoclonal antibody 10H. **B.** Densitometric quantification of A, normalized to signals obtained from binding of unfractionated PAR.

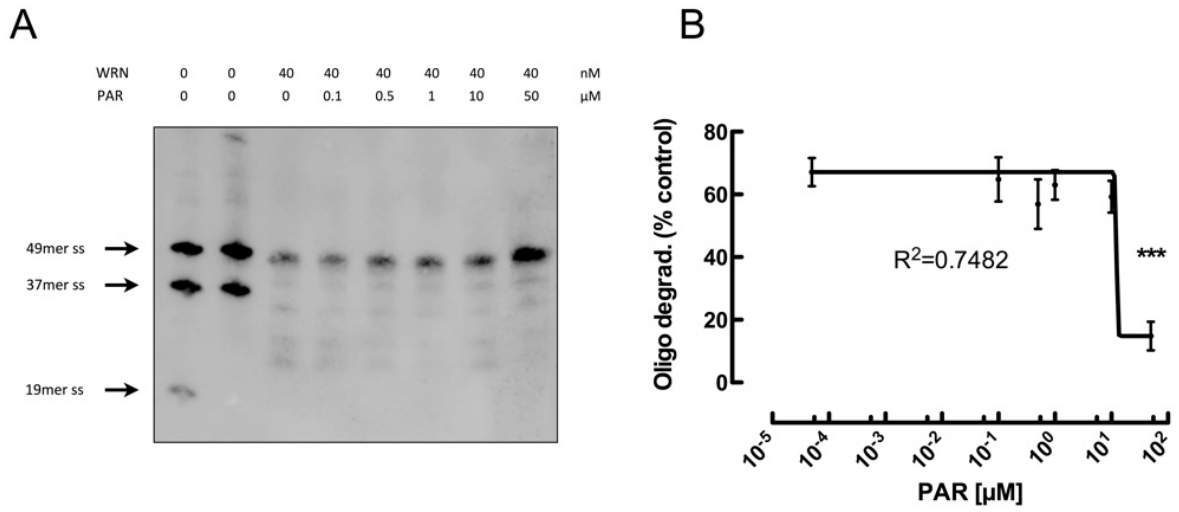

Supplementary Figure 7: Confirmation of the inhibitory effect of PAR on WRN's exonuclease activity.
The impact of non-covalent PAR binding on WRN exonuclease activity was assessed by detection of a 5'-biotin-end-labeled oligonucleotide on a sequencing gel. **A.** WRN (40 nM) was pre-incubated with increasing concentrations of PAR as indicated. Exonuclease reaction was started by addition 300 fmol of a forked oligoduplex and carried out for 15 min. Following electrophoretic separation, products were immobilized on a nylon membrane, and detected via streptavidin-POD. A decrease in degradation of the oligonucleotide by increasing concentrations of PAR is observable. **B.** Densitometric evaluation from four independent experiments (means ± SEM). Curve was fitted using a sigmoidal dose-response curve with variable slope. Statistical analysis was performed with ANOVA followed by Dunnett's multiple comparison post-test. *** $p < 0.001$.

Chapter IV: Differential and concordant roles for PARP1 and poly(ADP-ribose) in regulating WRN and RECQL5 activities

Prabhat Khadka, Joseph K. Hsu*, Sebastian Veith, Takashi Tadokoro, Aswin Mangerich, Raghavendra Shamanna, Deborah L. Croteau, and Vilhelm A. Bohr*

Molecular and Cellular Biology, 2015 Dec 1; 35(23): 3974-89

* Equal contribution

Abstract

Poly(ADP-ribose) polymerase 1 (PARP1) catalyzes the poly(ADP-ribosyl)ation (PARylation) of proteins, a post-translational modification which forms the nucleic acid-like polymer poly(ADP-ribose) (PAR). PARP1 and PAR are integral players in the early DNA damage response, since PARylation orchestrates the recruitment of repair proteins to the damage sites. Human RecQL helicases are DNA unwinding proteins that are critical responders to DNA damage, but how their recruitment and activities are regulated by PARPs and PAR is poorly understood. Here we report that all human RecQL helicases interact with PAR non-covalently. Furthermore, we define the effects that PARP1, PARylated PARP1 and PAR have on RECQL5 and WRN, using both *in vitro* and *in vivo* assays. We show that PARylation is involved in the recruitment of RECQL5 and WRN to laser-induced DNA damage and that RECQL5 and WRN have a differential response to PARylated PARP1 and PAR. Furthermore, we show that RECQL5 or WRN loss results in increased sensitivity towards PARP inhibition. In conclusion, our results demonstrate that PARP1 and PAR actively, and in some instances differentially, regulate the activities and cellular localization of RECQL5 and WRN, suggesting that PARylation acts as a fine-tuning mechanism to coordinate their functions in time and space during genotoxic stress response.

Introduction

Mammalian cells are constantly exposed to various environmental genotoxic stresses that can hamper genomic stability. To maintain genomic integrity, cells have developed various complex DNA repair machineries that effectively identify DNA lesions and activate DNA damage responses (DDRs) and DNA repair (Lord and Ashworth, 2012; Sancar et al., 2004). One of the early DDR mechanisms is the activation of poly(ADP-ribose) (PAR) polymerases (PARPs). PARP1 is the most ubiquitously expressed PARP family member and constitutes the majority of PAR synthesis in human cells (Gibson and Kraus, 2012; Kim et al., 2005). In response to DNA damage, such as single or double DNA strand breaks, PARP1 is activated and promotes PAR synthesis. It utilizes nicotinamide adenine dinucleotide (NAD^+) to form PAR at the DNA lesions or breaks thereby post-translationally modifying itself and other proteins of interest. Importantly, PAR formation is highly dynamic, because shortly after being synthesized, it is rapidly hydrolyzed by PARPs catabolic counterparts, PAR glycohydrolase (PARG) and ADP-ribosylhydrolase 3 (ARH3) (Barkauskaite et al., 2013a;

Meyer-Ficca et al., 2004; Min et al., 2010; Niere et al., 2008). However, neither enzyme is able to remove the last ADP-ribose moiety from acceptor proteins; macrodomain-containing proteins, such as MacroD1 and MacroD2, fulfill this task, leaving behind an unmodified amino acid that is readily available for the next round of PARylation (Jankevicius et al., 2013; Rosenthal et al., 2013). Formation of PAR can act as a docking site to promote protein recruitment and protein-protein interactions. This docking site serves to integrate diverse cellular signaling pathways, including DNA damage detection and repair, transcription, chromatin remodeling, and cell death (Mangerich and Bürkle, 2012). PAR formation plays a critical role in the rapid recruitment of the DNA repair proteins such as MRE11, NBS1, BRCA1 and ATM to DSBs (Haince et al., 2008; 2007; Li and Yu, 2013; Li et al., 2013). Mice lacking PARP1 are extremely sensitive to genotoxic stress, show defects in repair of damaged DNA and display genomic instability with high frequencies of sister chromatid exchanges and chromosomal breakages (Rouleau et al., 2010).

RecQL helicases are a highly conserved family of 3' to 5' DNA unwinding proteins that engage in various roles in DNA metabolic processes and DNA repair pathways to maintain genomic stability. In humans, there are five RecQL helicases: RECQL1, BLM, WRN, RECQL4, and RECQL5 (Brosh, 2013; Croteau et al., 2014). In addition to helicase activity, these RecQL proteins also possess the opposite activity as they can anneal two DNA strands. Furthermore, unlike the other RecQL helicases, WRN possesses a 3'-5' exonuclease activity. Activated PARP1 has been previously reported to covalently modify human RecQL helicases and to modulate their biological activities (Adelfalk et al., 2003; Veith and Mangerich, 2014; Woo et al., 2006). For example, activation of PARP1 can strongly repress RECQL1's ability to restore replication forks (Berti et al., 2013). The exonuclease and helicase activities of WRN are inhibited by the presence of PARP1 and PAR (Kobbe et al., 2004a; Popp et al., 2012). In addition, PARP1 binds to the C-terminal region of RECQL4 and pharmacological PARP inhibition affects RECQL4's nuclear distribution (Woo et al., 2006). Interestingly, $Parp1^{-/-}$ / $Wrn^{\Delta hel/\Delta hel}$ mice develop spontaneous tumors at early ages and the derived mouse embryonic fibroblasts show increased formation of chromosome fragments and chromosomal rearrangements (Lebel et al., 2003). Currently, it is unknown whether PARP1 plays a role in the regulation of RECQL5.

Compared with the other RecQL family members, RECQL5 is the least studied and most poorly understood. Even though no human genetic disorders have been reported to be associated with RECQL5 mutations, human RECQL5 knock-down cells display increased levels of endogenous DNA damage and PAR formation (Tadokoro et al., 2012b). RECQL5-

deficient mice are more susceptible to cancer and show increased levels of spontaneous DNA double-strand breaks (DSBs) and homologous recombination activities (Hu et al., 2007). Thus, RECQL5 may act as a tumor suppressor to maintain genomic integrity.

RECQL5 interacts with several proteins that participate in DNA replication, transcription, and recombination pathways. Previously, RECQL5 was reported to associate with the MRE11-RAD50-NBS1 complex at DSBs to regulate repair (Zheng et al., 2009). DSBs are critical DNA lesions that require an immediate cellular response because failure to do so can result in chromosomal rearrangements, genomic instability, and even cell death. It has been shown that RECQL5 interacts with RAD51 to inhibit RAD51 induced D-loop formation and sister chromatid exchange (Islam et al., 2012). Consistent with this finding, RECQL5 prevents RAD51 ssDNA filament formation by promoting synthesis-dependent strand annealing to mediate DSBs repair (Paliwal et al., 2013). Our previous studies used confocal laser microscopy to study RECQL5's recruitment kinetics to DSBs in real time in live cells (Popuri et al., 2012b). We demonstrated that its recruitment was independent of the activities of MRE11, RNA polymerase II and ATM.

The mechanisms that mediate RECQL5's and WRN's recruitment to DSBs still remain elusive and therefore we sought to further investigate this by exploring the role of PARP1 and PARylation in the recruitment of RECQL5 and WRN to DSBs. In this study, we show that RECQL5 is not a substrate for PARP1 but that RECQL5 can bind to PAR in a non-covalent manner. RECQL5's biochemical activities with or without PARP1 activation are systematically compared with that of WRN's. Both RECQL5 and WRN show helicase and ATPase inhibition by activated PARP1. In contrast, strand annealing by RECQL5 can be stimulated by PAR and to some extent PARylated PARP1 but is inhibited by PARP1. Additionally, we report that the early recruitment of RECQL5 to DSB sites is impaired when PAR synthesis is inhibited. PARP1 is involved in the same pathway as RECQL5 to regulate HR-mediated DSB repair.

Results

RECQL5 interacts with PAR and PARP1

It is well known that PARylation can modulate protein-protein interactions in the regulation of cell signaling pathways through recruitment of PAR-binding proteins. PAR regulates protein function through covalent modification, but also by specific high affinity non-covalent

interactions (Malanga and Althaus, 2011). WRN has recently been evaluated for its PAR binding via a PAR-binding motif (PBM) (Popp et al., 2012). PBMs are suggested to be loosely conserved stretches of amino acids (aa), about 22-25 aa long, that contain positively charged residues followed by basic and hydrophobic rich sequences (Barkauskaite et al., 2013b). Previous studies have shown that RECQL1 and WRN can interact with PAR non-covalently and that this interaction regulates their helicase activities (Berti et al., 2013; Popp et al., 2012). Here we performed a bioinformatic search to identify whether all of the RecQL helicases contain putative PBMs. These results revealed that all five human RecQL helicases do in fact contain putative PBMs (data not shown). To validate the bioinformatic findings, we examined each of the human RecQL helicase proteins, RECQL1, BLM, WRN, RECQL4, and RECQL5, for their ability to bind PAR using far western analysis. Purified recombinant proteins (15 pmol) were separated on an SDS-PAGE gel and then transferred to a nitrocellulose membrane. Immobilized proteins were then incubated with PAR, and the PAR-protein interactions were visualized through immunoblotting analysis. We found that each human RecQL helicase interacts with PAR in a non-covalent manner (Figure 25 A). Using unfractionated PAR, which consists of a mixture of short, long and branched polymer with chain lengths up to 200 ADP-ribose moieties, RECQL5 displayed the highest level of PAR binding compared with the other RecQL family members (Figure 25 A). To independently confirm these results for RECQL5, we employed an *in vitro* PAR-overlay slot blot assay (Figure 25 B). As can be seen low concentrations of RECQL5 were able to capture the PAR probe. EMSA analyses using end-biotinylated PAR of defined chain length (30-35-mer) as a probe (Figure 25 C) confirmed that the RECQL5 and PAR interaction also occurs in solution. From these experiments, we estimated that the K_d value for the RECQ5-PAR interaction is in the nanomolar range, similar to the WRN-PAR interaction (Suppl. Figure 8) and as observed previously for other PAR-interacting proteins (Fahrer et al., 2007). These results suggest that RECQL5 and WRN bind short PAR chains (*i.e.*, 30-35-mer) with similar affinities (Figure 25 C; see also Suppl. Figure 8), whereas unfractionated PAR, which consists mainly of long (>100mer) and branched polymers, is bound much stronger by RECQL5 compared to WRN (Figure 25 A). Further *in vivo* co-immunoprecipitation (IP) assays were performed after treatment of cells with hydrogen peroxide and with or without the PARP inhibitor veliparib (Figure 25 D). It revealed that GFP-RECQL5 can interact with both PARP1 and PAR.

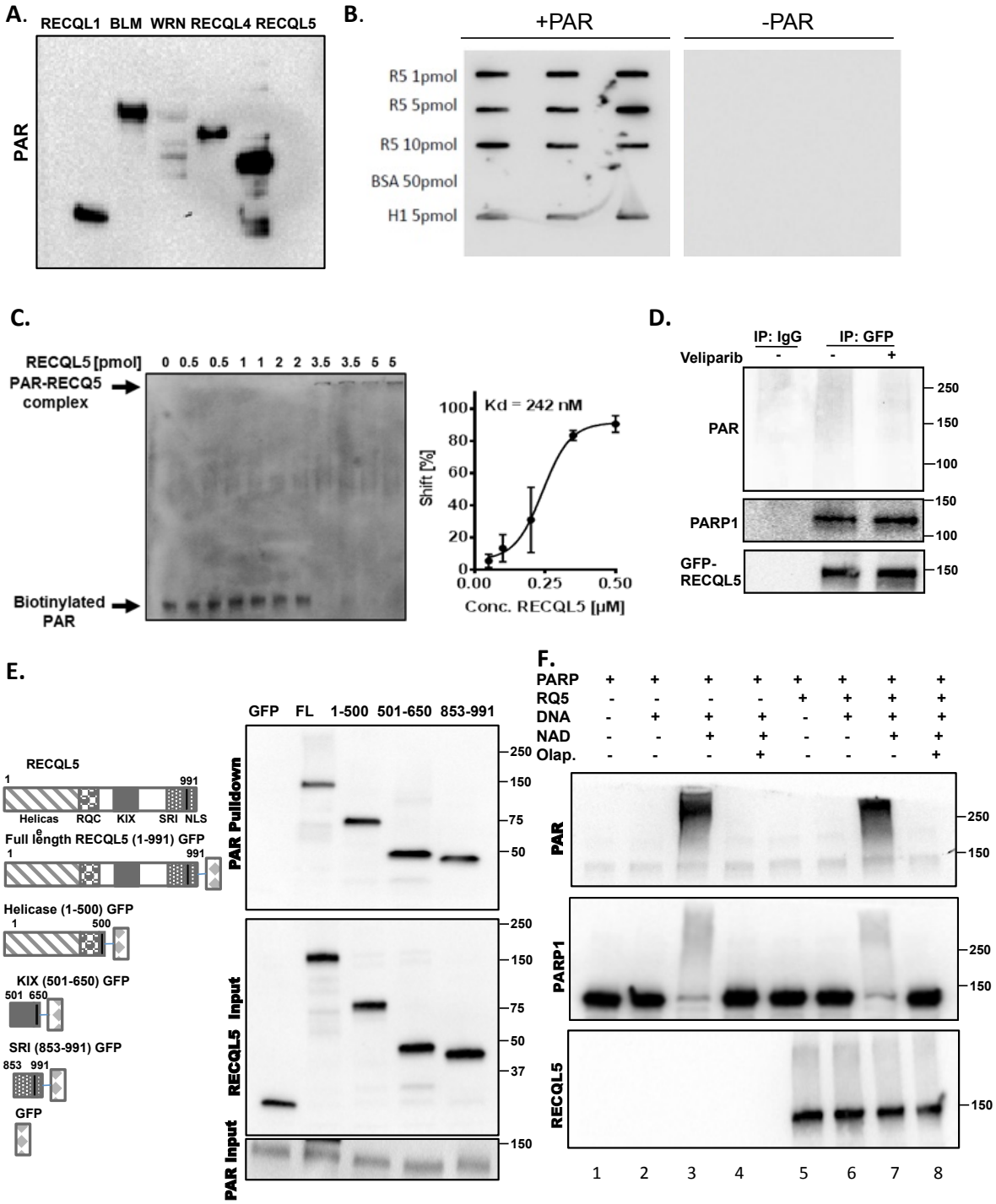

Figure 25: RECQL5 directly binds PAR and PARP1, but is not PARylated by PARP1.
A. Far western analysis showing PAR interaction with all of the human RecQL helicases: RECQL1, BLM, WRN, RECQL4, and RECQL5. Proteins were separated by SDS-PAGE and transferred to nitrocellulose membranes and then incubated with PAR. Immunoblotting was performed to detect the PAR. **B.** PAR-overlay slot blot assay to show interaction between PAR and RECQL5. **C.** Electrophoretic mobility shift assay with end-biotinylated PAR to examine RECQL5-PAR interaction in solution. Size-fractionated PAR (500 fmol) was incubated with increasing concentrations of RECQL5 as indicated, separated via native gel electrophoresis then PAR was detected via streptavidin-coupled HRP. **Right**. Quantitative evaluation of the RECQL5 gel shifts. Shift [%] indicates [signal intensity complexed PAR]/[complexed + free PAR]. Data are expressed as mean ± SEM of triplicates. **D.** HEK 293T cells overexpressing RECQL5-GFP were treated with 0.5 mM H_2O_2 for 10 min with or without 5uM veliparib. Co-immunoprecipitation shows that RECQL5 binds PAR and PARP1 *in vivo*. Input and immunoprecipitated samples were analyzed by western blotting with the indicated antibodies. **E.** Biotin-PAR pull-down assays with RECQL5 fragments. Cell lysates overexpressing control GFP, RECQL5-GFP or the various GFP-tagged RECQL5 domains (helicase, KIX, and SRI domains) were incubated with biotin-labeled PAR, then streptavidin beads were used to pull down the biotin-PAR. **F.** *In vitro* PARylation reactions carried out with the indicated purified recombinant proteins. PARP1 (50 nM), DNA (4 ng/ml), 500 μM NAD^+, 5 μM olaparib and 50 nM RECQL5 were used as indicated in the figure.

The five putative PAR-binding motifs in RECQL5 are shown in Suppl. Figure 9. RECQL5 can be broken down into several well defined domains called the helicase, KIX and SRI domains (Islam et al., 2010). The helicase and KIX domains each contain one putative PBM while there are three sites in the SRI domain. To identify which domains of RECQL5 can bind PAR, we tested the fragments of RECQL5 for PAR binding using PAR pull-down assays. Each of the fragments of RECQL5 displayed PAR binding and the GFP negative-control did not bind (Figure 25 E).

Since RECQL5 could interact with PARP1 and PAR, we investigated whether RECQL5 could be post-translationally PARylated by PARP1. *In vitro* PARylation assays were performed in the presence or absence of NAD^+, DNA, PARP1 and RECQL5. PARP1 was activated in the presence of NAD^+ and DNA (Figure 25 F, Lane 3) as PARylated PARP1 is clearly evident (Figure 25 F). As expected, PARP1 activation was inhibited when the samples were treated with the PARP1 inhibitor olaparib, which works by competing for the NAD^+ binding site on PARP1 (Murai et al., 2012). The same reactions were performed in the presence of RECQL5 to determine if RECQL5 could be a substrate for PARP1. In the presence of NAD^+, PARP1 and RECQL5, we still observed the PARP1 activation, however, there was no formation of high molecular weight modified RECQL5. These results reveal that RECQL5 is not PARylated by PARP1.

RECQL5 helicase is inhibited regardless of the modification status of PARP1

Previous studies show that WRN's catalytic activities are inhibited by PAR and PARP1 (Kobbe et al., 2004a; Popp et al., 2012). Therefore, the effect of PARP1 and PAR on RECQL5 helicase activity was investigated using a forked DNA substrate. RECQL5 exhibits weak helicase activity with intrinsic strand-annealing activity (Garcia et al., 2004), and it is possible that RECQL5's helicase activity might be masked by its intrinsic strand annealing activity *in vitro*, as reported for RECQL4 (Rossi et al., 2010b; Xu and Liu, 2009). Thus, an excess of unlabeled ssDNA was included to enhance the helicase activity of RECQL5 (Suppl. Figure 10). We performed RECQL5 and WRN helicase assays in the presence or absence of PARP1. As shown in Figure 26 A and D, WRN helicase exhibited better unwinding properties compared to RECQL5. Both RECQL5 and WRN helicase activities were inhibited with increasing PARP1.

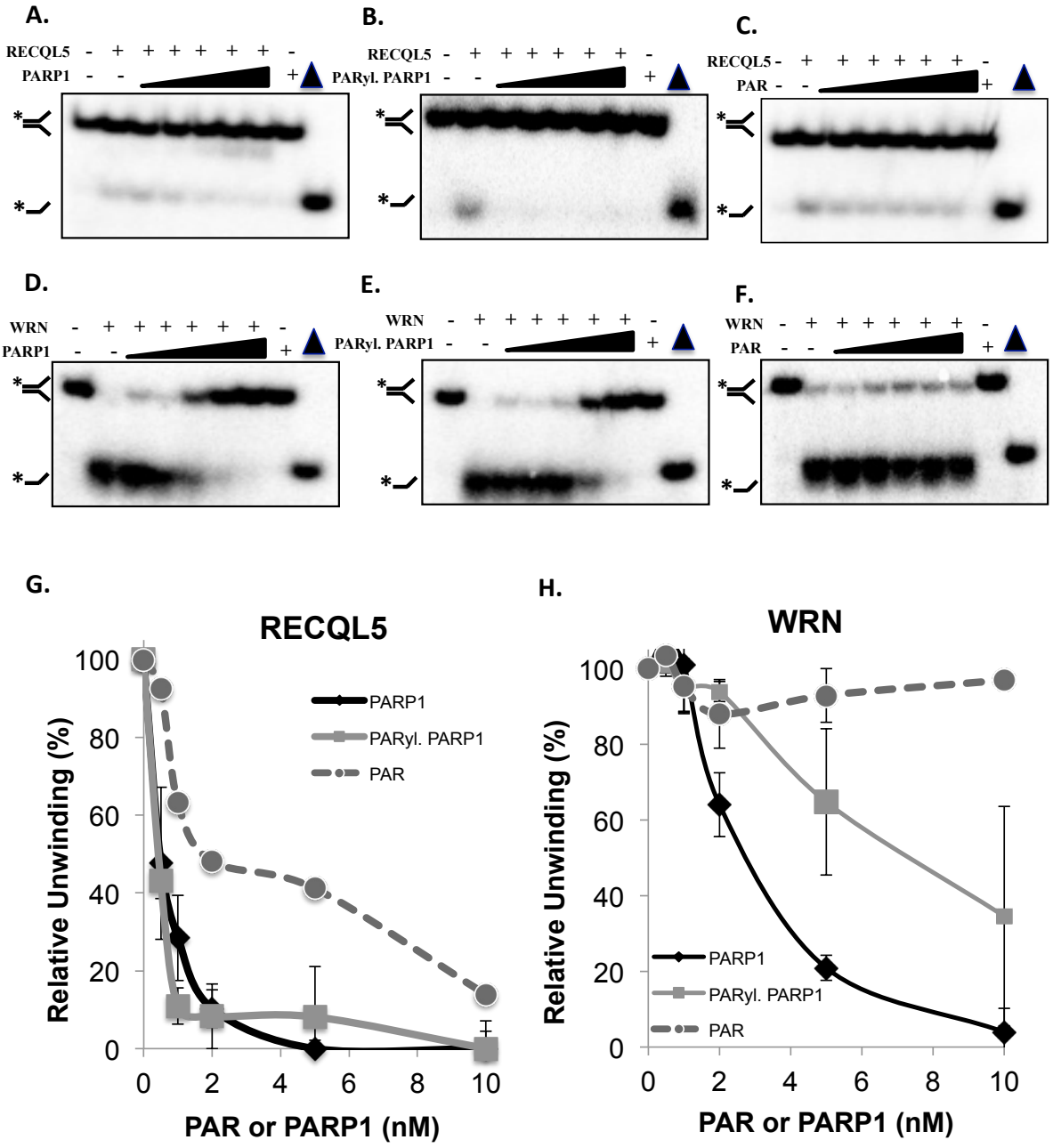

Figure 26: Both RECQL5 and WRN's helicase activities are regulated by PARP1, PARylated PARP1 and PAR. RECQL5's helicase activity in the presence of increasing concentrations (none, 0.5 nM, 1 nM, 2 nM, 5 nM, 10 nM) of PARP1 **(A)**, PARylated PARP1 **(B)** or PAR **(C)**. WRN helicase activity in the presence of none, 0.5 nM, 1 nM, 2 nM, 5 nM, 10 nM of PARP1 **(D)**, PARylated PARP1 **(E)** or PAR **(F)**. **G.** Quantitative analysis of A, B, and C. **H.** Quantitative analysis of D, E, and F. PARP1, PARylated PARP1, or PAR show no helicase properties and the symbol (Δ) marks the denatured substrate control. All experiments were repeated at least three times and the error bars represent standard error of the mean (SEM).

Next, the effect of activated PARP1 on RECQL5 (Figure 26 A&B) and WRN (Figure 26 D&E) helicase activity was analyzed. PARylated PARP1 had a strong inhibitory effect on RECQL5's ability to unwind the forked DNA structures. PARylated PARP1 also inhibited WRN helicase, but less than the non-PARylated form (Figure 26 G&H). The results for WRN are consistent with what has been previously reported (Kobbe et al., 2004a), and suggest that PARP1 differentially regulates the catalytic activities of RECQL5 and WRN.

To examine the effects of PAR-binding on helicase activities of RECQL5 and WRN, various doses of PAR were incubated with the helicases. We noted that RECQL5 helicase activity was inhibited by PAR in a dose dependent manner (Figure 26 C&G), but WRN was only minimally inhibited by PAR treatment (Figure 26 F&H). A previous report showed that WRN helicase activity can be strongly repressed by the presence of PAR (Popp et al., 2012). The difference between these two results can be explained by the PAR concentrations, as levels of PAR were a thousandfold lower in our experiments. Therefore, PARP1, PARylated PARP1, or PAR can inhibit the helicase activities of RECQL5 and WRN, but the extent of inhibition varies. Compared with WRN, RECQL5 showed higher sensitivity because it required lower amounts of PARP1 or PAR to be regulated. The effect of PARP1, PARylated PARP1 or PAR on RECQL5 or WRN's helicase activities are summarized in Table 1.

ATPase is inhibited by PARP1 activation

RecQL helicases hydrolyze ATP to drive unwinding of double stranded DNA. Thus, we investigated the effects of PARP1 and its activated form, PARylated PARP1, on RECQL5 and WRN ATPase activities. PARP1 was activated in the presence of NAD^+ to form PARylated PARP1. As shown in the western blot analysis (Figure 27 A), after incubating PARP1 and NAD^+ there was an increase of high molecular weight modified PARP1 and PAR production. In the presence of PARP1, there was no change on WRN or RECQL5's ATPase hydrolysis (Figure 27 A, lanes 4 versus 5 and lanes 7 versus 8). However, when incubated with PARylated PARP1, the ATPase activity of both WRN and RECQL5 decreased by 27% and 25%, respectively (Figure 27 B). Additionally, RECQL5's ATPase activity could be completely inhibited by high doses of PAR (Figure 27 C, lanes 8, 9, and 10). PAR can partially decrease WRN's ATPase activity, but not in a dose-dependent manner (Figure 27 E, lanes 8, 9, and 10). Increasing concentrations of PARP1 had no effect on ATPase activities of either RECQL5 or WRN.

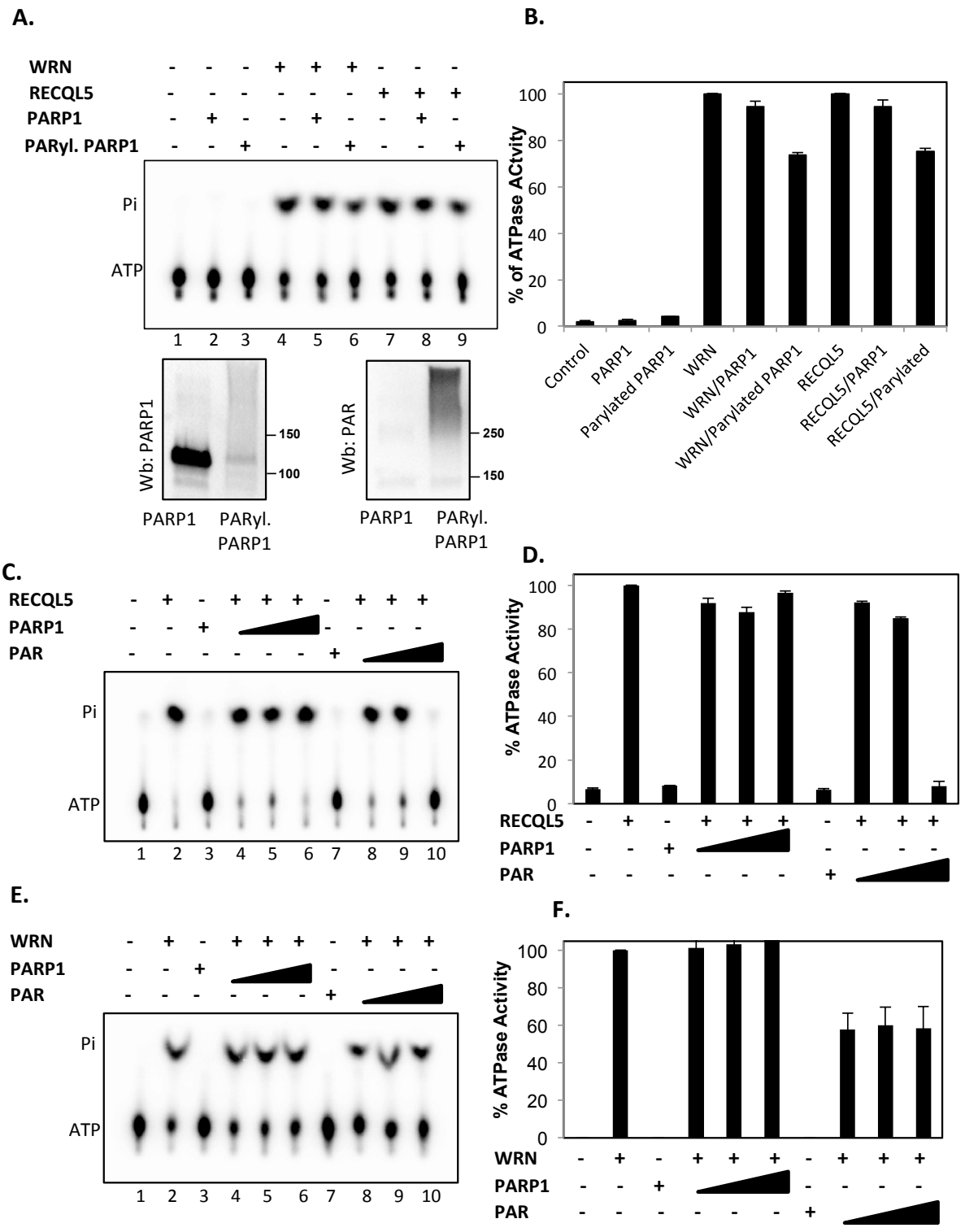

Figure 27: Activation of PARP1 alters the ATPase activities of both RECQL5 and WRN.
A. WRN (5 nM) and RECQL5 (5 nM) ATPase activity in the presence or absence of activated PARP1 (10 nM), as shown. In addition, western blotting showing PAR-staining to demonstrate the extent of PARP1 activation. **B.** Quantification of experiments in panel A. **C.** RECQL5 ATPase activity measured in the presence of increasing concentrations of PARP1 and PAR. None (lane 1), 100 nM PARP1 (lane 3), and 500 nM (PAR) show no ATP hydrolysis. RECQL5 alone (10 nM, lane 2) or with the 25 nM, 50 nM and 100 nM of PARP1 (lane 4, 5, 6) or with 100 nM, 250 nM, and 500 nM of PAR (lane 8, 9, 10). **D.** Quantification C. **E.** Similar to C but in the presence of WRN (5 nM), and quantification **(F).** The values represent an average of three independent experiments; error bars represent SEM.

Strand-annealing activities of RECQL5 are stimulated by PAR

Besides helicase and ATPase activities, RECQL5 and WRN also exhibit ATP-independent single-strand annealing activities. We investigated whether the single-strand annealing activities of RECQL5 or WRN are altered in the presence of PARP1, PARylated PARP1 or PAR. As shown in Figure 28 A, the ability of RECQL5 to mediate strand-annealing was inhibited by increasing concentrations of PARP1. Interestingly, the effect on RECQL5's DNA annealing was promoted by a low level of PARylated PARP1, but was inhibited at high levels of PARylated PARP1 (Figure 28 B). RECQL5's strand-annealing activity could be slightly enhanced by increased levels of PAR in the reaction, while PAR alone had no effect (Figure 28 C). Thus, PARP1, PARylated PARP1 and PAR show more complex effects on strand-annealing, distinct from their uniformly inhibitory effects on the helicase and ATPase activities of RECQL5.

On the other hand, WRN showed inhibition of strand-annealing activity with unmodified PARP1 (Figure 28 D) and PARylated PARP1 (Figure 28 E). It is very likely that PARylated PARP1 represses WRN's strand-annealing ability via steric hindrance. Low concentrations of PAR had no effect on WRN strand-annealing, whereas high PAR concentrations partially inhibited the strand-annealing of WRN (Figure 28 F). Thus, the two RecQL proteins show clear differences with respect to strand-annealing activity in the presence of PARP1, PARylated PARP1 and PAR (Figure 28 G&H). The effect of PARP1, PARylated PARP1 or PAR on RECQL5 or WRN's annealing activities are summarized in Table 1.

PARP activation mediates the early recruitment of RECQL5-GFP to DSBs

Our previous studies have shown that all RecQL helicase proteins are recruited to laser-induced DSB sites (Popuri et al., 2012b; Singh et al., 2010). RECQL5's recruitment to DSBs exhibited the same recruitment kinetic pattern as that of WRN and BLM. PARPs are activated early in response to DNA damage and promote PAR production to allow DNA repair proteins to be recruited to the damage sites. To investigate whether PARylation is important for RECQL5 recruitment to sites of damage, we performed laser micro-irradiation and observed RECQL5 recruitment to DSBs induced by 12% laser strikes from a 435 nm beam. We have previously shown that we generate a majority of DSBs under these conditions (Liberti et al., 2011). Our results indicate that PAR co-localized with the DSB marker 53BP1 at the laser sites 30 seconds after micro-irradiation (Figure 29 A). Using this methodology, we find that

endogenous RECQL5 and WRN as well as PAR can be recruited to the sites of the laser strike.

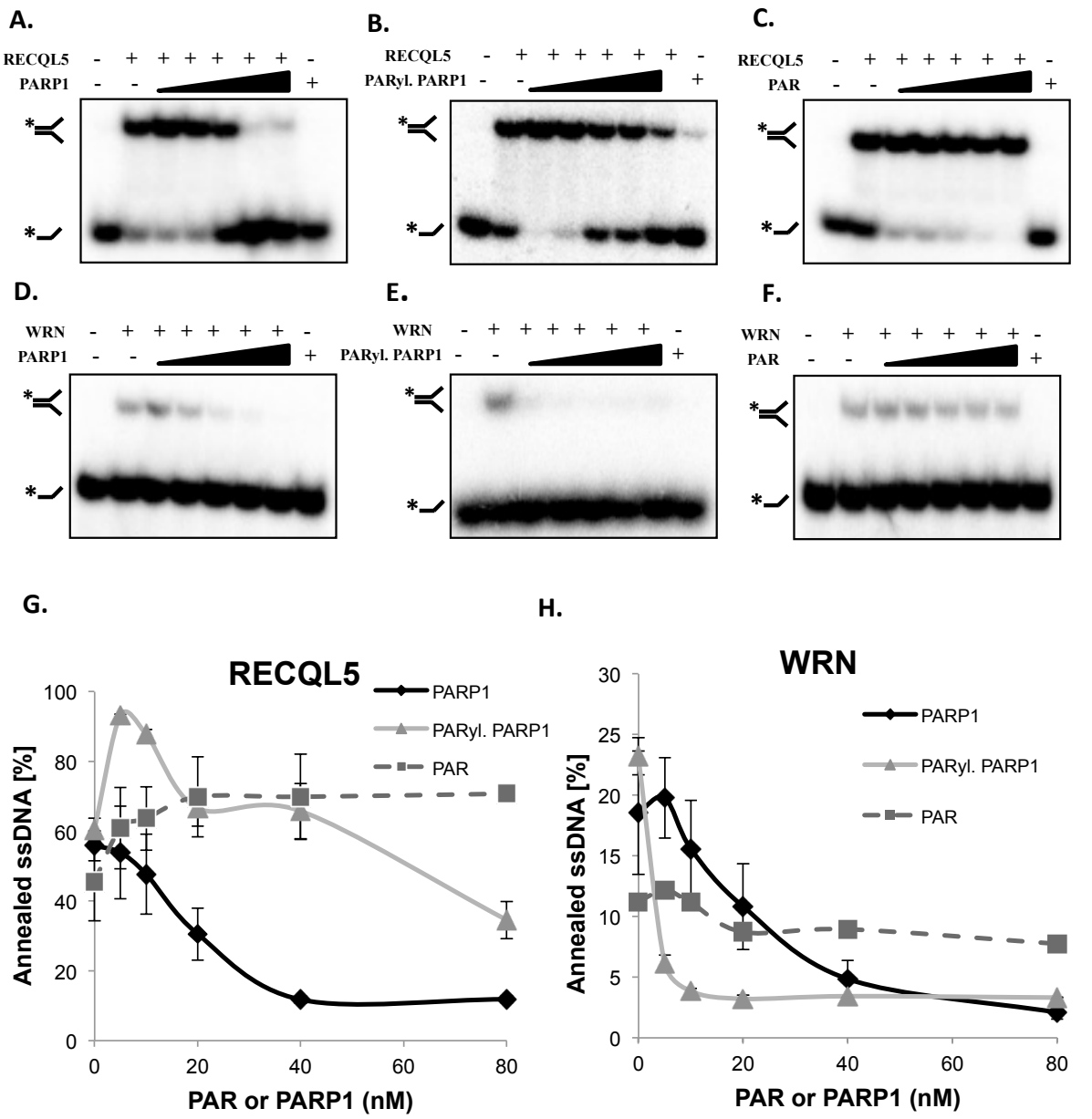

Figure 28: The effects of PARP1, PARylated PARP1 and PAR on single-strand annealing activities of RECQL5 and WRN.
Strand-annealing activity of RECQL5 (10 nM) examined in the presence of the increasing concentrations (none, 5, 10, 20, 40, and 80 nM) of PARP1 **(A)**, PARylated PARP1 **(B)**, and PAR **(C)** with the radiolabeled ssDNA fork DNA and its complimentary single-strand DNA. **G.** Quantitative results of A, B, and C. WRN's (10nM) strand-annealing activity measured in the presence of increasing doses of PARP1 **(D)**, PARylated PARP1 **(E)**, and PAR **(F)** same concentrations as for RECQL5. **H.** Quantification of D, E, and F. The values represent an average of three independent experiments; error bars represent SEM.

To determine if PAR or PARP1 regulate WRN and RECQL5 recruitment to sites of laser damage, we measured the recruitment kinetics of GFP-tagged RecQLs to the DSBs when PAR synthesis was inhibited by either olaparib or veliparib. Both inhibitors compete for PARP1's NAD^+ binding pocket and trap PARP1 at DNA strand breaks (Murai et al., 2012).

In response to laser micro-irradiation, RECQL5-GFP was rapidly recruited to DNA damage sites (Figure 29 B; see also Suppl. Figure 11 A-C). However, when cells were pre-treated with the PARP inhibitors, RECQL5 did not respond to the laser strikes immediately. RECQL5 eventually recruited to the damage site at later time points but the extent of recruitment was weaker. In control cells, 100% of RECQL5 recruited to the damage sites 10 min after the laser strikes whereas in PARP inhibitor treated cells, 30% (olaparib) and 52% (veliparib) of RECQL5 recruited to the sites (Figure 29 C). This suggests that PARP activation is mediating the early RECQL5 recruitment and the later recruitment of RECQL5 is independent of PAR synthesis or alternatively that DNA damage processing is delayed when PAR synthesis is inhibited and consequently RECQL5's recruitment is slowed.

In comparison, GFP-WRN was quickly able to relocate to the DNA damage sites right after the laser strikes, and like for RECQL5, GFP-WRN's recruitment to the DNA damage site was inhibited by PARP inhibitors because the overall extent of recruitment was lower after olaparib or veliparib treatment (Figure 29 D and E; see also Suppl. Figure 11 B-D). GFP-WRN recruitment level dropped to 64% (olaparib) and 74% (veliparib). These data demonstrate that PARP activity is required for both RECQL5 and WRN full recruitment to sites of laser-induced DSBs.

Pharmacological PARP inhibitors target all DNA damage dependent PARP homologs (*i.e.*, PARP1, PARP2, and PARP3). Since both RECQL5 and WRN interact with PARP1, we also wanted to determine whether recruitment of both proteins was dependent on the presence of PARP1. HeLa *PARP*1 knock-out cells generated by TALEN-mediated gene targeting were used to investigate the proteins' recruitment dynamics. These cells are completely null for PARP1 (see Suppl. Figure 12). Lack of PARP1 had a moderate effect on the recruitment of RECQL5-GFP and GFP-WRN (see Suppl. Figure 12 A-E). Recruitment of both proteins could be visualized at the earliest time points, however the proteins varied with respect to the extent of recruitment. While GFP-WRN eventually reached its full potential for recruitment between 400-600 sec, RECQL5-GFP did not, even after 10 minutes. In order to further suppress PARylation by other PARPs, veliparib was added to the cells and recruitment of the proteins was monitored. Curiously, veliparib had a more pronounced effect on the recruitment of GFP-WRN than RECQL5-GFP, as GFP-WRN showed a delay in its early recruitment dynamics. Decreased levels of RECQL5, however, could be visualized during both the early and later recruitment phases and veliparib treated cells showed no difference compared to the *PARP1* KO cells (see Suppl. Figure 12 D&E).

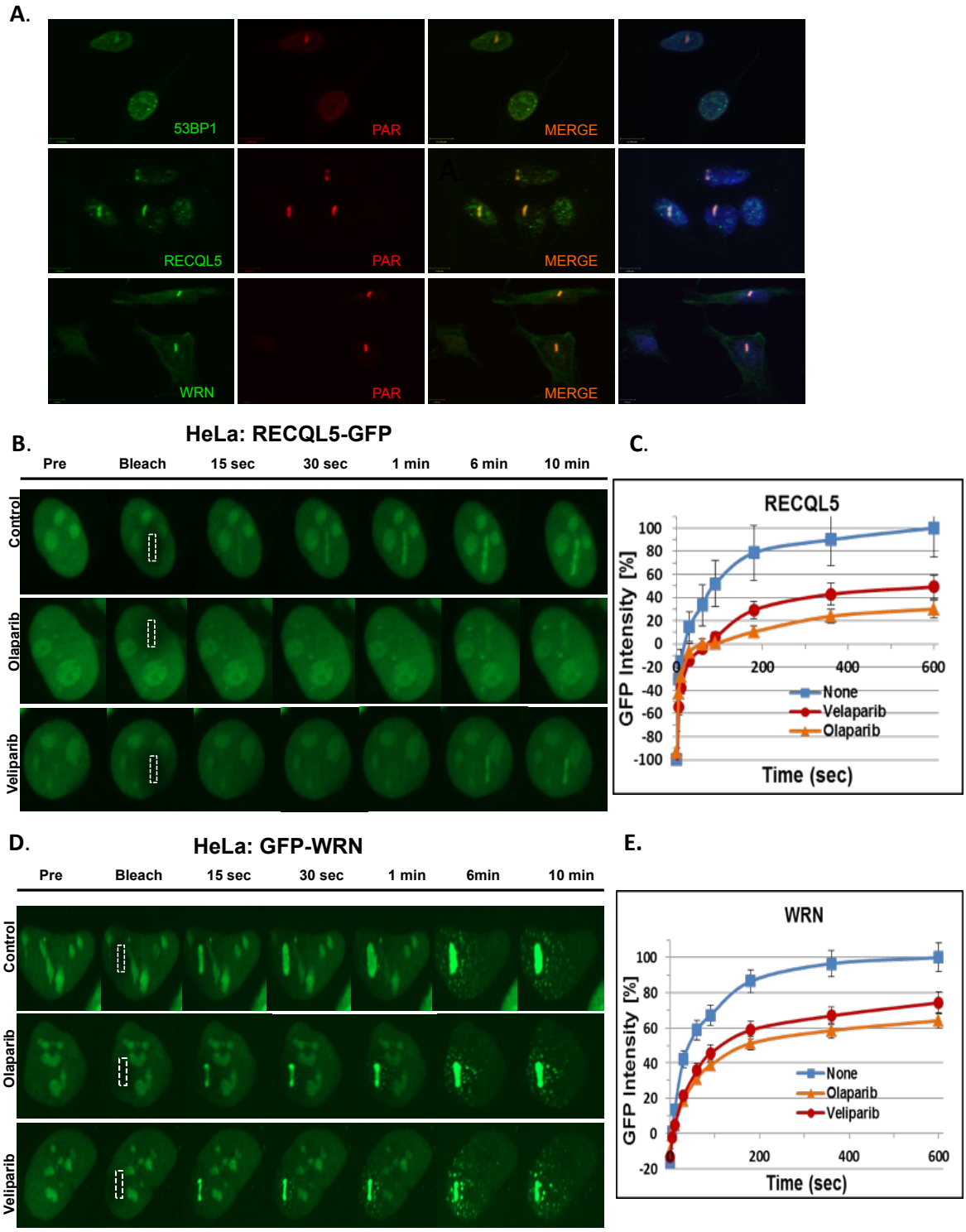

Figure 29: PARylation regulates the early recruitment of RECQL5 to laser induced DNA damage.
A. RECQL5 and WRN display co-localization with PAR at the DNA lesions. HeLa cells were struck with 12% laser strikes to induce DNA damage. Cells were immunostained with PAR and 53PB1, RECQL5, or WRN antibodies. GFP tagged **(B)** RECQL5 or **(D)** WRN were transiently transfected into HeLa cells for 24 h. The overexpressed cells were pre-treated for 3h with vehicle control, 5 µM olaparib or 5 µM veliparib, and then targeted with the 12% laser strike to induce DSBs. The cells were imaged at the indicated time points to observe recruitment of the proteins to the DNA damage. Recruitment kinetics of at least twenty cells from three independent experiments were quantified for RECQL5-GFP **(C)** and GFP-WRN **(E)** and the relative signal intensities at the laser line were calculated using velocity software and plotted versus time. The white box with the dotted outline indicates the laser striking area. Absolute values are reported in Suppl. Figure 11. The error bars represent SEM.

These results suggest that even though PARP1 is the most ubiquitously expressed PARP enzyme, other PARPs also contribute to PAR synthesis at sites of DNA damage. Finally, we summarized RECQL5 or WRN's recruitment at DSB sites in *PARP1* KO cell and with PARP inhibitors in Table 1.

Previously, we reported that RecQL helicase proteins are retained for several hours at sites of laser-induced DNA damage (Popuri et al., 2012b), therefore, we wanted to determine if the absence or presence of PARP1 could alter retention kinetics. As shown, GFP-RECQL5 is normally retained for more than three hours at laser strikes and that is also true in *PARP1* KO cells (see Suppl. Figure 12 F). In addition, we also examined the effects of DNA repair protein kinases on RECQL5's recruitment to DSBs. We still observed the recruitment of RECQL5 although the amount of recruitment varied after various treatments. We examined the effects of VE821 (an ATR inhibitor), KU55933 (a PI3K inhibitor), and Torin 2 (an ATR, ATM, DNA-PK, and mTOR inhibitor) (see Suppl. Figure 13). When co-treating with veliparib, RECQL5's recruitment, under both high dose KU55933 and Torin 2 conditions, was strongly impaired. Thus, these findings further support the notion that after DSBs the early recruitment of RECQL5 depends on the activation of PARPs, and that the later recruitment of RECQL5 might be associated with the activation of DNA signaling proteins, like ATM, ATR, and DNA-PK.

Loss of RECQL5 or WRN is associated with high sensitivity to PARP inhibitor

Since PARP inhibition was associated with significant inhibition of RECQL5 and WRN recruitment to DSB sites, we asked whether depletion of RECQL5 and WRN by siRNA would lead to an increased sensitivity to PARP-inhibition. To test this we used two different cell lines (HeLa and HEK293T) that expressed normal levels of RECQL5 and WRN (Figure 30 A&B). In both cell lines, transfection with RECQL5 and WRN siRNA efficiently depleted endogenous proteins (Figure 30 A&B). We next assessed PARP inhibitor sensitivity in the RECQL5 and WRN-depleted cells in the presence of increasing concentration of PARP inhibitor (veliparib at 0, 1, 10 and 100 nM) using a cell counter (Beckman Coulter Z1Coulter Particle Counter). Upon depletion of RECQL5 and WRN, we consistently observed a decrease in cell viability in the presence of increasing concentrations of veliparib (Figure 30 B) in both cell lines. The HeLa cells were generally more sensitive, so we observed the effect at lower concentrations of PARP inhibition.

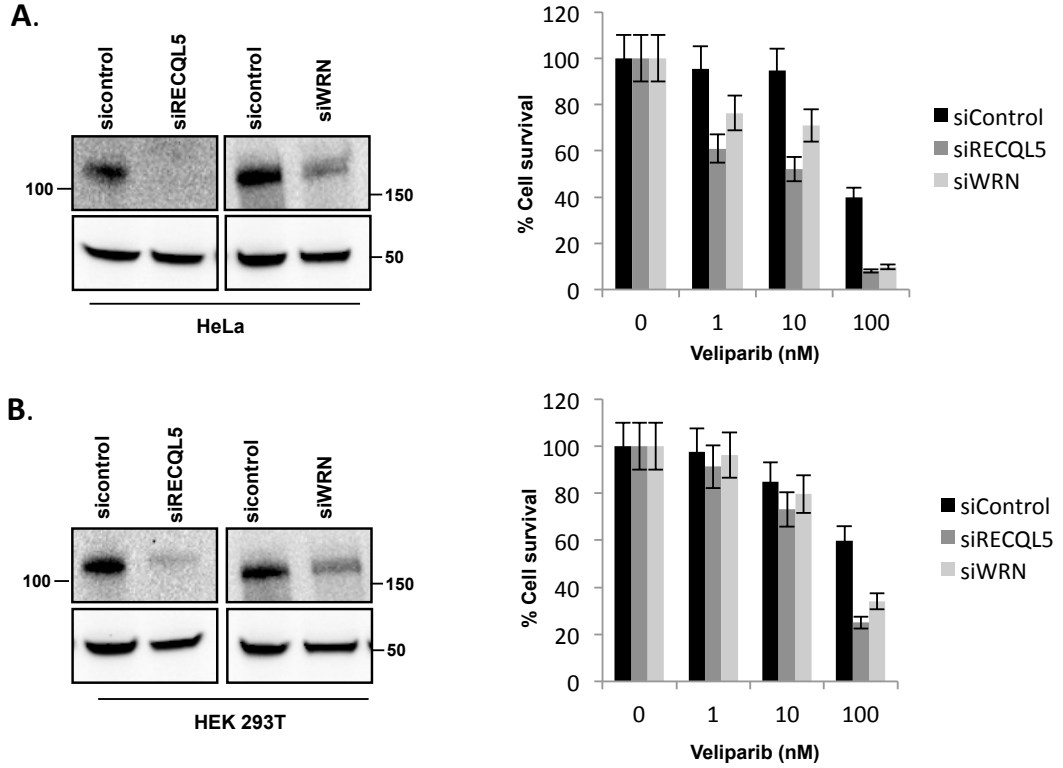

Figure 30: Cancer cell lines with loss of RECQL5 or WRN show increased sensitivity to PARP inhibitor.
A. Western blot demonstrating the expression status of RECQL5 or WRN in HeLa cell line, treated with respective siRNA **(Left Panel)**, demonstrating the sensitivity to the PARP inhibitor (veliparib 0 nM, 1 nM, 10 nM, 100 nM) in RECQL5 or WRN knock-down HeLa cell line **(Right Panel)**. **B.** Western blot demonstrating the expression status of RECQL5 or WRN in HEK293T cell line, treated with respective siRNA **(Left Panel)**, demonstrating the sensitivity to the PARP inhibitor (veliparib) in RECQL5 or WRN knock-down HeLa cell line **(Right Panel)**. Tubulin was used as loading control for western blot. All cell lines were treated in triplicates for 4 days. Survival is represented in percentage of the control (DMSO treated). The cell numbers were quantified using a colorimetric method (SRB). The error bars represent SEM.

PAR formation regulates the recruitment of RECQL5-GFP domains to DSB sites

Having demonstrated that early recruitment of RECQL5-GFP is impacted by olaparib and veliparib (Figure 29 A&B), we next sought to determine which RECQL5 domains are associated with the PAR-dependent DSBs recruitment. The three RECQL5 constructs, helicase, KIX, and SRI domains as shown in Figure 25, were evaluated. As shown in Figure 31, all three GFP-tagged RECQL5 domains displayed fast recruitment to the DNA damage sites. Unlike the full length protein and as we have reported previously (Popuri et al., 2012b), the three GFP-RECQL5 fragments were not retained but instead completely disappeared from the damage sites after three minutes. Upon treatment of cells with veliparib, there was a dramatic loss of the recruitment signal for each of the GFP-RECQL5 fragments. Interestingly, the GFP-KIX domain showed only minor recruitment to damage sites. These findings are in agreement with Figure 25 E that all three of RECQL5 domains can interact with PAR and here we show that recruitment of these fragments is altered by PARP inhibition. Thus,

without PAR formation, the helicase, KIX, and SRI domains of RECQL5 were not recruited to DNA damage sites. Taken together, these results strongly demonstrate that more than one domain of RECQL5 is needed for its full recruitment to DSB sites and that PARylation impacts recruitment of each of the GFP-RECQL5 fragments.

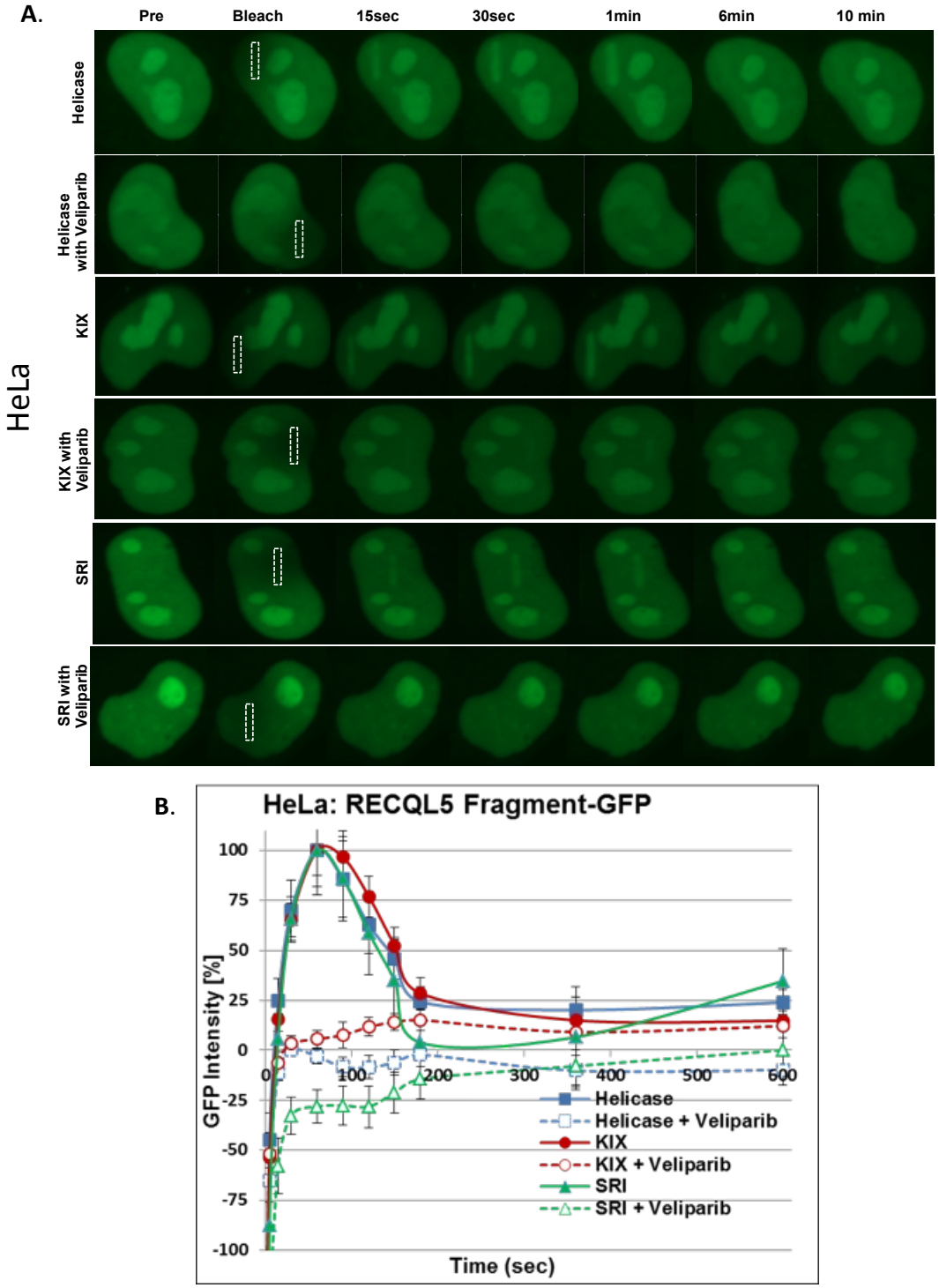

Figure 31: RECQL5-GFP fragment's recruitment to laser induced DSBs depends on PARP1's PARylation activity. **A.** The various C-terminally GFP-tagged RECQL5 domain constructs, helicase (1-500), KIX (501-650), and SRI domain (853-991), were expressed in HeLa cells. Before inducing DSB damage with the laser (12% intensity), the cells were treated for 3 h with vehicle control or 5 µM PARP1 inhibitor veliparib. **B.** Graphical quantification of the recruitment dynamics of the RECQL5-GFP fragments to the laser strike with or without veliparib treatment. The white box with the dotted outline indicates the laser striking area. Three independent experiments were performed and at least twenty cells were quantified for each sample and error bars represent the standard error of the mean (SEM).

RECQL5's role in homologous recombination DSB repair depends on PARP1

Homologous recombination (HR) and non-homologous end joining (NHEJ) are the two major pathways for DNA DSB repair. RECQL5 has previously been shown to mediate non-crossover HR DSB repair (Paliwal et al., 2013). Yet, it is unclear whether PARP1 plays a role in the process of the repair here or whether RECQL5 has any function in regulating NHEJ-mediated repair. Here, we investigated the effect of PARP1 on HR or NHEJ-mediated DSB repair plus or minus RECQL5 or WRN knock-down. We adopted an established U2OS/DR-GFP system to analyze HR-mediated DNA repair efficiency and HCA2 NHEJ-I9A and pEGFP-Pem1-Ad2 reporter systems to study NHEJ-mediated DNA repair capacity *in vivo* (Mao et al., 2008; Stark et al., 2004). After knock-down, the cells were transfected with a plasmid expressing the restriction enzyme I-SceI to induce DSBs in the reporter cassettes or with NHEJ reporter plasmid, pEGFP-Pem1-Ad2 cut with HindIII or I-SceI restriction enzymes, along with a control reporter plasmid DsRed. *In vivo* DSB repair efficiency was measured based on the expression of the green fluorescent protein (GFP), which is translated from the cassettes repaired either by HR (U2OS/DR-GFP cassette) or NHEJ (HCA2 NHEJ-19A and pEGFP-Pem1-Ad2 cassettes) pathway, by flow cytometry.

U2OS cells lacking RECQL5 or PARP1 showed decreased homology directed repair efficiency, but knock-down of WRN had no effect (Figure 32 B). Interestingly, when both WRN and PARP1 or RECQL5 and PARP1 were depleted, the extent of HR repair was reduced to similar levels as knock-down of PARP1 alone, indicating no additive effects. The importance of RECQL5 in NHEJ was tested *in vitro* and *in vivo* in U2OS and HeLa cells knocked down for RECQL5 (Figure 32C). Examination of end-joined products from *in vitro* NHEJ assays indicated that knock-down of RECQL5 had no significant effect on the generation of dimer, trimer and higher multimers (HM) (Figure 32 D). Further, analysis of EGFP fluorescence from the siRNA-knock-down cells transfected with HindIII and I-SceI linearized pEGFP-Pem1-Ad2 plasmid suggested that RECQL5 has no significant effect on the end-joining mediated by NHEJ *in vivo* (Figure 32 E). Similar results were obtained with the HCA2 NHEJ-I9A system (data not shown). Together these results suggest that RECQL5 participates in HR-mediated DSB repair pathway as PARP1, but not in the NHEJ.

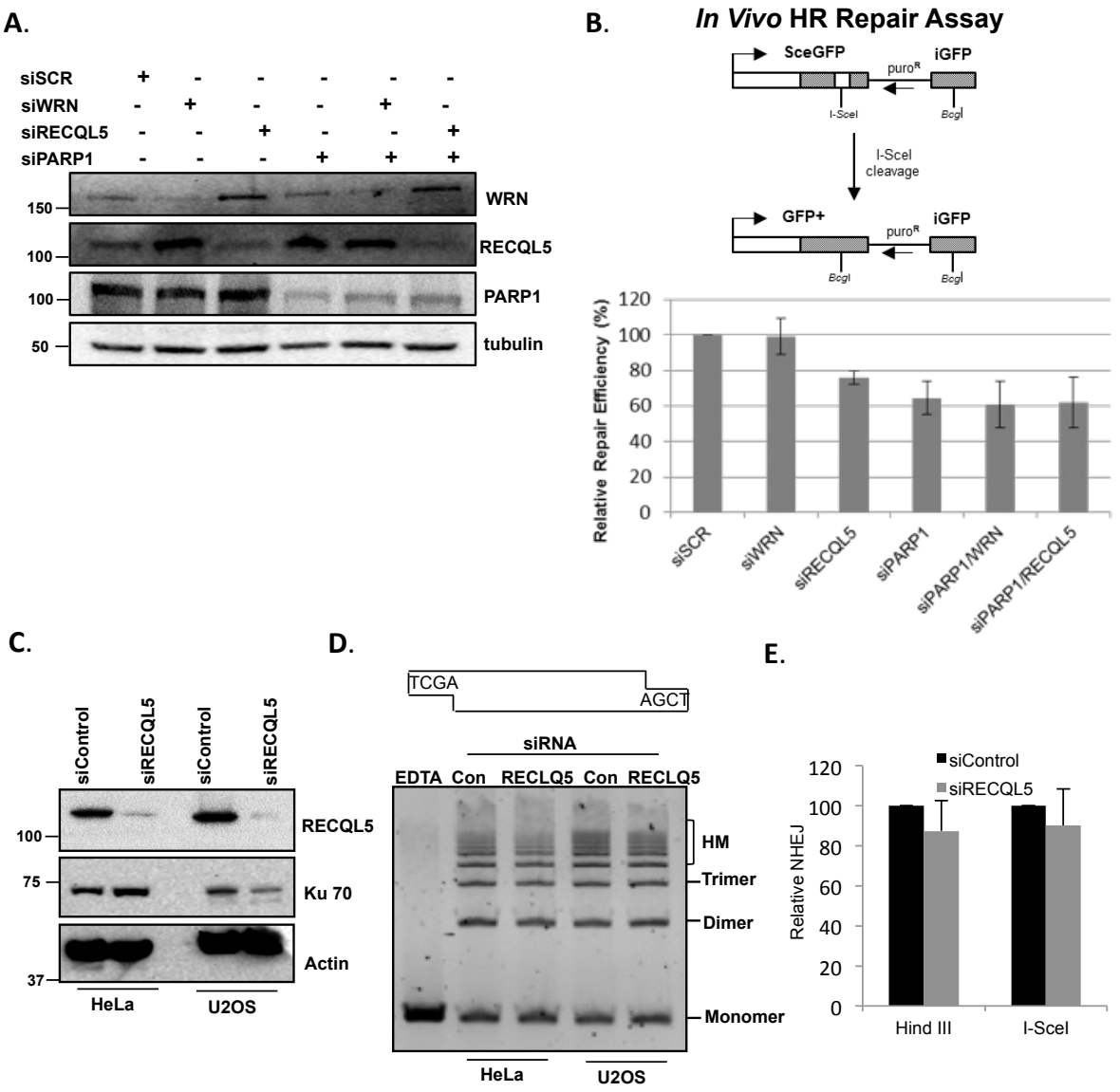

Figure 32: The effects of PARP1 on WRN or RECQL5 mediated HR or NHEJ DSB repair *in vivo*.
A. Western blot analysis of the U2OS/DR-GFP cells that were knocked down for WRN, RECQL5, PARP1, WRN & PARP1, and RECQL5 & PARP1. Cells were transfected with the indicated siRNA and cell extracts were analyzed by western blot and probed with the indicated antibodies. **B.** The effect of WRN, RECQL5, and PARP1 on the efficiency of repairing I-SCE mediated DSBs through HR. **Upper panel:** the scheme of the reporter cassette. Knock-down U2OS/DR-GFP cells were transfected with a plasmid expressing I-SCE. The cells, which repair the GFP cassette will express GFP and are measured by flow-cytometry. **Lower panel:** the repair efficiency of HR repair is relative to the siSCR condition, which is set arbitrarily to 100%. Fifty thousand events were collected for each point and five independent experiments were quantified and error bars indicate SEM. **C.** Cells were transfected with RECQL5 siRNA and cell extracts were analyzed by western blot and probed with the indicated antibodies and the same extracts were used for NHEJ assay. **D.** *In vitro* NHEJ assay on cohesive-end containing DNA substrate with cellular extracts prepared from siControl and siRECQL5 HeLa and U2OS cells. The end-joining assays were performed with *Sal*I-linearized pUC18 DNA substrate. The products were resolved by agarose gel electrophoresis, the gel shows the total end joining from three independent experiments. DNA substrate, with end sequence, used in the NHEJ is shown on the top of gel. EDTA marks the control reaction in the presence of EDTA. **E.** *In vivo* NHEJ assays with cohesive and non-cohesive end containing DNA substrates. U2OS siControl and siRECQL5 cells were transfected with either *Hind*III digested (cohesive ends) or *I-Sce*I digested (non-cohesive ends) linearized pEGFP-Pem1-Ad2 reporter plasmid. Twenty-four-hour post transfection, the cells were harvested and analyzed by flow cytometry for EGFP and DsRed positive cells. Bar graph represents the quantification of EGFP-positive cells normalized to DsRed-positive cells from three independent experiments. The error bars represent the standard deviation.

Table 1: Summary of interacting partner's effect on human RecQL protein activities.
RECQL5 and WRN's DNA strand annealing and helicase activities were performed in the presence of PARP1, PARylated PARP1 or PAR. (+) represents minimal stimulation, (+ +) represents greater stimulation, (-) represents minimal inhibition, (- -) represents greater inhibition, (- - -) represents greatest inhibition and NA represents not affected. Lower panel: effect of PARP1 protein or activity loss on recruitment of RECQL5 and WRN to double-strand break sites.

Interacting Partner	**Strand Annealing**		**Helicase Activity**	
	RECQL5	WRN	RECQL5	WRN
PARP1	- -	- -	- -	- - -
PARylated PARP1	+/-	- - -	- - -	- -
PAR	+ +	NA	-	NA

Cell line or treatment	**Recruitment at DSB Site**	
	RECQL5	WRN
PARP1 KO # 1 cell line	Delayed, relative to WT cells	Delayed, relative to WT cells
+ PARP1 Inhibitor (veliparib)	Delayed	Delayed
+ PARP1 Inhibitor (olaparib)	Delayed	Delayed

Discussion

Recently there has been a lot of interest in defining the role of PARP1 and PAR in the DNA damage response network. Many PAR binding partners have been reported to be DNA repair and checkpoint proteins and PAR formation can act as docking sites for signal recruitment of proteins to initiate DDR (Ahel et al., 2008; Pleschke et al., 2000). Targeting of these proteins to PAR depends on their PAR recognition domains. Thus far, six different protein modules that non-covalently interact with PAR have been identified. One, called PBM, is approximately 22-26 residues long containing a mix of basic and hydrophobic amino acids (Krietsch et al., 2012; Pleschke et al., 2000). A second one is called the macrodomain which is comprised of ~190 amino acids; PARP9, PARP14, PARP15 have been reported to contain macrodomains (Krietsch et al., 2012). A third one has been described as a PAR-binding zinc finger motif (Ahel et al., 2008). Furthermore, for proteins with WWE, BRCT or FHA domains it has been demonstrated that their recruitment to DNA damage sites depend on PAR binding (Li et al., 2013; Wang et al., 2012). Examination of the primary sequence of each of the human RecQL helicases reveals that they have multiple versions of the PBM-type motif and RECQL5's motifs are shown in Suppl. Figure 9. Consistent with this bioinformatics analysis, all five human RecQL helicases show PAR binding ability (Figure 25), with K_d values in the nanomolar range and RECQL5 showing the strongest affinity of all RecQL helicases to unfractionated, long and branched PAR.

PARP1 and PAR have been reported to regulate the activities of RECQL1 and WRN (Berti et al., 2013; Popp et al., 2012) and PARP1 has been reported to interact with RECQL4 (Woo et al., 2006), yet there have been no reports regarding PAR interaction with RECQL5. RECQL5 interacts with PARP1, but RECQL5 is not post-translationally modified by PARP1 (Figure 25). To further characterize the RECQL5 helicase, KIX, and SRI domains for PAR binding, we found that indeed each fragment was able to bind PAR. Additionally, the three domains all displayed fast recruitment to DSB sites but were poorly retained (Figure 30). This finding is in contrast to what we observed for the full-length protein, which is retained for hours (Suppl. Figure 11). Previously, we reported that only the helicase and KIX, but not the SRI domains, were recruited to DSBs (Popuri et al., 2012b). Perhaps, the two observations can be explained by the use of different laser intensities: the previous paper used 7% whereas here 12% was used. We are introducing more damage and more DSBs with the higher intensity. Even at higher laser intensity, recruitment of all three RECQL5 fragments was inhibited in the presence of veliparib, indicating that their recruitment depends on PARP activation. This

finding supports our PBM computation analysis and biotin-PAR pull-down findings that the three RECQL5 domains contain a *bona fide* PBM site (Suppl. Figure 9).

RECQL5 and WRN share many biochemical properties: helicase, ATPase and strand-annealing activity. Therefore, we sought to investigate how these activities are modulated by PARP1, PARylated PARP1 and PAR. Both RECQL5 and WRN helicase activities were inhibited by the presence of PARP1, PARylated PARP1, or PAR as shown in Figure 26. PARylated PARP1, but not unmodified PARP1, partially repressed the ATPase activity of both proteins. Taken together, the results suggest that PARP1, PARylated PARP1, or PAR inhibition of RECQL5 and WRN helicase activity might be simply associated with competition for substrate. Therefore PARP1 might prevent unwinding of a fork duplex by binding the DNA substrate with higher affinity than RECQL5 or WRN. Thus, the results suggest that the RecQL interaction with PARP1 or PAR structurally interferes with the activities of RECQL5 and WRN. Interestingly, strand-annealing analysis revealed differences between the proteins. PAR had no significant effect on WRN's single strand annealing activity, whereas it promoted single strand annealing by RECQL5. In contrast, PARP1 repressed both RECQL5 and WRN's abilities to mediate single strand annealing. It has been demonstrated that RECQL5 prevents the access of RAD51 to single strand DNA (ssDNA) to form D-loop DNA structures, which can promote homologous recombination events to form genomic instability (Hu et al., 2007). Our findings indicate that PAR may promote RECQL5's single strand annealing which may further impede RAD51's activity.

Consistent with our previous observation (Popuri et al., 2012b), both RECQL5 and WRN exhibit rapid re-localization to DNA lesions in response to laser-induced DSBs. PARP1 is well known for its role early in the steps of the DNA repair pathway by acting as a sensor of DNA breaks and becoming enzymatically activated to form PAR. We noted that by using PARP-specific inhibitors, olaparib and veliparib, RECQL5 and WRN recruitment to DSBs is affected. RECQL5 recruitment at early time points is abrogated to a greater extent than WRN (Figure 29; see also Suppl. Figure 11). Additionally, the extent of recruitment for both helicases is greatly reduced when treating cells with olaparib and veliparib. These findings indicate that PARP activation is important for RecQL response to DSBs. In the context of the *PARP1* KO cells plus veliparib (Suppl. Figure 13), WRN's early recruitment was more strongly affected by PARP inhibition, while RECQL5's later recruitment was nullified. As mutations in checkpoint and DNA repair pathways are associated with cancer, tumor cells defective in HR repair with diminished or deficient *BRCA1/2* gene function accumulate DNA

repair lesions and are more sensitive to PARP inhibitors (Bouwman and Jonkers, 2012; Farmer et al., 2005). We next determined whether lack of RECQL5 or WRN might sensitize RECQL5 and WRN-knock-down human cancer cells (HeLa and HEK293T) to PARP inhibitor. Accordingly, RECQL5 and WRN knock-down cells demonstrated increased sensitivity to PARP inhibitor treatment (Figure 30). Though we detected a similar pattern of sensitivity to HeLa and HEK293T cells at higher concentration of veliparib (100 nM), we found that HeLa cells were more sensitive than HEK293T cell.

DNA damage induction elicits cascades of post-translational modifications, including PARylation, phosphorylation, ubiquitination, and SUMOylation that orchestrate the aforementioned processes. These events are largely initiated by phosphatidylinositol 3-kinase–related kinases (PIKKs), such as ATM, ATR and DNA-PKcs which regulate both the activity and recruitment of various DDR proteins to DNA damage sites (Polo and Jackson, 2011). We therefore sought to assess whether ATM or ATR also regulate RECQL5 and WRN recruitment. Damage induced recruitment of RECQL5 and WRN was clearly impaired in the presence of each of these protein kinase inhibitors (Suppl. Figure 13). ATM, ATR and DNA-PKcs inhibitor KU-55933 markedly reduced the early recruitment of RECQL5 and WRN (Suppl. Figure 13). Importantly, these inhibitors also impaired the late retention time for RECQL5 and WRN compared to PARP inhibitor only (Suppl. Figure 13).

These findings support our proposal that both WRN and RECQL5 recruitment is regulated by PARP activation and PIKK proteins. This shows that, other than PARylation, phosphorylation also regulates the recruitment of RECQL5 and WRN at double strand break sites. Previously, it had been reported that RECQL5 enhances non-crossover DSB mediated HR repair (Paliwal et al., 2013). Indeed, our results support this finding and further show that RECQL5 and PARP1 participate in the same pathway (Figure 32). The observation that the lack of WRN shows no significant effect on HR-directed repair is also consistent with previous findings in WS cells (Chen et al., 2003). Instead, WRN plays a significant role in regulating NHEJ repair.

In general, the cellular activities of RecQL helicases must be tightly controlled until needed, because uncontrolled unwinding of the DNA (or nuclease activity in case of WRN) can cause genome instability, leading to catastrophic consequences for cells. Therefore, it is tempting to speculate that PARPs and PAR control the physico-chemical properties of RECQL5 and WRN in a spatio-temporal manner at the site of the damage. Due to its dynamic nature PARylation provides an excellent means to control RecQL function in time and space. Thus, it is likely that PARylation serves as signal to differentially modulate RecQL activities in order to “choose” the most appropriate RecQL protein at the right time to fulfill the relevant

task. Since PARylation is often induced in a dose-dependent manner with increasing levels of genotoxic stress, it is conceivable that this leads to a step-wise control of function and interactions among the different RecQL proteins dependent on the type and load of the cellular DNA damage. Here we provide a comparison of the coordinated control of WRN and RECQL5 by their interaction with PARP1 and PAR on a biochemical and cellular level during laser-induced DNA damage response. Many open questions remain, in particular on the mechanistic details of these processes.

Acknowledgements

HeLa *PARP1*$^{-/-}$ cells were a gift from Elisa Ferrando-May, A. M., and Alexander Bürkle (University of Konstanz). We thank Dr. Xiao-Fan Wang from Duke University for U2OS DR/GFP cell line and Dr. Gorbunova from University of Rochester for HCA2 NHEJ-I9A cell line. We thank Dr. Thomasz Kulikowicz for the recombinant dual-tagged WRN proteins. We thank Drs Beverly Baptiste, and Jaya Sarkar for reading and providing helpful comments on the manuscript. This work was supported in part by the Intramural Research Program of the National Institutes of Health, National Institute on Aging. S.V. was supported by a fellowship of the DFG-funded Research Training Group 1331.

Materials and Methods

Cell lines and transfection

Both HEK 293T and HeLa cells were growing in DMEM media (Gibco) containing 10% FBS and 1% Pen-Strep at 37°C in a 5% CO_2 humidified incubator. For live-cell imaging experiments, $5x10^4$ cells were seeded in 2-cm glass bottom plates. When cells were 60-70% confluent, they were transfected with the indicated plasmids using Lipofectamine 3000 (Invitrogen, Life Technologies) per manufacturer's directions. Cells were used for microscopic analysis 24 h after transfection. For co-immunoprecipitation and biotin-PAR pull-down assays, HEK 293T cells were plated at 60% confluence in 10 cm plates and transfected with10 µg of plasmid per plate as suggested by the jetPRIME^{TM} Polyplus DNA transfection protocol (VWR). Cells were harvested 36 h after transfection.

Recombinant proteins

As previously described, the recombinant RECQL5 protein was purified from the BL21 *E. coli* system (Janscak et al., 2003) and WRN was purified using a baculovirus/insect-cell expression system (Orren et al., 1999). High specific activity PARP1 enzyme was purchased from Trevigen.

Far western with PAR (PAR-overlay)

Recombinant RecQL proteins (15 pmol) were separated by SDS-PAGE and then transferred to nitrocellulose membranes. Membranes were incubated with indicated concentrations of unfractionated PAR O/N at 4°C, followed by high stringency washes with 1 M NaCl in Tris buffer saline plus 0.1% Tween-20 (TBST) (3x 5 min). Blots were blocked in 5% (w/v) milk, followed by incubation with PAR-specific antibody 10H 1:300 in 5% milk for 1 h (10H antibody is a kind gift from M. Miwa, Nagahama Institute of Bioscience and Technology, Japan, and T. Sugimura, National Cancer Center Research Institute, Tokyo, Japan (Kawamitsu et al., 1984)). Blots were washed 3-times for 5 min with TBST, followed by 1 h incubation with HRP-tagged anti-mouse secondary antibody (Dako, P0447) 1:2000 in 5% milk, followed by 3 washes with TBST. Bound PAR was detected using chemiluminescence detection at a LAS4000 mini using ECL (Lumigen ECL Ultra).

PAR overlay blot assay

Indicated amounts of recombinant proteins were vacuum-blotted onto a nitrocellulose membrane using a slot-blot manifold. The membrane was dried for 10 min at 50°C, followed by incubation with PAR in TBST O/N at 4°C. Bound PAR was detected as described above, by using 10H PAR antibody.

Peptide binding study

The PepSPOT Membrane was purchased from JPT Peptide Technologies (Berlin, Germany). Prior to the experiment the membrane was activated in 100% methanol for 5 min as recommended by the supplier. Subsequently, the membrane was washed 5 min in TNT, followed by a 1-h incubation in TNT. PAR incubation occurred O/N at 4°C with 0.2 µM unfractionated PAR in TNT. The membrane was washed 3 times for 5 min in TNT + 1 M NaCl, followed by two 5-min washes in TNT. Next, the membrane was blocked for 1 h in 5% milk powder in TNT, followed by 1-h incubation with anti-PAR antibody 10-H (1:300 in 5% milk-TNT). After three 5-min washes in TNT the membrane was incubated for 1 h in goat anti-mouse-HRP secondary antibody (1:2000 in 5% milk-TNT), again followed by three 5-min washes in TNT. The membrane was then developed using ECL and chemiluminescence signals were detected using a LAS 4000.

Electrophoretic mobility shift assay with end-biotinylated PAR (PAR-EMSA)

The PAR-EMSA was essentially conducted as described previously (Fahrer et al., 2007). Briefly, recombinant WRN or RECQL5 were equilibrated in EMSA buffer (40 mM Tris [pH 8.0], 4 mM $MgCl_2$, 0.1 mg/ml BSA, 0.1% NP-40, 5 mM diothiothreitol [DTT]) for 10 min at 25°C, followed by addition of 500 fmol end-biotinylated, size-fractionated PAR (30-35-mer). Reaction mixtures were incubated for another 20 min at 25°C to allow complex-formation in a total volume of 10 µl, followed by addition of 1 µl 10x loading dye (250 mM Tris [pH8.0], 0.2% (w/v) orange G) and subsequent separation on a 5% native TBE gel. The gel was semi-dry blotted onto a nylon membrane (GE, Hybond-N+), followed by a 1-h incubation at 90°C. The membrane was then blocked in 5% (w/v) milk powder in TBST, followed by 3x washing in TBST for 5 min. Next, the membrane was incubated for 1 h with streptavidin-coupled HRP (GE, RPN1051V) in TBST, followed by chemiluminescence detection. Quantitative analysis

of the band shift was performed using IMAGEJ. Relative band shift was calculated by dividing the signal intensity of the protein-PAR complex by the total signal intensity of unbound PAR and the protein-PAR complex.

Co-immunoprecipitation and immunoblotting

HEK 293T cells were transfected with various GFP tagged RECQL5 plasmids. Cell extracts were prepared with NTEN lysis buffer (20 mM Tris-HCl, [pH8.0], 100 mM NaCl, 1mM EDTA, and 0.5% NP-40) containing protease inhibitor cocktail (Thermo Scientific Pierce) and 1 μM ADP-HPD (Enzo Lifesciences) to inhibit PARG activity. Lysates were sonicated and then clarified by centrifugation at max speed at 4°C and the cell extracts were obtained. The supernatants were pre-cleared with protein G beads (GE Healthcare) for 30 min at 4°C. Ethidiumbromide (5 μg/ml, BioRAD) was added to the lysates to eliminate DNA-mediated interactions. The supernatants were incubated with indicated antibodies, as described in the figure legends, and the beads for 6 h at 4°C. The beads were washed five times with NTEN buffer (20 mM Tris-HCl [pH 8.0], 100 mM NaCl, 1 mM EDTA, and 0.5% NP-40) and then boiled in 2x Laemmli buffer (Sigma-Aldrich). Samples were loaded on SDS-PAGE gels (Bio-Rad) and then transferred to PVDF membranes. Membranes were blocked with 5% non-fat milk in TBST for 20 min at RT followed by incubation with primary antibody overnight at 4°C. The HRP-conjugated secondary antibodies (GE Biosciences) were added to the membranes. Blots were developed using the ECL western blotting substrate (Perkin Elmer) and images were obtained via the Bio-Rad ChemiDoc.

Biotin PAR pull-down

HEK 293T cells were transfected with various GFP tagged RECQL5 plasmids. Cell lysates were prepared with NTEN lysis buffer (20 mM Tris-HCl [pH8.0], 100 mM NaCl, 1mM EDTA, and 0.5% NP-40) with the cocktail protease inhibitors (Thermo Scientific Pierce). Cell lysates were sonicated, centrifuged at max speed at 4°C and supernatants were collected. The cell extracts were incubated with biotinylated-PAR (10 μM, Trevigen) and the pull-down was performed by using the Biotinylated Protein Interaction pull-down kit (Thermo Scientific Pierce). Samples were resolved on a SDS-PAGE gel and processed for immunoblotting analysis.

In vitro poly(ADP-ribosyl)ation assay

Human PARP1 (50 nM, Trevigen) was incubated with 4 ng/ml sonicated linear double stranded DNA (salmon sperm) in the presence or absence of 50 nM RECQL5 in reaction buffer (50 mM Tris HCl [pH8.0], 25 mM $MgCl_2$, 0.5 mM dithiothreitol [DTT]). The samples were treated with either 500 μM NAD^+ to induce PARylation activity or 5 μM Olaparib to inhibit PARP1 activity followed by 20 min at 37°C incubation. The reactions were terminated by boiling with Laemmli sample buffer. PARylation activity was observed by immunoblotting analysis.

Helicase assay

Recombinant WRN and RECQL5 were purified as described previously (Popuri et al., 2012a; Tadokoro et al., 2012a). PARP1 and PAR were obtained from Trevigen and Enzo. PARylated PARP1 was prepared as described in *In vitro poly(ADP-ribosyl)ation assay*. Helicase activity of RECQL5 with PARP1, PAR, and PARylated PARP1 proteins (at concentrations shown in the figure) were measured using 0.5 nM radiolabeled fork duplex for 30 min at 37°C in a reaction volume of 10 μl reaction buffer containing 30 mM Tris-HCl [pH 7.4], 50 mM KCl, 5 mM $MgCl_2$, 1 mM dithiothreitol [DTT], 100 μg/ml BSA, 10% glycerol, 5 mM ATP, and forked duplex substrates, which has been described previously (Tadokoro et al., 2013). The sequences of forked duplex substrates are shown as follows: 5′-TTTTTTTTTTTTTTGAGTGTGGTGTACATGCACTAC-3′, and 5′-GTAGTGCATGTACACCACACTCTTTTTTTTTTTTTT-3′. Reactions were stopped by the addition of stop buffer (30 mM EDTA, 0.9% SDS, 30% glycerol, 0.05% bromphenol blue, and 0.05% xylene cyanol). The reaction products were separated by electrophoresis on a 10% native polyacrylamide gel in 1x Tris-Borate-EDTA (TBE) running buffer at 200 V for 1 h. The gels were processed similar to the strand-annealing assay.

Strand annealing

DNA strand-annealing activity of RECQL5 was measured using complementary oligonucleotides to create a forked duplex. The top strand was labeled at the 5'-end using [γ-^{32}P] ATP and T4 polynucleotide kinase. Annealing reactions (10 μl) were carried out for 10 min at 37°C in buffer (30 mM Tris-HCl [pH7.5], 50 mM KCl, 1 mM dithiothreitol [DTT], 5

mM $MgCl_2$, BSA 100 µg/ml) with the indicated amounts of RECQL5, PARP1, PAR, or PARylated PARP1 proteins. The reaction products were separated by electrophoresis on a 10% native polyacrylamide gel in 1x TBE running buffer at 200 V for 1 h. The gels were exposed to a PhosphorImager screen (GE Healthcare, Piscataway, NJ), and imaged with a Typhoon scanner (GE Healthcare, Piscataway, NJ). ImageQuantTL version 5.2 was employed to analyze the phosphor-images and calculate the percentage of free versus annealed substrate in each reaction and each was normalized against background. Assays were performed at least in triplicates, and representative gels are shown.

ATPase assay

The recombinant protein concentrations were as listed in the figure legends. Reactions were incubated with 0.2 µM M13mp18 single stranded DNA (New England Biolabs) and 1 µCi [γ-32P] ATP (PerkinElmer Life Sciences, Waltham, MA) and PAR, PARP1, or PARylated PARP1 (as noted in figure legends) in 10 µl reaction buffer (50 mM TrisHCl [pH7.5], 50 mM NaCl, 2 mM $MgCl_2$, 1 mM dithiothreitol [DTT], 50 µg/ml BSA, 50 µM cold ATP) for 1 h at 37°C. Reactions were stopped by adding 166 mM EDTA. Reaction samples (2 µl) were spotted onto the Baker-flex cellulose polyethyleneimine thin-layer chromatography plates (J.T. Baker) and developed using a solution of 0.8 M LiCl and 1 M formic acid. The plates were exposed to a PhosphorImager screen, and then images were captured by the Typhoon Phosphorimager scanner (GE Healthcare, Piscataway, NJ) and analyzed using ImageQuantTL version 5.2 (GE Healthcare, Piscataway, NJ) to calculate the percentage of ATP hydrolysis.

Laser micro-irradiation and confocal microscopy

A Nikon Eclipse 2000E spinning disk confocal microscope with a laser imaging module and CCD camera (Hamamatsu, Tokyo, Japan) was used. The Stanford Research Systems (SRS) NL100 nitrogen laser by Micropoint ablation (Photonics Instruments, St. Charles, IL, USA) was employed for double strand break *in vivo* targeting as described previously (Liberti et al., 2011; Singh et al., 2010). Site-specific double stranded DNA damage was induced through SRS NL100 nitrogen laser that passed through a 435 nm dye cell. The laser power was regulated by Velocity software 4.3.1 (Improvision/Perkin Elmer, Coventry, UK). The laser intensity was applied at 12% to initiate double strand breaks. Images were taken and analyzed by Velocity software.

Cell survival assay

Cells were seeded in 6 cm plates and treated with the siRNA (RECQL5 or WRN) and next day equal numbers of cells were splitted from 6 cm plates and seeded in 6 well plates (n =3). Cells were subjected to veliparib treatment as indicated and media exchanged every other day. Cell growth was examined on day 4, using cell counter (Beckman Coulter Z1 Coulter Particle Counter). Mean cell numbers from three experiments were expressed as percentage of cell ± SE relative to siRNA-vehicle treated cells.

Immunofluorescence

HeLa cells were plated on Ibidi glass bottom dish Grid-50 at a density of 50,000-cells/plate for overnight, and then the cells were irradiated with 12% laser. After irradiation, the cells were fixed with 3.7% formaldehyde for 10 min at room temperature. Cells were washed three times with PBS for 5 min each followed by 5 min room temperature permeabilization treatment (0.1% Triton X-100 in PBS). Then cells were washed with PBS and blocked with goat serum, and then treated with antibodies. Following, the primary and secondary antibodies are used: Rabbit polyclonal anti-53BP1 (1:250; Novus Biologicals), rabbit polyclonal anti-WRN H-300 (1:250; Santa Cruz Biotechnology), rabbit polyclonal anti-RECQL5 (1:250; house made), mouse monoclonal anti-Poly(ADP-ribose) 10H (1:250; Enzo Life Sciences), donkey anti-rabbit Alexa Fluor 488 (1:1000; Invitrogen) and donkey anti-mouse Alexa Fluor 647 (1:1000; Invitrogen). The cells were also co-stained with DAPI. The images were captured with a Nikon Eclipse 2000E confocal microscope and analyzed by Velocity software.

In vivo DSB repair assays

U2OS/DR-GFP, HCA2 NHEJ-I9A and pEGFP-pem1-Ad2 transfected U2OS cells were used to measure *in vivo* DSB repair efficiency as described previously (Mao et al., 2008; Shamanna et al., 2011; Stark et al., 2004). Cells were knocked down with siRNA by transfecting twice with siControl (Qiagen; cat no. 1027310), siRECQL5 (CAGGAGGCUGAUAAAGGGUUA), siWRN (GUAAACAGCUCCUGAAAGA), siPARP1-A (CCGAGAAATCTCTTACCTCAA) and siPARP1-B (ACGGTGATCGGTAGCAACAAA) (GE Healthcare) using jetPRIME. 5 µg I-SceI or empty vector along with or without 0.025 µg

DsRed plasmid was transfected using AMAXA^{TM} cell line nucleofector kit V (Lonza) and NHDF nucleofector kit (Lonza). Three days after transfection, the GFP-positive cells were determined by flow cytometry and FACS analysis was performed using a BD Accuri^{TM} C6 flow cytometer.

In vitro end joining

The assays were performed by incubating 10 ng of 2.6 kb cohesive DNA substrate, generated from *Sal*I (New England Biologicals) linearized pUC18 plasmid (Shamanna et al., 2011), with 20 µg end-joining extracts for 1 h at 25°C in a 20 µl reaction containing 20 mM *N*-2-hydroxyethylpiperazine-*N*′-2-ethanesulfonic acid [pH 7.5], 10 mM $MgCl_2$, 80 mM KCl, 1 mM dithiothreitol (DTT), 1 mM ATP and 50 µM deoxyribonucleotide triphosphates. The reaction was stopped with 50 mM EDTA and 80 µg/ml RNaseA at 37°C, and deproteinized by incubating with proteinase K (2 mg/ml) for 60 min at 37°C. Ligation products were separated in a 0.7% agarose gel and stained with SYBR-Gold (Invitrogen). Fluorescence was detected with Molecular Imager Gel Doc XR system (Bio-Rad).

Data and statistical analysis

All graphs display cumulative data representing three independent experiments and standard error of mean (± SEM) was used to display data variability, unless stated otherwise.

Supplementary Data

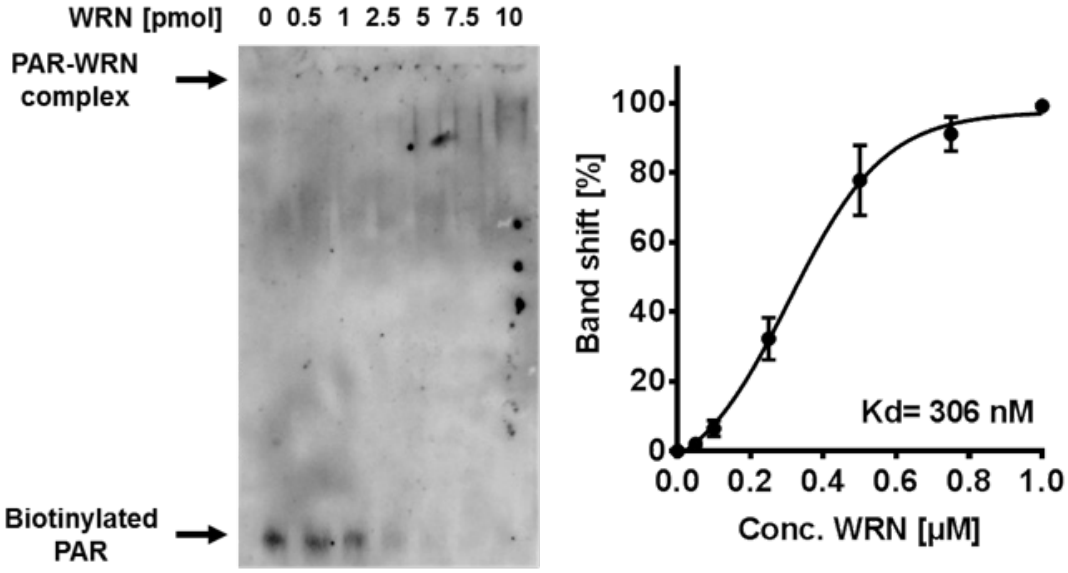

Supplementary Figure 8: EMSA with end-biotinylated PAR to examine WRN-PAR interaction in solution.
Size-fractionated PAR (500 fmol) was incubated with increasing concentrations of WRN as indicated, separated via native gel electrophoresis in 1xTBE buffer and semi-dry blotted. PAR was detected via streptavidin-coupled HRP. **Right.** Quantitative evaluation of RECQL5 gel shifts. Shift [%] indicates [signal intensity complexed PAR]/[complexed + free PAR]. Data are expressed as mean ± SEM of triplicates.

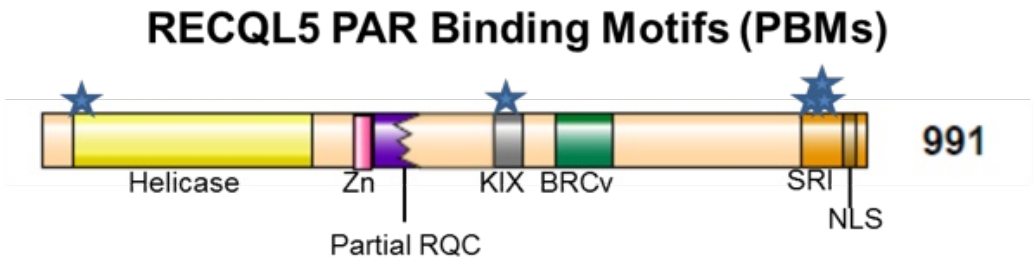

PepSPOT PAR-binding blot	Peptide sequence	AA position
RecQL5 PMB 1	HTTFPFDPERRVRSTLKKVF	5-24
RecQL5 PMB 1 - mut1	HTTFPFDPERRVRSTLAAVF	5-24
RecQL5 PMB 1 - mut2	HTTFPFDPEAAVASTLKKVF	5-24
RecQL5 PMB 1 - mut3	HTTFPFDPEAAVASTLAAVF	5-24
RecQL5 PMB 2	TFRNAKVANLYKASVLKKVA	587-606
RecQL5 PMB 2 - mut1	TFRNAKVANLYKASVLAAVA	587-606
RecQL5 PMB 2 - mut2	TFRNAKVANLYAASVLKKVA	587-606
RecQL5 PMB 2 - mut3	TFRNAKVANLYAASVLAAVA	587-606
RecQL5 PMB 3/4	KEGKFASKELFKGFARHLSH	928-947
RecQL5 PMB 3/4 - mut1	KEGKFASKELFKGFAAALSA	928-947
RecQL5 PMB 3/4 - mut2	KEGAFASAELFAGFARHLSH	928-947
RecQL5 PMB 3/4 - mut3	KEGAFASAELFAGFAAALSA	928-947
RecQL5 PMB 5	TSPGRSVKEEAQNLIRHFFH	953-972
RecQL5 PMB 5 - mut1	TSPGRSVKEEAQNLIAAFFH	953-972
RecQL5 PMB 5 - mut2	TSPGRSVAEEAQNLIRHFFA	953-972
RecQL5 PMB 5 - mut3	TSPGRSVAEEAQNLIAAFFA	953-972

Motif: basic amino acids before PBM pattern
PBM pattern: [HKR]-X-[AVILFWP]-[AVILFWP]-[HKR]-[HKR]-[AVILFWP]-[AVILFWP]

Site	Position	Comments
Site 1: 17-24;	tfpfdperrv_RStLKKVF_gfdsfktplq	lobe 1 of helicase (22-292 aa)
Site 2: 599-606;	rnakvanlyk_aSVLKKVA_dihraskdgq	in KIX domain (540-620 aa)
Site 3: 935-942;	pfhkegkfas_KELFKgFA_rhlshlltqk	in SRI domain (899-991 aa)
Site 4: 939-946;	egkfaskelf_KGFARHLs_hlltqktspg	sites 3 & 4 overlap in SRI domain
Site 5: 964-971:	spgrsvkeea_qNLIRHFF_hgrarcesea	in SRI domain (899-991 aa)

Basic amino acids before PBM pattern shown in orange and PBM pattern shown in all caps.
If amino acids fails to fit the consensus PBM pattern, that amino acid is not in capitalized.

Supplementary Figure 9: Five putative PAR binding motifs are identified in RECQL5.
Five PBM sites (*) in RECQL5 have been identified by searching the primary amino acid sequence (aa) as described in Popp *et al.* (Popp et al., 2012). One is located in the helicase region (aa 17-24) and one falls in the KIX domain (aa 599-606). Three PBM sites are shown in the SRI domain in close proximity to one another (aa 935-942, aa 939-946, and aa 964-971).

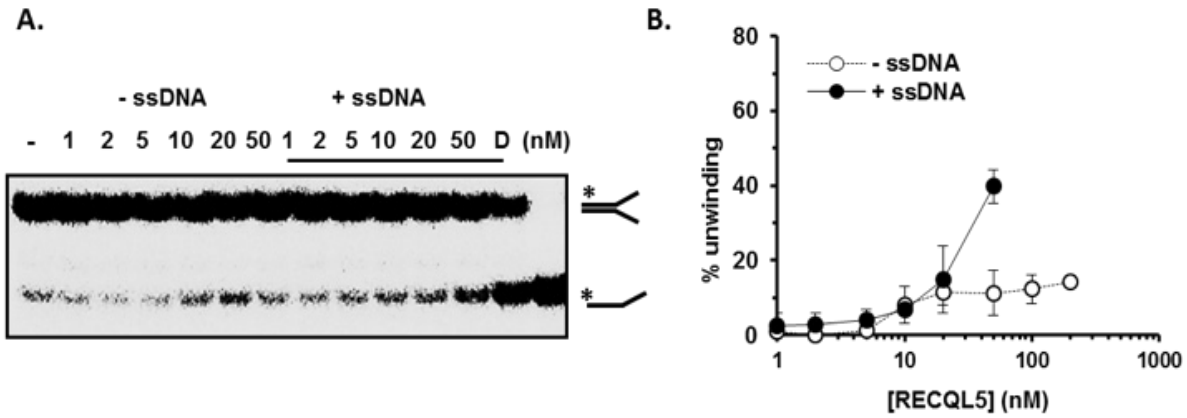

Supplementary Figure 10: The presence of single stranded DNA stimulates the helicase activity of RECQL5.
A. RECQL5 helicase activity in the absence and presence of excess of cold ssDNA (12.5 nM). **B.** Quantitative analysis of A. The error bar represents SEM from three independent experiments.

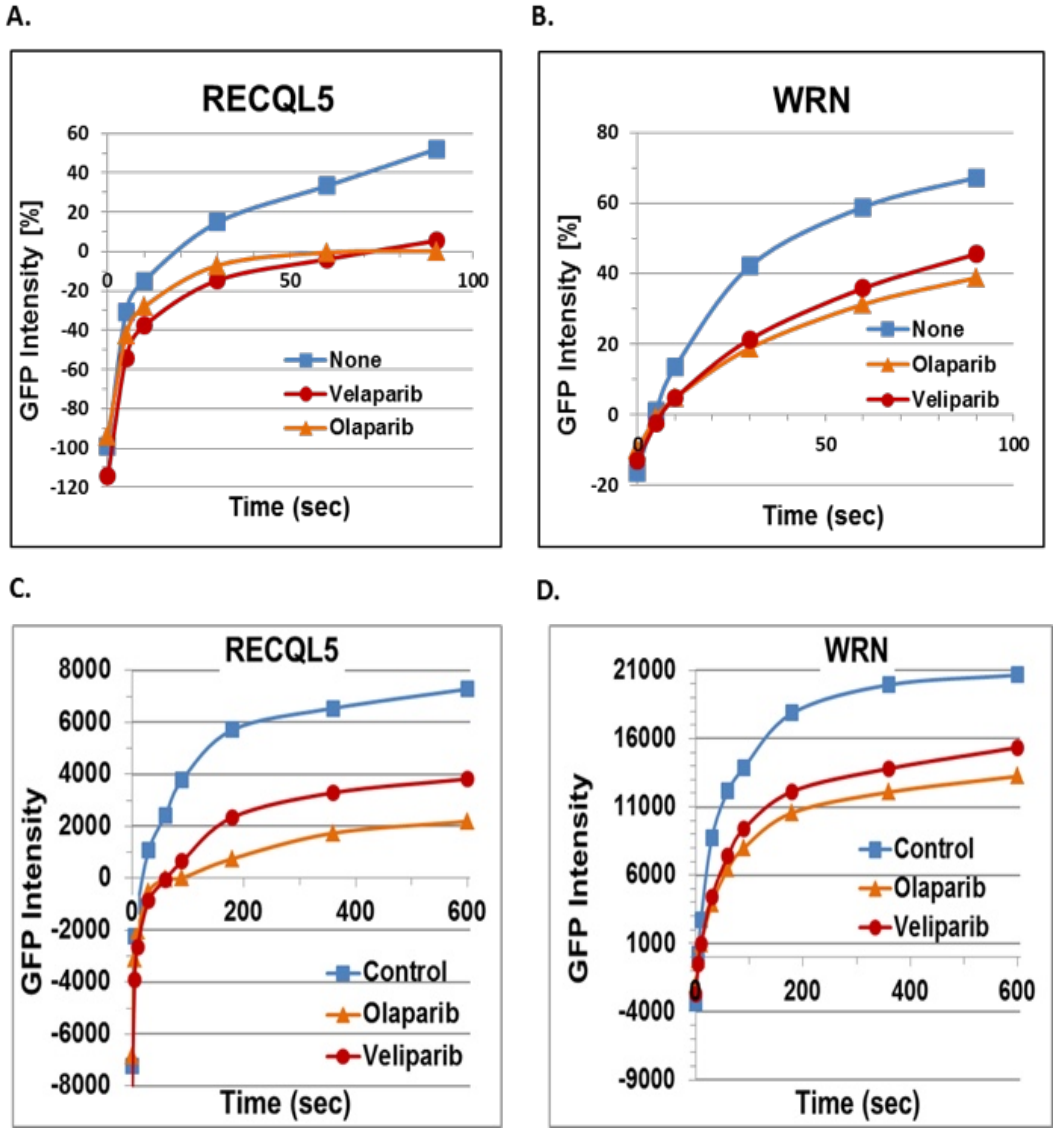

Supplementary Figure 11: PARylation regulates the recruitments of both RECQL5 and WRN to laser induced DNA damage.
A, B. Early recruitment kinetics (0-90 sec) for GFP tagged RECQL5 and WRN. RECQL5's recruitment to DSB is disrupted at the early time point, but not WRN. Recruitment to DSB data is same as that reported in Figure 29 but re-plotted to focus on the 0 to 90 sec time scale. **C, D.** Absolute values of the GFP intensity of RECQL5 and WRN from Figure 29.

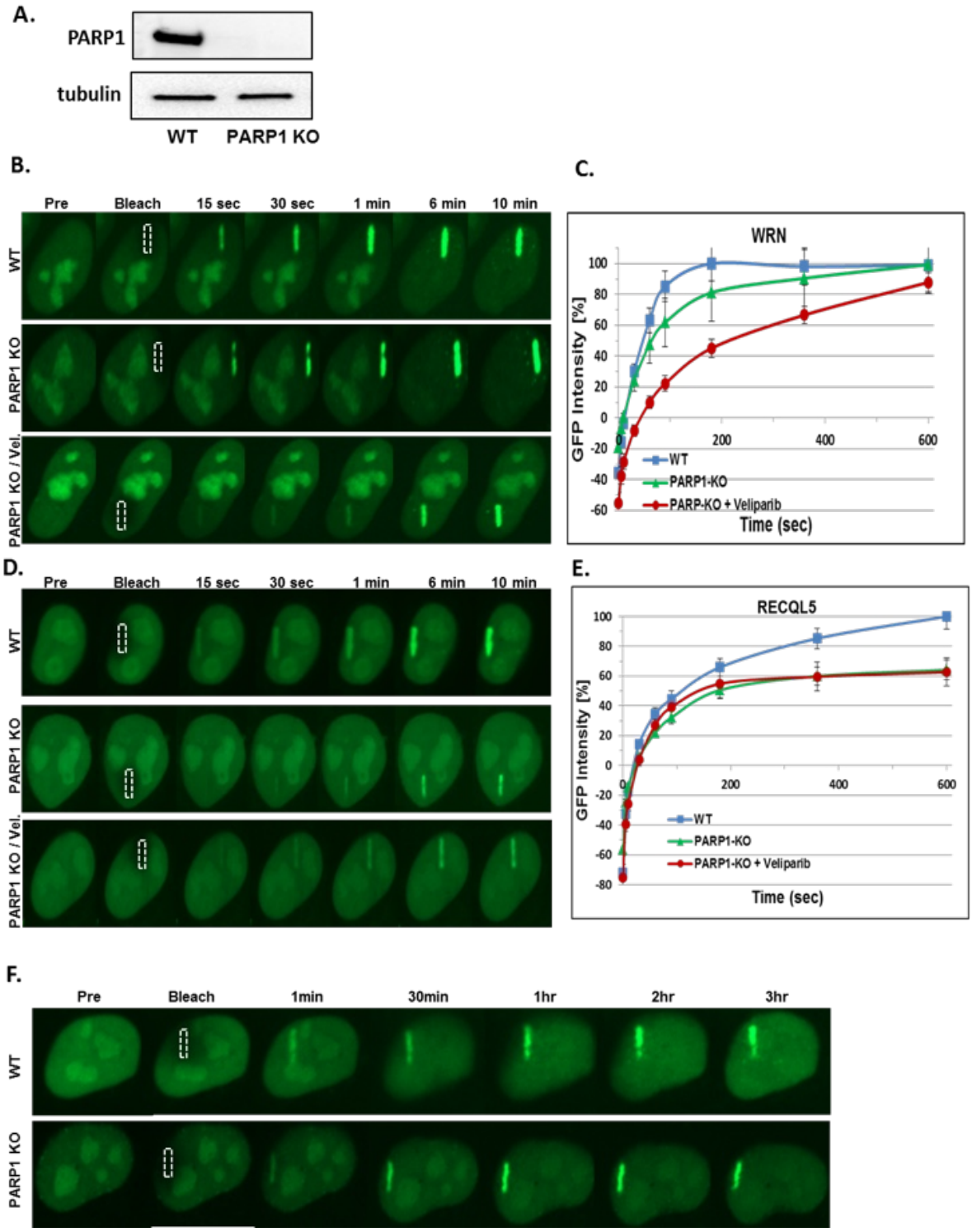

Supplementary Figure 12: RECQL5 and WRN are recruited to sites of DSBs in *PARP1* knock-out cells.
A. Western blot analysis of HeLa Kyoto wild type and *PARP1* knock-out cell lines. HeLa Kyoto wild type, *PARP1* knock-out, and *PARP1* knock-out cells with 5 ¥ M veliparib treatment overexpressing GFP tagged WRN **(B)** or RECQL5 **(D)** and subjected to 12% laser strikes. Protein recruitment dynamics were recorded in real-time. At least twenty cells from three independent experiments were measured and quantified and are shown in **(C)** and **(E)** with the error bars of SEM. **F.** RECQL5-GFP expressing HeLa Kyoto wild type and PARP1 deficient cells were targeted with 12% laser strikes and recruitment kinetics were recorded at the indicated time points to examine retention of RECQL5. The white box with the dotted outline indicates the laser striking area.

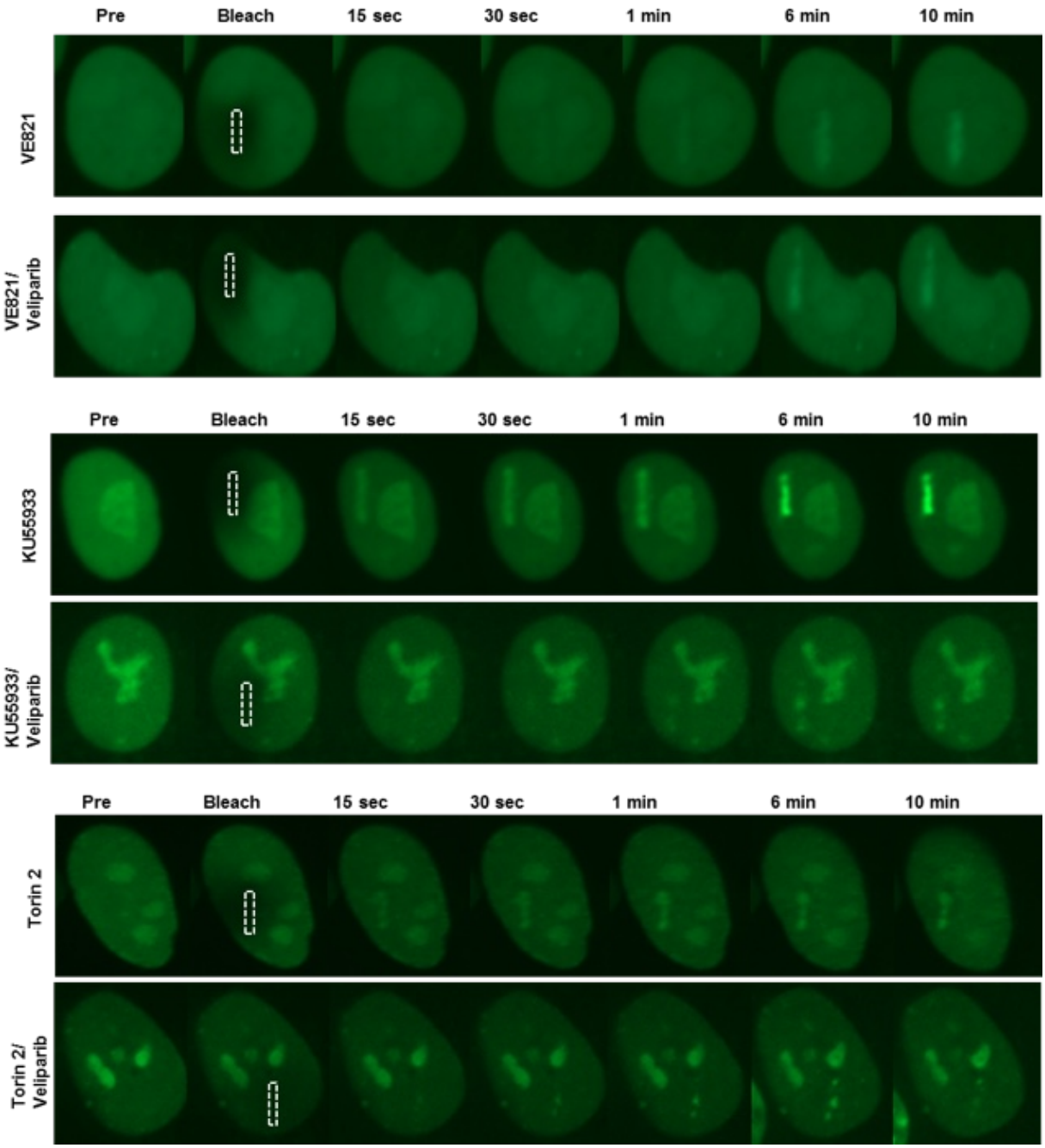

Supplementary Figure 13: RECQL5 recruitment to DSBs is abrogated when cells are treated with both veliparib and PI3 kinase inhibitors.
HeLa cells were transiently transfected with RECQL5-GFP. Cells were pretreated with the indicated PI3 kinase inhibitors, 1 ¦M VE821 (ATR inhibitor), 50 ¦MKU55933 (ATM inhibitor), and 1 ¦M Torin2 (ATM, ATR, DNA-PK and mTOR inhibitor), and with or without PARP inhibitor, 5 ¦M veliparib. After 3 h incubation, GFP expressing cells were struck with 12% laser and observed for RECQL5 protein recruitment for up to 10 min. The white box with the dotted outline indicates the laser striking area.

Chapter V: PARP1 is essential for oxidative stress-induced relocalization of WRN from nucleoli to sites of DNA damage

Sebastian Veith, Andrea Schink*, Alexander Bürkle and Aswin Mangerich*

Manuscript

* Equal contribution

Abstract

Poly(ADP-ribose) polymerase 1 (PARP1) and WRN are considered as guardians of the genome due to their roles in almost every aspect of DNA metabolism, especially DNA repair and response to genotoxic stress. They have overlapping fields of action, interact with each other and both are localized in the nucleus and also the nucleoli. Here we describe a novel role for PARP1 and poly(ADP-ribosyl)ation in the regulation of WRN's spatial distribution in the nucleus and the trafficking of WRN out of the nucleoli. We could show that WRN contains four PAR-binding motifs and one of them is located in its RQC domain, which is the binding site for PARP1 and necessary for nucleolar localization. We could demonstrate that PARP1 is essential for efflux of WRN from the nucleoli upon oxidative stress but not for its initial recruitment to, and the containment in, the nucleoli. On the other hand, PARP1 activity and non-covalent PAR-binding to WRN only play a minor role in WRN-trafficking out of the nucleoli, underlining the importance of direct protein-protein interaction between WRN and PARP1. In conclusion, we provide new insight into the role of PARP1 in WRN's spatio-temporal regulation in response to oxidative stress.

Introduction

The Werner Syndrome protein (WRN) is a member of the RecQL helicase family that comprises five members in humans (RECQL1, WRN, BLM, RECQL4 and RECQL5). So far, little is known about the specific roles or the interplay between the five RecQL helicases, but there is evidence that they can have redundant, synergistic or complementary roles (Croteau et al., 2014). Defects in WRN are the primary cause of the premature aging disorder Werner Syndrome (WS), which is characterized by an early onset of aging-related symptoms such as cataracts, diabetes, gray hair, atherosclerosis, osteoporosis and a higher incidence of cancer (Goto et al., 2013; Lauper et al., 2013). In addition to its helicase and single-strand annealing activities, WRN exhibits, unlike the other RecQL helicases, an exonuclease activity (Rossi et al., 2010a). It is largely agreed upon that WRN is predominantly located in the nucleoli and translocates from the nucleoli upon induction of cellular stress, however, little is known about what drives this process (Constantinou et al., 2000; Gray et al., 1997; Kanagaraj et al., 2012; Lan et al., 2005; Lee et al., 2005; Singh et al., 2012a). It has been implicated that the AAA ATPase VCP/p97 is involved in this process, however no underlying process has been described so far (Indig et al., 2004; Partridge et al., 2003). Over the last decade, several

publications have shown that acetylation plays an important role in WRN trafficking from and to the nucleolus (Blander et al., 2002; Karmakar and Bohr, 2005; Li et al., 2008; 2010). Recently, Lee *et al.* proposed a role of SIRT1 in WRN's relocalization from the nucleolus, thus strengthening the evidence for a role of acetylation in WRN trafficking (Lee et al., 2015). Furthermore, phosphorylation reactions appear to contribute to the return of WRN into the nucleoli (Karmakar and Bohr, 2005). WRN has been shown to play a role in almost every aspect of DNA metabolism, including DNA repair, replication, transcription and telomere maintenance (Croteau et al., 2014). Its role in these processes is regulated by protein-protein interactions but also by posttranslational modifications, *i.e.* phosphorylation, SUMOylation, acetylation or poly(ADP-ribosyl)ation (PARylation) (Adelfalk et al., 2003; Kusumoto et al., 2007; Rossi et al., 2010a). The synthesis of poly(ADP-ribose) (PAR) is catalyzed by poly(ADP-ribose) polymerases (PARP's) by cleaving NAD^+ into ADP-ribose and nicotinamide, with PARP1 being responsible for up to 97% of PAR-production under stress conditions (Shieh et al., 1998). Upon activation PARP1 modifies lysines, glutamates or aspartates at several hundred target proteins, but also heavily automodifies itself with PAR (Gagné et al., 2012; Kawaichi et al., 1981; Ogata et al., 1981). This modification can have various effects: it can in- or decrease enzymatic activity of target proteins, it can alter the spatio-temporal distribution of target proteins and it can lead to complex formation, with PARylated proteins acting as scaffolding factors (Gibson and Kraus, 2012; Mangerich and Bürkle, 2012). Besides covalent modification with PAR, proteins can interact non-covalently with PAR via PAR binding modules (Krietsch et al., 2012). So far, at least 7 different binding modules for non-covalent PAR interaction have been described, with the most prevalent and the least conserved being the PAR binding motif (PBM), first described by Pleschke and colleagues (Altmeyer et al., 2015; Pleschke et al., 2000; Veith and Mangerich, 2014). Proteins bearing a PAR binding module could interact with either PARylated proteins or with free PAR chains, generated by poly(ADP-ribose) glycohydrolase (PARG) or ADP-ribosylhydrolase 3 (ARH3) (Niere et al., 2008; Ueda et al., 1972). By now a lot of different roles for PARylation have been described, ranging from participation in spermatogenesis to inflammation, cell death and energy metabolism, but one of its most recognized roles is in DNA repair, where it is implicated in basically every major pathway (Krukenberg et al., 2015; Mangerich and Bürkle, 2012; Meyer-Ficca et al., 2004). Therefore, it does not come as a surprise that there is increasing evidence of interaction between PARylation and RecQL helicases in general, and with WRN in particular (Veith and Mangerich, 2014). Besides being covalently PARylated, which is still a matter of debate, WRN has been shown to interact with

both PARP1 and PAR and being inhibited by this interaction (Gagné et al., 2012; Khadka et al., 2015; Kobbe et al., 2003a; 2004a; Li et al., 2004; Popp et al., 2012). Also, like WRN, PARP1 is mostly localized in the nucleolus and also its exact functions there remain elusive (Dantzer and Santoro, 2013; Guetg et al., 2012; Meder et al., 2005). The direct interaction between PARP1 and WRN is mediated via PARP's BRCT and WRN's RQC domain, the same domain that is required for nucleolar localization of WRN (Kobbe et al., 2003a; 2004a; Lachapelle et al., 2011; Lebel et al., 2003). However, although there is a bulk of biochemical and some organismal evidence, it is still largely unclear what cellular or organismal consequences these interactions have (Deschênes et al., 2005; Lebel, 2002; Lebel et al., 2003; Veith and Mangerich, 2014). Here we show that the oxidative stress-induced WRN translocation from the nucleoli is regulated by PARP1 and PAR and that this process can, at least in part, be blocked by PARP inhibitor treatment.

Results

WRN interacts non-covalently with PAR via at least 4 different PBMs

We have previously reported that there are four putative PBM's in WRN and found that one non-covalently binds PAR strongly and two weakly (Popp et al., 2012). In a follow-up study, we wanted to examine this non-covalent WRN-PAR-interaction further by using several fragments of full length WRN, covering most of its sequence and all but one of the putative PBMs (Figure 33 B, light blue boxes). These fragments were expressed as recombinant proteins and were tested for PAR binding using a far-Western blot assay (PAR overlay). Unexpectedly, fragment aa 1-520, containing with PBM1 the strongest PBM in our previous screen, displayed only moderate PAR binding under these experimental conditions (Figure 33 A). Moreover, the fragment comprising the PBM that previously showed no PAR binding, revealed a very strong PAR-protein interaction (PBM4, fragment aa 910-1240), closely followed by the fragment containing PBM5, which was not tested before. Using a previously published search pattern we found five PAR-binding motifs in WRN (Figure 33 C) (Popp et al., 2012). Based on these findings we designed several peptides, including the WT sequences of each PBM and several mutated variants thereof (Figure 33 D), and had them synthesized on-membrane (PepSpot Membrane, JPT Technologies). The peptides were then tested for PAR-binding using the PAR overlay assay. In principle, the results of Figure 33 A were confirmed, establishing the putative WRN PBMs 1, 3, 4 and 5 as *bona fide* PBMs.

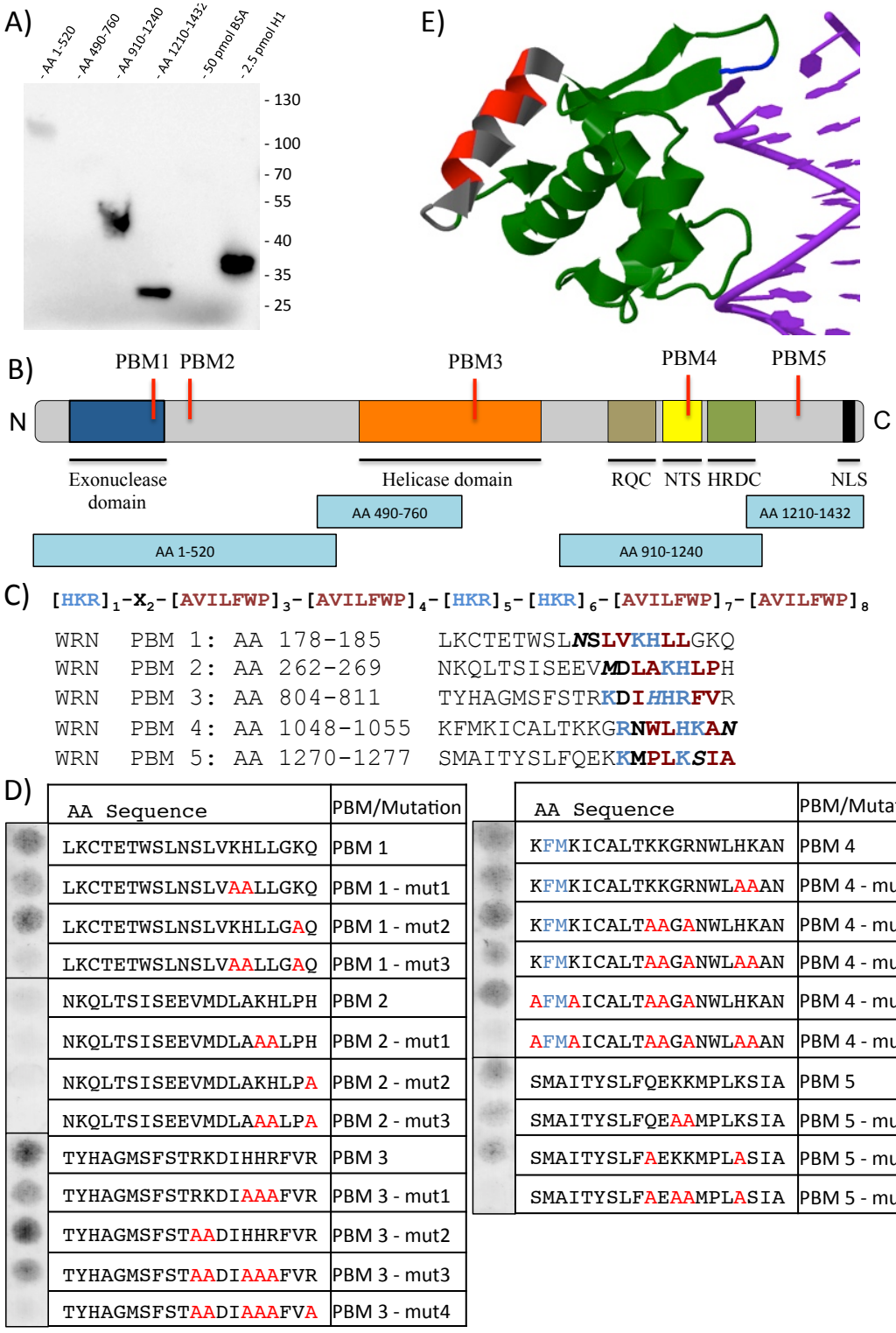

AA Sequence	PBM/Mutation
LKCTETWSLNSLVKHLLGKQ	PBM 1
LKCTETWSLNSLVAALLGKQ	PBM 1 - mut1
LKCTETWSLNSLVKHLLGAQ	PBM 1 - mut2
LKCTETWSLNSLVAALLGAQ	PBM 1 - mut3
NKQLTSISEEVMDLAKHLPH	PBM 2
NKQLTSISEEVMDLAAALPH	PBM 2 - mut1
NKQLTSISEEVMDLAKHLPA	PBM 2 - mut2
NKQLTSISEEVMDLAAALPA	PBM 2 - mut3
TYHAGMSFSTRKDIHHRFVR	PBM 3
TYHAGMSFSTRKDIAAAFVR	PBM 3 - mut1
TYHAGMSFSTAADIHHRFVR	PBM 3 - mut2
TYHAGMSFSTAADIAAAFVR	PBM 3 - mut3
TYHAGMSFSTAADIAAAFVA	PBM 3 - mut4

AA Sequence	PBM/Mutation
KFMKICALTKKGRNWLHKAN	PBM 4
KFMKICALTKKGRNWLAAAN	PBM 4 - mut1
KFMKICALTAAGANWLHKAN	PBM 4 - mut2
KFMKICALTAAGANWLAAAN	PBM 4 - mut3
AFMAICALTAAGANWLHKAN	PBM 4 - mut4
AFMAICALTAAGANWLAAAN	PBM 4 - mut5
SMAITYSLFQEKKMPLKSIA	PBM 5
SMAITYSLFQEAAMPLKSIA	PBM 5 - mut1
SMAITYSLFAEKKMPLASIA	PBM 5 - mut2
SMAITYSLFAEAAMPLASIA	PBM 5 - mut3

Figure 33: WRN has a PAR-binding motif in its nucleolar targeting sequence.
A. PAR overlay western blot of 4 WRN fragments, with BSA and H1 as negative and positive control for PAR-binding, respectively. **B.** Schematic representation of WRN, with the 5 putative PAR-binding motifs (PBMs) marked in red. RQC, RecQ C-terminal domain; NTS, nucleolar targeting sequence; HRDC, helicase and RNase D-like domain; NLS, nuclear localization signal. The light blue boxes below WRN depict the position and size of the four fragments used in A. **C.** Pattern that was used to search for PBMs in WRN's sequence using PattinProt. Blue, basic amino acids (aa); red, hydrophobic aa; X, any aa. Below are the five PBMs in WRN listed that the search yielded. Marked is the position of the core motif by aa number and by bold writing; italic, mismatch compared to search pattern. **D.** PAR overlay of the PepSpot membrane. Each spot resembles one peptide; the respective sequence is noted to the right. Each PBM found in WRN was tested, along with several mutations. Mutated aa are highlighted in red, essential aa for DNA binding are highlighted in blue. **E.** 3D structure of the RQC domain of WRN bound to DNA (PDB identifier: 3AAF). DNA is depicted in purple, WRN aa sequence in green, PBM4 in grey, essential aa for DNA binding in blue (Kitano et al., 2010) and crucial aa for PAR binding in red (based on PBM4-mut3).

By sequentially exchanging several basic aa in the PBM to alanines it was possible to disrupt the PAR-binding capabilities of the respective motif (Figure 33 D). PBM4, which bound strongest in the fragment screen and also strongly in the peptide screen is situated in the one domain of WRN that is necessary for its nucleolar localization, the RQC domain (Figure 33 B, yellow box) (Kobbe and Bohr, 2002). Furthermore, it is also the domain in WRN that is required for interaction with PARP1. We therefore speculated that PARP1, or its product PAR, might be involved in the translocation of WRN out of the nucleoli.

WRN translocates from the nucleoli upon genotoxic stress

Most prior publications reporting the nucleolar localization of WRN failed to use nucleolar proteins as marker to verify the nucleolar localization, thus weakening the results. In order to verify and validate these previous reports, showing that WRN translocates from the nucleoli upon stress induction, we challenged HeLa cells with H_2O_2 and monitored the time-dependent sub-nuclear relocalization of WRN. We could reproduce findings demonstrating that in unstressed cells WRN indeed localizes mainly in the nucleoli (Figure 34 A&D). After a 10-min treatment however, we observed the first major change in WRN localization: only 40% of the cells still displayed WRN in the nucleoli and more and more cells had a pan-nuclear distribution of WRN. The second change happened after 30 to 60 min, when suddenly even more WRN left the nucleoli, thus appearing devoid of any WRN (Figure 34 A&C). We classified cells into three different morphological stages during the time line experiment: (*i*) cells with nucleoli showing a strong WRN signal (full), (*ii*) cells in which WRN is evenly distributed throughout the nucleus, and (*iii*) cells with no or weak WRN signal in the nucleoli (empty) (Figure 34 B). Figure 34 D shows that the positive, strong WRN signal, as well as the weak WRN signal, correlates perfectly with the nucleolar marker nucleolin (C23), verifying WRN's nucleolar localization in unstressed cells. However, the prolonged H_2O_2 treatment seems to affect the nucleolar architecture, as the nucleolin signal was consistently weaker in treated than in untreated cells (Figure 34 D).

Strangely, sometimes we observed a lot of empty nucleoli even in unstressed cells 1-2 h after treatment. After systematically analyzing this phenomenon, we could demonstrate that the exchange of medium per se, *i.e.*, aspiration of old medium and replacement by fresh medium with or w/o stressor, is a sufficient stressor to trigger WRN's release from nucleoli (Suppl. Figure 14, uppermost red frame). We therefore modified our method accordingly, *i.e.* the medium was not aspirated for treatment but the stressor (or medium as control) was added to

achieve final concentration in the well. All experiments were conducted using this improved method.

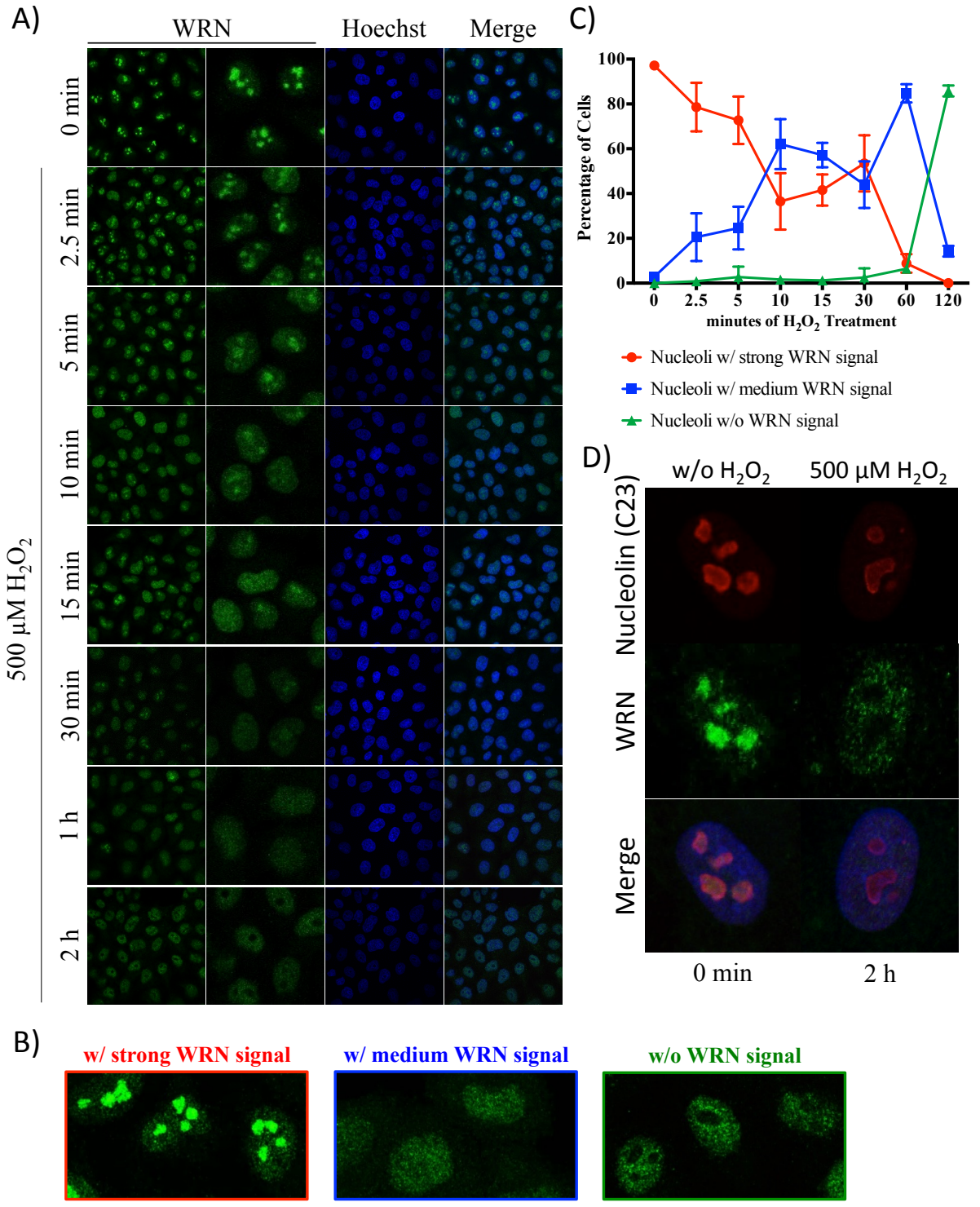

Figure 34: WRN relocalizes from nucleolus to nucleoplasm upon oxidative stress.
A. HeLa cells were treated with either 500 µM H_2O_2 or medium as control and were fixed using 4% PFA after the indicated treatment times. Pictures were taken using confocal microscopy. WRN is depicted in green, Hoechst nuclear staining in blue. The right-hand WRN pictures are blow-ups of the original picture for better illustration. Shown is one representative experiment out of three independent experiments. **B.** Exemplary pictures of the different conditions that were analyzed: nucleoli with strong (red), medium (blue) or no (green) WRN signal. **C.** Quantification of A, showing mean ± SD. At least 100 cells per experiment were analyzed, n=3. **D.** WRN resides mainly in nucleoli and leaves upon stress. Nucleolin as nucleolar marker is depicted in red, WRN in green and Hoechst in the merge picture in blue.

Next, we used camptothecin (CPT) as a stressor that induces a different kind of stress than H_2O_2, *i.e.* at submicromolar doses mostly replicative stress and strand-breaks, but also requires WRN for restart of the stalled forks (Thangavel et al., 2015). Since CPT treatment did not elicit such an immediate effect as H_2O_2 (Figure 34), the cells were treated for up to 6 h and fixed after each hour. When treated with 100 nM CPT, the WRN signal in the nucleoli changed from strong to medium after 1-2 h and most cells had empty nucleoli after 4 or more hours (Figure 35, middle part). With 1 µM CPT however, WRN was released much faster from the nucleoli to the nucleoplasm and the cells displayed empty nucleoli already 1 h after treatment (Figure 35, lowest part). DMSO, which was used as a solvent for CPT, had no effect on WRN's sub-nuclear localization.

PFA fixation can trigger artificial PAR formation

Even though the methanol:acetic-acid fixation is the method of choice for PAR immunofluorescence, we opted for a 4% PFA fixation method, thus enabling co-staining of WRN and PAR in the same experiment (the WRN antibody is incompatible with the methanol:acetic-acid fixation). In our initial immunofluorescence experiments, we often observed PAR signals in unstressed cells when using the 4% PFA fixation method, even at time point 0 min or in cells treated with PARP inhibitor (Suppl. Figure 15 A, red frame). Similar findings have previously been reported for ChIP experiments and possible suggested solutions were the use of methanol fixation or the use of PARP inhibitors (Beneke et al., 2012). Since the methanol:acetic-acid fixation was not an option we prevented artificial PARP1 activation during the 4% PFA fixation by adding the PARP inhibitor ABT-888 to the PFA solution, the PBS and the glycine solution. We rationalized that this blocks any artificial PARP activity during the fixation procedure until the cells are lysed with Triton X-100, which leads to a loss of PARP's substrate NAD^+. Indeed, our experiments show that with this modified approach no artificial PAR formation is observed (Suppl. Figure 15 B). Consequently, all experiments shown here were conducted using this modified protocol. Furthermore, our experiments revealed a more even PAR signal, when treatment of cells was performed in medium instead of PBS (data not shown). However, since medium inactivates H_2O_2 partly, the dose was increased accordingly (500 µM H_2O_2 in medium roughly corresponds to 100 µM in PBS).

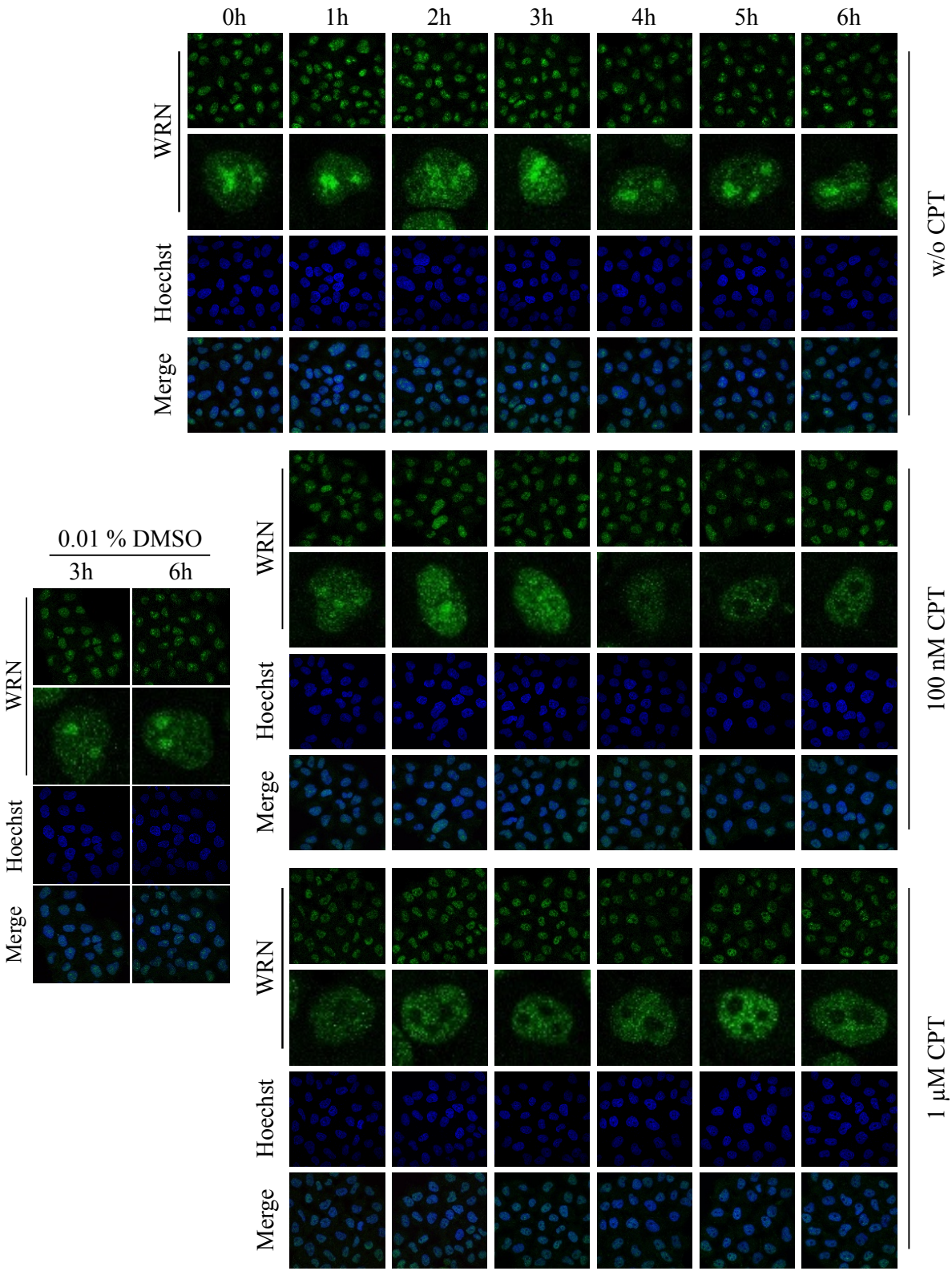

Figure 35: Stress-dependent WRN relocalization is not restricted to oxidative stress.
HeLa cells were treated with either 0.1 or 1 µM camptothecin (CPT) or medium as control for the indicated times and were fixed using 4% PFA. WRN is depicted in green, Hoechst nuclear staining in blue. The lower WRN pictures for each treatment condition are blow-ups of the original picture for better illustration. Experiment was conducted once. DMSO control was prepared as control for CPT treatment (dissolved in DMSO).

WRN's translocation from the nucleoli is almost exclusively PARP1-dependent

The translocation wave of WRN 10 min after H_2O_2 treatment (Figure 34C) fits very good within the time frame of PAR synthesis, which is strongest between 5 and 10 min after treatment (Martello et al., 2013). To test our hypothesis that PARP1 or PAR regulate WRN's translocation, we treated HeLa WT cells or HeLa *PARP1* KO1 cells (Rank/Veith *et al.*, in preparation (Chapter VI), Figure 36 C) with H_2O_2 and followed the localization of WRN in the nucleus (Figure 36). Since the most relevant time points seemed to be around 10 min (maximum of PAR formation) and after more than 60 min (complete release of WRN from nucleoli upon stress induction) (Figure 34), we focused on the time points 10 min and 2 h in the following experiments. In untreated cells, we did not observe any difference in the localization of WRN between HeLa WT and *PARP1* KO1 cells (Figure 36 A&B). In both cell lines WRN is mostly localized in the nucleoli while some cells show a pan-nuclear distribution (~10%, Figure 36 B, left two columns). This small percentage of cells with pan-nuclear distribution is to be expected since the nucleolar structure is dissolved during cell replication. After a 2-h treatment with H_2O_2 however, there was a significant difference between the cell lines. While in most WT cells WRN completely disappeared from nucleoli, only few of the *PARP1* KO1 cells show no or weak WRN signal in the nucleoli (~30%) and most have WRN still located in the nucleoli (~70%) (Figure 36 A&B, the two right-hand columns).

PARP activity plays a minor role in WRN translocation from the nucleoli

Since the presence of PARP1 is necessary for WRN's translocation we tested, whether it is through protein-protein interaction, or PARP1's catalytic activity, or both. To this end, HeLa WT cells were treated with H_2O_2 and additionally with one of the two different PARP inhibitors ABT-888 (veliparib) or olaparib (Figure 37). Both inhibitors were capable to suppress PARP activity completely as evident from the PAR channel of the immunofluorescence pictures (Figure 37 A). In contrast to the *PARP1* KO1 cells however, the inhibitors only partly, but significantly, blocked the stress-induced translocation of WRN from the nucleoli. Whereas almost all untreated cells showed nucleoli with a strong WRN signal, more than half of the H_2O_2-treated cells displayed empty nucleoli (Figure 37 A&B, the two left-hand columns). Samples treated additionally with PARP inhibitor showed a reduction in cells with WRN-empty nucleoli (~50% reduction) and also displayed some cells with strong WRN signal in the nucleoli, when compared to cells treated with H_2O_2 only. However,

the effect of the PARP inhibitors was not as strong as observed in *PARP1* KO1 cells (Figure 36), suggesting an important role of direct protein-protein interaction between WRN and PARP1.

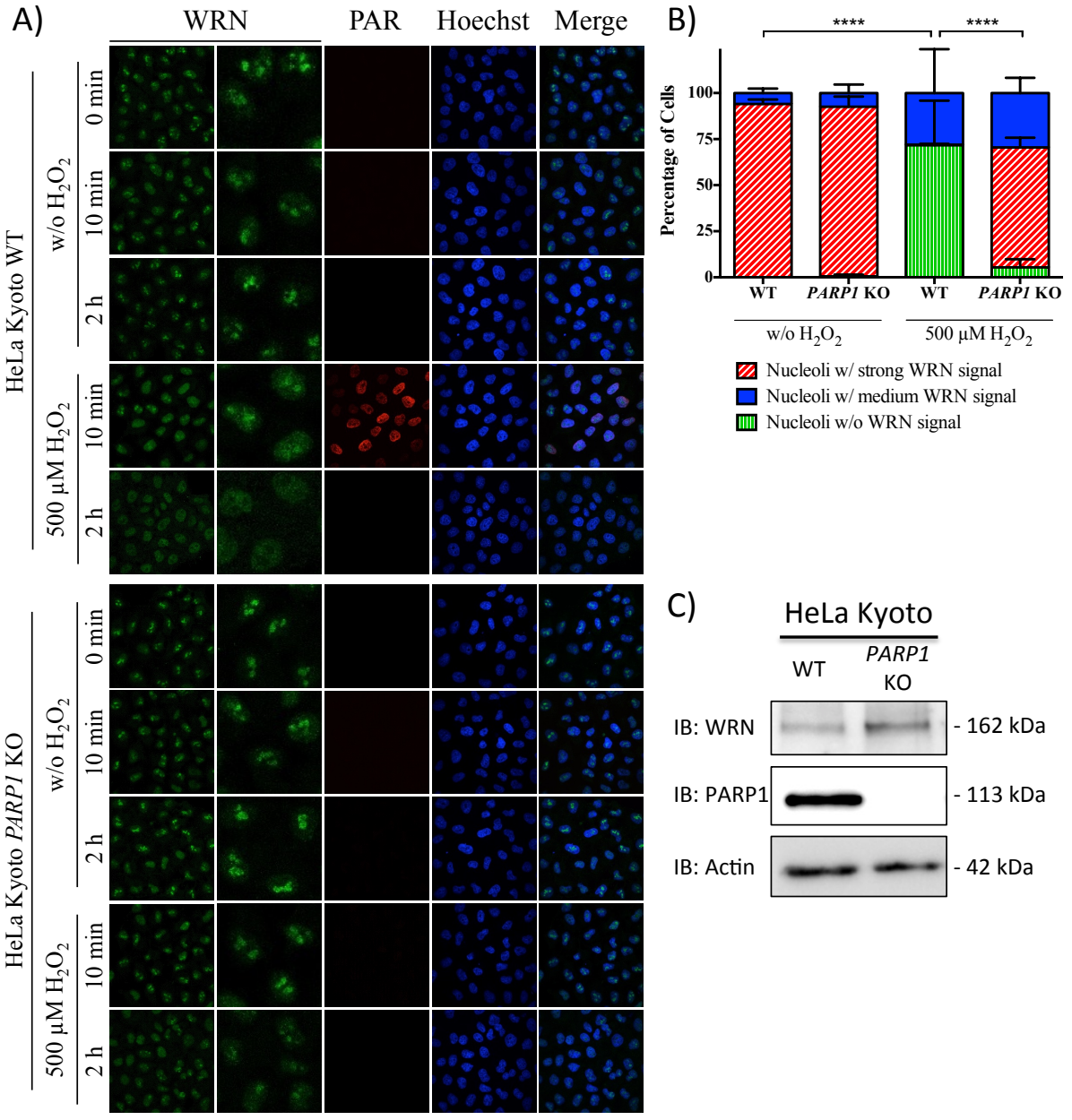

Figure 36: WRN relocalization is dependent on PARP1.
A. HeLa WT or HeLa *PARP1* KO cells were treated with either 500 µM H_2O_2 or medium as control and were fixed using 4% PFA. WRN is depicted in green, PAR in red and Hoechst nuclear staining in blue. The right-hand WRN pictures are blow-ups of the original picture for better illustration. Shown is one representative experiment out of three independent experiments. **B.** Quantification of A as mean ± SD. Only cells after two hours treatment were counted. Three independent experiments were analyzed and cells were divided into three categories: with strong, medium or no WRN signal in the nucleoli. At least 100 cells per experiment and treatment were analyzed. $p<0.0001$ = ****, Chi-squared analysis. **C.** Cell lysates of HeLa WT and HeLa *PARP1* KO cells were separated by SDS-PAGE and blotted on nitrocellulose. Immunoblotting against PARP1 confirmed that the HeLa *PARP1* KO cells are indeed deficient in PARP1.

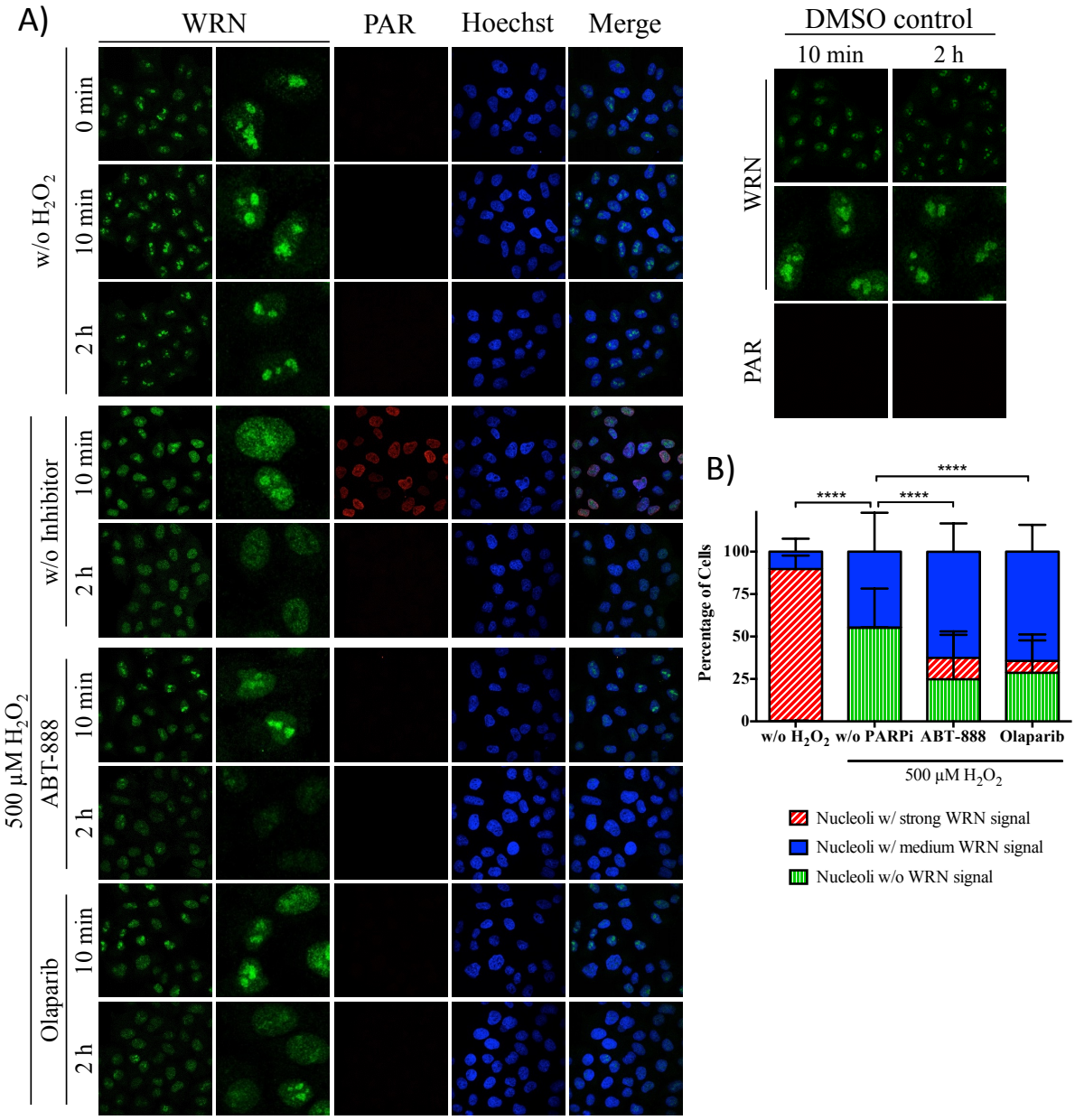

Figure 37: WRN relocalization is partially dependent on PARP activity.
A. HeLa WT cells that received additional PARP inhibitor treatment were pre-treated with either 10 µM olaparib or 10 µM ABT-888 for 30 min. Cells were then treated with either 500 µM H_2O_2 or medium as control and 10 µM of the respective inhibitor and were fixed using 4% PFA. WRN is depicted in green, PAR in red and Hoechst nuclear staining in blue. The right-hand WRN pictures are blow-ups of the original picture for better illustration. Shown is one representative experiment out of three independent experiments. **Right panel**. DMSO control was prepared as control for olaparib treatment (dissolved in DMSO). **B.** Quantification of A as mean ± SD. Only cells after two hours treatment were counted. Three independent experiments were analyzed and cells were divided into three categories: with strong, medium or no WRN signal in the nucleoli. At least 100 cells per experiment and treatment were analyzed. $p<0.0001$ = ****, Chi-squared analysis.

We found a strongly binding PBM in the RQC domain of WRN, which is both the interaction site with PARP1 and where the NTS is located (Figure 33). Since PARP inhibitors had a moderate effect on WRN relocalization from the nucleoli we asked ourselves whether the PBM4, located in the NTS, mediated this translocation of WRN. To that end, we generated a WRN-eGFP mutant that should bind PAR at PBM4 less efficiently (based on the Pepspot membrane, Figure 33 D, PBM4-mut3) by exchanging basic aa for alanines (WRNmPBM4-

eGFP). HeLa WT cells were then transfected with either WT WRN-eGFP or WRNmPBM4-eGFP and 24 h after transfection cells were challenged with 500 µM H_2O_2 for 2 h. Interestingly, the impaired PAR-binding capacity of WRNmPBM4 had no effect at all on the relocalization of WRN upon oxidative stress (Figure 38). Both WT and mPBM4 WRN were distributed similarly, almost exclusively in the nucleoplasm with empty nucleoli. However, while basically all untreated cells had WT WRN stored in the nucleoli, a considerable fraction of unstressed cells had WRNmPBM4 equally distributed throughout the nucleus (Figure 38 B, two left columns).

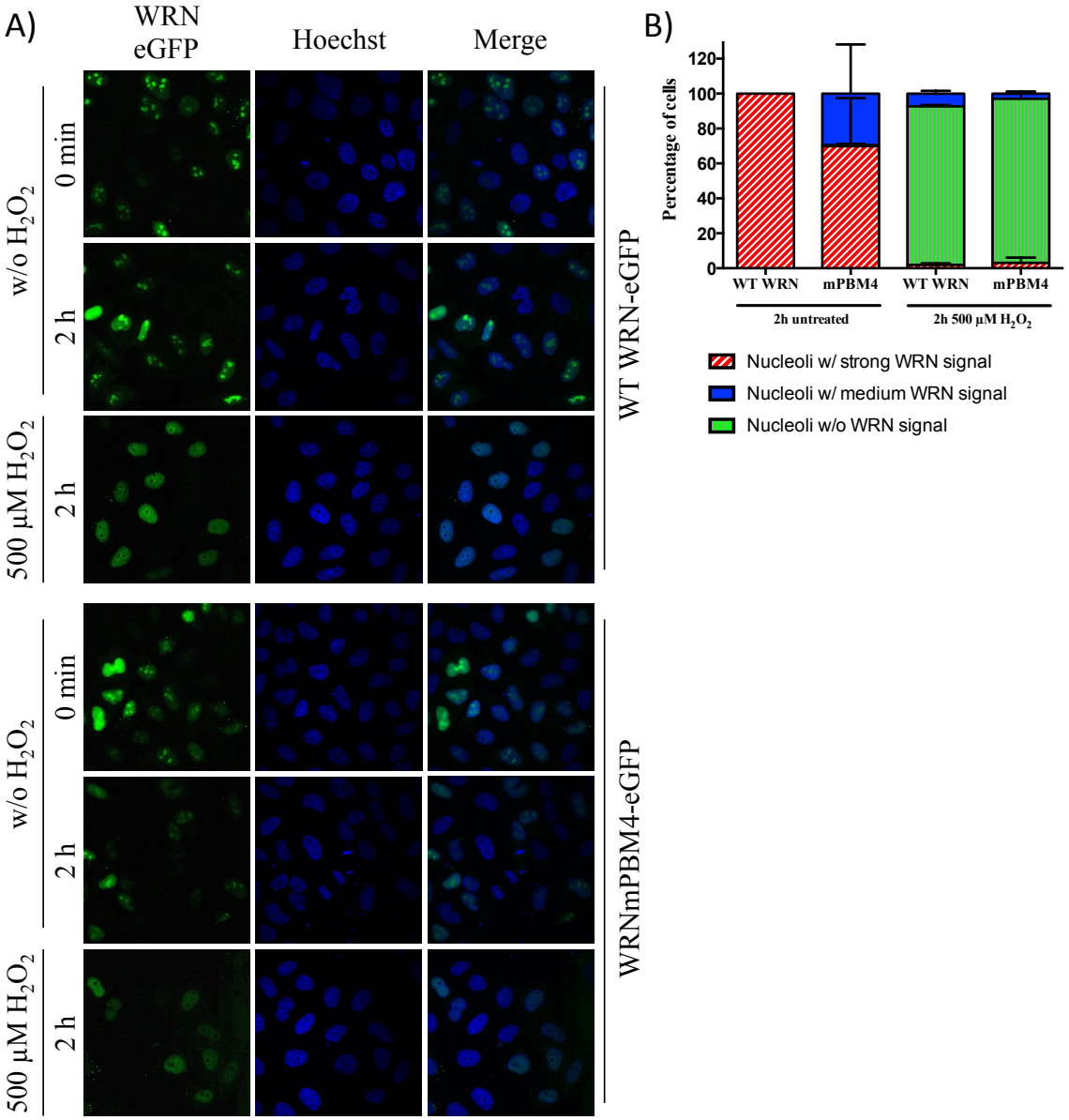

Figure 38: PBM4 is not relevant for WRN translocation.
A. HeLa WT cells were transfected with either WT WRN-eGFP or WRNmPBM4-eGFP, followed by treatment with either 500 µM H_2O_2 or medium as control and were fixed using 4% PFA. WRN is depicted in green and Hoechst nuclear staining in blue. Shown is one representative experiment out of two independent experiments. **B.** Quantification of A as mean ± SEM. Only cells after two hours treatment were counted. Two independent experiments were analyzed and cells were divided into three categories: with strong, medium or no WRN signal in the nucleoli. 30-100 cells per experiment and treatment were analyzed.

Since we only measured the WRN distribution up to two hours it is possible that the relocation in the *PARP1* KO cells is only delayed instead of being strongly reduced. Therefore, to discriminate between true reduction and a delay in relocalization of WRN, we conducted a long-time experiment for up to 24 h (Figure 39 and Suppl. Figure 16). The cells were treated for 30 min with either 500 µM H_2O_2 or medium as control, followed by exchange for fresh medium to allow recovery. In unstressed WT and KO cells there is no change in WRN localization visible and also no difference between the cell lines detectable, as expected (Figure 39 C&E, Suppl. Figure 16 B&C). Treated WT and KO cells, however, differ strongly in their WRN distribution over time. *PARP1* KO cells only display a minor reduction of full nucleoli to ~60% 1 h after stress release, recovering after ~2 h to the initial levels (~95% at 0 h) (Figure 39 B&F). WT cells, on the other hand, release WRN completely from the nucleoli (*i.e.* empty nucleoli) 2-4 hours after stress release (Figure 39 A&D). Also the recovery to the initial levels takes much longer (up to 8 hours).

PARP1 translocates from nucleoli to nucleoplasm upon oxidative stress

There have been reports that PARP1 is located in the nucleoli and, similar to WRN, relocates upon stress induction (Guetg et al., 2012; Meder et al., 2005). To the best of our knowledge, however, no one has investigated the time frame of this relocation so far. Therefore, to investigate whether PARP1 relocates from the nucleoli in a similar time frame as WRN, we repeated our initial experiment (Figure 34) with an immunofluorescence staining against PARP1. We found that, indeed, PARP1 is stored in the nucleoli in unstressed cell, albeit not to such a high degree as WRN (~70% vs. ~95%, Figures 34 and 40, respectively). Also, similar to WRN, PARP1 relocates from the nucleoli to the nucleoplasm but much faster: 5 min after stress induction almost all nucleoli are either completely devoid of PARP1 or display a pan-nuclear distribution (Figure 40). After 2 h most nucleoli are empty, similar to the results obtained for WRN.

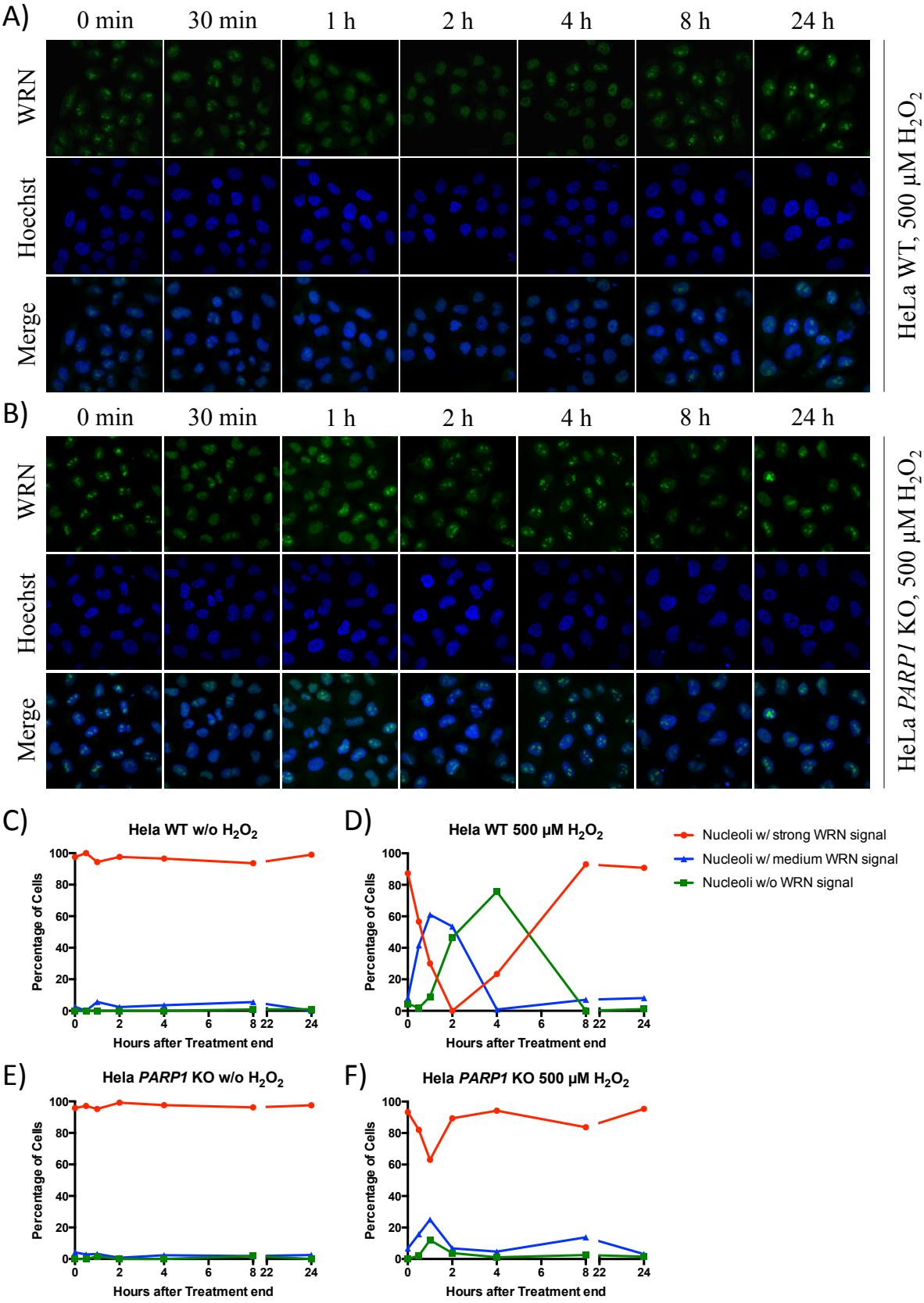

Figure 39: WRN returns to nucleoli after stress release.
A. HeLa WT cells, or HeLa *PARP1* KO cells **(B)**, were treated with 500 µM H_2O_2 for 30 min, followed by medium exchange for fresh medium. Cells were fixed and subjected to immunofluorescence at the indicated time points (Suppl. Figure 16A). WRN is depicted in green, Hoechst nuclear staining in blue. **C.** Quantification of Suppl. Figure 16 B. **D.** Quantification of A. **E.** Quantification of Suppl. Figure 16 C. **F.** Quantification of B. At least 100 cells per cell line and time point were analyzed and categorized according to Figure 34 B. N=1.

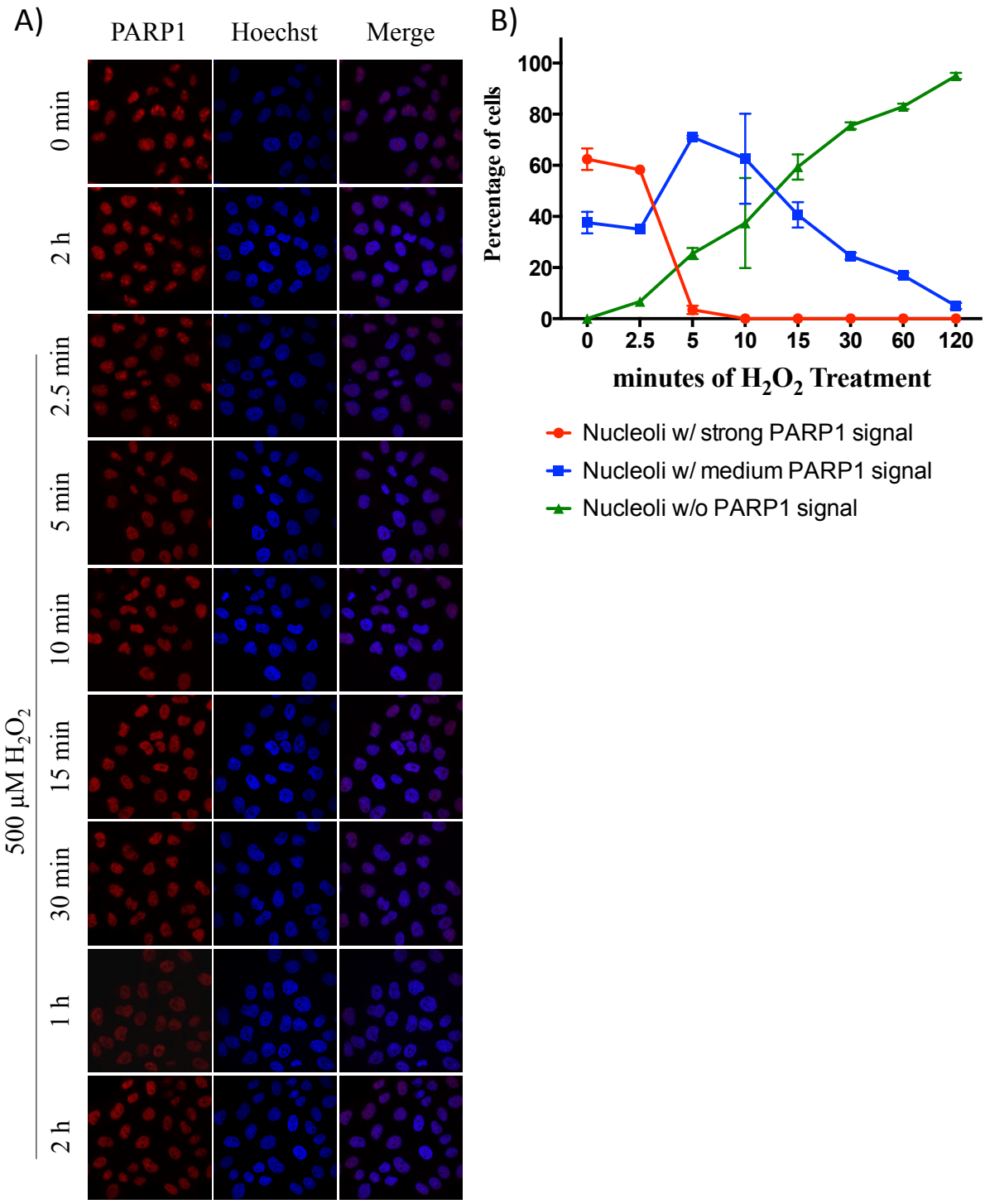

Figure 40: PARP1 relocalizes from nucleolus to nucleoplasm upon oxidative stress.
A. HeLa WT cells were treated with 500 µM H_2O_2 for the indicated time points (0 min and 2 h untreated controls), followed by fixation and immunofluorescence staining against PARP1. Shown is one representative experiment out of two independent experiments. **B.** Quantification of A as mean ± SEM. At least 100 cells per time point were analyzed and categorized according to Figure 34 B. N=2 (except time point 2.5 min: N=1).

Discussion

Previously, we reported the existence of four putative PBM's in WRN, of which at least 3 were shown to bind PAR (Popp et al., 2012). Here, we extend these studies by showing that the PBM3 in the helicase domain binds strongest, but closely followed by PBM1 and PBM 4 (PBM1, 3 and 4; Figure 33 D). This might also explain why we saw a much stronger impact of PAR-binding on WRN's helicase activity compared to its exonuclease activity (Popp et al., 2012). The reason, why we previously determined the PBM in WRN's EXO domain to be the strongest binder might be due to methodological differences: here, the peptides were synthesized on-membrane, ensuring equal amounts on each spot. In our previous study separately synthesized peptides were individually spotted on a membrane, allowing a higher variation in concentration. Equal concentration on the blot was verified by protein staining SyproRuby, which, as all protein dyes, is biased by its selectivity for certain AA. By performing PAR-binding assays with different recombinantly expressed and purified WRN fragments, we identified a novel PBM within the NTS (*i.e.*, PBM4). Albeit PAR binds to the protein fragment covering the nucleolar targeting sequence and the RQC domain, which is also essential for DNA binding, it is unlikely that it competes with DNA binding since both binding sites are on opposite sides of the RQC domain (Figure 33 E, PBM in grey, DNA binding residues in blue) (Kitano et al., 2010). PBM3 is positive for PAR binding in the peptide membrane overlay assay (this study) and also in a classical peptide binding study (Popp et al., 2012) but could not be tested in the protein since the respective fragment could not be overexpressed (data not shown). The fact that the helicase activity is the enzymatic activity of WRN that is strongest affected by PAR binding (Popp et al., 2012), combined with strong affinity for PAR in two independent assays, however, strongly implies PBM3 as a *bona fide* PBM in WRN, together with PBMs 1,4 and 5. A recent publication by ourselves confirms that helicase, ATPase and ss-annealing activity of WRN are inhibited by PAR interaction, albeit to a lesser degree than we have previously reported (Chapters III&IV) (Khadka et al., 2015; Popp et al., 2012). This is most likely due to much lower levels of PAR used. PBM1 is still among the strongest PAR binders in the peptides overlay assay, whereas the Fragment AA1-520, incorporating PBM1, displays only weak affinity for PAR (Figure 33 A vs. D). This implies that the structure of the PBM might play a role in non-covalent PAR-binding too, besides the semi-conserved sequence.

The results of a peptide PAR overlay assay can be used as a screening tool for novel PBMs, but as our experiments with longer fragments of WRN have shown it is necessary to confirm

these motifs in longer peptide sequences (full-length proteins or larger fragments thereof) where the secondary and tertiary structure play more important roles. Furthermore, the peptide assay is also a valuable tool to generate and evaluate possible mutations of the PBM's with minimal time and cost input. The advantage of this membrane, compared to individually synthesized peptides (as used in (Popp et al., 2012)), lies in its greater reproducibility. Also, the peptides are synthesized directly on the membrane, therefore minimizing the risk of dissolvation problems and guaranteeing equal amounts of peptide on each spot.

It has been known for some time that WRN is located primarily in the nucleoli and translocates to the nucleoplasm or to sites of DNA damage (foci) upon stress conditions (Constantinou et al., 2000; Gray et al., 1997; Kanagaraj et al., 2012; Kobbe and Bohr, 2002; Lan et al., 2005; Lee et al., 2005; 2015; Singh et al., 2012a). However, only little is known about the molecular mechanism of this phenomenon and why WRN is so prominently located in nucleoli in the first place. The explanations for the nucleolar localization range from a pure storage site to important functions of WRN in rRNA metabolism, which takes place in the nucleoli. Most likely however, both are true to some extent, since WRN can bind RNA/DNA-heteroduplexes and WS cells have been shown to have significantly decreased rRNA transcription (Shiratori et al., 2002; Suzuki et al., 1997). The fact that WRN leaves the nucleoli upon stress and returns after successful repair is, on the other hand, a strong indicator that the storage hypothesis might be correct (Karmakar and Bohr, 2005). Recent evidence suggests that the nucleolus functions as a sequestration site upon stress, thus allowing the shutdown of cellular processes that are not critical or might even interfere with the reaction to the stressor (Audas et al., 2012; Lam and Trinkle-Mulcahy, 2015). At the same time the nucleolus might release proteins to the nucleoplasm to cope with the stress, *e.g.* DNA repair proteins like WRN and PARP1, but which might otherwise be harmful to the cell homeostasis if allowed to roam freely in the nucleus.

Here we show that the WRN translocation from the nucleoli upon oxidative stress is almost completely PARP1 dependent: stressed *PARP1* KO1 cells display almost the same nuclear distribution of WRN as unstressed WT cells, *i.e.* most WRN is located in nucleoli (Figure 36 A&B). This implies that WRN is unable to leave the nucleoli in the absence of PARP1, even in the presence of strong oxidative stress. The reason for this might be either a direct interaction between PARP1 and WRN or the translocation is dependent on PARP activity, *i.e.* PAR synthesis. However, since PARP1 inhibitor treatment had only a mild to moderate impact on WRN translocation upon H_2O_2-treatment, it is likely that WRN translocation is not

dependent on PARP1 activity but rather direct protein interaction (Figure 37). This is supported by our finding that PAR-binding to the PBM located in RQC domain has no effect *in vivo*. We see no difference in WRN's localization when comparing WT WRN and WRNmPBM4 (Figure 38). However, this particular mutant should still have roughly 50% PAR-binding capacity at the mutated PBM4, compared to WT PBM4 (based on the peptide mutagenesis, Figure 33 D, PBM4-mut3). This might explain the lack of an effect in localization and, furthermore, it is still possible that another PAR-binding motif or, as discussed above, direct interaction with PARP1 is responsible for translocation or even that covalent modification plays a role in this. As a side note, it would be possible to decrease the PAR-binding capacity of PBM4 much stronger by exchanging two more aa (Figure 33 D, PBM4-mut5), however, these two aa directly flank the two aa that are crucial for DNA binding of WRN (aa F1037&M1038) (Kitano et al., 2010). Thus, tempering with these aa would most likely have severe consequences for WRN's functions and therefore the negative consequences of the mutagenesis would dwarf the potential benefits.

The importance of protein-protein interaction between WRN and PARP1 for WRN's nucleolar localization is also underlined by the fact that PARP's interaction site in WRN is located in the RQC domain (Kobbe et al., 2004a). Recently, a novel inhibitor of PARP1 protein-protein interactions has been described (Na et al., 2015). This inhibitor could be employed to determine whether the relocalization of WRN upon oxidative stress is dependent on direct interaction with PARP1 or whether other proteins are involved therein as well.

Since WRN is still mainly localized to the nucleoli in unstressed cells, despite the absence of PARP1, PARP1 seems to have no influence in the recruitment/detainment of WRN into the nucleoli. This process seems to be regulated by phosphorylation and possibly by VCP interaction with WRN (Indig et al., 2004; Karmakar and Bohr, 2005; Partridge et al., 2003).

Unexpectedly, medium change alone turned out to be a sufficient trigger to release WRN from the nucleoli (Suppl. Figure 14). Potentially the sudden short contact with air is sufficient to induce oxidative stress in the cells or sheer stress is induced by the aspiration and addition of medium, but this problem can be overcome with an optimized treatment protocol as reported in this study. In general, taking these results into account, it is advisable to evaluate data concerning the translocation of WRN with great care. Furthermore, our findings indicate that immunofluorescence stainings of PAR should be carefully planned and executed as artificial PAR formation can easily arise and be misinterpreted (Suppl. Figure 15). A similar effect has been previously described for ChIP assays with PAR (Beneke, 2012).

We wanted to test whether the reduction in empty nucleoli in *PARP1* KO cells is a real reduction, *i.e.* if much less WRN translocates from the nucleoli to the nucleoplasm after stress as in WT cells, or if the translocation is just delayed by the loss of PARP1. Therefore we observed the cells for a much longer time frame (24 h). The WRN levels in *PARP1* KO cells resemble nicely the values obtained in the first experiment (Figure 34). However, we do not see any stronger reduction of WRN levels in the nucleoli later than 2 h in the *PARP1* KO cells, thus eliminating the possibility that the loss of PARP1 merely delays the efflux of WRN out of the nucleoli. In WT cells WRN completely leaves the nucleoli after stress induction but returns in the course of the following 6 h. 8 h after stress release WRN levels in the nucleoli are back to the initial levels (Figure 39 D).
Of note, there is a small reduction of the WRN signal in the nucleoli in both WT and KO cells after 1 h detectable. This arises most likely from a necessary change in the experimental protocol: in order to relieve the cells from the stress we had to aspirate the H_2O_2-containing medium and replace it with fresh medium. Although this was executed as careful as possible, some stress could have been inflicted on the cells, causing a minor and short efflux of WRN from the nucleoli (Suppl. Figure 14).

Over time, several groups provided data, that acetylation as a posttranslational modification plays a significant role in WRN translocation (Blander et al., 2002; Karmakar and Bohr, 2005; Lee et al., 2015; Li et al., 2008; 2010). However, these papers strongly vary in their results and sometimes even contradict each other, *e.g.* Blander and colleagues show that WRN is acetylated by p300 and acetylation leads to an increase in translocation, whereas Lee *et al.* recently showed that inhibition of SIRT1 blocks translocation of WRN (Blander et al., 2002; Lee et al., 2015). Ignoring the publication from Lee and colleagues, however, the available data taken together paints the following picture: WRN is acetylated upon DNA damage by CBP or p300, causing the translocation from nucleoli to nucleoplasm where it can act on the DNA damage. The acetylation of WRN inhibits its catalytic activities until both the timing and the place is correct for DNA repair. It is then deacetylated by SIRT1 and/or other HDACs (histone de-acetylases) and can thus act on its substrates. Deacetylation, and/or potentially phosphorylation, then regulates the re-translocation of WRN into the nucleolus after successful repair (Blander et al., 2002; Karmakar and Bohr, 2005; Li et al., 2008; 2010). Sustained acetylation, *e.g.* by SIRT1 inhibition, may prevent WRN from repair and relocalization to the nucleoli and target it for degradation (Kahyo et al., 2008). Of note, one of these publications specifically states that WRN did not translocate upon UV damage and thus

the authors conclude that WRN is not involved in the NER repair pathway. They furthermore showed that WRN was neither acetylated nor phosphorylated upon UV damage, in contrast to cells treated with mitomycin C (MMC) or MMS (Karmakar and Bohr, 2005). This again strongly disagrees with Lee and colleagues, who used cisplatin as stressor, mimicking UV damage (Lee et al., 2015). On the other hand, all papers that show acetylation of WRN upon stress used stressors that induce damages primarily repaired via the NER or DSBR pathways (*i.e.* IR, cisplatin, UV, MMC, MMS) (Blander et al., 2002; Karmakar and Bohr, 2005; Lee et al., 2015; Li et al., 2008; 2010). Taken together, this suggests that acetylation of WRN is a specific regulatory mechanism of WRN in NER and DSBR. There is no evidence so far that acetylation is involved in the spatio-temporal regulation of WRN upon oxidative damage. This strongly supports our data that show that WRN's translocation upon oxidative stress is mediated by PARP1, which is also implicated in the repair of oxidative lesions. To date, however, it is unclear what role PARP activity might play in this regard and whether PARP1 is also necessary for translocation back into the nucleoli.

The varying data for WRN's translocation in and out of the nucleolus suggest that there is not one system or interaction regulating the translocation, *i.e.* (de-)acetylation, phosphorylation or PAR(P) interaction, but more likely a mixture of these. Also, these results were generated under strongly varying conditions, thus making it more likely that there are different systems for different circumstances, which might work alone or in concert with others. In total, this might represent an adaptive system to release WRN only when it is needed to cope with the induced damage and otherwise retains it in the nucleolus (Karmakar and Bohr, 2005).

Material and Methods

Cell culture and treatment conditions

HeLa Kyoto and HeLa Kyoto *PARP1* knock-out 1 (KO1) cells (Rank/Veith *et al.*, in preparation) were kept at 37°C, 5% CO_2 and 95% humidity. The cells were cultured in DMEM (41966-029, Gibco) supplemented with 10% FBS (Biochrom), 2 mM L-Glutamine (Sigma-Aldrich) and 1% penicillin/streptomycin (Gibco). Cells were seeded on cover slips for immunofluorescence and treated for the indicated times with H_2O_2 (Merck-Millipore; diluted in medium) or camptothecin (CPT; Sigma-Aldrich; dissolved in DMSO, diluted in medium). PARP inhibitors, when employed, were added to the cells 30 min prior to treatment with H_2O_2 or CPT and were also present during the treatment. ABT-888 (veliparib, Selleckchem) was dissolved in MilliQ-water, olaparib (AZD2281, Selleckchem) was dissolved in DMSO. In order to avoid stress generation that also causes WRN to leave the nucleoli both inhibitors (Suppl. Figure 14), H_2O_2 and CPT were added to the medium to the indicated final concentration instead of aspirating and replacing the whole medium.

Immunofluorescence microscopy

After treatment, the cover slips bearing the cells were briefly washed with PBS, followed by 20 min fixation with 4% paraformaldehyde (PFA, Merck-Millipore) in PBS. The fixation process was stopped by treatment with 100 mM glycine for 1 min, followed by a 5-min wash in PBS. Cells were permeabilized with 0.4% Triton X-100 (Roth) in PBS for 3 min, followed by another 5-min wash step in PBS. The cover slips were then blocked for 1 h in 5% milk powder in PBS with 0.2% Tween 20 (Sigma) (PBSMT), followed by 1-h incubation with primary antibody in PBSMT at 37°C (H-300 rabbit anti-WRN 1:50, Santa Cruz; mouse anti-C23 (nucleolin) Clone D6 1:500; Santa Cruz; 10H mouse anti-PAR 1:300). Next, the cover slips were washed thrice for 10 min with PBS, followed by 1-h incubation with secondary antibody in PBSMT at 37°C (goat anti-rabbit Alexa-488 and goat anti-mouse Alexa-647, both 1:400; Life Technologies). The cover slips were again washed thrice for 10 min with PBS, followed by nuclear staining with Hoechst 33342 (Life Technologies) for 5 min. The cover slips were washed again thrice for 10 min with PBS, mounted in Aqua Polymount (Polysciences) and left for hardening over night. In case of PARP1, all blocking steps and

antibody incubation steps were performed in 1% BSA solution (mouse anti-PARP1 CII-10, 1:300). The rest was performed as described above.

For the methanol:acetic-acid fixation (Léger et al., 2014) the cells were also briefly washed in PBS after treatment, followed by a 7-min fixation step with ice-cold methanol:acetic-acid (3:1) at -20°C. The cells were then washed twice with PBS for 5 min. After that, the cells were blocked in PBSMT and were further treated as described above.

To ensure that no artificial PAR production occurred during the fixation procedure PARP inhibitor ABT-888 was present in PBS, 4% PFA and glycine in a final concentration of 10 μM until permeabilization of the cells (Suppl. Figure 15).

Microscopy pictures were taken using a Zeiss LSM 510 Meta microscope with a 63x/1.4 Oil DIC objective. Microscopy of treated and untreated cells and counting of nucleoli was done blinded for an unbiased analysis.

Plasmids

pEGFP::C3-WRN-WT was a kind gift from Vilhelm Bohr, NIA, Baltimore, USA. pEGFP::C3-WRNmPBM4 was generated by two successive rounds of site-directed mutagenesis' using a modified protocol from Zheng *et al.* (Zheng et al., 2004) with the following primer pairs:

5'-TGGCTTGCTGCAGCTAATACAGAATCTCAGAGCCTCATC-3' and

5'-TATTAGCTGCAGCAAGCCAATTTCTACCCTTTTTCGTAAGG-3';

5'-CGCCCTTACGGCAGCGGGTGCAAATTGGCTTGCTGCAGCTAATAC-3' and

5'-CAATTTGCACCCGCTGCCGTAAGGGCGCAAATCTTCATAAATTTG-3'.

The mutated bases are underlined. The successful base-exchange was checked by DNA sequencing (GATC Biotech).

Transfections

Twenty four hours after seeding, HeLa cells were transfected with pEGFP::WRN-WT or pEGFP::WRNmPBM4 using Lipofectamine 3000 (Invitrogen). The cells were transfected according to the manufacturer's instructions. 24 hours post-transfection cells were treated and immunofluorescence was performed as described above. GFP was detected using an anti-GFP antibody (Roche, 11814460001, 1:150 in PBSMT).

In silico search for PAR binding motifs

WRN was screened for PAR-binding motifs (PBM) using PATTINPROT (https://npsa-prabi.ibcp.fr/cgi-bin/npsa_automat.pl?page=npsa_pattinprot.html) as previously described (Pleschke et al., 2000; Popp et al., 2012). The pattern [HKR]-X-[AVILFWP]-[AVILFWP]-[HKR]- [HKR]-[AVILFWP]-[AVILFWP] was searched against the full-length protein sequence of WRN (http://www.uniprot.org/; Q14191 WRN_HUMAN), allowing one mismatch.

Far-western blot with PAR (PAR-overlay blot)

The PepSpot peptide membrane was purchased from JPT, with acetylated N-termini for enhanced stability. According to the manufacturer's instructions the membrane was activated in 100% methanol for 5 min, followed by a 5-min wash in TNT (150 mM NaCl, 10 mM Tris-HCl pH8.0, 0.05% (v/v) Tween 20) and a 1-h incubation in TNT. PAR incubation occurred over night at 4°C with 0.2 µM unfractionated PAR in TNT. PAR was synthesized and purified as previously described (Popp et al., 2012). The membrane was washed thrice for 10 min with high salt buffer (1 M NaCl in TNT), followed by three 5-min washes with TNT. Next, the membrane was blocked in 5% milk powder in TNT for 1 h, followed by 1-h incubation with anti-PAR antibody 10-H (1:300 in 5% milk in TNT). After three more 5-min washes with TNT, the membrane was incubated with goat-anti-mouse-HRP antibody (1:2000 in 5% milk in TNT) for 1 h. After three final washes in TNT, the chemiluminescent signal was detected using a LAS 4000 mini (GE Healthcare).
The recombinant WRN fragments were size-separated on a 4-20% SDS gel (Biorad) and blotted on a PVDF membrane. The blot was then incubated for 1 h at RT with 0.2 nM unfractionated PAR in TNT. The rest of the procedure was performed as described above.

Generation and purification of recombinant WRN fragments

The WRN fragments were generated by PCR extraction using the 6xHis-WRN-FLAG/pFastbac1-InteinCBDAla construct kindly provided by T. Kulikowicz and V. Bohr (NIA) (Tadokoro et al., 2012a). The vector backbone containing the N-terminal His-tag and the C-terminal InteinCBD-tag was PCR-extracted using the following primer pair:

5’-GTGATGGTGATGGTGATGAG-3’ and 5’-GATTACAAGGATGACGACGA-3’. The four fragments were PCR extracted from the same vector using the following 5’-phosphorylated primer pairs:
Fragment 1-520 AA: 5’-AGTGAAAAAAAATTGGAAACAACTG-3’ and 5’- TTCCCCTTCATTAGCTTCATTTT-3’; Fragment 490-760 AA: 5’- CTGGGTCTTCCTACTAAAGAAG-3’ and 5’-CAGATCCTGAAGGATATTCCCT-3’; Fragment 910-1240 AA: 5’-AAATATCTTCATTCTAGCAGATGTAG-3’ and 5’-ATTTTTTGCTACCAGACTCGT-3’; Fragment 1210-1432: 5’-GACCTCTTTTCAAGTACAAAACC3’ and 5’-ACTAAAAAGACCTCCCCTTTTC-3’. The phosphorylated inserts and the vector backbone were ligated using the Roche Quick Ligation Kit. The obtained plasmids were checked for mutations and correct orientation by DNA sequencing. Bacmids and baculoviruses of the four fragments were then generated using the Bac-to-Bac TOPO Cloning Kit (Invitrogen) as per the manufacturers instructions. HighFive insect cells were transfected with the respective baculovirus with an MOI of 10 and were harvested after 48 h.

The proteins were purified as previously described (Tadokoro et al., 2012a). Briefly, the cell pellets were lysed in lysis buffer using ultra sonication. Cell debris was spun down using centrifugation and the lysate was further clarified by filtration through a 0.22 µm filter. The proteins were purified using an ÄKTA FPLC with a 5 ml Ni-Sepharose FF column (GE Healthcare). Protein-containing fractions were identified by coomassie staining and pooled for the second step of the purification. The pooled fractions were loaded on a column packed with chitin-sepharose beads (NEB) and the flow-through was re-loaded twice onto the column. The proteins were incubated on-column over night at 4°C with 2-mercaptoethanol to allow intein-self-cleavage. The tag-free proteins were then eluted and concentrated using Amicon 10-kD cut-off centrifugal filters (Merck-Millipore). The proteins were shock-frozen in liquid nitrogen and stored at -80°C.

Supplementary Data

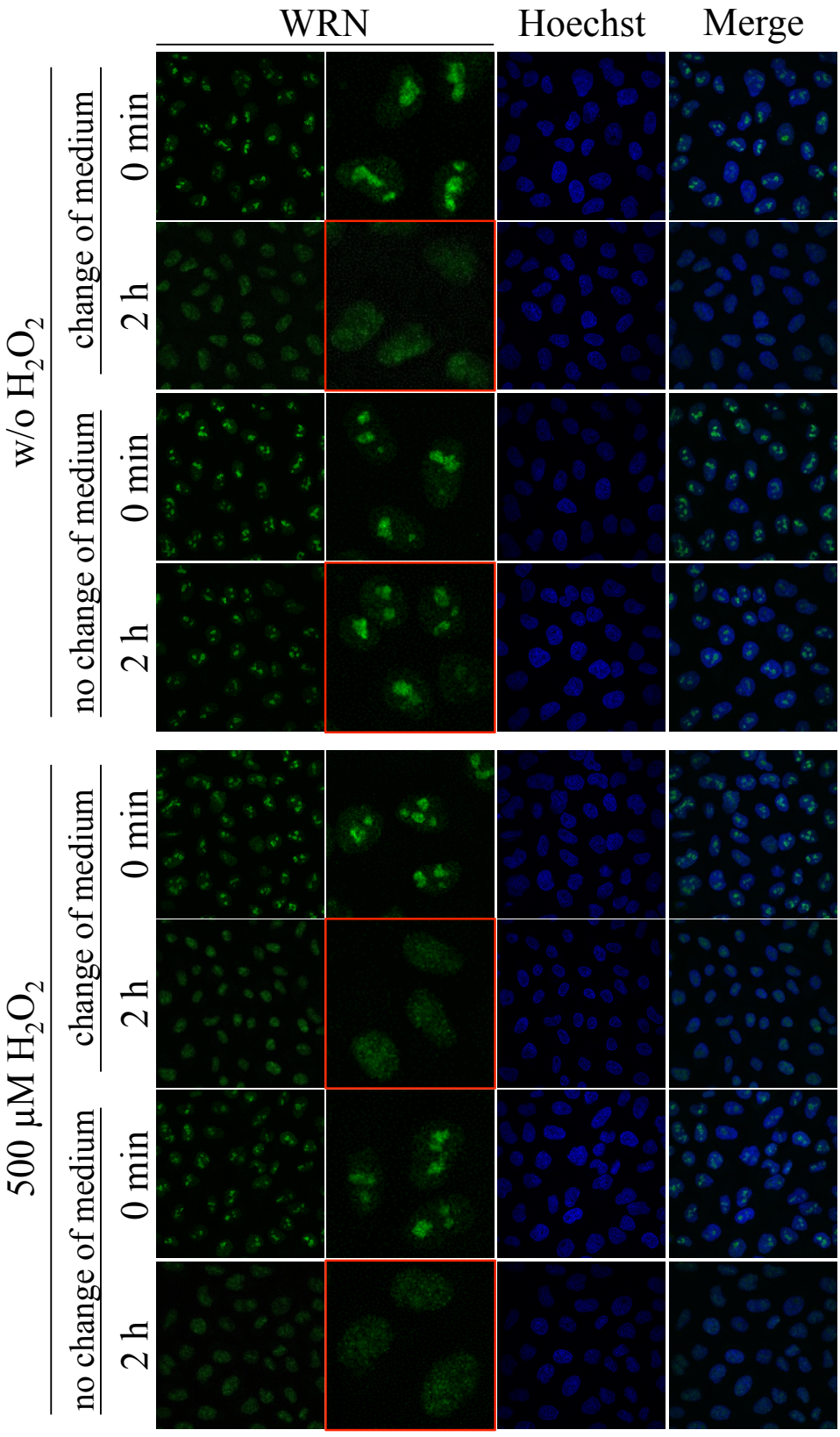

Supplementary Figure 14: Medium change is a sufficient stressor to trigger WRN relocalization.
HeLa WT cells were treated with either 500 µM H_2O_2 or medium as control for the indicated times. The medium was either completely aspirated and replaced by H_2O_2 in medium or the H_2O_2 was added carefully in a higher concentration to the medium to achieve the working concentration of 500 µM. WRN is depicted in green and Hoechst nuclear staining in blue. The right-hand WRN pictures are blow-ups of the original picture for better illustration.

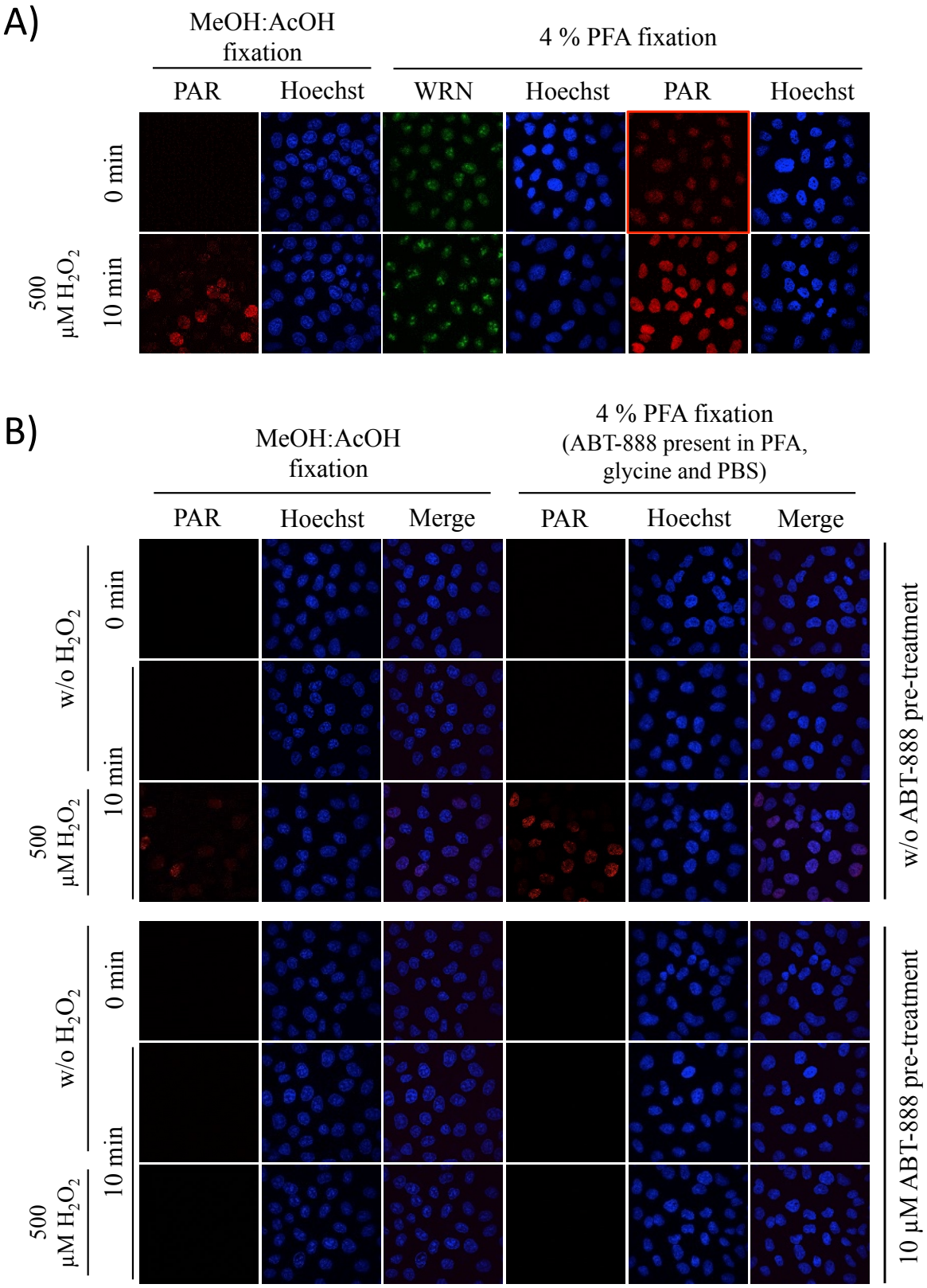

Supplementary Figure 15: Optimization of PFA fixation procedure.
A. HeLa WT cells were treated with either 500 µM H_2O_2 (10 min) or were fixed at 0 min. Cells were fixed either by methanol:acetic-acid protocol or by 4% PFA protocol. With 4% PFA fixation PAR is induced during the fixation procedure (marked red). **B.** HeLa WT cells were treated with either 500 µM H_2O_2 or medium as control for 10 min or were fixed at 0 min. In the lower half of the figure cells were additionally treated with 10 µM ABT-888 during H_2O_2 treatment and 30 min prior to treatment. Cells were fixed either by methanol:acetic-acid protocol or by a modified 4% PFA protocol with 10 µM ABT-888 present in PFA, glycine and PBS. PAR is depicted in red, Hoechst nuclear staining in blue and WRN in green.

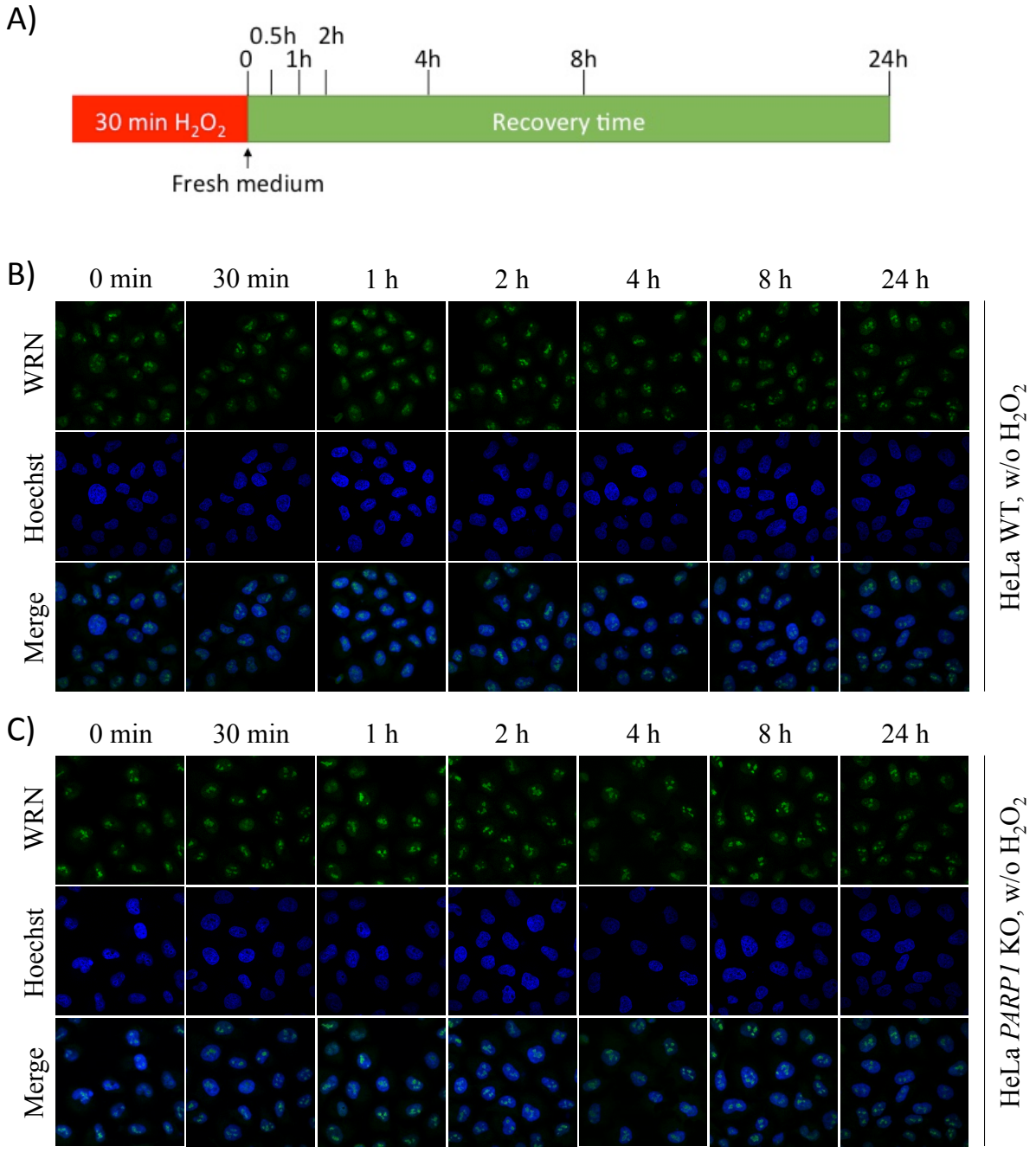

Supplementary Figure 16: Recovery of WRN nucleolar distribution.
A. Scheme of the experimental setup. HeLa cells were treated for 30 min with 500 µM H_2O_2 or medium as control, followed by an exchange for fresh medium to allow recovery. Cells were fixed and substituted for immunofluorescence at the indicated time points. **B.** HeLa WT cells treated according to A with medium as control. WRN is depicted in green and Hoechst nuclear staining in blue. **C.** HeLa *PARP1* KO cells treated according to A with medium as control. WRN is depicted in green and Hoechst nuclear staining in blue. Quantifications for B and C are shown in Figure 39 C&E, respectively.

PARP1 and PARylation

Chapter VI: Analyzing structure-function relationships of PARP1 by reconstituting HeLa *PARP1* knock-out cells with artificial and natural PARP1 variants

Lisa Rank, Sebastian Veith*, Eva Gwosch, Janine Demgenski, Magdalena Ganz, Marjolijn Jongmans, Christopher Vogel, Arthur Fischbach, Stefanie Bürger, Anna Stier, Sascha Beneke, Jan M F Fischer, Christina Renner, Roland P Kuiper, Alexander Bürkle, Elisa Ferrando-May, and Aswin Mangerich*

Manuscript

* Equal contribution

Abstract

Various forms of genotoxic stress activate PARP1, resulting in the synthesis of the post-translational modification poly(ADP-ribose) (PAR). Here we generated a genetic knock-out of *PARP1* in one of the most widely used human cell systems, *i.e.*, HeLa *PARP1* KO cells, via TALEN-mediated gene targeting and characterized these cells with regards to PARylation metabolism and genotoxic stress response. Furthermore, by reconstituting HeLa *PARP1* KO cells with a series of artificial and natural PARP1 variants, we analyzed structure-function relationships of PARP1 in a cellular environment without interfering with endogenously expressed WT-PARP1. We confirmed that the PARP1\E988K mutant exhibits mono(ADP-ribosyl)ation activity, and extended previous reports by demonstrating that the PARP1\L713F mutant is constitutively active in a cellular environment, leading to high cellular PAR levels even in unchallenged cells. Additionally, both mutants exhibited significantly altered recruitment and dissociation kinetics at sites of laser-induced DNA damage, which can partially be attributed to non-covalent PARP1-PAR interaction via at least one specific PAR binding motif located in zinc finger 2 of PARP1. Consistent with strong changes in their cellular biochemistries, expression of both mutants had distinct cellular consequences. *E.g.*, while the expression of PARP1\L713F itself triggered apoptosis, PARP1\E988K led to alterations in cell cycle distribution and sensitized cells to CPT treatment. Interestingly, pharmacological PARP inhibition mitigated effects of the E988K mutant, suggesting distinct functions of mono-ADP-ribosylation. Finally, by reconstituting *PARP1* KO cells with a natural cancer-associated PARP1 SNP variant (V762A) as well as a newly identified inherited PARP1 mutation present in a patient with pediatric colorectal carcinoma (F304L-V762A), we demonstrate that these variants exhibit altered biochemical and cellular properties, potentially supporting carcinogenesis. Together, this study establishes a novel model for PARylation research and reveals new insight into the structure-function relationships of artificial as well as natural PARP1 variants in a cellular environment, with implications for PARP research in general.

Introduction

Poly(ADP-ribosyl)ation (PARylation) is a post-translational modification that plays key roles in cellular physiology and stress response (Gibson and Kraus, 2012; Hottiger, 2015; Mangerich and Bürkle, 2012). It mainly occurs in the nucleus and to a lesser extent in the cytoplasm. The reaction is carried out by enzymes of the family of poly(ADP-ribose) polymerases (PARPs), which use NAD^+ to synthesize poly(ADP-ribose) (PAR), a biopolymer with variable chain length and branching. Of the 17 members of the human *PARP* gene family, at least five have been shown to be true PARPs, *i.e.*, these do exhibit PAR-forming capacity, while other family members act as mono(ADP-ribosyl) transferases or are catalytically inactive. PARP1 is a highly abundant, chromatin-associated protein that exhibits PARylation activity. Upon binding to DNA damage, in particular to strand breaks, and subsequent conformational rearrangements, PARP1 is catalytically activated and is thought to contribute to the bulk of the cellular PAR formation (Gibson and Kraus, 2012). This can happen either in *cis*, by activation of a single PARP1 molecule, or in *trans*, by PARP1 dimerization at sites of DNA damage (Ali et al., 2012; Coquelle and Glover, 2012; Langelier and Pascal, 2013; Langelier et al., 2012; Mendoza-Alvarez and Alvarez-Gonzalez, 1993). Apart from DNA damage-dependent activation, PARP1 activity is also regulated by post-translational modifications, such as phosphorylation, acetylation, and SUMOylation (Cohen-Armon et al., 2007; Hassa et al., 2005; Kauppinen et al., 2006; Messner et al., 2009; Walker et al., 2006), as well as by direct protein-protein interactions (Berger et al., 2007; Guastafierro et al., 2008; Krukenberg et al., 2014; Midorikawa et al., 2006). Catalytic activation leads to covalent PARylation of hundreds of target proteins (Jungmichel et al., 2013; Zhang et al., 2013), however, PARP1 itself is the main target of its modification (*i.e.*, PARP1 automodification) (Gagné et al., 2015). In addition to covalent PARylation, PAR can interact with other proteins non-covalently via distinct PAR binding modules (Krietsch et al., 2012). Importantly, PARylation is highly dynamic (Alvarez-Gonzalez et al., 1999; Martello et al., 2013), because shortly after being synthesized, PAR is rapidly hydrolyzed by poly(ADP-ribose) glycohydrolase (PARG) and other catabolizing enzymes (Barkauskaite et al., 2015; Jankevicius et al., 2013; Niere et al., 2012; Rosenthal et al., 2013). Thereby, PARylation transiently modulates physico-chemical properties and spatio-temporal activities of target proteins, including chromatin, DNA repair factors, and PARPs themselves (Altmeyer et al., 2015; Fischer et al., 2014; Mangerich and Bürkle, 2012; Popp et al., 2012). On the cellular level, PARylation fulfills pleiotropic functions in genome maintenance, including DNA

repair, telomere length regulation and re-initiation of stalled replication forks (Bai, 2015; Robert et al., 2013). Moreover, it is involved in a host of further cell functions, such as chromatin remodeling, transcription, epigenetics, signaling, cell cycle, and regulation of cell death (Hottiger, 2015). There is also evidence that some functions of PARP1 are independent of its enzymatic activity, such as its action as a co-activator or repressor of certain transcription factors (Hassa et al., 2005; 2003; Kraus and Hottiger, 2013). On the organismic level, these functions link PARP1 and PARylation to mechanisms of inflammation and metabolism, as well as aging and cancer biology (Bai, 2015; Bai and Cantó, 2012; Mangerich and Bürkle, 2012). Notably, several PARP inhibitors are currently tested in clinical cancer therapy, either in combination with classical chemo- or radiotherapy or as stand-alone drugs following the concept of synthetic lethality in *BRCA1/2*-deficient tumors (Curtin and Szabo, 2013; Mangerich and Bürkle, 2011; Sonnenblick et al., 2015).

A lot of our knowledge on PARP1 and PARylation has been obtained through a plethora of studies using three independently generated *Parp1* knock-out mouse models and immortalized mouse embryonic fibroblasts (MEFs) derived thereof (de Murcia et al., 1997; Masutani et al., 1999; Shall and de Murcia, 2000; Wang et al., 1995). Strikingly, a genetic double knock-out of *Parp1* and *Parp2* resulted in embryonic lethality in the mouse, thereby demonstrating the key function of PARylation during development (Ménissier-de Murcia et al., 2003). To the best of our knowledge, no genetic deletion of *PARP1* in a human system has been described to date. Notably, at present no *PARP1* mutations have been directly related to human heritable diseases – because such mutations presumably lead to embryonic lethality beforehand. Yet, several *PARP1* polymorphisms exist that have been associated with an increased risk for cancer development and inflammatory diseases. For example, a *PARP1* polymorphism, causing the amino acid exchange V762A (Cottet et al., 2000), leads to reduced enzymatic activity of purified PARP1 protein (Beneke et al., 2010; Wang et al., 2007). Notably, the PARP1\V762A variant is associated with an increased risk for the development of several types of cancers, especially in the Asian population (Hua et al., 2014; Qin et al., 2014). How the V762A variant and other potentially disease-associated *PARP1* polymorphisms and mutations affect cellular functions is so far unknown.

Here we report the generation of a full genetic knock-out of *PARP1* in one of the most widely used human cell systems, *i.e.*, HeLa *PARP1* KO cells, via TALEN-mediated gene targeting. We characterized these cells with regards to PARylation metabolism and genotoxic stress resistance. By reconstituting HeLa *PARP1* KO cells with a series of PARP1 variants we then analyzed structure-function relationships of PARP1 in a cellular environment, without

interfering with endogenously expressed WT PARP1. These variants included two sets of artificial and natural variants in order to exemplify the potential of this system for its wider usage in PARylation research. The first set included two artificial PARP1 mutants that are of high interest to understand the cellular biochemistry of PARylation, *i.e.*, a hypomorphic (E988K) and a hypermorphic (L713F) PARP1 variant. Using a second set of PARP1 variants, we then analyzed cellular consequences of naturally occurring PARP1 variants, *i.e.*, the PARP1 polymorphism leading to the V762A aa exchange and a newly identified germline PARP1 mutant (F304L) in a patient with pediatric colorectal carcinoma (*N.B.* in addition the patient carried the V762A polymorphism and a pathogenic mutation in *BRCA2*). We characterized functional consequences of the PARP1-reconstituted HeLa *PARP1* KO cells to obtain a deeper understanding into the cellular biochemistry and functional significance of PARP1 and PARylation during physiology and pathophysiology.

Results

Generation and characterization of HeLa PARP1 knock-out cells

To date, three independent *Parp1* knock-out mouse models have been established that have been widely used as model systems in PARylation research (de Murcia et al., 1997; Masutani et al., 1999; Shall and de Murcia, 2000; Wang et al., 1995). To the best of our knowledge, no characterization of a genetic *PARP1* knock-out (KO) in a human cellular system has been reported so far. To this end, we set out to generate and establish a genetic *PARP1* KO in one of the most widely used human cellular model systems, *i.e.*, HeLa cells. Recently the HeLa Kyoto genome has been fully sequenced (Adey et al., 2013; Landry et al., 2013), enabling us to use the TALEN technology to target exon 1 of the *PARP1* gene [MIM 173870] (Figure 41 A). After two rounds of TALEN transfection and clone selection by limiting dilution, we identified two independent cell clones, termed *PARP1* KO1 and KO2. Both displayed a complete abrogation of PARP1 expression, as evaluated by single-cell fluorescence microscopy (Figure 41 B) and Western blotting (Figure 41 C). DNA sequencing of PCR amplicons of the genomic region of interest confirmed successful targeting and introduction of small genomic deletions in *PARP1* exon 1 in both clones (data not shown). Next, we characterized how the loss of PARP1 affects PAR metabolism in HeLa cells. To this end, we treated HeLa WT and KO clones with doses of 10 µM to 1 mM H_2O_2. As evident from single-cell immuno-epifluorescence microscopy using the anti-PAR specific antibody 10H, *PARP1* KO cells did not form any detectable levels of PAR even at the highest treatment dose of 1 mM H_2O_2 (Figure 41 D). Next, we tested if the loss of PARP1 affects NAD^+ levels under non-stress conditions as well as upon H_2O_2 treatment by using an enzymatic NAD^+ cycling assay based on (Jacobson and Jacobson, 1976). Figure 41 E shows that under non-stress conditions the loss of PARP1 did not lead to a significant change in basal NAD^+ levels. As expected, treatment of HeLa WT cells with H_2O_2 led to a dramatic drop in cellular NAD^+ levels. In contrast, NAD^+ levels did not significantly change in *PARP1* KO cells upon H_2O_2 treatment (Figure 41 E). In order to analyze cellular PAR metabolism in more detail in HeLa *PARP1* KO clones, we used a recently developed bioanalytical method based on isotope-dilution mass spectrometry (Martello et al., 2013). Compared to immunochemical-based technologies, this method is sensitive enough to quantify basal PAR levels in unstressed cells with unequivocal chemical specificity. When treating HeLa WT cells with up to 200 µM H_2O_2, this led to a 100-fold increase in cellular PAR levels. As expected, this effect could be

largely inhibited by treating cells with the pharmacological PARP inhibitor ABT-888 (10 µM) (Figure 42 F).

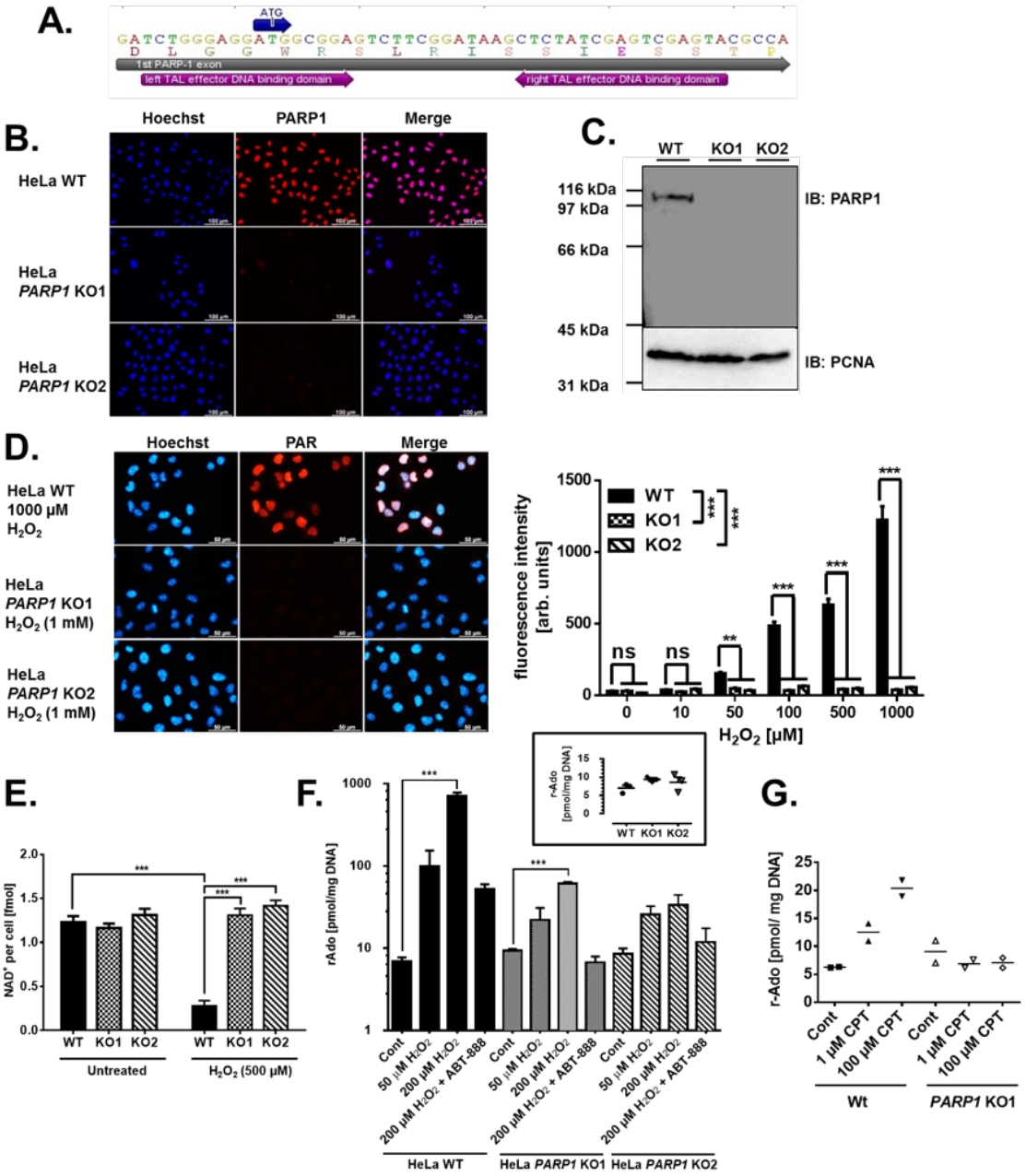

Figure 41: TALEN-mediated gene targeting of *PARP1* in HeLa cells and its consequences on PAR metabolism.
A. Binding sites of TAL effector DNA binding domains within the 1st exon of the *PARP1* gene. **B.** Single cell immuno-epifluorescence analysis of PARP1 expression in HeLa WT and in two independently generated *PARP1* knock-out (KO) clones (KO1 and KO2). **C.** Western blot analysis of PARP1 expression in HeLa WT and *PARP1* KO clones. PCNA served as a loading control. **D.** Single cell immuno-epifluorescence analysis of PAR formation in HeLa WT and *PARP1* KO clones. WT cells showed a dose-dependent increase in cellular PAR levels upon H_2O_2 treatment (for 5 min), while PAR levels in *PARP1* KO cells remained close to background signal intensities. Means ± SEM, densitometric analysis of n>70 cells. Statistical analysis was performed via 2-way ANOVA testing and Sidak's post-test. **E.** Intracellular NAD^+ levels in WT and *PARP1* KO cells ± H_2O_2 treatment for 7 min as measured by an enzymatic NAD^+ cycling assay. Means ± SEM of n=3 independent experiments. Statistical analysis was performed using 2-way ANOVA testing and Sidak's post-test. **F.** Quantification of basal and H_2O_2-induced PAR levels in WT and *PARP1* KO cells via isotope dilution mass spectrometry (LC-MS/MS) using a previously published method (Martello et al., 2013). Prior to analysis, cells were treated with 10 µM ABT-888 for 45 min and H_2O_2 for 5 min. Insert: Basal PAR levels in WT and *PARP1* KO cells without H_2O_2 treatment. Means ± SEM of n=3 independent experiments. Statistical analysis was performed using 1-way ANOVA testing and Sidak's post-test. **G.** LC-MS/MS analysis of PAR levels ± camptothecin (CPT) treatment for 30 min. Means of n=2 independent experiments. R-Ado indicates ribosyl-adenosine.

In contrast, HeLa *PARP1* KO cells showed only a 5-7-fold increase in PAR levels, which could be completely inhibited by ABT-888 treatment. These results demonstrate that upon induction of severe genotoxic stress in HeLa cells, PARP1 contributes to >90% of cellular PAR formation. The residual PAR forming ability can be probably attributed to other DNA damage dependent PARPs, such as PARP2 and PARP3 (Beck et al., 2014). Importantly, while stress-induced PAR formation was almost completely abolished in *PARP1* KO cells, basal PAR levels remained constant, indicating that under physiological, non-stress conditions other PARPs can compensate for the loss in PARP1 (Insert in Figure 42 F). Recently, it has been shown that PARP1 plays a crucial role in the response of cells to camptothecin (CPT) treatment (Berti et al., 2013; Patel et al., 2012). Using our highly sensitive LC-MS/MS technique, we analyzed if CPT treatment directly stimulates PARP activity in HeLa cells. As shown in Figure 41 G, CPT treatment for 30 min led to a significant induction of PARP activity, yet this was far more moderate than after H_2O_2 treatment. Thus, a 10-µM treatment led to ~2 fold and a 100-µM CPT treatment to 4-fold higher PAR levels compared to basal PAR levels in untreated cells. Importantly, this increase in PAR can be completely attributed to PARP1 activity, since no increase in PAR levels was observed in *PARP1* KO cells.

After having analyzed PAR metabolism in HeLa *PARP1* KO clones, we characterized cellular and functional consequences of the genetic deletion of *PARP1* in our cellular system. When culturing HeLa *PARP1* KO cells, it became apparent that these cells grew considerably slower compared to their WT counterparts. In agreement with this observation, a proliferation analysis revealed that both *PARP1* KO clones showed significantly slower proliferation rates compared to WT, while the overall cell cycle distribution appeared to be unaffected (Figure 42 A&B). A plethora of reports from *Parp1* KO mice and human cell culture studies using RNA interference and pharmacological inhibition of PARP activity showed that loss of PARP1 leads to a sensitization of cells towards genotoxic stimuli (Godon et al., 2008; Shall and de Murcia, 2000). In order to validate our model we tested if the same holds true for our HeLa *PARP1* KO cells. To this end, we performed a clonogenic survival analysis of HeLa WT and *PARP1* KO cells upon H_2O_2 treatment. Consistent with data from other mammalian systems, loss of PARP1 led to a significant sensitization of HeLa cells towards low-dose H_2O_2 treatment (Figure 42 C). In a next step, we then analyzed how PARP1 deficiency affects the response of HeLa cells to CPT treatment by performing cell viability and cell cycle analyses. Figure 42 D demonstrates that HeLa *PARP1* KO clones were significantly sensitized to CPT treatment, resulting in significantly lower cell viability two days after CPT treatment, which could be attributed to both increased apoptosis as well as necrosis rates.

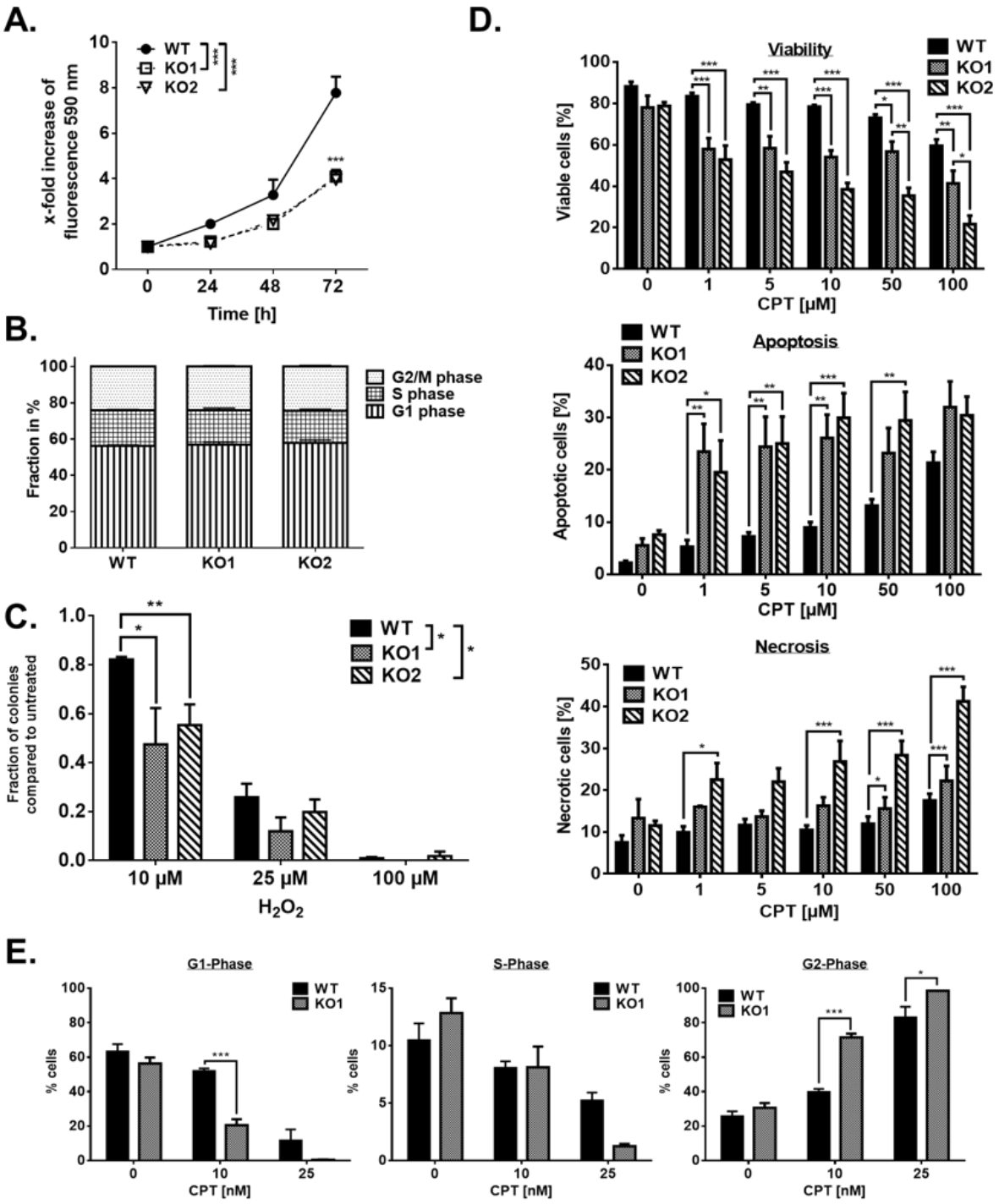

Figure 42: Functional consequences of *PARP1* deletion in HeLa cells.
A. Cell proliferation of HeLa WT and *PARP1* KO cells as analyzed by ALAMAR Blue assay for 3 days. Means ± SEM of n=3 independent experiments. Statistical analysis was performed using 2-way ANOVA testing and Sidak's post-test. **B.** Cell cycle analysis of untreated WT and *PARP1* KO cells via PI staining and subsequent flow cytometric analysis. Means ± SEM of 3 independent experiments. **C.** Clonogenic survival analysis. WT and *PARP1* KO cells were treated with H_2O_2 in concentrations as indicated for 5 min and then plated and cultivated for 12 days prior to colony counting. Means ± SEM of n=3 independent experiments. Statistical analysis using 2-way ANOVA testing and Sidak's post-test. **D.** Cytotoxicity analysis via annexinV / PI staining and subsequent flow cytometric analysis 2 days after treating WT and *PARP1* KO cells treated ± CPT in concentrations as indicated. Viable cells refer to annexin V / PI-double negative cells; apoptotic cells to annexin V-positive, PI-negative cells; and necrotic and late-apoptotic cells to annexin V/PI-double positive cells (ratios compared to total cell numbers). Means ± SEM of n≥4 independent experiments. Statistical analysis was performed using 2-way ANOVA testing and Sidak's post-test. **E.** Cell cycle analysis via PI staining and flow cytometric analysis 2 days after treatment of cells ± CPT in concentrations as indicated. Means ± SEM of n≥3 independent experiments. Statistical analysis was performed using 2-way ANOVA testing and Sidak's post-test.

Interestingly, in terms of necrosis, the two independently generated *PARP1* KO clones showed significant differences, with clone KO2 showing considerable higher necrosis induction than clone KO1. Such slight differences in the phenotypes of the two clones are not unexpected, since selection processes may occur during culturing of the clones, before initial biochemical analysis by immunofluorescence microscopy and Western blotting. For further analyses, we focused on the usage of clone KO1, since this clone showed full abrogation of PARP1 expression, however milder effects in CPT-induced cytotoxicity. In order to analyze if also nanomolar doses of CPT, which are assumed to induce primarily replicative stress without directly inducing DNA strand breaks, lead to a sensitization of *PARP1* KO cells, we performed a cell cycle analysis two days after CPT treatment (Figure 42 E). These experiments revealed that CPT treatment caused a strong G2 arrest in HeLa cells that was significantly increased by the loss of PARP1.

In summary, we have generated a complete genetic knock-out of *PARP1* in HeLa cells in two independent clones. Furthermore, we provide a detailed characterization of these cells with regards to their PAR and NAD^+ metabolism, their growth characteristics, and their cellular responses after application of the genotoxins H_2O_2 and CPT.

Reconstitution of HeLa PARP1 knock-out cells with PARP1 variants

Next, we used this cellular system for reconstitution studies testing the cellular biochemistry and functional consequences of select PARP1 variants of interest. To exemplify the potential of this system for its usage in PARylation research, we analyzed a first set of two artificial PARP1 mutants that are of high interest to understand the cellular biochemistry of PARylation, *i.e.*, a hypomorphic and a hypermorphic PARP1 variant (E988K and L713F, respectively). Using a second set of PARP1 variants, we then analyzed cellular consequences of naturally occurring PARP1 variants, *i.e.*, a PARP1 polymorphism that has been associated with increased risk for certain cancers (V762A) and a newly identified inherited PARP1 mutant in a patient with pediatric colorectal carcinoma (F304L). Figure 43 A shows the localization of the different aa exchanges within the PARP1 structure and Figure 43 B gives an overview of the biochemical parameters of the different variants as reported in the literature and the current study (see below). We generated eukaryotic expression constructs of the PARP1 variants of interest using site-directed mutagenesis (data not shown). In order to detect PARP1 expression in transfected HeLa cells and to monitor recruitment to sites of DNA damage, all variants were C-terminally tagged with eGFP. As it is evident from Western

blot analysis (Figure 43 C), reconstitution of HeLa *PARP1* KO cells with these constructs led to a strong expression of the different PARP1 variants, which was ~4-6-fold higher than endogenous PARP1 expression in HeLa WT cells, with the exception of the PARP1\L713F variant, which showed expression levels comparable to WT cells.

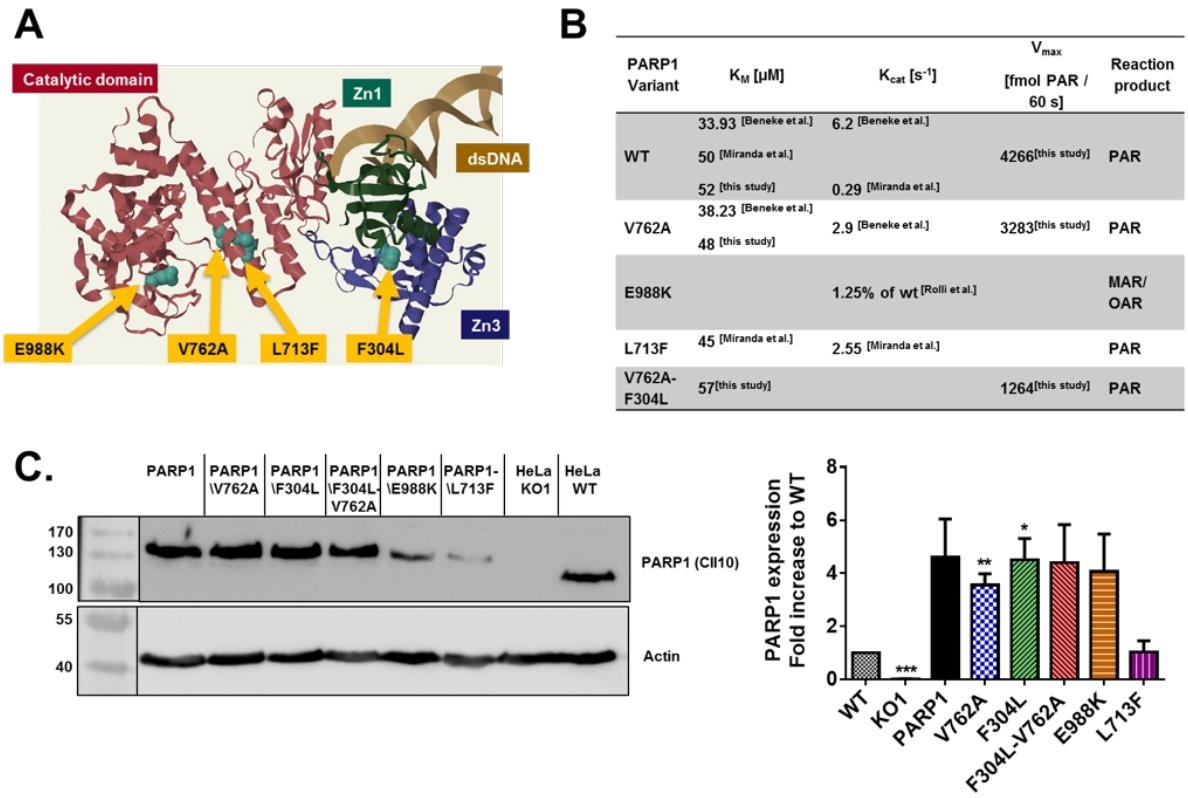

Figure 43: Overview of PARP1 variants included in this study.
A. PARP1 structure (without Zn2 and WGR domains) in complex with a double-stranded DNA molecule [PDB code 4DQY (Langelier et al., 2012)]. Amino acid exchanges of PARP1 variants as used in this study are highlighted in turquoise. **B.** Biochemical parameters derived from rec. enzymes of the different PARP1 variants used in this study. Values were determined in the present study (*cf.* Figure 49) or taken from the literature as indicated. PAR indicates poly(ADP-ribose); MAR, mono(ADP-ribose); and OAR, oligo(ADP-ribose). **C.** Western-blot analysis of PARP1 protein levels in HeLa *PARP1* KO cells reconstituted with different PARP1-eGFP variants 2 days after transfection. The panel on the *left* shows a representative experiment out of ≥4. The panel on the *right* shows the densitometric analysis of Western-blot signal intensities after taking into account transfection efficiencies. Means ± SEM of n=4 independent experiments. Statistical analysis was performed using 1-sample t-test.

Reconstitution of HeLa PARP1 knock-out cells with wild-type and artificial PARP1 variants

In the first set of PARP1 variants, we focused on a hypomorphic PARP1 variant, with an aa exchange from glutamate to lysine at position 988 (E988K), and on a hypermorphic PARP1 variant, with an aa exchange from leucine to phenylalanine at position 713 (L713F). Previously, the PARP1\E988K mutant was shown to exhibit mono- or oligo(ADP-ribosyl)ation activity in biochemical studies using recombinant enzymes (Beneke et al., 2010; Marsischky et al., 1995; Rolli et al., 1997) and its cellular behavior has been characterized by

reconstituting mouse embryonic fibroblasts derived from *Parp1* knock-out mice (Mortusewicz et al., 2007; Patel et al., 2012). The PARP1\L713F mutant was originally identified as a gain-of-function mutant in a random mutagenesis screen and has been characterized on a biochemical level (Langelier et al., 2012; Miranda et al., 1995). Thus, this mutant mimics the effect of DNA-binding-induced distortions in the catalytic domain, thereby increasing PARP1 DNA-independent activity up to 20-fold and elevating the catalytic efficiency of PARylation, while not affecting its affinity for NAD^+ (Langelier et al., 2012) (*cf.* biochemical parameters in Figure 43 B). To the best of our knowledge, so far this variant has not been characterized in a cellular environment.

Cellular PAR and NAD^+ metabolism of artificial PARP1 mutants

To provide a basis for the analysis of cellular consequences of PARP1-reconstituted HeLa *PARP1* KO cells, we conducted a detailed characterization of the cellular biochemistry of the different PARP1 variants with regards to PARylation and NAD^+ metabolism as well as PARP1 localization dynamics at sites of DNA damage. Using triple-color single-cell immuno-epifluorescence microscopy and image evaluation by an automated KNIME workflow, we examined the PARylation response upon treatment of PARP1-reconstituted cells with increasing doses of H_2O_2. As expected, PARP1-reconstituted cells showed a dose-dependent PAR formation (Figure 44 A&B), similar to the dose-response that had been observed in HeLa WT cells (*cf.* Figure 41), while PARP1\E988K-reconstituted cells did not reveal any significant increase in PAR-derived fluorescent intensities (Figure 44 A&B). These results are in agreement with time-course analysis of PAR formation in PARP1-reconstituted cells upon H_2O_2 treatment, which revealed a transient PARylation response with peak levels of PAR formation at ~5 min after treatment. Thirty minutes after H_2O_2 treatment, PAR levels returned to basal levels, due to the activity of PAR-degrading enzymes such as PARG (Figure 44 C) (Barkauskaite et al., 2015). Furthermore, time-course analysis confirmed the inability of the PARP1\E988K variant to produce PAR. On the other hand, cells reconstituted with PARP1\L713F produced high amounts of PAR even in the absence of exogenous DNA damage, indicating that it is constitutively active not only in a cell-free system (Langelier et al., 2012), but also in a cellular environment (Figure 44 A&B). Interestingly, treating PARP1\L713F-reconstituted cells with H_2O_2 for 5 min did not lead to a further increase in PAR levels. Time-course analysis of H_2O_2-treated PARP1\L713F-reconstituted cells, however, revealed that 30 min after the genotoxic stimulus, PAR levels declined to basal level

as observed in untreated HeLa WT cells (Figure 44 C and Suppl. Figure 17). These results indicate that (*i*) PARP1\L713 can still be stimulated by DNA damage probably leading to a depletion of NAD^+ and (*ii*) that PAR-degrading enzymes are constantly active in these cells.

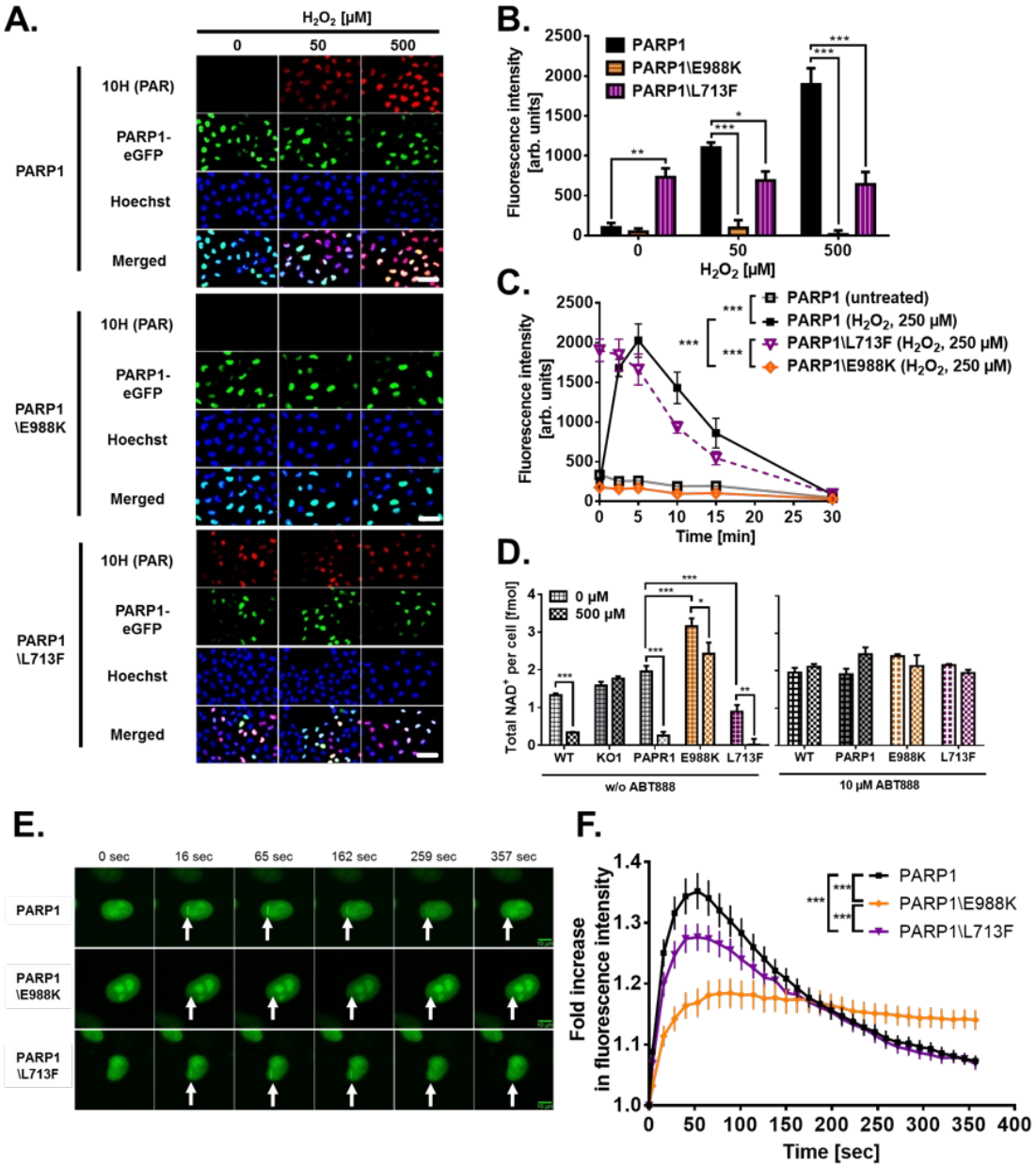

Figure 44: Cellular biochemistry of artificial PARP1 mutants.
HeLa *PARP1* KO cells were transfected with eGFP-coupled constructs of PARP1, PARP1\L713F, and PARP1\E988K. Analyses were performed 2 days after transfection. **A.** Representative images from single cell immuno-epifluorescence analysis of PARP1-eGFP and PAR after treatment of PARP1-reconstituted cells ± H_2O_2 as indicated for 5 min. Scale bars indicate 30 µM. **B.** Densitometric analysis of imaging data as shown in A. >100 cells were analyzed per experiment and condition in a semi-automated manner using a KNIME workflow. Means ± SEM of n=4 independent experiments. Statistical analysis using matched 2-way ANOVA testing and Sidak's post- test. **C.** Time-course analysis of PAR levels in PARP1-reconstituted cells after treatment of cells with 250 µM H_2O_2. For representative raw data refer to Suppl. Figure 17. Means ± SEM of n=4 independent experiments, >100 cells were analyzed per experiment and condition. Statistical analysis was performed using matched 2-way ANOVA testing and Sidak's post-test. **D.** NAD^+ levels in PARP1-reconstituted cells upon treatment ± H_2O_2 for 7 min as measured by an enzymatic NAD^+ cycling assay. Means ± SEM of n=3 independent experiments, except for -888-treated samples, n=2. Statistical analysis was performed using 2-way ANOVA testing and Sidak's post-test. **E-F.** Recruitment and dissociation kinetics of PARP1-eGFP at sites of laser-induced DNA damage. **E.** Representative imaging data. Scale bars indicate 10 µm. **F.** Densitometric quantification of signal intensities from imaging data as shown in E. Means ± SEM of n=3 independent experiments, >29 cells were analyzed per experiment and condition. Statistical analysis was performed using 2-Way ANOVA testing and Sidak's post-test.

In order to obtain further insight into the PARP1 activity in PARP1-reconstituted cells, we analyzed NAD^+ levels in untreated as well as in H_2O_2- and PARP inhibitor-treated cells. Transfection efficiencies of individual samples were measured in parallel via flow cytometric analysis and have been taken into account in the graphical presentation in Figure 44 D. These experiments confirmed that, as expected, cells reconstituted with PARP1 for two days responded similar as HeLa WT cells by showing a drastic drop in NAD^+ levels upon H_2O_2 treatment, which could be completely inhibited by ABT-888 (Figure 44 D). Interestingly, cells that had been reconstituted with PARP1\E988K, displayed a significant increase in total NAD^+ amounts per cell compared to PARP1-reconstituted cells. Furthermore, H_2O_2 treatment led to a moderate, but statistically significant, drop in NAD^+ levels, which is consistent with the fact that the PARP1\E988K mutant acts as a mono- or oligo(ADP-ribose) transferase, which is incapable to form PAR chains that can be recognized by the 10H antibody. Strikingly, the increase in NAD^+ levels in PARP1\E988K-reconstituted cells could be completely inhibited by PARP inhibitor treatment (Figure 44 D), suggesting that the mono- or oligo(ADP-ribosyl)ation activity of PARP1\E988K is responsible for the observed effect. Consistent with our PARylation analysis, NAD^+ levels in PARP1\L713F-reconstituted cells were reduced by >40% under basal conditions and showed a total exhaustion in H_2O_2-treated cells. These effects could be completely inhibited by PARP inhibitor treatment.

In summary, these results demonstrate that single aa exchanges within the PARP1 molecule can cause dramatic effects on PARP1's enzymatic activation, PAR forming ability, and NAD^+ metabolism. This holds true for both (*i*) a hypomorphic exchange, such as E988K, thereby generating a mono- or oligo(ADP-ribosyl) transferase, or (*ii*) a hypermorphic exchanges, such as L713F, thereby generating a constitutively active PARP1 variant, whose enzymatic activity appears to be partially uncoupled from its DNA binding ability.

DNA recruitment and dissociation dynamics of artificial PARP1 mutants

Since enzymatic PARP1 activation is in many cases directly related to its DNA binding status, we analyzed the spatio-temporal recruitment of PARP1-eGFP to sites of laser-induced DNA damage using multi-photon excitation microscopy (Tomas et al., 2013). For PARP1\WT, we observed a fast and strong recruitment to sites of DNA damage with peak intensities of PARP1-eGFP ~1 min after laser irradiation and a constant dissociation thereafter (Figure 44 E&F). In contrast, for PARP1\E988K, the recruitment to sites of DNA damage was only about half as efficient as for PARP1\WT. Interestingly, however,

PARP1\E988K molecules that were recruited to sites of DNA damage stayed there persistently, without showing any considerable dissociation 6 min after laser damage induction. These results are largely consistent with recruitment kinetics of PARP1\E988K reported in a mouse system (Mortusewicz et al., 2007) and indicate that PARP1 activity is necessary for efficient recruitment as well as dissociation of PARP1 at DNA damage sites. Remarkably, the constitutively active mutant PARP1\L713F, also efficiently associated and dissociated from site of laser damage with similar kinetics as PARP1\WT, however with significantly lower peak intensities.

Non-covalent PARP1-PAR interaction

In many instances, recruitment of DNA repair factors is mediated by non-covalent PAR-protein interactions (Krietsch et al., 2012). The impaired recruitment of PARP1\E998K to sites of DNA damage suggests that PARP1 itself may be recruited to such sites by non-covalent binding to locally formed PAR. Therefore, we tested if PARP1 and PAR interact non-covalently, which could lead to an accumulation of PARP1 molecules at sites of DNA damage. Previously, some studies incidentally reported a non-covalent PARP1-PAR interaction (Huambachano et al., 2011; Robu et al., 2013), however, a comprehensive characterization of this interaction has so far not been reported. Non-covalent PARP1-PAR interaction may lead to conformational changes within the secondary and tertiary structure of PARP1, thereby regulating its binding to DNA.

We used three different biochemical approaches to characterize the non-covalent PARP1-PAR interaction. We performed Western blotting of SDS-PAGE-separated rec. PARP1, incubated membranes with or without *in-vitro* synthesized PAR, and detected bound PAR after high-stringency washing. Figure 45 A demonstrates that PARP1 clearly interacts with PAR. This result was further confirmed by an immuno-slot blot technique, which keeps the protein in native condition (*i.e.* not denatured) (Figure 45 B). Since both techniques analyze binding of PAR to rec. PARP1 immobilized on a membrane, we performed a modified EMSA using biotin-end-labeled PAR of defined chain length as bait to analyze PARP1-PAR interaction in solution. This technique further confirmed that PARP1 interacts with PAR, which leads to the formation of three defined macromolecular complexes (Figure 45 C). Non-covalent PAR-protein binding can be mediated by several different PAR-binding modules (Krietsch et al., 2012).

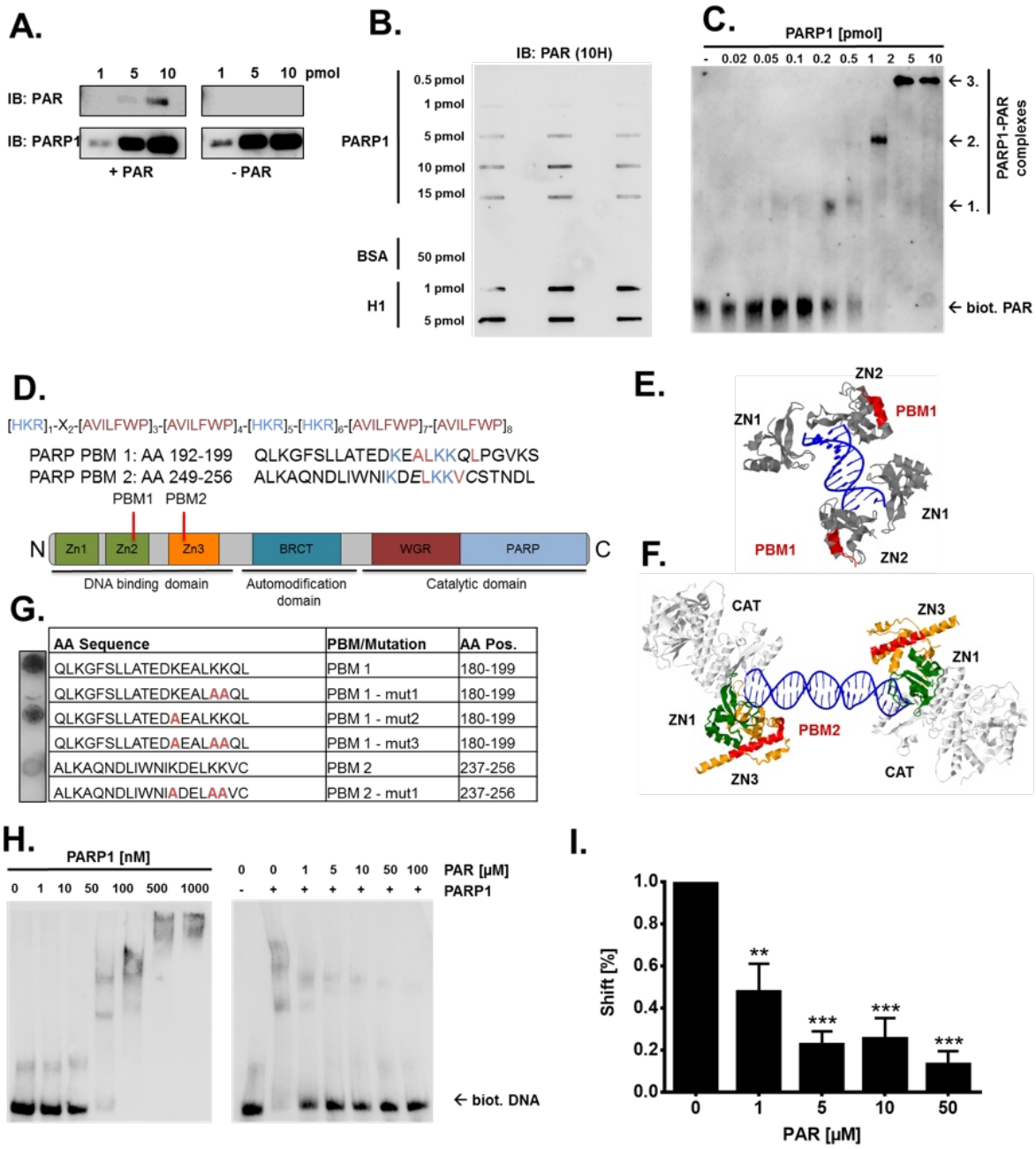

Figure 45: Non-covalent PARP1-PAR interaction.
A. Analysis of PARP1-PAR interaction by PAR overlay assay upon SDS-PAGE and Western-blotting (Far-Western) using increasing amounts of rec. PARP1 as indicated. After protein transfer, membranes were incubated with (left) or without (right) PAR (0.2 µM), and PAR binding was detected by immunochemical analysis using the 10H antibody, after high-stringency washing to remove unspecifically bound PAR. **B.** Immuno slot-blot PAR-binding assay using increasing amounts of rec. PARP1 that were immobilized on a nitrocellulose membrane. Afterwards, membranes were incubated with PAR (0.2 µM) and bound PAR was detected using the 10H antibody after high-stringency washing. **C.** Analysis of PARP1-PAR interaction in solution using a modified PAR-EMSA. End-biotinylated PAR of defined chain length (30-35 mer, 0.5 pmol ADP-ribose) was incubated with rec. PARP1 and afterwards PARP1-PAR binding was assessed by native TBE gel electrophoresis and Western-blotting. Three distinct complexes (1.-3.) were observed that were formed in a PARP1 dose-dependent manner. **D.** *In silico* search for putative PAR-binding sites within the PARP1 sequence using the search sequence displayed at the top. Two potential PAR binding motives (PBMs), *i.e.*, PBM1 (1 mismatch) and PBM2 (2 mismatches), were identified in Zn2 and Zn3, respectively. **E.** Localization of PBM1 with Zn2. Structure based on PDB code 4AV1 (Ali et al., 2012). **F.** Localization of PBM2 with Zn2. Structure based on PDB code 4DQY (Langelier et al., 2012). **G.** PAR binding ability to peptides comprising aa sequences of PBM1/2 and peptides comprising aa exchanges potentially responsible of PBM-PAR interactions using a Pepspot analysis. "AA pos." indicates aa positions within full-length PARP1 sequence. **H.** DNA-PARP1 EMSA using a known biotinylated double-stranded DNA oligonucleotide (200 fmol). ***Left***. DNA-PARP1 interaction in the absence of PAR. ***Right***. Rec. PARP1 (100 nM) was incubated with increasing concentrations of PAR as indicated. **I.** Densitometric evaluation of EMSAs as shown in H. Means ± SEM of n=3 independent experiments. Statistical analysis was performed using 1-way ANOVA testing and Sidak's post-test.

The one that is most abundant within the human proteome is termed the PAR-binding motif (PBM) and comprises a weakly conserved consensus sequence, containing a basic/hydrophobic core helix. Using a previously published target sequence (Pleschke et al., 2000; Popp et al., 2012), we searched for putative PBMs within the PARP1 aa sequence and came up with two potential binding sites within Zn2 and Zn3, respectively (Figure 45 D-F). To test if these aa stretches are capable of PAR binding *in vitro*, we used membrane-immobilized peptides (Pepspot approach) in combination with a PAR overlay assay. As it is evident from the dotblot in Figure 45 G**,** PBM1 showed a strong and PBM2 a weak PAR binding. By exchanging potentially critical lysines with alanines, PAR-binding of PBM1 and PBM2 could be completely abolished. Next, we were interested in potential functional consequences of the PARP1-PAR interaction. Based on the presence of a PBM within Zn2 we speculated that the non-covalent PARP1-PAR interaction could directly affect the ability of PARP1 to bind to DNA. To test this hypothesis we performed EMSAs using PARP1-DNA substrate. Figure 45 H&I demonstrate that PARP1 binds to this DNA substrate in a dose-dependent manner and, more importantly, this binding could be already inhibited by the presence of PAR in a molar ratio of 1:10 (PAR:PARP1).

In summary, these results demonstrate that PARP1 activity is necessary for efficient recruitment as well as dissociation of PARP1 to and from sites of laser-induced DNA damage. Furthermore, apart from the previously published electrostatic repulsion and chromatin remodeling triggered by covalent modification of PARP1, direct non-covalent PARP1-PAR interaction can contribute to these effects (*i*) by efficiently attracting further PARP1 molecules to sites of active PARylation and (*ii*) by supporting the release of highly modified PARP1 molecules from DNA.

Cellular consequences of PARP1 reconstitution

After having analyzed the cellular biochemistry of the PARP1\E988K and PARP1\L713F mutants in the absence of any potentially interfering endogenous WT-PARP1, we were interested in the cellular consequences of the modulated PARylation metabolism in PARP1-reconstituted cells. First, during microscopic and flow cytometric analysis, we recognized that PARP1\E988K-reconstituted cells showed considerable alterations in cellular morphology. Thus, we observed that PARP1\E988K reconstitution led to significant changes in flow cytometric dot-blots. As displayed in Figure 46 A forward (FSC) and side scatter (SSC) intensities were significantly increased. Furthermore, when we quantified the areas of nuclei

from epi-fluorescence microscopic images of PARP1-reconstituted cells, we observed that nuclei of PARP1\E988K-reconstituted cells were ~50% enlarged compared to WT, *PARP1* KO and other PARP1-reconstituted cells (Figure 46 B). In addition, 3D deconvolution microscopy of Hoechst33342 staining of PARP1- and PARP1\E988K-reconstituted cells revealed morphological changes in the nuclear architecture of PARP1\E988K-expressing cells. Thus, nucleoli of PARP1\E988K-reconstituted cells appeared enlarged and surrounded by highly compacted perinucleolar heterochromatin (Figure 46 C).

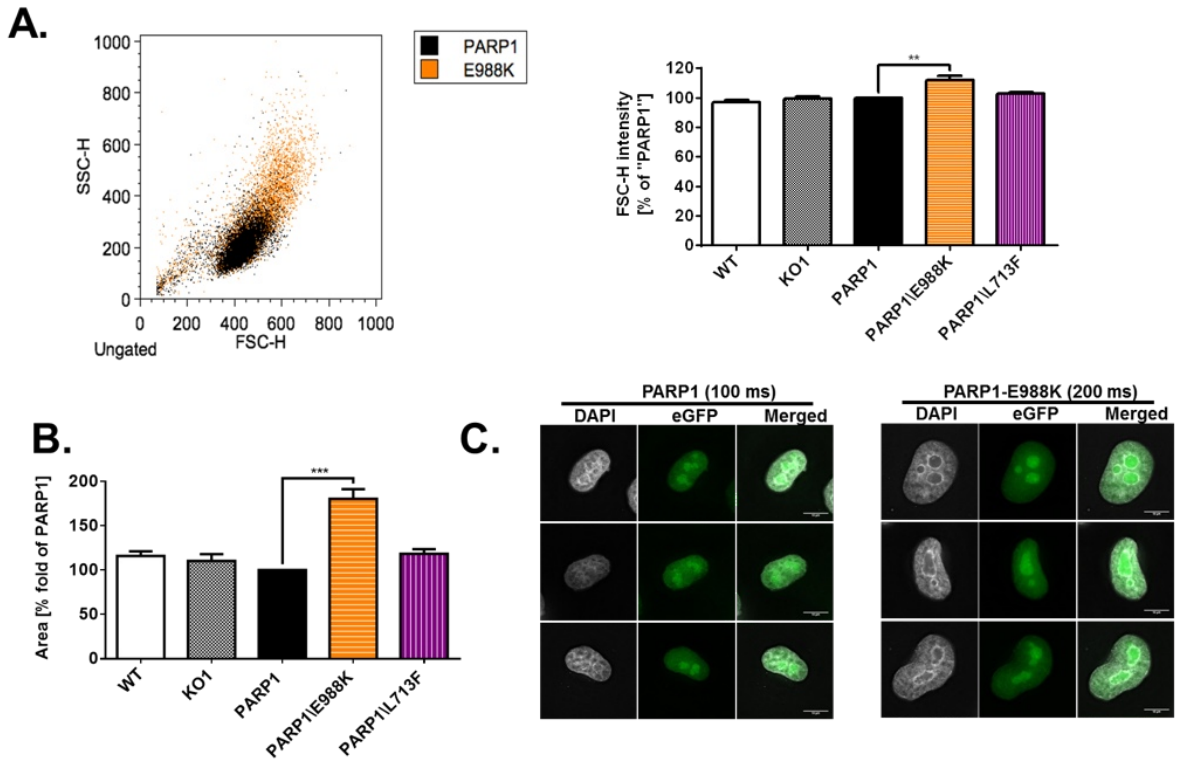

Figure 46: PARP1\E988K mutant affects nuclear architecture.
A. Evaluation of cell morphology by flow cytometric analysis. ***Left***. Representative dot blot of eGFP-positive cells 2 days after transfection with PARP1 or PARP1\E988K. SSC indicates side scatter; FSC, forward scatter. ***Right***. Quantification of FSC intensities of WT, *PARP1* KO and PARP1-reconstituted cells. Means ± SEM of n=4 independent experiments. Statistical analysis was performed using 1-way ANOVA testing and Sidak's post test. **B.** Quantification of nuclear sizes of WT, *PARP1* KO, and PARP1-reconstituted cells 2 days after transfection. Means ± SEM. Evaluation of DAPI staining of >100 cells from ≥4 independent experiments. Statistical analysis was performed using 1-way ANOVA testing and Sidak's post-test. **C.** Evaluation of DAPI staining and eGFP fluorescence by 3D deconvolution microscopy using a DeltaVision OMX super-resolution microscope indicates changes in nuclear morphology, as evident by strong perinucleolar staining. Exposure time for PARP1-transfected cells, 100 ms, and for PARP1\E988k-tranfected cells 200 ms.

Since enlarged nuclei can be a consequence of changes in the chromatin status, we analyzed the tri-methylation status of lysine 27 on histone H3, *i.e.*, H3K27me3 in PARP1-reconstituted cells (Suppl. Figure 18). H3K27me3 is associated with transcriptional repression (Young et al., 2011) and it has been recently reported that PARP inhibition and knock-down of PARP1 results in increased global H3K27me3 levels in lymphoblastoid B cells and HeLa cells (Martin et al., 2015). Our analysis, using immunofluorescence confocal microscopy, revealed an increase in H3K27me3 staining in PARP1-reconsituted cells compared to HeLa WT and

PARP1 KO cells (Suppl. Figure 18). It can be speculated that this effect is caused by moderate PARP1 overexpression, which would be consistent with the notion that PARP1 protein by itself contributes to chromatin compaction (Wacker et al., 2007). On the other hand, we did not observe any significant differences in H3K27me3 staining intensities in cells reconstituted with the different PARP1 variants, including PARP1\E988K, although at this stage, we cannot exclude that alterations in chromatin status may become more apparent, when analyzing this at a more detailed level. Another cause for differences in nuclear sizes may be alterations in cell cycle regulation (Umen, 2005). To test if PARP1\E988K reconstitution led to alterations in cell cycle distribution, we analyzed the cell cycle status of PARP1-reconstituted cells via PI staining and subsequent flow cytometric analysis. While expression of the PARP1\L713F mutant did not seem to influence the HeLa cell cycle without the application of additional stress, remarkably, expression of the PARP1\E988K mutant for three days, led to a strong G2 arrest (Figure 47 A). Interestingly, PARP inhibitor treatment of PARP1-reconstituted cells did not affect the cell cycle status at all, remarkably however, normalized the cell cycle distribution of PARP1\E988K-expressing cells completely. These results are consistent with our analysis of the NAD^+ status in PARP1\E988K-reconstituted cells and hints at an active role of mono- or oligo(ADP-ribosyl)ation in inducing the observed effects. Typically, a G2 arrest in cell cycle progression can be caused by accumulating DNA damage. To test if PARP1\E988K expression leads to a DNA damage response, we analyzed several key factors of DNA damage signaling in PARP1-reconstituted cells, such as phosphorylated p53 at serine 15 (ph-p53), γH2A.X, and p16 (Figure 47 B). Western-blot analysis revealed that two days after PARP1 reconstitution, PARP1\L713F-expressing cells showed slightly enhanced γH2A.X levels and PARP1\E988K-expressing cells showed strongly induced γH2A.X and ph-p53 staining, while p16 expression was not affected.

Since PARP1\E988K-expressing cells entered a G2 arrest, we assumed that expression of this variant could induce cell death in HeLa cells. Indeed, when analyzing cell viability via AnnexinV / PI staining in PARP1-reconstituted cells three days after transfection, PARP1\E988K-expressing cells showed a higher rate of early as well as late apoptotic/necrotic cells compared to PARP1\WT-reconstituted cells, at a similar level to mock-transfected HeLa *PARP1* KO cells (*i.e.*, labeled with GFP-cont. in Figure 48 A). More strikingly, however, expression of PARP1\L713F in HeLa *PARP1* KO cells revealed to be highly cytotoxic reducing viability from 80% for PARP1\WT-reconstituted cells to ~40-50% for PARP1\L713F-reconstituted cells (Figure 48 A). Interestingly, most of this effect could be attributed to AnnexinV-positive, but PI-negative cells indicating that high basal PAR levels in

these cells could drive cells into apoptosis without any obvious induction of cell cycle arrest in viable cells (at least under the conditions tested). Since the loss of PARP1 in HeLa cells led to a significant sensitization towards CPT treatment, we examined if PARP1-reconstitution could rescue this effect. When treating cells with increasing doses of CPT two days prior to analysis, PARP1\WT reconstitution could significantly rescue the sensitization effect observed in *PARP1* KO cells (Figure 48 A). Interestingly, neither reconstitution with PARP1\E988K nor with PARP1\L713F were able to rescue the *PARP1* KO effect, indicating that full PARP1 functionality is necessary to protect cells form CPT-induced genotoxic stress.

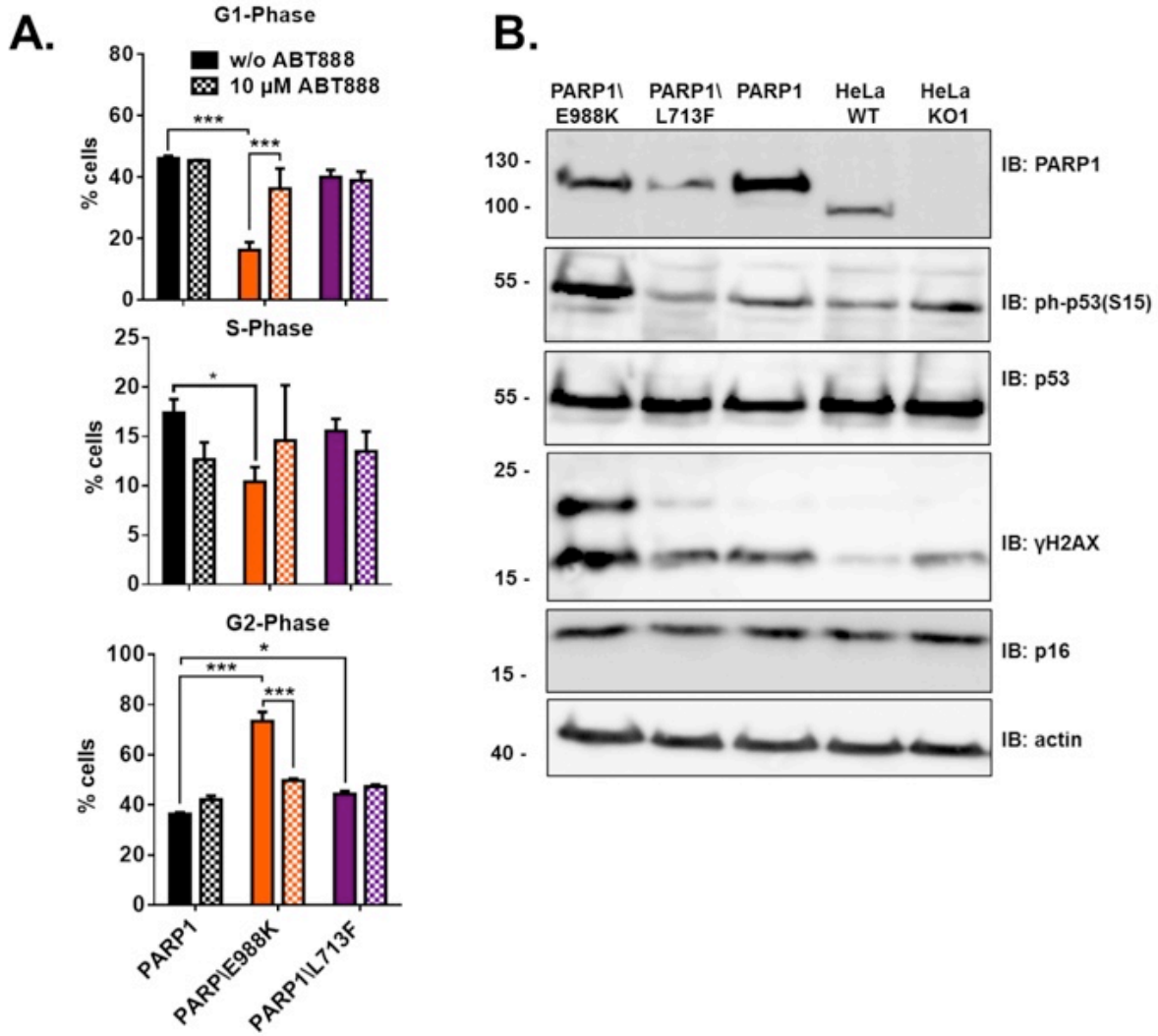

Figure 47: PARP1\E988K affects cell cycle regulation and induces DNA damage signaling.
A. Cell cycle analysis by PI staining and subsequent flow cytometric analysis 3 days after transfection of HeLa *PARP1* KO cells with PARP1, PARP1\E988K, and PARP1\L713F. PARP1\E988K induces a G2 arrest, which can be rescued by treating cells with 10 µM ABT-888. Means ± SEM of n=6 independent experiments, except of ABT-888-treated samples, n=2. Statistical analysis was performed using 2-way ANOVA testing and Sidak's post-test. **B.** Analysis of DNA damage response markers, *i.e.*, phospho-S15-p53, γH2A.X and p16 in WT, *PARP1* KO, and PARP1-reconstituted cells as indicated 2 days after transfection. Cells reconstituted with PARP1\E988K displayed increased phospho-S15-p53 and γH2A.X levels and cells reconstituted with PARP1\L713F showed slightly elevated γH2A.X levels. Immunochemical detection of PARP1, P53, and actin served as controls. Shown is a representative experiment out of three.

Furthermore, CPT-induced cell death could be mostly attributed to the induction of necrotic cell death, while apoptosis was only slightly induced in PARP1 and PARP1\E988K-reconstituted cells and stayed at a constant high level in PARP1\L713F-reconstituted cells (Figure 48 A). Consistent with these results, treatment of PARP1-reconstituted cells with CPT in the low nM range, led to a G2 arrest in cells reconstituted with all three variants, but with the strongest effects observed for PARP1\E998K-reconstituted cells (Figure 48 B).

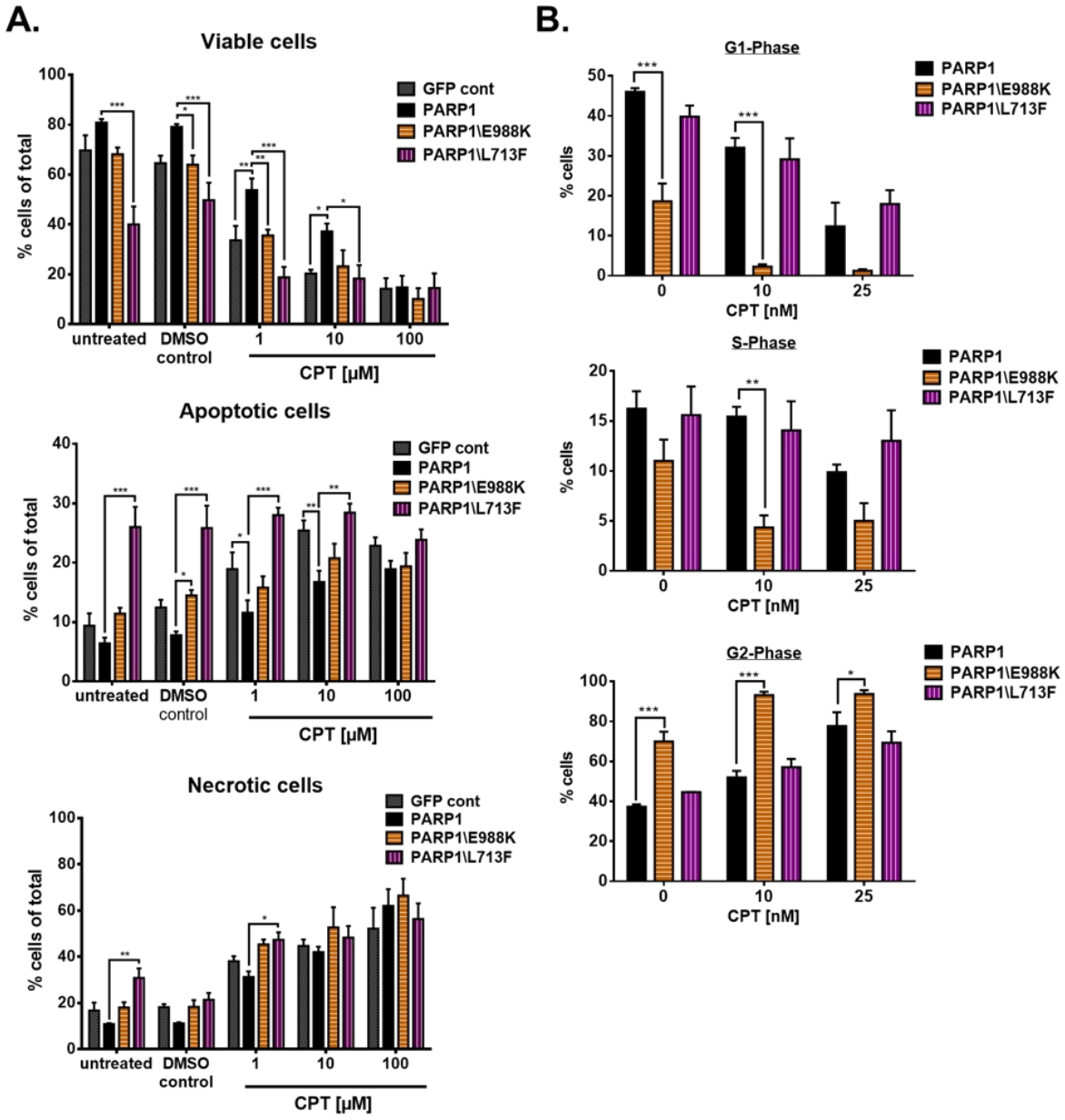

Figure 48: PARP1 mutants influence cell viability and cell cycle progression upon CPT treatment.
A. Analysis of viable, apoptotic and necrotic cells 3 days after transfection of HeLa *PARP1* KO cells with PARP1, PARP1\E988K, and PARP1\L713F by annexinV / PI staining and subsequent flow cytometric analysis. Cells were treated with CPT in concentrations as indicated 24 h after transfection. Viable cells refer to annexin V / PI-double negative cells; apoptotic cells to annexin V-positive, PI-negative cells; and necrotic and late-apoptotic cells to annexin V/PI-double positive cells (ratios compared to total cell numbers). Means ± SEM of n≥3 independent experiments. Statistical analysis was performed using 2-way ANOVA testing and Sidak's post test. **B.** Cell cycle analysis of PARP1-reconstituted cells as indicated 3 days after transfection and 2 days after CPT treatment via PI staining and subsequent flow cytometric analysis. Means ± SEM of n=3 independent experiments. Statistical analysis was performed using 2-way ANOVA testing and Sidak's post-test.

In summary, these experiments reveal remarkable cellular consequences by interfering with PARylation metabolism, such as higher apoptosis rates induced by increased basal PAR levels through expression of the constitutively active PARP1\L713F variant, or severe effects on cell cycle progression by expression of the mono(ADP-ribosyl) transferase PARP1\E988K.

Reconstitution of HeLa PARP1 knock-out cells with natural PARP1 variants

In a second set of PARP1 variants, we analyzed two variants naturally occurring in humans. These included (*i*) the V762A polymorphic variant (valine to alanine exchange at aa position 762) (Cottet et al., 2000). This variant displays reduced enzymatic activity as evaluated mainly by *in vitro* studies using rec. PARP1 (Beneke et al., 2010; Wang et al., 2007). This variant is associated with higher risks for specific types of tumors in certain ethnicities, in particular in the Asian population (Hua et al., 2014; Qin et al., 2014). To the best of our knowledge, at present, PARP1\V762A has not been characterized in detail in a cellular environment. (*ii*) Using exome sequencing of peripheral blood DNA from a patient with pediatric colorectal cancer, we identified the V762A polymorphism to co-occur with a novel rare PARP1 mutation, *i.e.*, a genomic 910T>C mutation leading to a phenylalanine to leucine exchange at the protein level at position 304, *i.e.*, F304L. This mutation was maternally inherited. Importantly, although not in the focus of the present study, the paternal family history of this patient was positive for breast and ovarian cancer, which can be explained by an accompanying pathogenic frameshift mutation c.2808_2811del (p.A938fs) in the *BRCA2* gene [MIM 600185]. This aberration was found to be present in the patient as well. Predisposition to pediatric CRC in *BRCA2* mutation carriers has not been reported before, but germline biallelic *BRCA2* mutations cause Fanconi anemia, a condition that predisposes to pediatric cancer (Howlett et al., 2002). Before performing exome sequencing, we therefore assessed this patient for the presence of a second germline mutation in *BRCA2*, which was not found. Subsequent whole exome sequencing revealed no *de novo* mutations, nor mutations affecting both alleles of one gene. The c.910T>C (p.F304L) variant in the *PARP1* gene (Figure 49 A), which was one of the rare candidate pathogenic variants, was analyzed in more detail in tumor tissue-derived DNA of this patient. Of the chromosome 1q42.12 region, which harbors *PARP1*, two copies were present, and SNP array data revealed no indication for acquired uniparental disomy of this region in the tumor tissue. After Sanger sequencing of *PARP1* on tumor DNA no second hit mutation was found (Figure 43 A). The F304 residue of

PARP1 is a highly conserved residue at the homodimer interface within the third zinc-binding domain, which may be important for PARP1 dimerization and DNA-dependent enzyme activation (Figure 43 A) (Langelier et al., 2008). At present it is not clear if this *PARP1* mutation may have contributed to colon carcinogenesis. In order to test this hypothesis, we first tested if the F304L exchange disturbs PARP1 enzymatic activity. To this end, we generated mutant *PARP1* cDNAs by site-directed mutagenesis, coding for either a phenylalanine or leucine at position 304 and either a valine or alanine at position 762. The rec. proteins carrying the four different combinations at these two aa positions were over-expressed in the *Sf*9/baculovirus protein expression system and purified. Activity testing of PARP1 variants was performed using a well-established biochemical immuno-slot blot assay (Suppl. Figure 19 A) (Beneke et al., 2010). These experiments confirmed previous results showing that the V762A exchange is associated with reduced PARP1 activity (Figure 49 B). Importantly, the PARP\F304L variant showed reduced PARP1 activity by about 50% compared to respective WT, both in the absence and presence of the V762A polymorphism (Figure 49 B). Of note, PARP1\F304L\V762A - as found in the patient - exhibited only 30% of the maximum activity compared to PARP1\WT. These results indicate that the presence of both the F304L and V762A variants in PARP1 in the patient resulted in a cumulative reduction in enzymatic activity.

In a next step, we analyzed the cellular properties of these two natural PARP1 variants. This paves the way towards a molecular risk assessment also of other natural occurring PARP1 variants in order to assess the risk of carriers of these variants for disease development.

Figure 49 C shows that the enzymatic activities of the different natural PARP1 variants behave very similar in a cellular environment compared to the *in vitro* setting as shown in Figure 49 B. Thus, when reconstituting HeLa *PARP1* KO cells with the different natural PARP1 variants, treating them with 50 µM H_2O_2, and subsequently analyzing their PAR forming ability via single-cell immuno-epifluorescence microscopy, PAR formation was reduced by ~31% and ~42% in cells reconstituted with the PARP1\V762A and PARP1\F304L variants, respectively (Figure 49 C). Strikingly, under those conditions the activity of the PARP1\V762A\F304L variant declined by ~57% compared to PARP1\WT. Treatment of cells with higher doses of H_2O_2 (500 µM) resulted in more moderate differences in PAR formation, with a ~20%-reduced PAR formation for the PARP1\V762A\F304L variant compared to PARP1\WT (Figure 49 C and Suppl. Figure 19 B). This indicates that the maximum PAR forming ability in a cellular environment is similar for the different variants,

since under such treatment conditions with high concentrations of H_2O_2, the PAR formation in the cellular system is already saturated.

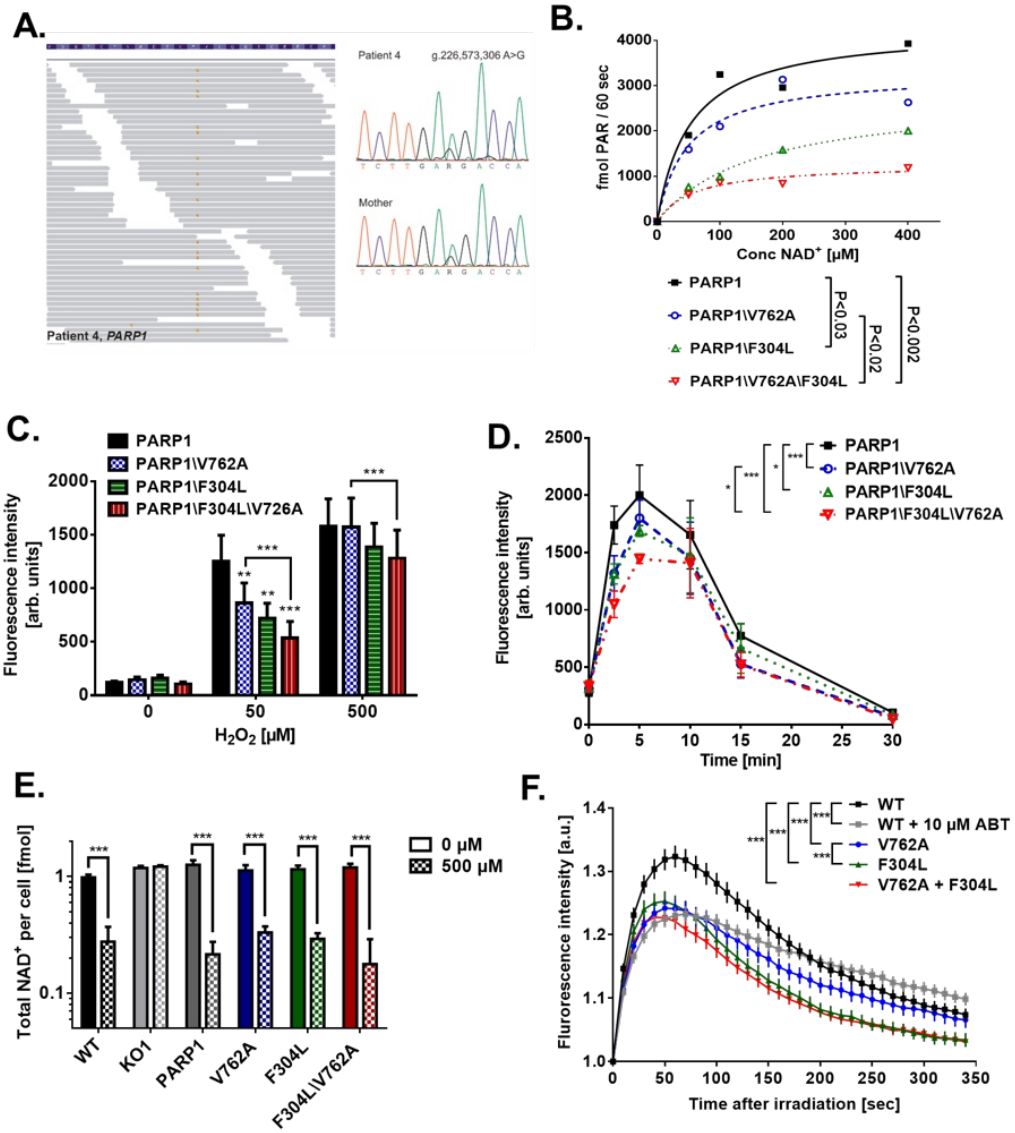

Figure 49: Biochemical and cellular characteristics of natural PARP1 variants.
A. PARP1 mutation identified by exome sequencing in a patient with pediatric colorectal cancer. The panel on the ***left*** shows a subset of the individual sequencing reads spanning the individual mutations (data based on hg19); the panel on the ***right*** shows the validation by Sanger sequencing in the child and the maternal samples to indicate the mode of inheritance. **B.** Biochemical characterization of natural PARP1 variants as used in this study. Rec. enzymes were expressed in the *Sf*9 / baculovirus system and purified via size-exclusion and affinity chromatography. PARP1 activity was examined by incubating 5 nM PARP1 with increasing concentrations of NAD^+ as indicated in a reaction mixture as described in material and methods section. Afterwards 15% of reaction mixtures were slot-blotted on a nylon membrane (see Suppl. Figure 19 A) and PAR content was analyzed by immunochemical staining using the 10H antibody. Means of n=3 independent experiments, error bars were omitted for clarity. A non-linear Michaelis-Menten model was used for curve fit. Statistical analysis using 2-way ANOVA testing. **C.** Analysis of intracellular PARP1 activity in *PARP1* KO cells reconstituted with PARP1 variants as indicated 2 days after transfection by single cell immuno-epifluorescence microscopy as shown in Figue 45 (for representative raw data refer to Suppl. Figure 19 B). Cells were treated with H_2O_2 for 5 min in concentrations as indicated, and PAR levels of eGFP-positive cells were examined using the anti-PAR-specific mAB 10H. Means ± SEM of n=5 independent experiments. Statistical analysis was performed using matched 2-way ANOVA testing and Sidak's post-test. **D.** Time-course analysis of PAR formation in PARP1-reconstituted cells after treatment of cells with 250 µM H_2O_2. Means ± SEM of n=4 independent experiments (>100 cells per experiment). Statistical analysis using matched 2-way ANOVA testing and Sidak's post-test. **E.** NAD^+ levels in WT, *PARP1* KO, and PARP1-reconstituted cells ± H_2O_2 treatment for 7 min as evaluated by an enzymatic NAD^+ cycling assay. Means ± SEM of n=3 independent experiments. Statistical analysis was performed via 2-way ANOVA testing and Sidak's post-test. **F.** Recruitment and dissociation kinetics of natural PARP1 variants at sites of laser-induced DNA damage. For representative raw data refer to Suppl. Figure 20. Means ± SEM. Evaluation from ≥35 cells from 3 independent experiments. Statistical analysis was performed using 2-way ANOVA testing and Sidak's post-test.

Consistent with results from the dose-response analysis, also time-course studies revealed reduced activities for the PARP1\V762A and the PARP1\F304L variants (Figure 49 D). NAD^+ levels in cells reconstituted with the different natural PARP1 variants revealed no differences under non-stress conditions and only minor differences after challenging cells with H_2O_2 (Figure 49 E). This suggests that PARP1 variants still keep their NAD^+ hydrolyzing (NADase) activities (Desmarais et al., 1991) largely active, which is consistent with the findings of similar K_m values of the different variants (Figure 43 B).

In a next step, we were interested if aa exchanges of the natural PARP1 variants influence not only their enzymatic activities, but also their localization dynamics at sites of laser-induced DNA damage. To this end, we used multi-photon excitation microscopy to site-specifically irradiate HeLa cells and monitored the localization of PARP1-eGFP at site of DNA damage over time (Figure 49 F and Suppl. Figure 20).

Interestingly, PARP1\WT-reconstituted cells that were treated with ABT-888 shortly before irradiation, showed similar recruitment and dissociation behavior as the PARP1\E988K variant, *i.e.*, reduced peak levels of recruitment, but longer persistence at the site of the damage (*cf.* Figure 44 F). When analyzing cells reconstituted with the different natural PARP1 variants, it became evident that all variants showed strongly reduced recruitment to sites of laser-damage with the strongest effects observed for the PARP1\V762A\F304L variant (Figure 49 F and Suppl. Figure 20). Interestingly, while the peak intensities at sites of laser-damage between the PARP1\V762A and the PARP1\F304L variant were quite similar, both variants showed significant differences in their dissociation behavior, since the PARP1\V762A variant persisted longer at sites of laser-damage than the PARP1\F304L mutant.

In summary, we have identified a novel PARP1 mutant (*i.e.,* PARP1\F304L\V762A) in a patient with pediatric colorectal carcinoma and provide a biochemical characterization of enzymatic properties of this variant. Furthermore, we analyzed the cellular properties of the PARP1\F304L, PARP1V762A, PARP1\F304L\V762A variants, which revealed significant alterations in their enzymatic activities and localization dynamics at sites of DNA damage that might contribute to the higher risk of disease, which may be present in carriers of these variants.

Discussion

Genotoxic stress, in particular DNA strand breaks, induce an immediate and transient PARylation response that is largely mediated by PARP1. This PARylation response has strong effects on chromatin structure, the spatio-temporal composition of DNA repair factors and their physico-chemical properties at the site of the damage, as well as pronounced signaling effects and consequences on cellular energy metabolism (Gibson and Kraus, 2012; Hottiger, 2015; Mangerich and Bürkle, 2012). Specifically, PARP1-dependent PARylation is involved in base excision and single-strand break repair (BER/SSBR), double-strand break repair (DSB) through homologous recombination (HR) and non-homologous end-joining (NHEJ), as well as nucleotide excision repair (Robert et al., 2013). Much of our knowledge on PARP1 and PARylation has been obtained through studies using genetically engineered mice as well as MEFs derived thereof, pharmacological PARP inhibitor studies, as well as RNA interference approaches in various cellular systems (Blenn et al., 2012; de Murcia et al., 1997; Godon et al., 2008; Masutani et al., 1999; Shall and de Murcia, 2000; Wang et al., 1995). Although these models proved to be extremely informative, there is a lack of systems with a complete genetic deletion of *PARP1* in a human setting. Recently, gene editing technologies have been become commonly available, such as TALEN or CRISPR/Cas technologies, which allow genetic modification in human cancer cell lines (Kim and Kim, 2014). Here we used the TALEN technology to generate a complete genetic deletion of *PARP1* in one of the most widely used human cell culture systems, *i.e.* HeLa cells. We extensively characterized such HeLa *PARP1* KO cells with regards to their PARylation metabolism and stress-response phenotype. Furthermore, we used this system to test a spectrum of artificial and natural human PARP1 variants of interest in a cellular environment without interference of endogenously expressed PARP1 to improve our understanding on the cellular biochemistry and functions of PARP1.

HeLa *PARP1* KO cells did not express detectable levels of PARP1 nor did they reveal any H_2O_2-induced PARP activity, when analyzing intracellular NAD^+ levels or using the 10H antibody in immunofluorescence microscopy. This suggests that in HeLa cells, PARP1 is responsible for most of the genotoxic stress-induced PARylation and that PARP2 does only play a minor role in this cell type. In contrast to these findings, Ame *et al.* showed that 3T3 fibroblasts derived from *Parp1* KO mice still produce significant amounts of PAR after H_2O_2 treatment (as evaluated by 10H-immunofluorescence microscopy), which led to the discovery

of *Parp2* (Amé et al., 1999). However using highly sensitive isotope dilution LC-MS/MS (Martello et al., 2013), we did indeed observe low-level induction of PARylation upon H_2O_2 treatment, which is consistent with the notion that PARP2 can in part compensate the loss of PARP1 also in HeLa cells. Strikingly, basal levels of PAR were not affected at all in HeLa *PARP1* KO cells, demonstrating that under unstressed conditions other PARPs can fully compensate for the loss of PARP1. Our functional analysis revealed that HeLa *PARP1* KO cells showed reduced proliferation rates and were more sensitive towards the treatment with H_2O_2 and CPT, thereby largely confirming the central role of PARP1 in genotoxic stress response as previously reported from mouse, PARP inhibitor, and RNAi studies (Robert et al., 2013).

Reconstitution studies with the PARP1\E988K mutant verified previous results that this variant acts as a mono- or oligo(ADP-ribosyl)transferase (Beneke et al., 2010; Marsischky et al., 1995; Rolli et al., 1997). In addition, with regards to its recruitment and dissociation kinetics at sites of laser-induced DNA damage, our results revealed that the PARP1\E988K variant behaves similar in a human cellular system as it does in a mouse system (Mortusewicz et al., 2007). Thus, as observed by Mortusewicz *et al*., the PARP1\E988K mutant showed impaired recruitment, yet longer persistence, at sites of DNA damage. Generally, it is thought that localization of PARP1 at sites of DNA damage is regulated by its automodification status, since the presence of the highly negatively charged PAR molecules covalently attached to PARP1 may lead to electrostatic repulsion of PARP1 from negatively charged DNA (Zahradka and Ebisuzaki, 1982). Here we extent this view by presenting the possibility that a complementary mechanism can also contribute to the regulation of the PARP1-DNA interaction, *i.e.*, non-covalent interaction of PARP1 with PAR via at least two PAR binding motifs (PBM1/2). Our finding that PAR inhibits the PARP1-DNA interaction is in agreement with the fact that PBM1 is located in Zn2, which is necessary for PARP1 binding to DNA strand breaks (Ali et al., 2012), and the PBM2 is located at the Zn3-Zn1 interface (Langelier and Pascal, 2013). On the other hand, the impaired recruitment of the PARP1\E988K mutant to DNA damage suggests that initial PAR formation at the site of DNA damage is necessary for subsequent second-wave recruitment of PARP1 molecules (Mortusewicz et al., 2007). In accordance with this, results by Mortusewicz *et al.* show that DNA-binding deficient PARP1 mutants still recruited to sites of laser-induced damage in MEFs and this recruitment could be inhibited by PARP inhibitor treatment (Mortusewicz et al., 2007). Consistent with our cytotoxicity and cell cycle analyses of CPT-treated, PARP1\E988K-reconstituted HeLa cells,

previous results showed that the PARP1\E988K reconstitution sensitized *Parp1* KO MEFs to CPT treatment in a colony formation assay (Patel et al., 2012). These effects can presumably be attributed to trapping of the PARP1\E988K mutant at sites of DNA damage and therefore manifesting the damage (Murai et al., 2012). On the other hand, our finding showing that PARP1\E988K expression by itself leads to a G2 arrest, which goes along with higher NAD^+ levels per cell and increased nuclei sizes, is probably unrelated to a potential trapping affect, since PARP inhibitor treatment completely abolished these effects. Because PARP1\E988K is still catalytically active, as shown by our NAD^+ measurements, the PARP1\E988K-triggered G2 arrest is possibly caused by its mono(ADP-ribosyl)ation activity. This remarkable possibility suggests that PARP1-mediated mono(ADP-ribosyl)ation, which may occur upon certain stimuli or as intermediates in PAR catabolism, exerts pronounced and distinct cellular functions.

The PARP1\L713F mutant was originally described as a gain-of-function variant with an over 9 times increased K_{cat}, but similar K_m value compared to WT-PARP1 (Miranda et al., 1995). These results were recently extended by a biochemical study from Langelier *et al.*. These authors demonstrated that the L713F exchange in the hydrophobic core domain (HD) of the catalytic domain (CAT) mimics the effect of DNA damage-induced HD distortions, increasing PARP1 DNA-independent activity up to ~20-fold and elevating the catalytic efficiency of PARylation while not affecting affinity for NAD^+ (Langelier et al., 2012). The HD mutants studied by Langelier *et al.* did not show an increased level of DNA-dependent activity compared to WT PARP-1, indicating that these mutants act through the same mechanism as DNA to stimulate PARP-1 catalytic activity. Our results revealed that the L713F mutant is constitutively active in a cellular environment leading to high PAR levels within cells, even without exogenously-induced DNA damage. Thus, PARP1\L713F-reconstituted cells represent a valuable tool to analyze cellular consequences of PAR overproduction with or without application of genotoxic stress. In this regard, our experiments provide first evidence that PAR overproduction significantly affects cell viability, since PARP1\L713F expression drove cells directly into apoptosis, even without DNA damage induction. If this effect is exerted via the parthanatos pathway, *i.e.*, the PAR-triggered release of AIF from mitochondria, which subsequently translocates to the nucleus to trigger caspase-independent apoptosis (Wang et al., 2011), awaits clarification in future studies. In support of such a scenario, it was previously shown that PAR production upon MNNG treatment leads to AIF release and induction of apoptosis in HeLa cells (Ethier et al., 2007). Since PARP1-

dependent cell death has been implicated in several neurodegenerative and neuroinflammatory diseases, such as Parkinson's disease and ischemia reperfusion damage (Fatokun et al., 2014), the PARP1\L713F mutant can be very useful to study mechanisms of disease related to PAR overproduction in a cellular setting.

Apart from studying the cellular biochemistry of PARP1 and molecular mechanisms of PARylation, the cell culture model reported in this study can be used to analyze structure-function relationships of naturally occurring *PARP1* variants. One of such variants that has been extensively studied in recent years is a SNP in the *PARP1* gene leading to the V762A aa exchange (Cottet et al., 2000). This variant has been associated with an increased risk for gastric, cervical, and lung cancers and a generally increased cancer risk in the Asian population, while being associated with a decreased risk for brain tumors (Hua et al., 2014; Qin et al., 2014). Consistent with the notion that changes in PARP activity might be responsible for these correlations, previous results revealed a reduced enzymatic activity of the PARP1\V762A variant on the biochemical level (Beneke et al., 2010; Wang et al., 2007). On the other hand, studies of human cells derived from V762A carriers revealed inconsistent results, with one study observing a gene-dose-dependent reduction of PARP activity (Lockett et al., 2004), whereas another one did not find such an effect (Zaremba et al., 2009). Our results from reconstituted HeLa *PARP1* KO cells provide clear proof for decreased activity of PARP1\V762A in a cellular environment under conditions of genotoxic stress, thereby strongly supporting a causative link for the increased tumor risk in V762A carries due to reduced PARP1 activity.

In a patient with pediatric CRC, who inherited a frameshift mutation in *BRCA2* from his father, we identified a maternally inherited missense variant in *PARP1* (F304L) combined with the V762A polymorphism, which significantly reduced PARP1 activity on the biochemical and cellular level. Furthermore, the PARP1\F304L\V762A mutant showed reduced recruitment efficiency to sites of laser-induced DNA damage. In cells deficient in PARylation activity single-stranded (ss) DNA breaks can accumulate, which, when encountered during DNA replication, may result in the accumulation of double-stranded (ds) DNA breaks. These dsDNA breaks are repaired via HR, which requires proper functioning of BRCA2. Therefore, cells that are deficient in BRCA2 are highly sensitive to PARP1 inhibition, resulting in cell death by apoptosis (Bryant et al., 2005; Farmer et al., 2005). The tumor in the CRC patient was deficient for BRCA2 due to an inherited pathogenic mutation in

one allele and an acquired somatic loss of the second wild-type allele (data not shown). This functional loss of both *BRCA2* alleles, in conjunction with the inherited heterozygous PARP1 variant, may have resulted in an increase in genomic instability and, as a consequence, early-onset cancer development in the colon. Complete loss of PARP1 through a second hit in the tumor most likely would have resulted in cell death due to synthetic lethality (Bryant et al., 2005; Farmer et al., 2005). Therefore, in retrospect, this patient might have benefited from a PARP1 inhibitor therapy. The drastic impairment of PARP1 activity due to the cumulative effect of the F304L variant and the V762A polymorphism in combination with the *BRCA2* mutation, may well have resulted in predisposition for CCRC development in this patient, however this needs to be clarified in detailed follow-up experiments. Reports on digenic inheritance, with germline mutations in genes with synergistic interactions, are scarce. This mode of inheritance has been described in patients with extreme phenotypes, *i.e.*, exceptionally early ages of onset or severe clinical presentations. Examples of these are digenic inheritance in early onset Parkinson's disease [MIM 605909] and severe insulin resistance [MIM 125853] (Savage et al., 2002; Tang et al., 2006).

In conclusion, this study establishes a novel human cell culture model to decipher the role of PARP1 and PARylation in cellular functions, *i.e.*, a complete *PARP1* KO in HeLa cells. Reconstitution of these cells with different PARP1 variants enabled us to study PARP1 hypomorphy (E988K) as well as hypermorphy (F713L) in an easy to handle and exceptionally well-characterized human cancer cell line. Furthermore, we used this approach to correlate epidemiological and clinical findings on naturally occurring PARP1 variants with the cellular properties of this variants. This provides a basis for molecular risk assessment of these and other naturally occurring PARP1 variants in order to judge if carriers may be predisposed to the development of certain diseases.

Material and Methods

Generation of HeLa PARP1 KO cells by TALEN-mediated gene targeting

TALENs were custom synthesized by Cellectis Bioresearch (75013 Paris ‐ France) and were designed to target the first exon of the *PARP1* gene in close proximity to the start codon (Figure 41 A). For the generation of stable cell lines HeLa Kyoto cells were transfected with 1 µg of each TALEN arm DNA using Effectene transfection reagent (Qiagen). After 24 hours, cells were subcloned using a limited dilution approach. Single clones were expanded and PARP1 protein levels were analyzed using immunoflourescent analysis and Western blotting. Cells were cultured in DMEM with 10% FBS, 2 mM L-glutamine and 1% penicillin/streptomycin at 37°C, 5% CO_2 and 95% humidity.

Orthologous expression and purification of recombinant PARP1

Baculovirus expression constructs of PARP1 were generated according to manufacturer's instructions (BD). Recombinant (rec.) PARP1 was overexpressed in *Sf*9 insect cells with an MOI of 1 and an incubation time of 60 h. Thereafter, cells were harvested, pelleted and stored at -80°C. Rec. PARP1 was purified as described previously (Beneke et al., 2000), with modifications. Briefly, cell pellets were lysed for 20 min in lysis buffer (1 ml per 1.5×10^7 cells; 25 mM Tris-HCl pH 8.0, 10 mM EDTA pH8.0, 50 mM glucose, 0.2% Tween 20. 0.2% NP-40, 0.5 M NaCl, 1 mM PMSF and 1 mM 2-mercaptoethanol) and cell debris was cleared by centrifugation at 20,000 × *g* for 20 min. Protamine sulfate (1 mg/ml) was added to the supernatant and samples centrifuged again for 10 min at 20,000 × *g*. Next, ammonium sulfate was added to 30% saturation, followed by centrifugation at 25,000 × *g* for 20 min. Ammonium sulfate saturation in the supernatant was increased to 80%, and centrifuged again at 20,000 × *g* for 15 min. For desalting, the PARP1-containing pellet was dissolved in Buffer 2 (1 ml per 1.5×10^7 cells; 100 mM Tris-HCl pH 7.4, 0.5 mM EDTA pH 7.4, 10% glycerol, 1 mM PMSF and 2 mM 2-mercaptoethanol) and loaded onto a Sephadex G-100 column (Sigma-Aldrich). Proteins were eluted with 10 ml Buffer 3 (50 mM Tris-HCl pH 8.0, 0.5 mM EDTA pH 8.0, 5 mM $MgCl_2$, 5% glycerol, 1 mM PMSF and 2 mM 2-mercaptoethanol) and fractions were separated on a 10% SDS gel, followed by Coomassie staining and Western blotting to identify the PARP1 containing fractions. These fractions were pooled and loaded onto a dsDNA-cellulose column (Sigma-Aldrich). Proteins were eluted with Buffer 3,

containing increasing concentrations of KCl (100 mM, 200 mM, 400 mM, and 1 M). Fractions were collected and the PARP1-containing fractions were identified using Coomassie staining and Western blotting. The PARP1 fractions were then pooled and concentrated using an Amicon 50-kD cut-off spin filter, for buffer exchange (storage buffer, 20% glycerol in PBS). Protein concentration was determined using the Bradford assay and the purified rec. PARP1 samples were aliquoted, snap-frozen in liquid N_2 and stored at -80°C until further usage.

PARP1 activity assay

PARP1 activity assays were performed as previously described (Beneke et al., 2010), with modifications. Reaction buffer (100 mM Tris-HCl pH 7.8, 1 mM DTT, 10 mM $MgCl_2$ and 25 µg/ml of dsDNA activator oligonucleotide, *i.e. Eco*RI linker) was pre-incubated at 30°C for 60 s. The reaction was started by addition of 5 nM PARP1 and varying concentrations of NAD^+ (50-400 µM) and was stopped by addition of an equal volume ice-cold 20% TCA. Each sample (15% of total) was loaded per slot on a slotblot manifold in technical triplicates and vacuum aspirated on a Hybond-N^+ nylon membrane (GE Healthcare). Purified PAR in different concentrations (200-1500 fmol) was applied as technical standards. The slots were washed with 10% TCA and 70% ethanol before heat-crosslinking for 1 h at 90°C. Afterwards, the membrane was blocked in M-TNT, followed by incubation with anti-PAR antibody 10H (1:300 in M-TNT) for 1 h. Next, the membrane was washed thrice in TNT for 5 min, followed by incubation with secondary antibody goat anti-mouse-HRP (1:2000 in M-TNT) for 1 h. The membrane was again washed thrice in TNT, followed by chemiluminescent detection at LAS 4000 mini (GE Healthcare). The band intensities were evaluated densitometrically using ImageJ software.

In silico search for PAR binding motifs

PARP1 was screened for PAR-binding motifs (PBMs) using the PATTINPROT tool (https://npsa-prabi.ibcp.fr/cgi-bin/npsa_automat.pl?page=npsa_pattinprot.html) as described previously (Popp et al., 2012). The PBM-pattern [HKR]-X-[AVILFWP]-[AVILFWP]-[HKR]- [HKR]-[AVILFWP]-[AVILFWP], first described by Pleschke and colleagues (Pleschke et al., 2000), was searched against the full-length protein sequence of PARP1

(http://www.uniprot.org/; P09874 PARP1_HUMAN), allowing for one (PBM1) or two mismatches (PBM2).

Far-western PAR binding assay

Rec. PARP1 was either size-separated using SDS-PAGE and subsequent western blotting on a PVDF membrane, vacuum-aspirated onto a nitrocellulose membrane using a slotblot manifold (Roth), or, in case of the peptide studies, purchased as a membrane with covalently attached peptides (PepSpot membrane with on-membrane synthesized peptides, JPT Technologies). The PepSpot membrane was activated in 100% methanol for 5 min according to the manufacturer's instructions, followed by a 5-min wash in TNT [150 mM NaCl, 10 mM Tris-HCl pH 8.0, 0.05% (v/v) Tween 20] and 1-h incubation in TNT. The membrane was then incubated over night with 0.2 µM unfractionated PAR in TNT at 4°C. Negative controls were incubated with TNT only, *i.e.*, w/o PAR. The blots were subjected to three 10-min washes with high salt buffer to remove unspecifically bound PAR. Next, membranes were washed twice with TNT for 10 min and blocked with 5% milk powder in TNT (M-TNT) for 1 h. Subsequently, blots were incubated for 1 h with anti-PAR-specific primary antibody 10H (1:300 in M-TNT), followed by three 5-min TNT washes. The blots were then incubated for 1 h with secondary antibody goat anti-mouse-HRP (Dako Cytomation, 1:2000 in M-TNT), followed by three 5-min washes in TNT and subsequent chemiluminescence detection. Slotblot and western blots were stripped, blocked again and re-probed with mouse anti-PARP1 antibody CII-10 (1:300 in M-TNT) as loading control.

Biotinylation and size-fractionation of poly(ADP-ribose)

Biotinylation of PAR was performed as described previously (Fahrer et al., 2007) with some modifications. Briefly, 400 µM of purified PAR were incubated for 8h at RT in a buffer consisting of 100 mM sodium acetate buffer pH 5.5, 1 mM $NaBH_3CN$, 4 mM EZ-Link Hydrazide-Biocytin (Thermo Scientific). After dialysis against 100 mM sodium acetate buffer pH 5.5 with a 2 kDa cut-off Slide-A-Lyzer Dialyis cassette G2 (Thermo Scientific) the PAR was ethanol-precipitated. Concentration of PAR was determined with UV absorbance at 258 nm. The biotinylated PAR was separated from non-biotinylated PAR by affinity purification using the Pierce Monomeric Avidin Kit (Thermo Scientific) according to the manufacturer´s instructions. The elution fractions were dialyzed against 100 mM sodium acetate buffer, pH

5.5, followed by ethanol-precipitation. HPLC fractionation of the biotinylated PAR was performed as described previously (Fahrer et al., 2007). Briefly, the biotinylated PAR was fractionated using an Agilent 1100 series HPLC with a semi-preparative DNAPac^{TM} PA100 BioLC column (Thermo Scientific), by applying a multistep NaCl gradient in 25 mM Tris-HCl pH 9.0, modified from (Kiehlbauch et al., 1993). The 258 nm UV absorbance signal was used to collect PAR fractions manually, followed by ethanol-precipitation.

Electrophoretic mobility shift assays (EMSAs)

EMSAs were performed as described previously (Popp et al., 2012). Briefly, rec. PARP1 in increasing concentrations was incubated for 20 min with 200 fmol biotinylated double-stranded DNA oligonucleotide (5'-biotin-$(TTT)_5$-TTAGGGTTAGGGTTAGGGT-TAGGGCATGCACTAC-3' and 5'-GTAGTGCATGCCCTAACCCTAACCCTAACCC-TAA-$(TTT)_5$-3') in EMSA buffer (40 mM Tris-HCl pH 8.0, 5 mM DTT, 4 mM $MgCl_2$, 0.1 mg/ml BSA and 0.1% NP-40) at RT. Then, samples were mixed with 10× loading dye (40% glycerol, 0.05% orangeG and 0.05% bromphenol blue) and loaded on a 5% native TBE gel. The gel was then blotted onto a nylon membrane, followed by heat-crosslinking (1 h at 90°C). The blot was blocked for 1 h in M-TNT, washed thrice for 5 min in TNT and then incubated for 1 h with streptavidin-HRP (1:1000 in TNT). Afterwards, membranes were washed thrice for 5 min in TNT followed by chemiluminescence detection. When the effect of PAR binding on PARP's DNA binding ability was tested, PARP1 was pre-incubated with unfractionated PAR (in amounts as indicated) for 20 min at RT before addition of the DNA substrate. The band intensities were measured using ImageJ to calculate relative band shifts.

PAR-EMSAs were essentially performed as described previously (Fahrer et al., 2007), with modifications. Briefly, rec. PARP1 in increasing concentration was mixed with EMSA buffer (see above) and incubated at 25°C for 10 min. After addition of 500 fmol size-fractionated biotinylated PAR (30-35mer) the samples were again incubated at 25°C for 20 min. The samples were mixed with 10x loading dye (40% glycerol and 0.05% orangeG), separated on a 5% native TBE gel by electrophoresis, semi-dry blotted on nylone membrane, followed by drying at 90°C for 1 h. After 1-h blocking in M-TNT, the blots were washed thrice for 5 min with TNT followed by 1-h incubation with streptavidin-HRP (1:1000 in TNT). Afterwards, the blots were washed again thrice with TNT, followed by chemiluminescence detection.

Identification of F304L variant in a patient with pediatric colorectal carcinoma

This patient, with non-polyposis microsatellite stable colorectal cancer, diagnosed at 13 years of age, was included in a study to identify novel CRC predisposing genes by applying exome sequencing on germline DNA of the child. Clinical data, tumor tissue and DNA samples were obtained. The patient and the parents provided informed consent and the studies were approved by the Medical Ethics Committee of the Radboud university medical center in Nijmegen (no. 2012/271). DNA was extracted from peripheral blood cells and tumor tissues using standard procedures.

The exome sequencing procedures used were essentially as reported before (Vissers et al., 2010). Briefly, exome enrichment was performed using an AB SOLiD optimized SureSelect human exome kit v1 (Agilent, Santa Clara, CA, USA). Small insertions and deletions were detected using the SOLiD Small InDel Tool. All variants were annotated using an in-house developed analysis pipeline (Hoischen et al., 2011; Vissers et al., 2010). For prioritization, we selected high confident non-synonymous variants that had a high probability of being pathogenic, and were absent in dbSNPv132 and our in-house variant database containing at time of analysis 1,302 in-house analyzed exomes. The candidate mutations were validated by Sanger sequencing in peripheral blood DNA of the child and its parents.

Generation of PARP1-GFP expression constructs and cell transfection

PARP1 mutants were generated by site-directed mutagenesis. Plasmids pET15b::PARP1-V762 and pET15b::PARP1-A762 were used as templates to generate the mutants pET15b::PARP1-V762-L304 and pET15b::PARP1-A762-L304 using the primer pair 5'-AATGCTCGGGTCAGCTGGTCCTCAAGAGC-3' and 5'-GCAGTAATAGGCATC-GCTCTTGAGGACCAGCT-3'. For rec. protein expression in *Sf*9 cells the *PARP1* sequences were PCR-extracted (5'- AAACTGGCGGCCGCATGGCGGAGTCTTCGGATA-AGC-3' and 5'-TCGAGTGCGGCCGCTTACCACAGGGAGGTCTTAA-3') and sub-cloned into the pJET1.2 vector using the CloneJET PCR cloning kit (Thermo Fisher), thereby introducing *Not*I restriction sites up- and downstream of the *PARP1* sequences (underlined in primer sequence). Using these restriction sites the *PARP1* sequences were cloned into the MCS of the baculovirus expression vector pVL1393 (BD). peGFP-N1::PARP1-V762A, peGFP-N1::PARP1-F304L and peGFP-N1::PARP1-F304L-V762A were generated using the pVL1393 plasmids as donors. Therefore, the respective pVL1393 plasmids and pEGP-N1::PARP1 were digested with *Bss*HII and *Eco*RV. The resulting fragments were ligated in

the pEGP-N1::PARP1 backbone. peGFP-N1::PARP1-E988K and peGFP-N1::PARP1-L713F were generated by site-directed mutagenesis using peGFP-N1::PARP1 as a template. For peGFP-N1::PARP1-E988K the primer pair 5'-CCTCTCTACTATATAAC**A**AGTACATTG-TCT-3' with 5'-CATAGACAATGTACT**T**GTTATATAGTAGAG-3' was used. For peGFP-N1::PARP1-L713F the primer pair 5'-GCATACTCCATC**T**TCAGTGAG-3' with 5'-GGACCTCACTGA**A**GATGGAG-3' was used. Correct orientation of the inserts and successful mutagenesis were verified by DNA sequencing (GATC Biotech). All primers were purchased from Sigma-Aldrich; mutated bases are marked by bold underlining.

Immuno-chemical detection of PARP1 and PAR by fluorescence microscopy

HeLa WT and HeLa *PARP1* KO cells were seeded on glass cover slips in 12-well plates. For reconstitution experiments, *PARP1* KO cells were transfected with different eGFP-N1::PARP1 plasmids using Effectene (Qiagen), according to the manufacturer's instructions. PAR formation was induced by H_2O_2 treatment for 5 min, 48 h after transfection. After treatment, cells were washed once with PBS and fixed in 4% (w/v) PFA in PBS for 20 min. All subsequent incubation steps were performed at RT on a shaker. In order to stop fixation, 100 mM glycin in PBS was added for 1 min followed by washing of the slides in PBS. For permeabilization, the slides were incubated for 3 min in 0.4% Triton X-100 in PBS, followed by washing with PBS.

For immunofluorescence staining, the slides were blocked in PBS containing 20% (w/v) non-fat milk powder and 0.2% (v/v) Tween 20 (PBSMT) for 1 h. Then, samples were incubated with the primary antibodies mouse-anti-PAR (10H) or mouse-anti-PARP1 (FI-23) at 37°C for 1 h. In case of H3K27me3 slides were blocked in 5% BSA for one hour and incubated with rabbit anti-H3K27me3 (Abcam) 1:200 in 5% BSA and 0.1% Tween 20. Subsequently, the slides were washed thrice for 10 min in PBS, followed by incubation with the secondary antibodies goat anti-mouse/rabbit IgG coupled to Alexa546 (1:400 in PBSMT). Next, the slides were washed thrice for 10 min in PBS, nuclei were stained with Hoechst33342 (0.1 µg/ml in PBS) for 5 min, slides were again washed in PBS thrice for 10 min, and mounted with Aqua Polymount. Microscopic images were acquired using a Zeiss Axiovert 200M microscope. Image data were analyzed using an automated KNIME workflow. Antibody controls, prepared without the primary antibody were used to determine background fluorescence. Only cells with a fluorescence intensity higher than 1.5-fold of the mean

background fluorescence intensity were considered GFP-positive and analyzed for PAR-fluorescence.

Western blot analysis

Protein lysates were prepared by washing the cells with PBS, followed by cell lysis on ice using ice-cold high-salt RIPA buffer [500 mM NaCl, 50 mM Tris-HCl pH 7.4, 1% Triton X-100, 1% sodium-deoxychelate, 0.1% SDS and 1× complete protease inhibitor cocktail (Roche)] or SDS loading dye [93.75 mM Tris-HCl pH6.8, 9 M urea, 7.5% (v/v) 2-mercaptoethanol, 15% (v/v) glycerol, 3% (w/v) SDS and 0.01% (w/v) bromphenol blue]. The lysates were transferred to reaction tubes and DNA was sheared through syringes with decreasing diameter. Protein concentrations were determined via Bradford assay. Protein lysates (15-25 µg or 1.5×10^5 cells) were loaded per lane, run on 10% SDS gels and semi-dry blotted on nitrocellulose membrane. Membranes were blocked for 1 h in M-TNT or in TNT with 5% BSA (in case of antibodies detecting phosphorylated proteins), followed by 1-h incubation with primary antibodies [mouse anti-PARP1 CII-10 (1:300); mouse anti-p53 (1:1000, Cell Signaling); rabbit anti-p16 (1:2000, Abcam); mouse anti-actin (1:50000, Millipore) in M-TNT and rabbit anti-ph-p53(Ser15) (1:1000, Cell Signaling); mouse anti-γH2A.X (1:2000, Millipore) both in TNT with 5% BSA] and three 5-min washes in TNT. Next, membranes were incubated 1 h with the respective secondary antibodies [goat-anti rabbit-HRP 1:2000 in M-TNT (Dako); goat-anti mouse-HRP 1:2000 or 1:5000 in M-TNT (Dako)], again followed by three 5-min washes in TNT and chemiluminescence detection.

LC-MS/MS quantification of cellular PAR

Quantification of cellular PAR levels by isotope dilution mass spectrometry (LC-MS/MS) was conducted as previously described (Martello et al., 2013), with modifications. Briefly, cells were treated with H_2O_2 in concentrations as indicated for 5 min at 37°C. Then, cells were washed briefly with ice-cold PBS, placed on ice and lysed with 1 ml 20% TCA. The lysed cells were harvested using a cell scraper and the lysate was centrifuged for 5 min at 3000 x *g* and 4°C. The supernatant was discarded, the pellet washed twice with 500 µl ice-cold 70% ethanol and centrifuged for 5 min at 3000 x *g* at 4°C. The pellet was air-dried at 37°C, resuspended in 255 µl 0.5 M KOH by constant shaking until completely dissolved and was then neutralized with 50 µl 4.8 M MOPS buffer. For DNA concentration determination

30 µl were removed. To each 30-µl sample 390 µl MOPS:KOH (1 M:0.5 M) and 2.1 µl Hoechst 33342 (1 mg/ml) were added and fluorescence intensities were measured with an extinction wavelength of 360 nm and an emission wavelength of 460 nm utilizing a VarioskanFlash Fluorescence Reader (Thermo Scientific). The DNA concentration of a sample was calculated by using a standard curve from defined amounts of calf thymus DNA (Sigma-Aldrich). Heavy-isotope labeled, undigested PAR (12 pmol) was added as an internal standard to the residual sample. DNA and RNA were digested for 3 h at 37°C by incubating samples with 0.1 mg/ml DNase 1 (Roche), 0.1 mg/ml RNase A (Sigma-Aldrich), 50 mM $MgCl_2$ and 100 mM $CaCl_2$. Then, 1.25 µl of 40 mg/ml proteinase K (Roche) were added and samples were incubated at 37°C over night. Thereafter, PAR was purified using the High Pure miRNA Isolation kit (Roche) according to the manufacturer's instructions. PAR was eluted in 100 µl RNase-free water and then digested into its subunits with 10 U PDE1 (Affymetrix) and 0.5 U alkaline phosphatase (Sigma-Aldrich) for 3 h at 37°C. Next, the samples were filtered through a 10-kD Nanosep filter (Pall) and subsequently dried in a speedvac. The samples were then resolved in 100 µl MilliQ water and subjected to LC-MS/MS analysis as described previously (Martello et al., 2013).

NAD^+ cycling assay

HeLa WT or HeLa *PARP1* KO1 cells were seeded in 6-well plates and transfected with the different eGFP-N1::PARP1 plasmids using Effectene (Qiagen). Two days after transfection, NAD^+-cycling assays were performed. To this end, PAR formation was induced by treating cell with 500 µM H_2O_2 for 8 min. Subsequently, cells were harvested using trypsin/EDTA and kept on ice during all following steps. The cell numbers were determined using a CASY cell counter (Roche) and $5x10^5$ cells were used for analysis. Cell pellets were resuspended in 500 µl PBS and lysed by addition of 24 µl 3.5 M perchloric acid. After a 15-min incubation, samples were centrifuged to remove cellular debris. The supernatant was mixed with 350 µl phosphate buffer (0.33 mM K_2HPO_4, 0.33 mM KH_2PO_4 pH 7.5) followed by a 15-min incubation to allow precipitation. After centrifugation, the supernatant was incubated on ice for 20 min followed by another round of centrifugation. The resulting supernatant was used in the NAD^+-cycling assay. As a reference, a standard curve was determined in each experiment. To this end, NAD^+ was diluted to concentrations ranging for 0 µM to 0.48 µM. Each sample was measured in technical triplicates and therefore 40 µl of the supernatant were diluted in 160 µl diluent (0.5 M H_3PO_4, 0.5 M NaOH). To each well 100 µl of a reaction mix [0.48 M

bicine (pH8), 4 mg/ml BSA, 0.02 M EDTA, 2.4 M ethanol, 2 mM MTT, 0.96 mg alcoholdehydrogenase and 5.7 mM phenazine ethosulfate] were added. Absorption at 550 nm was measured 30 min after incubation at 30°C using 690 nm as a reference wavelength (Spectra 96-well plate reader). The intracellular NAD^+ concentration was calculated with the help of the standard curve and normalized to the transfection efficiencies as determined by FACS analysis performed in parallel.

Cytotoxicity analysis

HeLa Kyoto WT and *PARP1* KO cells were seeded in 6-well plates and transfected with the different eGFP-N1::PARP1 plasmids using Effectene (Qiagen). In case of treatment, camptothecin (CPT; Sigma-Aldrich) or DMSO as solvent control were added to the medium 24 h after transfection. Two days after treatment, cells were harvested using trypsin/EDTA. The supernatants containing the dead and viable cells were collected together and the cell concentration was determined using a CASY cell counter (Roche). A number of $2.5x10^5$ cells was pelleted and resuspended in annexin V binding buffer (10 mM HEPES pH 7.4, 140 mM NaCl, 2.5 mM $CaCl_2$). A volume of 195 µl of the cell suspension was mixed with 5 µl annexin V-FITC (for untransfected cells) or annexin V-APC (for transfected cells) and incubated in the dark at RT. Finally, 200 µl of propidium iodide (PI) solution (10 µg/ml PI in annexin V binding buffer) were added and the cells were analyzed using a FACSCalibur (BD). For each sample, 10,000 transfected cells were analyzed with a maximum flowrate of 500 cells/s.

Cell cycle analysis

HeLa WT or HeLa *PARP1* KO cells were seeded in 6-well plates and transfected with the different eGFP-N1::PARP1 plasmids using Effectene (Qiagen). Three days after transfection, the cells were harvested using trypsin-EDTA, pelleted, and resuspended in PBS. Then, 700 µl ethanol were added for fixation, cells were incubated for 20 min followed by centrifugation. The pellet was washed with PBS, centrifuged again and resuspended in 30 µl PBS. A volume of 120 µl of DNA extraction buffer (4 mM citric acid, 0.2 M Na_2HPO_4, pH 7.8) was added and the samples were incubated for 20 min on a shaker at RT. After centrifugation the samples were resuspended in PI-staining solution (PBS, 0.2 mg/ml RNAase A, 20 µg/ml PI)

and analyzed using a FACSCalibur (BD). For each sample, 10,000 transfected cells were measured with a maximum flowrate of 500 cells/s.

Clonogenic survival assay

Cells ($1x10^6$ cells/ml) were incubated for 5 min in the presence of H_2O_2 in concentrations as indicated. Subsequently, 500 cells were seeded in 6-cm plates and incubated for 2 weeks at 37°C, 5% CO_2 and 95% humidity. Then, medium was removed and colonies were fixed and stained for 1 h using a 10% formaldehyde solution (Sigma-Aldrich) mixed with 0.1% crystal violet. The culture dishes were washed and colonies consisting of at least 20 cells were counted using a stereomicroscope (Leica).

Recruitment studies

For recruitment studies, $1x10^5$ HeLa Kyoto *PARP1* KO cells were seeded on µ-slides (ibidi) 24 h before transfection with the different eGFP-N1::PARP1 constructs using Effectene (Qiagen) according to the manufacturer's instructions. The proteins were expressed for 48 h. On the day of irradiation the medium was changed to phenolred-free DMEM (Gibco).
DNA damage was induced with a commercially available 780 nm femtosecond-pulsed fiber laser (Toptica, Munich, Germany) coupled into a LSM700 confocal laser-scanning microscope (Zeiss) through an independent scanner system (Rapp Optoelectronics, Hamburg, Germany). Within the GFP-positive cell nuclei a 6 µm line was irradiated for a total irradiation time of 3.78 sec using 5 mW average power and a repetition rate of 40 MHz. The kinetics of the proteins were observed using a Zeiss EC-Plan-Neofluar 40x/1.3 oil immersion objective and a 488 nm solid-state imaging lasers with an open pinhole. Imaging was facilitated by an automated macro (LIC macro, University of Freiburg, Germany) and analysis was performed with a line analysis macro for ImageJ, which is available for download on http://www.bioimaging-center.uni-konstanz.de (BIC tool box, University of Konstanz, Germany).

Deconvolution microscopy

For deconvolution microscopy the slides were prepared as for immunofluorescence experiments.

Statistical analysis

Statistical testing was performed using GraphPad Prism and tests were applied as indicated in Figure legends. "*" indicates $P \leq 0.05$, "**" $P \leq 0.01$, "***" $P \leq 0.001$.

Acknowledgements

We like to thank Dr. Martin Stöckl for help with the 3D deconvolution microscopy and Dr. Jennifer Baur for help with the establishment of the KNIME workflow. Furthermore, we would like to thank Christina Renner for her work.

Funding

This work was supported by the Young Scholar Fund (YSF), Research Training Group (RTG) 1331, Konstanz Research School Chemical Biology (KoRSCB), Collaborative Research Center (CRC969), and Stichting Kinderen Kankervrij (KiKa project 127). Funding for open access charge: University of Konstanz.

Supplementary Data

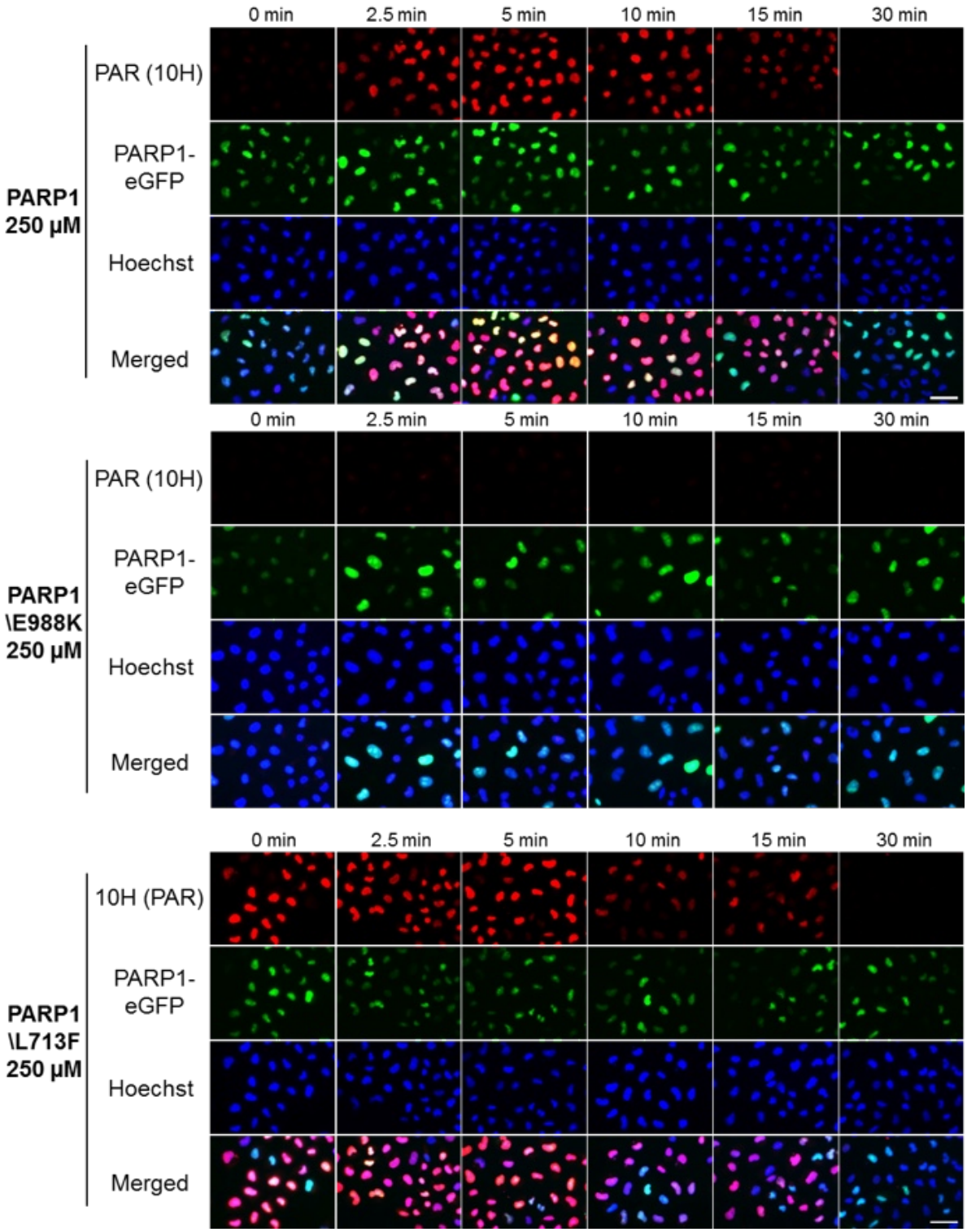

Supplementary Figure 17: Time course analysis of cellular PARylation capacity of artificial PARP1 mutants.
HeLa *PARP1* KO cells were transfected with eGFP-coupled constructs of PARP1, PARP1\L713F, and PARP1\E988K. Analyses were performed 2 days after transfection. Representative images from single cell immuno-epifluorescence analysis of PARP1-eGFP and PAR after treatment of PARP1-reconstituted cells with 250 µM H_2O_2 for the indicated times. Scale bars indicate 30 µM.

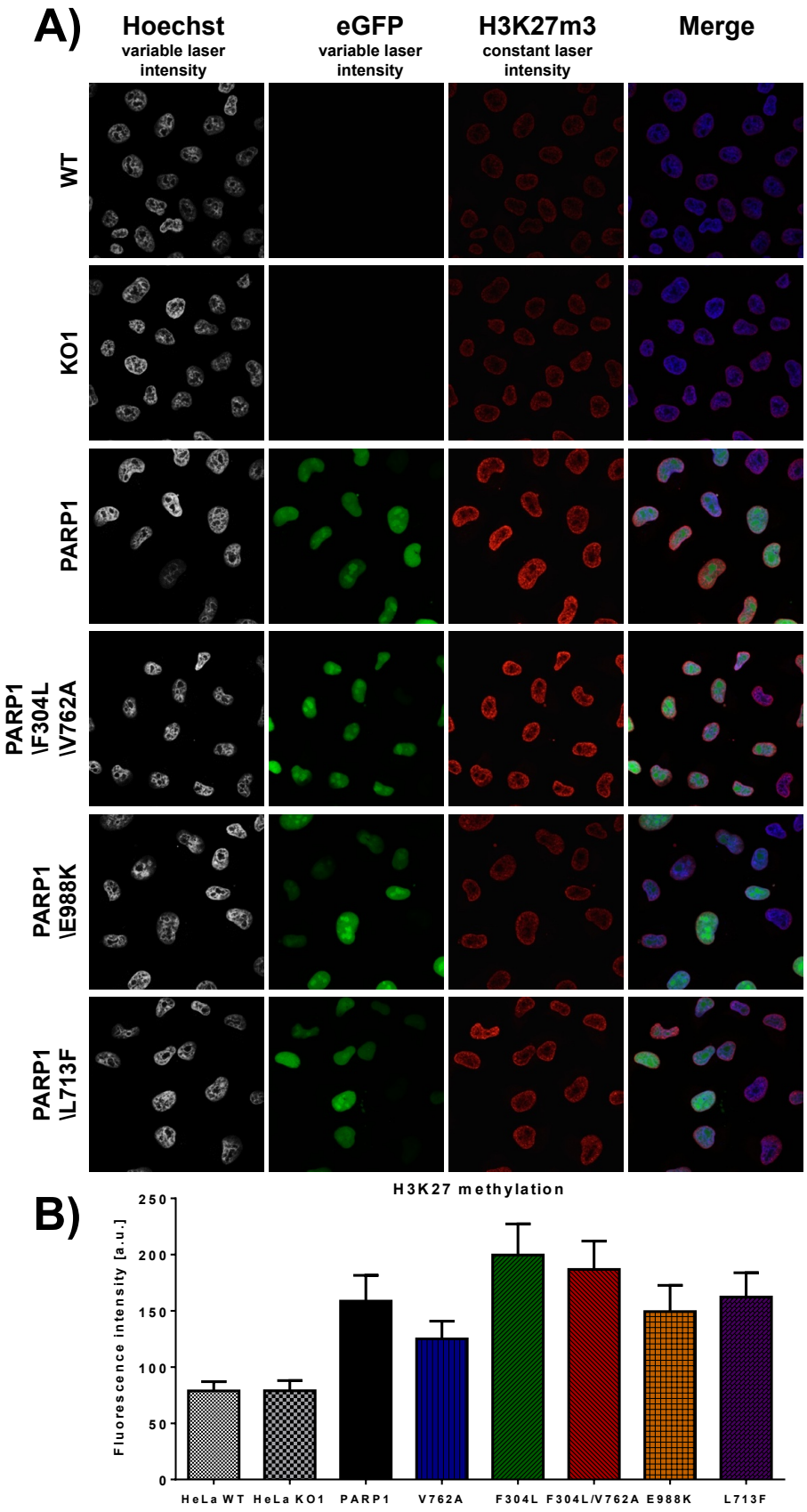

Supplementary Figure 18: Overexpression of different PARP1 variants changes H327K methylation status.
HeLa *PARP1* KO cells were transfected with eGFP-coupled constructs of PARP1, PARP1\L713F, PARP1\E988K, and PARP1\V762A\F304L. Analyses were performed 2 days after transfection. HeLa Kyoto WT cells were analyzed as control. **A.** Representative images from single cell immuno-epifluorescence analysis of PARP1-eGFP and H3K27m3 of PARP1-reconstituted cells. **B.** Densitometric analysis of imaging data as shown in A. >40 cells were analyzed per experiment and condition. Means ± SEM of n=2 independent experiments.

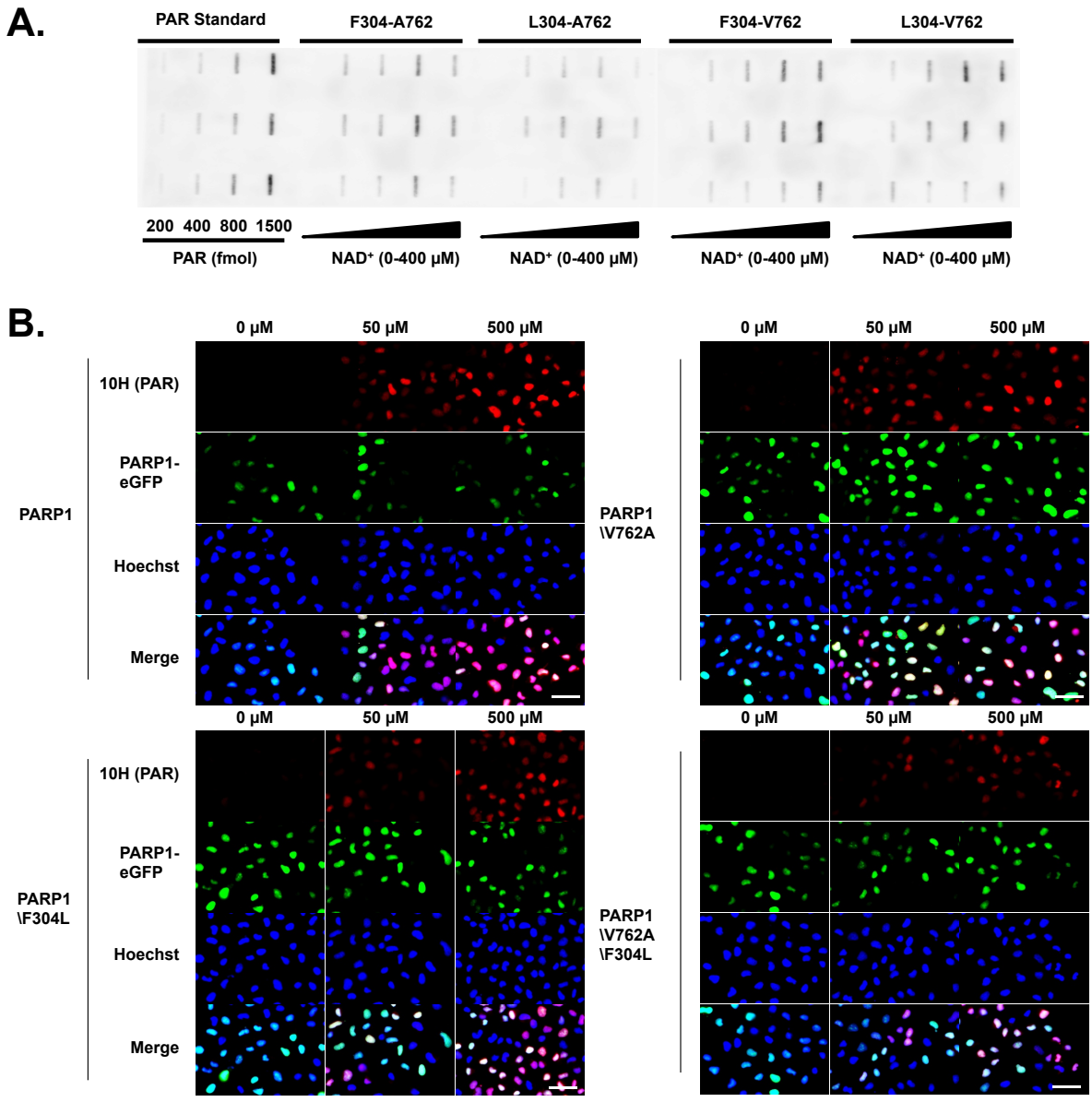

Supplementary Figure 19: Biochemical and cellular characteristics of natural PARP1 variants.
A. Biochemical characterization of the four natural PARP1 variants used in this study. Rec. enzymes were expressed in the Sf9 / baculovirus system and purified via size exclusion and affinity chromatography. PARP1 activity was examined by incubating 5 nM PARP1 with increasing concentrations of NAD+ as indicated. Afterwards, 15% of reaction mixtures were slot-blotted on a nylon membrane in technical triplicates and PAR content was analyzed by immunochemical staining using the 10H antibody. Displayed here are representative slot-blots of each PARP1 variant; purified PAR was used as standard. **B.** HeLa *PARP1* KO cells were transfected with eGFP-coupled constructs of PARP1, PARP1\V762A, PARP1\F304L and PARP1\V762A\F304L. Analyses were performed 2 days after transfection. Representative images from single cell immuno-epifluorescence analysis of PARP1-eGFP and PAR after treatment of PARP1-reconstituted cells ± H_2O_2 as indicated for 5 min. Scale bars indicate 30 µM.

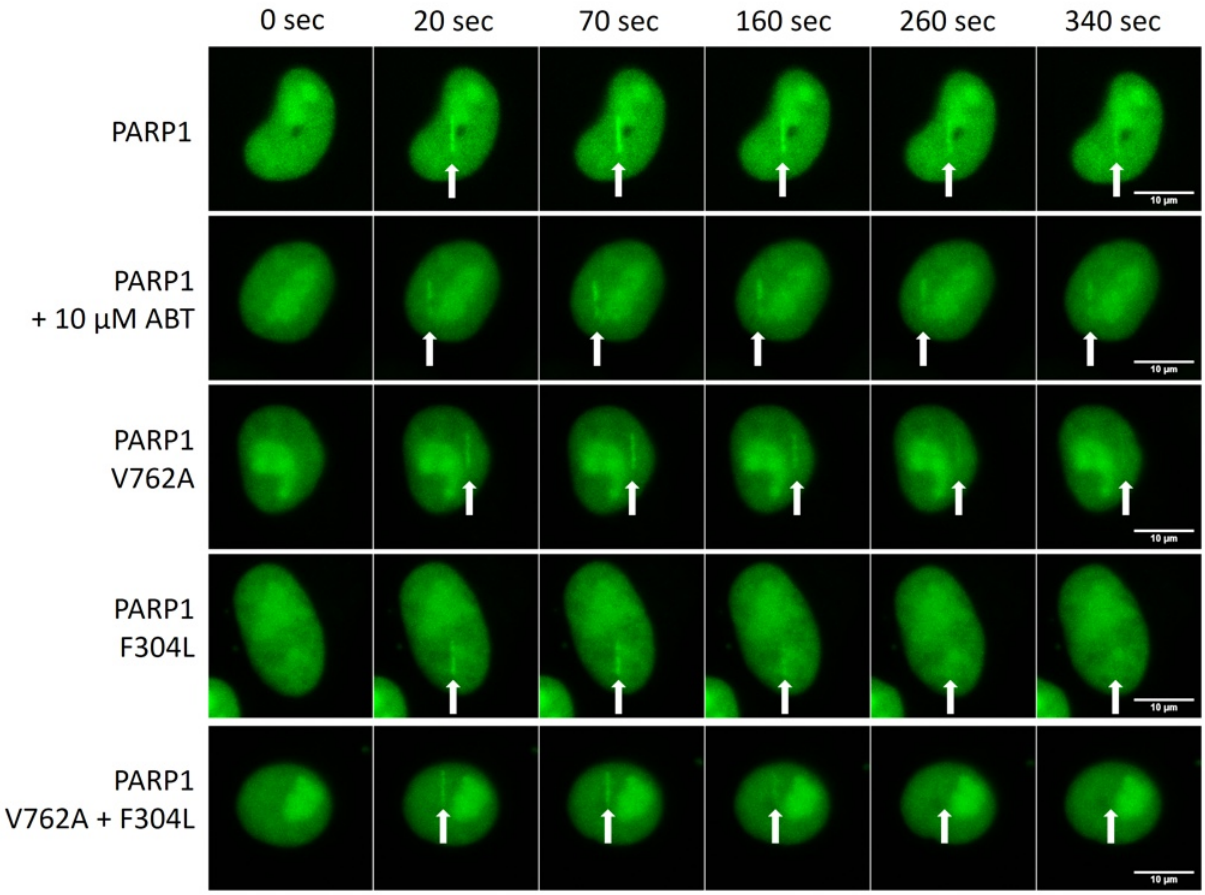

Supplementary Figure 20: Recruitment of natural PARP1 variants to sites of laser-induced DNA damage.
HeLa *PARP1* KO cells were transfected with eGFP-coupled constructs of PARP1, PARP1\V762A, PARP1\F304L and PARP1\V762A\F304L. Analyses were performed 2 days after transfection. Displayed are representative pictures showing the recruitment and dissociation of natural PARP1 variants at sites of laser-induced DNA damage at representative time points. The white arrow indicates the site of the laser strike. Scale bars indicate 10 µm.

Additional Data

Reciprocal regulation of CSB and PARylation

CSB, one of the two proteins responsible for Cockayne Syndrome, is an important player in DNA repair, more precisely in TC-NER and in mitochondrial BER. It has been reported previously that PARP1 and CSB directly interact and it was suggested they interact in BER in response to oxidative stress. However, little is known so far about this interaction and CSB's involvement in BER in general (Stevnsner et al., 2008; Thorslund et al., 2005). Our work aimed to increase our knowledge about the cooperation of CSB and PARP1 and we could demonstrate that CSB also interacts non-covalently with PAR, which has functional consequences for PARP1 and CSB.

Results

Since CSB is able to interact with PARP1 we wanted to investigate whether it can also interact non-covalently with PAR. Therefore, we utilized two different PAR-overlay assays in which the proteins were either size-separated by SDS-PAGE followed by western blotting or directly aspirated on a membrane. This allows to distinguish between PAR binding to denatured proteins (western blot) or proteins in native conformation (slot blot). In both cases we could demonstrate that PAR strongly and specifically interacts with full-length CSB non-covalently (Figures 50 A and 51 F).

Employing a previously established search pattern for PBMs we could identify four putative PBMs in CSB (Figure 50 B) (Popp et al., 2012). PBM1&2 are located in the N-terminal part of CSB that is necessary to interact with PARP1 while PBMs 3 and 4 are located in the helicase domain (Figure 51 G). All PBM's were tested for PAR binding using a Pepspot membrane where equal amounts of each peptide are directly synthesized on-membrane. All four PBM's displayed PAR binding, albeit to a different degree: PBMs 2,3 and 4 seem to bind PAR equally strong while PBM1 binds PAR to a lesser extent. Exchange of basic aa in the PBM to alanines abrogates PAR binding almost completely in three of the PBMs (1, 3 and 4).

Besides the non-covalent interaction with PAR we wanted to further investigate the direct PARP1-CSB interaction. Using an electromobility shift assay with CSB and PARP1 it was found that the binding pattern of PARP1 to DNA changes with increasing amounts of CSB,

i.e. the shift band of PARP1 vanishes with increasing CSB amounts (Figure 51 A). This indicates that CSB might influence the binding of PARP1 to DNA.

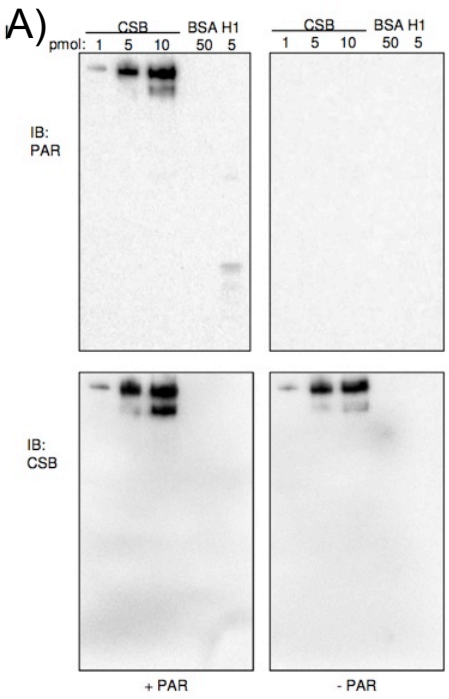

B)

[HKR]$_1$-X$_2$-[AVILFWP]$_3$-[AVILFWP]$_4$-[HKR]$_5$-[HKR]$_6$-[AVILFWP]$_7$-[AVILFWP]$_8$

CSB	PBM 1: AA 292-299	KLSFERKKQGCNKRAARKAP
CSB	PBM 2: AA 333-340	LSKKEERLKKHIKKLQKRAL
CSB	PBM 3: AA 501-508	DAEFDEGFKVPGFLFKKLFK
CSB	PBM 4: AA 975-982	LTAGTIEEKIYHRQIFKQFL

C)

AA sequence of PBM	PBM#/Mut	# of AA
KLSFERKKQGCNKRAARKAP	PBM 1	280-299
KLSFERKKQGCNAAAAAAAP	PBM 1 - mut1	280-299
LSKKEERLKKHIKKLQKRAL	PBM 2	321-340
LSKKEERLKKHIAALQAAAL	PBM 2 - mut1	321-340
DAEFDEGFKVPGFLFKKLFK	PBM 3	489-508
DAEFDEGFKVPGFLFAALFA	PBM 3 - mut1	489-508
LTAGTIEEKIYHRQIFKQFL	PBM 4	963-982
LTAGTIEEKIYAAQIFAQFL	PBM 4 - mut1	963-982

D) **PAR levels in reconstituted CSB cells (CS1AN.S3.G2)**

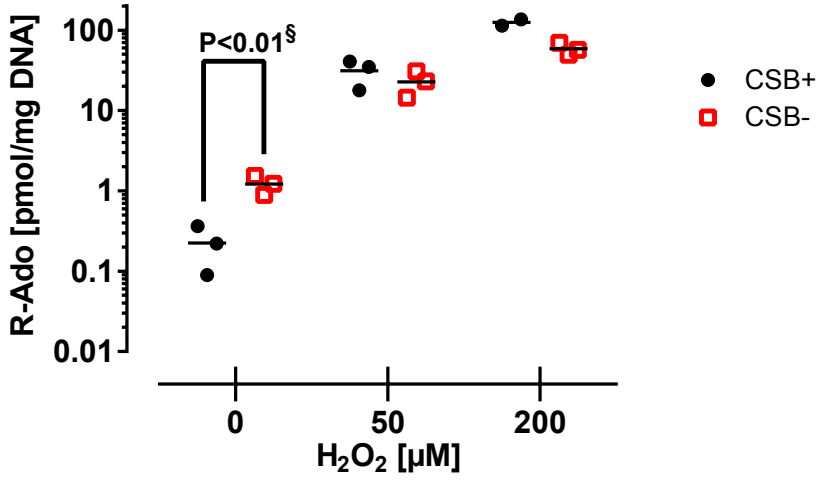

§ t-test (corrected for multiple comparison by Holm-Sidak)

Figure 50: CSB interacts with PAR non-covalently and influences the cellular PARylation capacity.
A. Representative western blot demonstrating non-covalent binding of full-length CSB and PAR. **Upper part:** immunostaining against PAR, only left blot was incubated with free PAR. H1, positive control; BSA, negative control. **Lower part:** immunostaining against CSB, loading control. **B.** Search pattern used to screen CSB's aa sequence for PAR binding motifs with one mismatch allowed. Below are the four identified PBMs listed. Bold, PBM core motif; italic, mismatch; red, basic aa; blue, hydrophobic aa. **C.** The four identified PBMs in CSB and mutants thereof were synthesized as peptides on-membrane and tested for non-covalent PAR binding. Red, exchanged aa. **D.** PARylation capacity of WT (CSB-) and CSB-reconstituted CS1AN cells measured by MS analysis after 5 min treatment with different doses of H_2O_2. Experiments were performed in triplicates (except CSB+, 200 µM; N=2). Panel A adapted from supplementary files of (Scheibye-Knudsen et al., 2014), data for panel D taken from Bokun Yin's Bachelor Thesis.

It has been reported previously that CSB can displace proteins from DNA and to investigate if PARP1 is displaced by CSB too, a previously established BamHI cleavage assay was utilized (Berquist and Wilson, 2009). PARP1 bound to a dsDNA oligonucleotide (containing a BamHI restriction site) is not released from the DNA strand, irrespective of the CSB concentration. Surprisingly however, automodified PARP1 is displaced from the ds oligonucleotide by increasing CSB concentrations, indicated by increased BamHI cleavage of the oligonucleotide (Figure 51 B).

Recently, it has been shown that PARP1 is also activated by UV damages, thus indicating an involvement in the NER pathway (Robu et al., 2013). Therefore, the PARP1 activity in the presence of increasing CSB concentrations with both undamaged and UV-damaged DNA as substrate was analyzed. With undamaged DNA there is no difference in PARP1 activity detectable. However, there is a stronger induction of PARP1 activity by UV-damaged DNA, which is further enhanced by equimolar amounts of CSB. A 4-fold excess of CSB, on the other hand, decreased PARP1 activity considerably (Figure 51 C).

As a follow up to this, the PARylation capacity in immortalized CSB-negative patient cells (CS1AN, CSB) and CSB-complemented cells (WT) was investigated after treatment with 5 J/m^2 UV light. CSB-deficient cells displayed a much stronger PARP activity as well as a prolonged PARylation response compared to CSB-complemented cells after UV damage. However, even in unstressed cells, PARylation is much stronger in CSB-deficient cells (Figure 51 D). These results are well in line with the previous findings that CSB displaces activated PARP1 from the damage site. We also measured the PAR levels in the same cell lines after H_2O_2 treatment and found the same enhanced basal PAR levels in CSB-deficient cells (Figure 50 D). However, with increasing H_2O_2-doses the differences in PARylation capacity between the cell lines vanished.

Since CSB activity is influenced by its interaction with PARP and PAR it was investigated how PARylation influences CSB's spatio-temporal distribution upon DNA damage. Accordingly, CSB recruitment to, and retention at, sites of laser-induced DNA damage with or without PARP inhibitors was measured. There was no difference in the recruitment to the damage observable, however, without PARP inhibition CSB was retained longer at the damage site (Figure 51 E). This indicates that PARP activity, *i.e.* the interaction of PAR with CSB, is important for retention of CSB at the site of DNA damage while having no influence on the initial recruitment of CSB. To verify the relevance of non-covalent PAR interaction in this context the experiment were repeated using a PAR-binding impaired GFP-CSB. This was

achieved by mutating the two first, conserved PBMs in CSB through an exchange of basic aa to alanines (Figure 50 C, PBM1&2, exchanged aa in red; Figures 51 G&H).

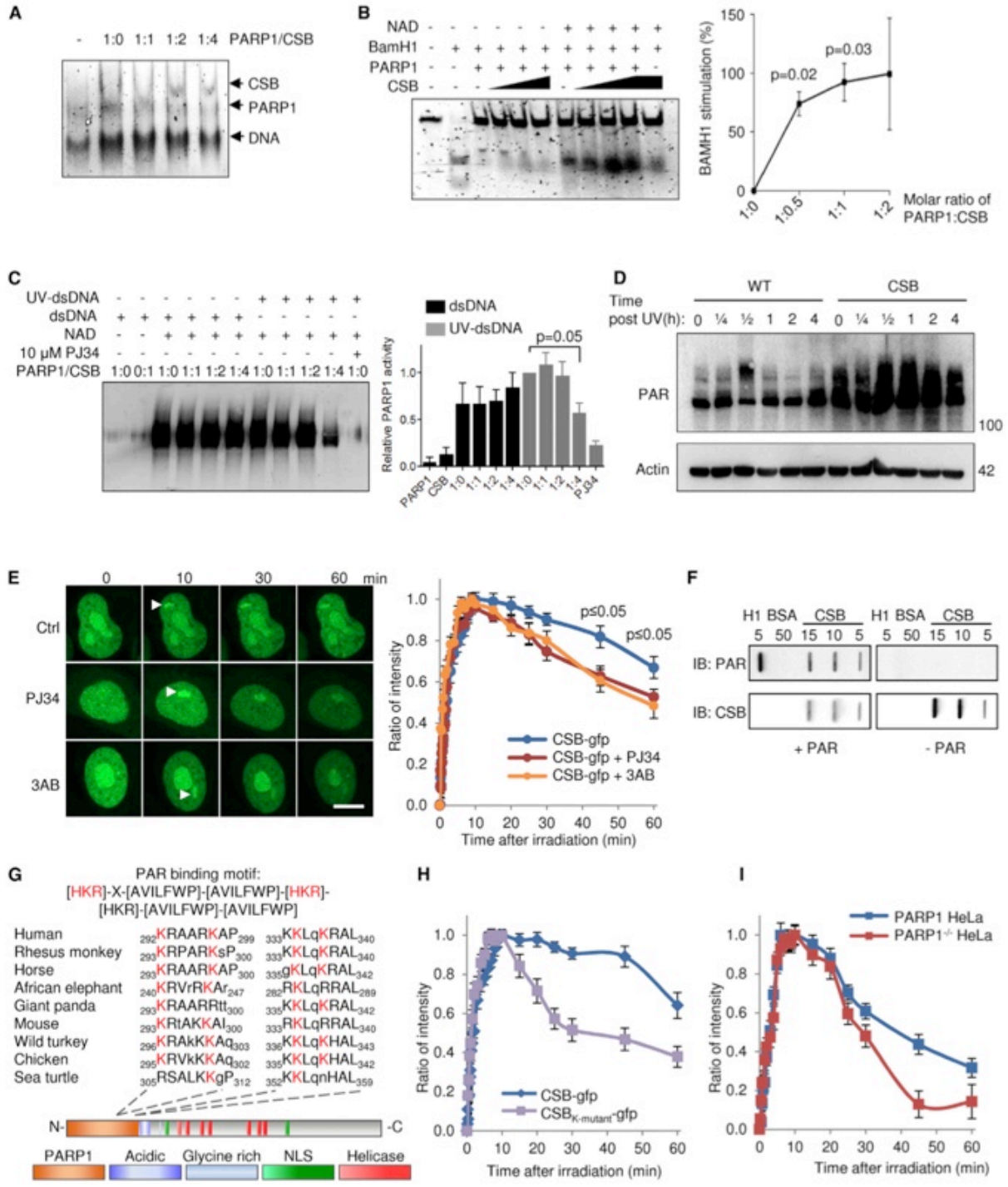

Figure 51: CSB inhibits PARP1 activation *in vitro* and *in vivo* through displacement of PARylated PARP1 from DNA. **A.** Electromobility shift assay (EMSA) of PARP1 and CSB binding to double-stranded DNA. **B.** BamH1 incision of a 42-mer oligonucleotide preincubated with 250 nM PARP1 and with increasing amounts of CSB with or without NAD^+ (n = 3, mean ± SEM). **C.** Representative immunoblot and quantification of *in vitro* poly(ADP-ribosyl)ation (PARylation) of CSB and PARP1. Reactions were performed with recombinant proteins in the presence of undamaged or damaged DNA (n = 3, mean ± SEM). **D.** Representative immunoblot of whole cell (PARylation) after 5 J/m^2 treatment in WT and CSB-deficient cells at various time points. **E.** Recruitment of GFP-tagged CSB to laser-induced DNA damage after 1 h preincubation with PARP inhibitors 3AB or PJ34. **F.** Representative slot-blot showing non-covalent interaction between CSB and PAR. **G.** The PAR-binding motif in CSB. **H.** Recruitment to laser-induced DNA damage of GFP-tagged WT CSB or CSB harboring K to A mutations in the four conserved lysines. **I.** Recruitment of GFP-tagged WT CSB to laser-induced DNA damage in WT HeLa or $PARP1^{-/-}$ HeLa cells. Adapted from (Scheibye-Knudsen et al., 2014).

The effect of an impaired CSB retention was even stronger than with PARP inhibition, confirming the huge importance of non-covalent PAR interaction on the retention of CSB at sites of DNA damage. Again, no difference in the initial recruitment of CSB was observed. When the retention was measured in cells that had a genetic knock-out of *PARP1* (PARP1$^{-/-}$ HeLa) an even more dramatic reduction in CSB retention was observed. This implies that, besides the non-covalent PAR interaction, also the protein PARP1 itself is important in CSB retention at laser-induced sites of DNA damage (Figure 51 I). Of note, the retention of CSB was also reduced in the control cells, compared to the previous experiments (Figures 51 E and H vs. I).

Discussion

Although both PARP1 and CSB are important players in DNA repair, information about their possible interaction has been scarce so far. It has been shown that they physically interact with each other, that CSB is covalently modified by PARP1 and that this modification decreases CSB's ATPase activity (Thorslund et al., 2005). Consequently, it has been proposed that this interaction is important for BER.
Here, a novel interaction of PARP1 and CSB in response to UV damage, *i.e.* in the NER pathway, could be demonstrated. We provide evidence that the non-covalent interaction of CSB with PAR plays an important role in the spatio-temporal regulation of CSB at sites of DNA damage. The PARylation status in the cells influences the retention of CSB at sites of laser-induced DNA damage, though the recruitment to the damage is not affected.

The results from the Pepspot PAR overlay experiment and the recruitment experiments suggest that only PBM1, but not PBM2, is relevant for retention of CSB at sites of DNA damage. The mutagenesis of PBM1 abrogates PAR-binding almost completely while the exchange of basic aa to alanines in PBM2 hardly shows an effect (Figure 50 C). Thus, either the performed mutagenesis is not sufficient enough to abolish PAR-binding to PBM2 or the interaction with PBM2 is not relevant. Either way, it would be interesting to investigate whether the other two PBMs are responsible for the remaining ~50% of CSB retention at the site of damage or if the retention is, at least in part, also regulated by other factors (Figure 51 H). Surprisingly, of all four PBM's PBM1 seems to play the most important role in a physiological context although it is the weakest PAR-binder according to the Pepspot PAR overlay (Figure 50 C).

The almost complete loss of retention in *PARP1* KO cells implies that the direct interaction with PARP1 also might play an important role (Figure 51 I, red graph). However, as retention of CSB is also reduced in the HeLa Kyoto WT cells, compared to the HeLa S3 cells in the other recruitment experiments, it is possible that the different genetic background of these cell lines comes into play (Figures 51 E, H and I, blue graphs).
Strikingly, the reported site of covalent PAR modification in CSB is in the same part where also PBM1 is located (Figures 50 and 51) (Thorslund et al., 2005). One could speculate that the previously reported covalent modification is in fact a non-covalent interaction. Since the non-covalent PAR-binding is an extremely strong interaction it is necessary to use very harsh conditions to discriminate between covalent and non-covalent interaction, *i.e*. SDS or urea treatment (Panzeter et al., 1992). Since such stringent conditions were not used in the previous study it is mandatory to clarify in future studies whether CSB is truly covalently modified with PAR or interacts non-covalently with PAR or both. This is necessary for a proper evaluation of the importance of the CSB and PARP1 interaction in the different repair pathways (*i.e*. BER and TC-NER, see below).

We could demonstrate by two different experiments that unstressed CSB-negative cells have significantly higher basal PAR levels (Figures 50 D and 51 D). However, only cells treated with UV light as stressor, not H_2O_2, display consistently higher PAR levels and also a prolonged PARP activation. This is consistent with the finding that CSB can displace activated and modified PARP1 from the DNA. Thus, in the absence of CSB PARP1 is longer active and produces more PAR. The finding that there is no difference in PAR levels between CSB positive and negative cells upon oxidative stress contradicts the previous findings that CSB and PARP1 interact in the response to oxidative stress (Thorslund et al., 2005). However, it is well in line with the bulk of literature proving that oxidative lesions are repaired by the BER pathway. CSB on the other hand, is mainly implicated in the NER pathway, although there is some evidence linking it to the BER pathway, especially the mitochondrial BER (Stevnsner et al., 2008). A potential explanation for these contradicting results might be that oxidative lesions arising on transcriptionally active sites are repaired by NER, thus explaining the interaction of CSB and PARP1 (as outlined below). This scenario is at least partially supported by literature, although there is also contradictory data.

Summarizing the findings, a potential model that explains the role of PARylation in CSB regulation upon UV damage could be postulated: PARP1 is recruited and activated upon DNA damage, *i.e.* damage repaired by NER (this might as well be oxidative damage, as discussed above). The damage is also recognized by CSB, which is attracted to the site of damage. CSB is retained by non-covalently binding to PAR and can displace the modified PARP1 from the damage. One could speculate that CSB's ATPase activity, which is necessary for unwrapping of DNA, is impaired by PAR interaction until PARP1 is displaced (assuming the reported covalent modification is in fact a non-covalent interaction). The displacement of PARP1 is necessary in order to proceed with the repair process by allowing access for other repair factors. PARylation, however, may also play a role in recruitment of these factors, as has been demonstrated for XPA, but in general the role of PARylation in NER is poorly understood (Fischer et al., 2014). However, the findings that CSB, XPA and UV-DDB interact with PARP1 and PAR indicates that PARylation plays a role in both global-genome and transcription-coupled repair, the two sub-pathways of NER (Fischer et al., 2014; Gagné et al., 2012; King et al., 2012; Pines et al., 2012; Robu et al., 2013). Considering that PARP1 produces less PAR when CSB is present it would be interesting to investigate whether CSB senses the activity of PARP1 by polymer length. This could be evaluated by analyzing whether CSB displays different binding affinities for PAR polymer of varying length, as it has been demonstrated for XPA and p53 (Fahrer et al., 2007). It might be necessary that PAR covalently attached to PARP1 reaches a certain length for CSB to recognize it in order to allow sufficient time for other proteins to be attracted to the site of damage.

Material and Methods

Material and Methods were taken from the supplementary material of (Scheibye-Knudsen et al., 2014). The Pepspot membrane PAR overlay was performed as described in the methods section of Chapter V. PAR quantification employing LC-MS/MS was performed as described in Chapter VI and (Martello et al., 2013).

Western, far-western and slot-blotting

Poly(ADP-ribose) was synthesized and purified as described previously (Popp et al., 2012). Purified recombinant proteins were either separated via denaturing polyacrylamide gel electrophoresis followed by semi-dry blotting or were directly immobilized on a nitrocellulose membrane using a slotblot manifold and vacuum. Subsequently, membranes with immobilized proteins were incubated with 0.2 μM poly(ADP-ribose) in TBST over night at 4°C, followed by high-stringency washes using 1M NaCl in TBST (3 times for 5 min at RT). Non-covalently bound poly(ADP-ribose) was detected using the anti-poly(ADP-ribose)-specific mAB 10H, anti-mouse HRP-coupled secondary antibody, and chemiluminescence detection.

Biochemistry and recombinant proteins

PARP1 was purchased from Trevigen. Recombinant CSB was a gift from Dr. Tinna Stevsner. PARP1 activity was investigated by incubating 30 nM PARP1 with increasing doses of purified CSB in the presence of 10 nM double stranded DNA in the reaction buffer (1 mM NAD+, 10 mM Tris-HCl pH 8.0, 1 mM MgCl2, 1 mM DTT) for 10 min at 37°C. The product was visualized by western blotting. UV-damaged DNA was generated by exposing a 39-mer double-stranded DNA oligonucleotide to UV radiation for 10 min. Electro-mobility shift assay (EMSA) was performed by incubating PARP1 with DNA for 10 min at 37°C after which increasing doses of CSB were added and further incubation was done for another 20 min at 37°C. Reactions were performed in 20 mM HEPES-OH pH 8.0, 50 mM KCl, 200 μg/mL BSA, 5 mM DTT, and 5% (v/v) glycerol. Finished reactions were run on a 4% native polyacrylamide gel and visualized by Sybr Gold staining (Invitrogen, Carlsbad, CA, USA) on a ChemiDocTM MP (Bio-Rad, Hercules, CA, USA). BamH1 assay was performed by preincubating a 42-mer oligonucleotide containing a single BamH1 restriction site with 250

nM PARP1 for 20 min at 37°C with or without NAD+. 125, 250 or 500 nM of CSB and 0.2 U BamH1-HF (New England Biolabs, Ipswich, MA, USA) was subsequently added and the reaction was further incubated 30 minutes at 37°C. The reaction was performed in 20 mM HEPES-OH pH 8.0, 50 mM KCl, 4 mM MgCl2, 200 µg/mL BSA, 5 mM DTT, and 5 % (v/v) glycerol. The finished reaction was run on a 10% native gel and visualized by Sybr Gold staining (Invitrogen, Carlsbad, CA, USA) on a ChemiDocTM MP (Bio-Rad, Hercules, CA, USA).

Site-directed mutagenesis for substitutions K292A, K297A, K334A and K337A in CSB-GFP plasmid

Multiple substitutions for K292A, K297A, K334A and K337A on CSB in CSB-GFP plasmid were performed using QuikChange II Site-Directed Mutagenesis Kit (Agilent Technologies). The specific nucleotide change corresponding to K292A and K297A on CSB in the plasmid was completed and then substitution for K334A and K337A was carried out. The two primer sets contain the relevant nucleotide changes of K292A/K297A (forward primer; 5'-GTAATGCAAGAGCAGCTAGAGCAGCTCCAGCCCCAGTCACG-3', reverse primer; 5'-CTCGACGAGATCGACGAGAACGTAATGTTGGAACGAAGAA-3'), or K334A/K337A (forward primer; 5'- CCCTGGAACTGCAAAGCCCTCGCCTGGAGTGCCTTGATGTGC TTTTTCAAACG-3', reverse primer; 5'- CGTTTGAAAAAGCACATCAAGGCACTCCA GGCGAGGGCTTTGCAGTTCCAGGG-3'), respectively. PCR was carried out according to the manufacturer's instruction. After digestion with DpnI (TaKaRa, Shiga, Japan), the DNA mix was transformed into NEB 5-alpha Competent E. coli (High Efficiency) (New England Biolabs) and then selected clones were sequenced confirmed by Eurofins Genomics (Huntsville, AL, USA).

Protein recruitment and retention experiments

To monitor protein recruitment and retention to laser induced DNA damage, localized microirradiation was performed as previously described in detail (McNeill et al., 2013). In brief, HeLa cells ($2.0x10^5$ cells) were precultured in a 35-mm glass bottom culture dish with 10 mm diameter microwells (MatTek Corporation, Ashland, MA, USA) for 24 h. GFP-tagged CSB (CSB-GFP) plasmid was transfected using JetPrime reagent (Polyplus-transfection, Illkirch, France) according to the manufacturer's standard protocol. The transfected cells were

incubated for 24 h before micropoint laser experiment. A 5x20 pixel (0.16 μm/pixel) region internal to the nuclei of the cells was targeted using a Plan Fluor ×60/1.25 numerical aperture oil objective. Throughout the experiment, the adherent cells were maintained at 80% humidity, 5% CO2, and 37°C using a live cell environmental chamber (Slonet Scientific, Segensworth, UK). To determine the effects of PARP inhibition on recruitment of CSB, 10 μM PJ-34 or 1 mM 3AB was added to the media one hour prior to laser microirradiation. The images were recorded using identical gain, exposure, sensitivity, and contrast settings, and analyzed with the Volocity software 6.2 (PerkinElmer, Waltham, MA, USA).

Discussion

Non-covalent PAR interaction as a regulator of protein functions

Although it has been known for several decades that PAR can interact non-covalently with proteins, examples for the significance of this interaction remained scarce (Althaus et al., 1999; Honjo et al., 1968; Nakazawa et al., 1968; Panzeter et al., 1992; Sauermann and Wesierska-Gadek, 1986). However, only recently several groups could demonstrate some functional consequences of the non-covalent PAR interaction. Among these are the control of protein degradation via PAR-dependent ubiquitin-transferase Iduna/RNF146, PAR-mediated cell death via AIF (*i.e.* parthanatos), chromatin relaxation through histone modification and regulation of DNA repair (DaRosa et al., 2015; Krietsch et al., 2012; Wang et al., 2011; Zhang et al., 2011). Besides the binding per se, the length and the degree of branching may determine the effect of the PAR-protein interaction, depending on the protein of choice, as our group has previously demonstrated (Fahrer et al., 2007; Fischer et al., 2014). Interestingly, it is still a matter of debate whether it is truly free PAR that interacts with proteins or if it is proteins with covalently attached PAR, which bind to the PAR-binding modules.
This thesis provides evidence that all five RecQL helicases bind PAR non-covalently and that WRN and RECQL5 are differentially regulated by this interaction (*N.B.:* non-covalent interaction of PAR and RECQL1 has been published elsewhere previously (Berti et al., 2013)). Furthermore, we could confirm that PARP1 is able to bind PAR non-covalently too, and establish CSB as a novel PAR-binding protein. The interaction of PARP1 and PAR with CSB has very relevant consequences for the pathogenesis of CS, as will be discussed in a separate section.

WRN is regulated by PARPs and PARylation

More than a decade ago, the first hints from mouse studies appeared that PARP1 and WRN interact with each other. Lebel and co-workers found that *WRN/PARP* double KO mice were more prone to cancer than single KO or WT animals and that they displayed a reduced life span. They also provided the first evidence of a direct interaction of WRN and PARP1 by co-immunoprecipitation experiments (Lebel et al., 2003). A year later it was confirmed that PARP1 and WRN directly interact with each other (Kobbe et al., 2004a). This interaction had,

at least biochemically, functional consequences for WRN: unmodified PARP1 inhibits both WRN's exonuclease and helicase activity, while automodified PARP1 does not bind to, and therefore does not inhibit, WRN.

We could extend this knowledge by providing evidence that free PAR interacts non-covalently via at least 4 different PAR-binding motifs (Figures 19, 25 and 33). Furthermore, this interaction inhibits WRN's interaction with DNA and both its exonuclease and helicase activity (Figures 21-23) (Popp et al., 2012). We could also confirm the inhibitory effect of PARP1 on WRN's exonuclease activity, employing a novel LC-MS/MS exonuclease assay (Figure 13) (Mangerich et al., 2012).

In contrast, in our more recent study we found that PARylated PARP1 has a strong inhibitory effect on both helicase and ss-annealing activity (Figures 26 & 28; exonuclease activity was not tested) (Khadka et al., 2015). Moreover, only modified, but not unmodified PARP1, inhibits WRN's ATPase, although only slightly (Figure 27). Free PAR also inhibits WRN's helicase and ss-annealing activity, albeit to a lesser degree than modified PARP1.

The differences in the reported effects of free PAR on WRN's helicase activity can have several reasons. The first and most obvious is easy to identify: the great difference in the used PAR concentrations between the two studies (*cf.* Figures 22 and 26). In Khadka *et al*. 100-fold lower concentrations of PAR were used, compared to our first study (Popp et al., 2012). On the other hand, also 25-fold lower WRN concentrations were used. Another reason for the observed differences could be the composition of the utilized PAR. Depending on several parameters like duration of reaction, concentrations of both PARP and acceptor proteins, reaction temperature and concentration of DNA substrate, PAR can have a substantially different composition regarding mean and absolute chain length and branching frequency (our lab, unpublished observations). However, exactly these characteristics could have a huge impact on PAR interaction with WRN, as our lab has demonstrated previously for other proteins (Fahrer et al., 2007). Although we have shown that chain length has only little impact on PAR-binding to WRN (Figure 18 B), it is possible that it affects its catalytical functions differently. This remains to be tested, in conjunction with the relevance of the branching frequency for WRN-PAR interaction. Therefore, it is very well possible that differences in the composition of the utilized PAR account for the observed differences, at least in part.

The same argumentation can of course be employed to explain the differences in the experiments with PARylated PARP1. PARP1 might be differently modified regarding chain length and branching, as well as which amino acids are covalently modified with PAR,

depending on the assay conditions. Additionally, PARP1 itself might be modified with PAR non-covalently (see below).
The decrease in WRN activity with increasing PARylated PARP1 can also, at least partly, be attributed to the assay design. For simplicity, automodified PARP1 was used directly in its reaction buffer for WRN assays, without prior purification. However, thereby also the activator DNA was transferred to the WRN reaction and could thus falsify the results by adding additional substrate for WRN. One way to avoid those pitfalls would be to purify modified PARP1 after the automodification reaction, thus getting rid of the additional DNA. However, the inconsistency in chain length and chain position on PARP1 could only be addressed by precise chemical modification of PARP1 with PAR chains of defined length and branching at defined aa positions. This is however, at the time of writing, not yet possible.
Of note, there might be also NAD^+ left over in the buffer that is carried over to the WRN reaction mix, thus potentially allowing PARP1 to modify WRN covalently. Strangely, although there are reports that WRN is covalently modified by PARP1, no further investigations have been conducted on the effect of this posttranslational modification (Adelfalk et al., 2003; Jungmichel et al., 2013).

We found that WRN recruits less efficiently to sites of laser-induced DNA damage under PARP inhibition (Figure 29). This could be confirmed by employing our novel HeLa *PARP1* KO cells (Suppl. Figure 12), although the effect was not as pronounced as with inhibitor treatment. Interestingly, WRN was again less efficiently recruited when the cells received additionally PARP inhibitor treatment, comparable to the effect of PARP inhibition alone, thus implying that other PARPs may play a role in the regulation of WRN, too. The prime suspect here would be PARP2 as it already has been shown to interact with WRN, with a similar affinity as WRN and PARP1. This is further supported by the fact that H_2O_2 mainly induces damages that are repaired by BER and that both WRN and PARP2 are implicated in BER (PARP1 too, of course) (Beck et al., 2014; Croteau et al., 2014). As previously demonstrated, this interaction had no impact on WRN's functions (Kobbe et al., 2004a). However, as our recent publication on the WRN-PARP1 interaction challenges some previous findings from von Kobbe *et al.,* it is tempting to speculate that there is also more to the WRN-PARP2 interaction than meets the eye. Therefore, it would be of great interest to re-evaluate whether the PARP2-WRN interaction has functional consequences for either protein. It would be of particular interest to analyze the potential interaction between automodified PARP2 and WRN since this was not investigated in the original publication.

PARP3 on the other hand might be another interesting candidate as it has recently been shown to steer the choice of DSBR pathways with a bias towards NHEJ, a pathway in which WRN is also involved. Additionally, it is also a nuclear PARP, capable of forming PAR polymers (Beck et al., 2014; Croteau et al., 2014).

That WRN and RECQL5 are still recruited to sites of DNA damage, even with a *PARP1* KO and additional PARP inhibition, can be explained by assuming some kind of backup system. Both WRN and RECQL5 are present throughout the nucleoplasm and therefore it is very likely that they will recruit to the damage by diffusion and stay there, albeit slower than through recruitment by PAR. Supporting this, it has been demonstrated recently that WRN actively scans the DNA to find damaged sites (Bendtsen et al., 2014). Taken together, this indicates a backup system that guarantees the recognition of DNA damages even in the absence of the primary damage sensor PARP1. Adding to these cues, WRN was found to recruit autonomously to DSBs via its HRDC domain (Lan et al., 2005).
It is also quite likely, that different kinds of damages are induced by the laser-irradiation that trigger different repair pathways. Some of these pathways might rely on PAR for recruitment while others do not. This has been demonstrated for XRCC1, which is recruited PAR-dependent to SSBs but not to oxidative lesions that are repaired by BER (Campalans et al., 2013). Interestingly, in cases where XRCC1 recruitment is dependent on PAR it is entirely dependent on it, in contrast to WRN and RECQL5. This is again well in line with the DNA-scanning hypothesis.

RECQL5 is differentially regulated by PARylation

Although most RecQL helicases received increased attention over the last years, RECQL5 was largely neglected and thus remains the least well studied RecQL helicase (Croteau et al., 2014). Therefore it is no surprise that there was no solid data available whether PAR or PARP interact with RECQL5. However, some studies reported that RECQL5 depletion decreased PARP1 levels while at the same time increasing PAR formation (Popuri et al., 2013; Tadokoro et al., 2012b). Additionally, a proteomics approach several years ago identified RECQL5 as a potential PAR-binding protein, with a putative PBM situated in the C-terminus (aa 937-947) (Gagné et al., 2008).
Indeed, our own experiments established RECQL5 as a novel PAR-binding protein, together with RECQL4 and BLM (Figure 25). Using an established search pattern we identified five

putative PBM's in RECQL5, of which two are interlaced and resemble the previously predicted motif (Gagné et al., 2008; Khadka et al., 2015; Popp et al., 2012). Moreover, we could show that all five PBM's bind PAR non-covalently and that RECQL5 directly interacts with PARP1. In contrast to WRN, however, RECQL5 is not covalently modified by PARP1 (Figure 25).

While basically all of WRN's functions are inhibited by PARP1, PARylated PARP1 or PAR, the situation is different for RECQL5. Here, PAR and PARylated PARP1 increase the ss-annealing activity, while unmodified PARP1 had an inhibitory effect. Helicase and ATPase were, similarly to WRN, inhibited.

Both WRN and RECQL5 are crucial in the response to replicative stress and seem to fulfill both complementary and redundant roles (Popuri et al., 2012a). The results of our recruitment studies indicate that RECQL5 is regulated only by PARP1, in contrast to WRN, which seems to be controlled by at least one other PARP1. This, together with the differing impact of PAR-interaction, hints at a differential regulation of WRN and RECQL5 in the response to genotoxic stress. Although both WRN and RECQL5 are capable of binding PAR non-covalently it is still unclear whether they are recruited directly by PAR-interaction or via other proteins. For example, it was found that MRE11 and NBS1 recruitment to DSBs is supported by PARP1 (Bryant et al., 2009; Haince et al., 2008) and that the MRN complex plays an important role in recruitment of RECQL5 (Zheng et al., 2009). Along this line, we found a diminished, but not abrogated, recruitment of RECQL5 to sites of laser-damage with PARP1 loss or under PARP inhibition, which could be caused by a weaker recruitment of MRE11 and NBS1 (Haince et al., 2008). Taken together, this points to an indirect influence of PARP1 on RECQL5 in the recruitment to sites of laser-induced damage.

Of note, while the recruitment to laser-induced damage provides a valuable tool to investigate the DNA damage response regulation, it also has its drawbacks. The strong damage that is induced by the laser strike most likely overpowers and saturates the cells repair capacity, which is evident from the fact that almost all cells die several hours after the laser strike (own observations). Furthermore, it is impossible to selectively induce only a specific kind of damage, thus making it difficult to differentiate between the different repair pathways.

Taken together, we established a novel interaction between PARP1, PAR and RECQL5 and demonstrated that PARP1 is involved in the process of RECQL5 recruitment to sites of DNA damage. Moreover, RECQL5's catalytic functions are differentially regulated by PAR interaction, in contrast to WRN.

Non-covalent PAR-binding might regulate PARP1 multimerization and displacement from damage sites

Previously, two studies reported that PAR can bind non-covalently to PARP1 (Huambachano et al., 2011; Robu et al., 2013). While Robu *et al.* did not comment at all on this finding, Huambachano and colleagues described the non-covalent PAR-binding to PARP1 in the Zn2, Zn3, DsDB and WGR domains. They argued that PAR-binding to Zn2 or the DsDB domain could displace PARP1 from the DNA and thus terminate the catalytic reaction.

Independently from Huambachano *et al*., we identified two possible PBMs in PARP1 (in Zn2 and Zn3) and verified experimentally that PARP1 binds PAR non-covalently. In line with our *in silico* and *in vitro* results, our recruitment data suggest that the recruitment of PARP1 to DNA damage is, at least in part, dependent on PARP activity. This is evident from the fact that the mono(ADP-ribosyl)ating PARP1 variant E988K recruits significantly weaker than WT PARP or PARP1\L713F (Figure 44).

Intriguingly, one of the two PBMs is located in the third zinc finger, a domain that might be important for dimerization (Langelier et al., 2008). It is therefore very well possible that PARP activity is necessary for efficient dimerization of PARP1, which has been suggested to be important for PARP1 activation (Ali et al., 2012; Mendoza-Alvarez and Alvarez-Gonzalez, 1993). Supporting this idea, our group has previously demonstrated that PAR-binding can modulate p53 complex formation (Fahrer et al., 2007). Similarly, PAR might be necessary for proper PARP1 dimerization, as our PAR-EMSAs suggest (Figure 45). It is, on the other hand, also thinkable that PAR-binding is a way to push the dimer apart, representing a potential mode to regulate and end the PAR-synthesis reaction. This is in agreement with our finding that the non-covalent interaction of PAR with PARP1 inhibits DNA-binding of PARP1 very efficiently already at nanomolar doses (Figure 45). Furthermore, it is also in agreement with Huambachano's hypothesis that PAR interaction with PARP1 abrogates the PARP1-DNA interaction (Huambachano et al., 2011).

Another model of PARP1 activation suggest a *cis*-activation of PARP1, *i.e*. only one PARP1 molecule is required for activation by DNA binding. It is therefore conceivable that PAR-binding to a PBM in Zn3 is necessary to induce the conformational change that is required for full catalytic activity (Gibson and Kraus, 2012). A first binding of Zn1 to DNA would start the PARylation reaction and PAR-binding to Zn3 would then initiate a conformational change that fully activates PARP1. Likewise, it is also possible that PAR-binding to either PBM in PARP1 abrogates PARP1-DNA interaction, as discussed above for the *trans*-activation model. Of course, a two-step model is conceivable, whereby "light" PARylation is necessary

for full PARP1 activation while strongly PARylated PARP1 promotes its own displacement and thus the end of the catalytic reaction.
Moreover, it is still a matter of debate whether dimerization is necessary for full PARP1 activation and whether this might be depending on the damage substrate (Coquelle and Glover, 2012). Although we could verify and extend the findings by Huambachano and colleagues, there is still a lot of open questions on the exact nature and the relevance of the non-covalent PAR-PARP1 interaction.

That PARP1\E988K is also longer retained at sites of DNA damage can be explained by our above-discussed findings as well (Figure 44). Huambachano *et al*. described that PAR needs to be at least 30 subunits long to interact with PARP1, which is well in line with the results of our own biochemical studies (our utilized PAR had a mean length of ~100 subunits). Since PARP1\E988K is only able to form mono(ADP-ribose) (MAR) it cannot initiate its displacement from the DNA. Consistently, WT PARP1 under PARP1 inhibition mirrors the recruitment and retention pattern of PARP1\E988K, thus reinforcing our hypothesis (Figure 49). On the other hand, the longer retention is also explainable by our findings on the CSB-PAR interaction (Figure 51). As PARP1\E988K only forms MAR it is not able to recruit CSB (or another protein with similar properties) to the damage site and thus induce its own displacement by CSB (*cf*. "Additional Data"). It is tempting to speculate that this is a more general mode of PARP1 regulation that can be performed by proteins other than CSB as well. However, most likely a mixture of both explanations is true, considering the idea that the substrate, *i.e.* different types of DNA damage, determines PARP1's multimerization status (Coquelle and Glover, 2012). Thereby, other proteins like CSB could displace single PARP1 molecules from the DNA while PARP1 dimers could displace each other upon sufficient activation.
Analogous to CSB, both WRN and RECQL5 could use their helicase activity to displace activated, and thus PARylated, PARP1 from the DNA. This would allow other repair factors, such as the RecQL helicases themselves, access to the damage and to proceed with the repair. This idea is supported by the results of the recruitment experiments with PARP1, WRN, RECQL5 and CSB. WT PARP reaches its maximum recruitment already after 60 sec and starts to dissociate from the damage site from that time point on. WRN, RECQL5 and CSB, however, are only recruited to ~50% of the maximum recruitment after 1 min and reached their individual maximum after more than 5 min. This is also well in line with the data

obtained in our nucleoli experiments: PARP1 leaves the nucleoli considerably faster than WRN (Figures 34 vs. 40).
Consequently, PARP1\L713F, a constitutively active PARP1 variant, recruits weaker than WT PARP1 but stronger than PARP1\E988K. Since it can form polymers it recruits similar as the WT, however, the constant activity and thus constant automodification leads to a faster displacement that is in conflict with the recruitment. This manifests in a weaker total recruitment (Figure 44).

Our collaborators in the Netherlands, Marjolijn Jongmans and Roland Kuiper, identified a novel PARP1 mutation, F304L, which was found in a patient with CCRC. Additionally, this patient carried the well-described V762A polymorphism (Beneke et al., 2010; Lockett et al., 2004; Qin et al., 2014). Our biochemical and *in vivo* data demonstrate that this novel PARP1 variant has considerably less catalytic activity than WT PARP1 or the single variants (Figure 49). Consequently, PARP1\V762A\F304L also displays less efficient recruitment to laser-induced DNA damage.
Besides the PARP1 mutation, the above-mentioned patient also had a deficiency in *BRCA2* in the tumor tissue. Therefore, following the concept of synthetic lethality, this patient might have benefited from treatment with PARP inhibitors. This would have shut down two of the most important repair pathways, SSBR and HR, and thus made the tumor extremely susceptible to anti-cancer treatments, *i.e*. chemotherapy or irradiation treatment (Bryant et al., 2005). The discovery of these mutations in the patient's tumor by exome sequencing and the resulting potential treatment options emphasize the importance of personalized medicine for efficient and successful treatment of cancer.

WRN's spatio-temporal distribution in response to oxidative stress is regulated by PARP1

It has been known for some time that WRN is primarily localized in the nucleoli and that it translocates into the nucleoplasm and to sites of DNA damage upon stress induction (Karmakar and Bohr, 2005; Kobbe and Bohr, 2002). Additionally, it has been demonstrated that acetylation and phosphorylation play an important role in this process, although it is not yet clear how exactly the translocation is regulated and whether it is damage specific (Blander et al., 2002; Karmakar and Bohr, 2005; Li et al., 2008; 2010). However, the selection of the employed stressors (*i.e.* IR, UV, cisplatin and MMC) strongly suggests that acetylation might

be regulating the release of WRN in relation to NER and DSBR as all these stressors cause bulky adducts, helix-distorting lesions or strand breaks.

We, on the other hand, could reveal that WRN's release from the nucleoli upon oxidative stress is entirely dependent on the presence of PARP1, but only weakly on PARP activity. The recruitment to sites of laser-induced damage is, in contrast, PAR-dependent (see above). It is, however, not yet clear whether this nucleolar export is mediated by direct PARP1-WRN interaction or through yet unknown intermediary factors. Also, it remains to be elucidated whether acetylation plays a role in the oxidative stress-related nucleolar export of WRN. The recent description of a novel protein-protein interaction inhibitor for PARP1, (-)-gossypol, offers an interesting new opportunity to determine whether the direct interaction between PARP1 and WRN regulates WRN's nucleolar export or whether this is mediated by another factor (Na et al., 2015).

Surprisingly though, the PARP1-dependency for WRN's translocation seems to be strongly damage-dependent as CPT-induced relocalization of WRN was not affected in *PARP1* KO cells (data not shown). Although PARP1 translocates similar to WRN in response to oxidative stress it is not yet clear whether it also translocates in response to CPT. However, since we detected only a weak PARylation response to CPT treatment, it is likely that PARP1 plays no or only a minor role in response to CPT-induced stress (Figure 41). Thus, it can be assumed that WRN's translocation is regulated by different interactions, be it PTMs or protein-interactions, depending on the kind of damage. Both WRN and PARP1 have been implicated in the oxidative stress response before, which is in support of our finding that WRN's nucleolar release is oxidative damage-specific [reviewed by (Croteau et al., 2014; Robert et al., 2013; Veith and Mangerich, 2014)].

It has been demonstrated that all RecQL helicases localize predominantly to the nucleoli with the exception of RECQL4, which seems to be mostly distributed evenly throughout the nucleus or absent from nucleoli. The other four translocate from the nucleoli to DNA damage sites upon a variety of different stressors (*e.g.* H_2O_2, mitomycin C, cisplatin, IR, UV, CPT), however, as of now, it is unclear whether they respond differently to the same stressors (Bendtsen et al., 2014; Khadka et al., 2015; Kobbe and Bohr, 2002; Popuri et al., 2012a; 2012b; Sharma and Brosh, 2007; Singh et al., 2010). Their differing roles in DNA metabolism suggest this, but it warrants further investigation. Interestingly, RECQL4 is recruited to the nucleoli upon oxidative stress and this can be abrogated by PARP inhibition, thus displaying the completely opposite behavior of WRN (Woo et al., 2006). We and others have speculated that non-covalent PAR-binding could induce a conformational change,

thereby exposing a NTS (Boamah et al., 2012; Léger et al., 2014; Rancourt and Satoh, 2009; Veith and Mangerich, 2014).

The fact that PARP inhibition only mildly inhibits WRN's translocation from the nucleoli can be explained by our recruitment results: because of the PARP inhibition WRN is not actively recruited to the damage site but rather passively, and thus slower, by diffusion. Hence, less WRN leaves the nucleoli.

In conclusion, physical presence of PARP1 is necessary for the release of WRN from the nucleoli upon oxidative stress while PARP activity is, at least in part, necessary for WRN's recruitment to sites of DNA damage. So far, however, there is no conclusive explanation how PARP1 exactly controls the release of WRN from the nucleoli, although it seems to be independent from PARP activity. Strikingly, it seems to be a specific reaction to oxidative stress and thus enforces the idea of a differential regulation of release and recruitment of WRN upon stress induction, depending on the type of damage. Our findings, combined with the literature, suggest that PARPs and PARylation might orchestrate the dynamic distribution of RecQL helicases upon genotoxic stress, in concert with other post-translational modifications (*e.g.* acetylation and phosphorylation).

PARylation and NAD^+ metabolism play pivotal role in Cockayne syndrome

Our investigations on the interplay of PARylation and CSB were part of a bigger study, trying to uncover and explain the underlying mechanism of Cockayne syndrome. CS is caused primarily by the loss of CSB (20% caused by loss of CSA) and the symptoms include progressive neurodegeneration, growth retardation, accelerated aging, mitochondrial deficiencies and weight loss (Natale, 2011; Scheibye-Knudsen et al., 2013a). It has been hypothesized that the loss of CSB leads to prolonged and enhanced PARP1 activation as a response to defective repair pathways (*i.e.* BER and NER). This would subsequently deplete NAD^+ levels and consequently also the ATP levels. Consequently, this leads to a decrease in uncoupling proteins (UCPs) as an effort to increase ATP production by the mitochondria. However, a side effect thereof is also an increase in ROS that leads to even more (DNA) damage, thereby creating a vicious cycle (Scheibye-Knudsen et al., 2013a).

Indeed, PARP1 is longer and stronger active as a response to UV-damage in CSB-negative cells (Figure 51). It could be shown that recruitment of CSB to sites of DNA damage is independent of PARP or PAR; however, the retention at the damage site is PAR-dependent. Moreover, CSB is necessary to efficiently displace PARP1 from the damage site, thereby

displaying a reciprocal regulation of the two proteins. In conclusion, PARP activity is necessary to recruit CSB to sites of UV damage, but thereby also regulates its own presence at the damage site.

SIRT1 activity was decreased in CSB-negative cells, which is not surprising considering that it also uses NAD^+ as a substrate, whose levels were also decreased. The decrease in SIRT1 activity led to a stronger histone methylation and consequently to a reduction in transcription (Scheibye-Knudsen et al., 2014). This might explain the inability of CS cells to resume transcription after UV damage (Mayne and Lehmann, 1982).

The resulting decrease in UCP proteins led to an increase in mitochondrial potential and subsequent mitochondrial dysfunction. This mitochondrial dysfunction on the one hand explains some of the CS phenotype and on the other hand generates ROS, which even more increases mitochondrial dysfunction and also leads to nuclear DNA damage. This, in turn, activates PARP1, thus feeding the vicious cycle.

Since different dietary interventions can alter neurodegenerative phenotypes, CS mice were supplied with different diets: high-fat diet (HFD), calorie restriction (CR), and resveratrol supplementation. Strikingly, a HFD rescued both the metabolical and the neurodegenerative phenotype of the CS mice (Scheibye-Knudsen et al., 2014). The ketone body β-hydroxybutyrate (β-OHB) increased both SIRT1 expression and activity in CSB-deficient cells, thereby attenuating the mitochondrial membrane potential and decreasing ROS levels. Interestingly, dual treatment of CS-nematodes with ketones and PARP inhibitor had no additive effect, but both treatments rescued the CS phenotype and extended the lifespan of the worms. This fosters the argumentation that SIRT1 and PARP1 are active in the same pathway in the pathogenesis of CS.

In conclusion, the interplay of PARP1, PAR and CSB plays a pivotal role in the development of the CS phenotype and CS might be the first inheritable disease that could benefit from PARP1 inhibitor treatment (besides cancer therapy). This is also the first study that provides evidence for an involvement of non-covalent PAR interaction in the pathogenesis of a disease. It would be of interest to investigate whether patients that display CS-like symptoms but express the protein have mutations in the PBM's of CSB. The resulting reduced retention of CSB at DNA damage sites, as demonstrated by the recruitment studies, could explain the CS symptoms (due to reduced PARP1-displacement, as discussed above).

Summary

Taken together, we could demonstrate that non-covalent PAR interaction plays an important role in the enzymatic and spatial regulation of the RecQL helicases WRN and RECQL5. We could show that both WRN and RECQL5 interact with free PAR, PARP1 and PARylated PARP1. Even though there are some inconsistencies with the literature, we have strong evidence that these interactions inhibit WRN's catalytic functions. RECQL5's functions however, are differentially modulated by PAR-interaction. While both proteins physically interact with PARP1 only WRN might be covalently modified. PARP1 not only regulates their recruitment to sites of DNA damage by PARP activity, but it is also essential for the release of WRN from the nucleoli upon oxidative stress. Moreover, there is evidence implying at least one other PARP in the recruitment of WRN to DNA damage sites, presumably PARP2, thus strengthening the importance of the WRN-PARP interaction in DNA repair. We could furthermore demonstrate that the non-covalent PAR-interactions are also very important for the spatio-temporal regulation of PARP1 itself in response to DNA damage. Instrumental for this progress in PARP and PARP-related research was the establishment of a novel *PARP1* HeLa KO cell line.
Beyond that, we could establish CSB and APE1 (data not shown) as *de novo* PAR-binding proteins and, in the case of CSB, reveal an important cellular function of this interaction. Additionally, we developed a novel LC-MS based method to determine exonuclease activity, which could be employed for inhibitor screenings and extended analysis of WRN's exonuclease functions *in vivo*.

Integrating our findings into the current literature I propose the following model: Upon DNA damage PARP1 is recruited to the site of DNA damage and activates itself either in *cis* or *trans*, depending on the type of damage. Repair proteins are recruited to the damage upon PARP1 activation and either proteins like CSB, WRN, or RECQL5 or the PARP1 molecules themselves displace PARylated PARP1 from the DNA. This allows CSB, WRN, RECQL5 and other repair factors to act on the damage while simultaneously limiting PARP1's catalytic activity to the necessary levels, thus protecting the cells from NAD^+ depletion. This is of course a highly speculative model, which needs to be verified by more experimental evidence. However, it is well supported by experimental data from ourselves and others and it stresses the importance for non-covalent PAR-interaction in the proper response to DNA damage.

Outlook

The work presented in this thesis provides deeper insight into the roles of PAR and PARP1 in the regulation of RecQL helicases, particularly WRN and RECQL5. However, despite and because of the advances being made, there is a plethora of new questions spiked by our results and old questions still unanswered that warrant further investigation:

(i) *Of what relevance is the inhibition of WRN and RECQL5 by non-covalent PAR interaction in a cellular context?* To answer this question PBMs must be identified, experimentally verified and separately investigated by side-directed mutagenesis, analogous to our work on CSB. We have only started to address this point and so far we have evidence that PBM4 in WRN has no influence on its localization (*cf.* Figure 38). We do, however, see a decrease in WRN and RECQL5 recruitment to sites of DNA damage under PARP inhibition. Our experiments with *PARP1* KO cells and additional PARP inhibitor treatment suggest the involvement of at least one other PARP. Of course, a *WRN* KO cell line analogous to our HeLa *PARP1* KO cells would be highly beneficial to study the effects of WRN PBM mutants *in vivo*. There are cell lines from WS patients available; however, they possess similar drawbacks as cancer cell lines since they have probably adapted to cope with the WRN loss.

(ii) *Does WRN or RECQL5 interact in vivo with free PAR?* It is still a matter of debate whether there actually is free PAR in the cell and to what extent. Another, more likely, explanation for the non-covalent interaction with PAR is an interaction with covalently PARylated proteins. This is a well-established model and it is thought that automodified PARP1 provides a scaffold to recruit and retain proteins at sites of DNA damage (Mangerich and Bürkle, 2012). This is a good hypothesis for WRN's interaction with PAR(P) since WRN is less efficiently recruited to a laser-induced damage when PARP is inhibited. However, the use of free PAR as model to analyze the non-covalent interaction is a good approximation as the identification of the respective PARylated interaction partners would be several magnitudes more difficult. The interaction with PARylated proteins, on the other hand, might have different effects on PAR-binding proteins than free PAR, as our own experiments with PARylated PARP1 and free PAR suggest.

(iii) *Does interaction with PAR affect multimerization?* It has been shown that WRN and other RecQL helicases can form different multimeric complexes, *e.g.* dimers, trimers, tetramers and hexamers (Choudhary et al., 2004; Compton et al., 2008; Huang et al., 2000; Xue et al., 2002). However, these were purely biochemical studies and it is still unclear if and what multimers WRN forms *in vivo*. Since PAR-dependent formation of higher-molecular p53 complexes has been demonstrated (Fahrer et al., 2007), it is tempting to speculate that interaction with PAR can influence the multimerization of WRN, or other RecQL helicases too, either by disrupting the multimers or by facilitating their formation. As our biochemical studies suggest, it is quiet likely that PARP1 dimerization is influenced by PAR-interaction (Chapter VI).

(iv) *What consequences has a covalent modification of WRN and the other RecQL helicases with PAR?* Covalent modification with PAR can have profound consequences for the respective proteins and the cell, such as dissociation or organization of complexes, targeting for proteasomal degradation or inhibition of protein-nucleic acid interactions (Gibson and Kraus, 2012). Regarding the RecQL helicases, it has been shown that RECQL1, WRN and RECQL4 are covalently PARylated, while RECQL5 is not (Adelfalk et al., 2003; Berti et al., 2013; Khadka et al., 2015; Woo et al., 2006). However, these results are contradictory as other groups have published opposing results (Li et al., 2004; Sharma et al., 2012). Furthermore, it is notoriously difficult to distinguish between covalent and non-covalent interaction as PAR has very high affinities for the PBMs and needs harsh treatments for dissociation (Panzeter et al., 1992). Taken together, as of now, it is rather unclear if and at which positions RecQL helicases are covalently modified. This uncertainty warrants further research as covalent PARylation could have a strong impact on the RecQL functions, analogous to the non-covalent interactions.

(v) *Is the response of RecQL helicases to genotoxic stress differentially regulated by post-translational modifications?* All RecQL helicases are regulated by various PTMs (Croteau et al., 2014). However, it is largely unclear if and to what extent these PTMs regulate the response of RecQLs to DNA damage. To complicate it even more, it is very well possible that they could interfere with each other and thus regulate the proteins. Such a crosstalk seems to regulate WRN's distribution upon DNA damage, where acetylation, phosphorylation and PARylation seem to play a decisive role (Blander et al., 2002; Karmakar and Bohr, 2005; Li et al.,

2008; 2010)(this thesis). However, the various possibilities of covalent modification, combined with the potentially mediating proteins and the possible crosstalks, make this line of investigation extremely arduous and labor-intensive.

(vi) *Do PARPs and PAR orchestrate the release of other RecQL helicases from the nucleoli?* Our results show that the presence of PARP1 is necessary to mediate the release of WRN from the nucleoli upon oxidative stress, while PARP activity contributes only weakly. Since other RecQL helicases also localize to the nucleoli and vacate them upon different kinds of stressors it will be interesting to investigate whether the release of other RecQLs is also mediated by PARP1 or PAR.

(vii) *Is the recruitment of repair factors to damage sites dependent on PAR composition?* It has been demonstrated by our group that length and branching of the PAR chains can determine their interaction-properties with proteins (Fahrer et al., 2007; Fischer et al., 2014). Therefore, it is conceivable that the composition of PAR orchestrates the regulation of different repair proteins to different DNA damages. Along that line, it is tempting to speculate that the type of DNA damage determines of which composition the resulting PAR chains are and thus, which repair proteins are recruited. However, investigating this hypothesis will be time-consuming and difficult. To that end, our *PARP1* HeLa KO cells could be employed. They could be supplemented with different PARP1 variants (*e.g*. no branching, mono(ADP-ribose)ylation, no automodification capabilities), ideally under the original *PARP1* promotor, to study their effects on the recruitment and regulation of repair proteins.

(viii) *Is there a reciprocal regulation of RecQL helicases and PARPs?* The results on XPA and CSB suggest that it is quite likely that the RecQL helicases also influence PARP activity and distribution (Fischer et al., 2014; Scheibye-Knudsen et al., 2014). This is supported by the findings that PAR levels differ strongly in various *RecQL*-deficient patient cell lines. While loss of RECQL5 results in decreased PARP1 expression levels, suggesting a transcriptional regulation, cells from WS patients are deficient in their PARylation response to genotoxic stress (Kobbe et al., 2003a). It is still unclear whether this happens through direct interaction or via other proteins, although experiments with overexpressed WRN RQC domain indicate that it is mediated through direct interaction.

(ix) *Of what significance are other PARPs in the non-covalent PAR-RecQL interaction?* There is evidence from the Bohr group that PARP2 interacts with WRN, however, the significance of this interaction was never further explored (Kobbe et al., 2004a). Our recruitment data indicate that at least one other PARP is involved in the recruitment of WRN to DNA damage, with the prime candidate being PARP2, although PARP3 is also a possibility. As of now, there is no evidence of another RecQL helicase interacting with other PARPs than PARP1. However, the fact that WRN interacts with PARP2 and both PARP2&3 are able to catalyze the formation of PAR suggests possible interactions. To analyze the putative interaction of WRN and PARP2 a previously by our group established transient PARP2 KD system could be employed, analogous to the *PARP1* KO cells (PhD Thesis B. Hanf).

(x) *Of what relevance is a putative RecQL-PAR(P) interaction at the telomeres?* Telomeres, the end-caps of the chromosomes, have been associated with the aging process for decades now. Interestingly, most RecQL helicases specifically interact with DNA substrates that resemble telomeric structures such as telomeric D-loops or G-quadruplexes and telomeric proteins (Croteau et al., 2014). Also, PARP1&2 have been long known to be associated with telomeres (Beneke et al., 2008; Dantzer et al., 2004; Gomez et al., 2006). Furthermore, the close association of all RecQL helicases with the telomeres increases the likelihood of an interaction with the two telomere-associated PARPs TNKS1&2 (Smith et al., 1998). Recently, PARP3 has been mentioned as a repressor of telomerase, thus implying it in telomere biology too. The recent generation of G-quadruplex-specific antibodies offers interesting research opportunities as it is now possible to analyze G-quadruplexes *in vivo* (Biffi et al., 2013; Henderson et al., 2014; Lam et al., 2013). Taken together, this offers an exciting future field of research, especially since telomeres are also closely associated with aging, similar to RecQL helicases and PARylation (Blasco, 2007).

Record of Contributions

Chapter I: RecQ helicases and PARP1 team up in maintaining genome integrity

First authorship. The review was jointly written by myself and A. Mangerich, including review and selection of the literature and preparation of Figures.

Chapter II: Quantitative analysis of WRN exonuclease activity by isotope dilution mass spectrometry

Own contributions: Shared first authorship (together with A. Mangerich). Significant contributions to the design and conduction of the study and the experiments, data evaluation, preparation of the figures and writing of the manuscript. The method was developed as part of my Master's thesis in 2011. Experiments leading to the data shown in Figures 13 C, 14, Suppl. Figures 3 C&D and Suppl. Figure 4 were conducted by myself during the manuscript revision process as part of my PhD thesis. I also contributed to the rewriting of the manuscript during the revision process.

Chapter III: Site-specific non-covalent interaction of the biopolymer poly(ADP-ribose) with the Werner syndrome protein regulates protein functions

Own contributions: Shared first authorship (together with O. Popp). Significant contributions to the design and conduction of the experiments, data evaluation, preparation of the figures and writing of the manuscript. Most experiments that were conducted by myself were performed during my Master's thesis in 2011. Experiments for manuscript revisions were performed by myself as part of my PhD thesis, which included protein purifications and PAR synthesis and the blots shown in Figure 18 A, right panel. I also conducted experiments that were requested by the reviewers and which were presented in the revision letter only. In addition, I contributed to the rewriting of the manuscript during the revision process.

Chapter IV: Differential and concordant roles for PARP1 and poly(ADP-ribose) in regulating WRN and RECQL5 activities

Own contributions: Contributions to the experimental design (in part), performance of experiments (in part), data evaluation (in part), editing and discussion of the manuscript. Experiments depicted in Figure 25 A-C and Suppl. Figures 8&9 were performed by myself.

Chapter V: PARP1 is essential for oxidative stress-induced relocalization of WRN from nucleoli to sites of DNA damage

Own contributions: Significant contributions to the design of the study and the experiments, conduction of experiments (in part), supervision of experiments and preparation of figures. Experiments leading to the data depicted in Figure 33 and the cloning work for all utilized GFP vectors (except WRN WT) were performed by myself. Lead in the writing of the manuscript.

Chapter VI: Analyzing structure-function relationships of PARP1 by reconstituting HeLa PARP1 knock-out cells with artificial and natural PARP1 variants

Own contributions: Significant contributions to the design of experiments (in part), performance of experiments (in part), supervision of experiments (in part), data evaluation (in part), preparation of figures (in part). Contribution to the writing of the manuscript. Experiments leading to the data depicted in Figure 41 F and Figure 45 were performed by myself.

Additional Data: CSB and PARylation

The experiments leading to the data shown in Figures 50 A-C and 51 E&F were performed by myself. Figures 50 A & 51 were published as is in (Scheibye-Knudsen et al., 2014). I contributed intellectual input to the rest of Figure 51 and the general manuscript and participated in discussion of results and in the writing of the manuscript.

Appendix

Abbreviations

53BP1	Tumor suppressor p53-binding protein 1
6-4PP	6-4 photoproduct
8oxodG/dA	8-oxo-2'-deoxyguanosine/deoxyadenosine
AA/aa	Amino acid
ADP	Adenosine diphosphate
AIF	Apoptosis inducing factor
ALT	Alternative lengthening of telomeres
ANOVA	Analysis of variance
AP	Alkaline phosphatase
AP-site	Apurinic/apyrimidinic site
APB	ALT-associated PML body
APC	Allophycocyanin
APE1	Apurinic/apyrimidinic endonuclease 1
APLF	Aprataxin and PNK-like factor
APTX	Aprataxin
ARH3	ADP-ribosylhydrolase 3
ARTD	Diphtheria toxin-like ADP-ribosyltransferase (≙PARP)
ATM	Ataxia telangiectasia mutated
ATP	Adenosin triphosphate
ATPase	ATP hydrolase
ATR	Ataxia telangiectasia and Rad3-related protein
BER	Base excision repair
BGS	Baller-Gerolds syndrome
BLM	Bloom syndrome protein (RECQL3)
bp	Basepair
BPB	Bromophenol blue
BRCA1/2	Breast cancer type 1/2 susceptibility protein
BRCT	BRCA1 C-terminal domain (of PARP1)
BS	Bloom syndrome
BSA	Bovine serum albumine
$CaCl_2$	Calcium dichloride
cAMP	Cyclic adenosinmonophosphate
CAT	Catalytic domain (of PARP1)
CBD	Chitin-binding domain
CBP	CREB-binding protein
CCRC	Childhood CRC
cDNA	Complementary DANN
CEN2	Centrin-2
ChIP	Chromatin immunoprecipitation
CHK1	Checkpoint kinase 1
CO_2	Carbon dioxide
Conc.	Concentration
CPD	Cyclobutane pyrimidine dimer
CPT	Camptothecin
CR	Calorie restriction
CRC	Colorectal cancer
CREB	cAMP response element-binding protein
CRISPR	Clustered regularly interspaced short palindromic repeats
CS	Cockayne syndrome
CSA/CSB	Cockayne syndrome, complementation group A/B (ERCC8/6)
D-loop	Displacement loop
DAPI	4',6-diamidino-2-phenylindole

dC	2'deoxycytidine
DDB1/2	DNA damage-binding protein 1/2
DDR	DNA damage response
DEK	Protein DEK
dG	2'-deoxyguanosine
dGMP	2´-deoxyribonucleosidemonophosphate
DMEM	Dulbecco's modified eagles medium
DMSO	Dimethyl sulfoxide
DNA	Deoxyribonucleic acid
DNA-PKcs	DNA-dependent protein kinase, catalytic subunit (needs Ku complex for full functionality)
DNA2	DNA replication ATP-dependent helicase/nuclease DNA2
DNase	Deoxyribonuclease
dNMP	2'-deoxyribonucleosidemonophosphate
ds	Double strand
DSB	DNA double-strand break
DSBR	DNA double-strand break repair
DsDB	Double-stranded DNA-binding domain (of PARP1)
DTT	Dithiothreitol
e.g.	*Exempli gratia* (lat.: for example*)*
E/S	Enzyme to substrate ratio
ECL	Enhanced chemiluminescence
EDTA	Ethylenediaminetetraacetic acid
eGFP	Enhanced GFP
EMSA	Electromobility shift assay
ERCC1	Excision repair cross-complementing 1
Et al.	*Et alii* (lat. and others)
EXO	Exonuclease domain (of WRN)
EXO1	Exonuclease 1
FACS	Fluorescence assisted cell sorting
FBS/FCS	Fetal bovine/calf serum
FEN1	Flap endonuclease 1
FHA domain	Forkhead-associated domain
FITC	Fluorescein isothiocyanate
FPLC	Fast protein liquid chromatography
FSC	Forward scatter
GFP	Green-fluorescent protein
H2A	Histone H2A
H_2O_2	Hydrogen peroxide
HCl	Hydrochloride
HD	Hydrophobic core domain (of PARP1)
HDAC	Histone deacetylase
HEK293T	Cell line derived from human embryonic kidney cells
HeLa	Henrietta Lacks (donor patient of HeLa cell line)
HEPES	4-(2-hydroxyethyl)-1-piperazineethanesulfonic acid
HFD	High-fat diet
HGPS	Hutchinson-Gilford progeria syndrome
HIF-1	Hypoxia inducible factor 1
HJ	Holliday junction
HM	Higher multimers
HPLC	High pressure/performance liquid chromatography
HR	Homologous recombination
HR23B	UV excision repair protein RAD23 homolog B
HRDC	Helicase and RNase D-like C-terminal domain
i.e.	*Id est* (lat.: that is)
IgG	Immunoglobuline G
iPS cells	Induced pluripotent stem cells
IR	Ionizing radiation
kB	Kilobases
K_{cat}	Turnover number
KCl	Potassium chloride
KD	Knock-down

K_d	Dissociation constant
kD/kDa	Kilo dalton
KIX	Interactor of kinase inducible domain
K_m	Michaelis constant
KNIME	Konstanz information miner
KO	Knock-out
KOH	Potassium hydroxide
Ku70/80	Also: XRCC6/5
LC-MS/MS	Liquid chromatography coupled to tandem mass spectrometry
LiCl	Lithium chloride
LIG1/2/3 (I/III/IV)	DNA Ligase 1/2/3 (I/III/IV)
LMNA	Prelamin-A/C
m/z	Mass to charge ratio
MAD	Aswin „MAD“ Mangerich
MAR	Mono(ADP-ribose)
MEF	Mouse embryonic fibroblast
$MgCl_2$	Magnesium chloride
MGMT	O^6-methylguanine methyl transferase
MIM	Mendelian Inheritance in Man (genetic disorder database)
miRNA	Micro RNA
Mlh1	MutL homolog 1
MMR	Mismatch repair
MMS	Methyl methanesulfonate
MOI	Multiplicity of infection
MOPS	3-(N-morpholino)propanesulfonic acid
mPBM	Mutated PAR-binding motif
MRE11	Meiotic recombination 11 homolog
MRM	Multiple reaction monitoring
MRN	MRE11, Rad50, NBS1
Msh2/3/6	MutS protein homolog 2/3/6
mTOR	Mechanistic/mammalian target of rapamycin
N-/C-terminus	Amino-/carboxy-terminus
N.B.	*Nota bene* (lat.: note well)
n.d.	Not detectable
NaCl	Sodium chloride
NAD^+	Nicotinamide adenine dinucleotide (oxidized)
NADase	NAD^+ hydrolase
NBS1	Nibrin
NEIL1/2	Endonuclease VIII-like 1/2
NER	Nucleotide excision repair
NF-κB	Nuclear factor kappa-light-chain-enhancer of activated B cells
NHEJ	Non-homologous end-joining
NLS	Nuclear localization signal
NTS	Nucleolar targeting signal
OAR	Oligo(ADP-ribose)
OB fold	Oligonucleotide/oligosaccharide-binding fold
OGG1	8-Oxoguanine glycosylase
P/S or Pen-Strep	Penicillin-Streptomycin
p300	E1A binding protein p300
p53	Tumor protein p53
PAGE	Polyacrylamide gel electrophoresis
PAR	Poly(ADP-ribose)
PARG	Poly(ADP-ribose) glycohydrolase
PARP	Poly(ADP-ribose) polymerases
PARylation	Poly(ADP-ribose)ylation
PBM	PAR-binding motif
PBMC	Peripheral blood mononuclear cell
PbR	PAR-binding regulatory motif
PBS	Phosphate-buffered saline
PBSMT	5% milk in PBS with Tween
PCNA	Proliferating cell nuclear antigen
PCR	Polymerase chain reaction

PDE	Phosphodiesterase
PFA	Paraformaldehyde
PI	Propidium iodide
PIKK	Phosphatidylinositol 3-kinase-related kinases
PIPES	Piperazine-N,N'-bis(2-ethanesulfonic acid)
PMS2	Mismatch repair endonuclease PMS2
PMSF	Phenylmethylsulfonyl fluoride
PNK	Polynucleotide 5'-hydroxyl-kinase
POD/HRP	Horseradish peroxidase
Pol	Polymerase
POT1	Protection of telomeres protein 1
PTM	Post-translational modification
PVDF	Polyvinylidene difluoride
R-Ado	Ribosyl-adenosine
Rad50/51/52/54	DNA repair protein RAD50/51/52/54
rDNA	Ribosomal DNA
Rec.	Recombinant
RNA	Ribonucleic acid
RNase	Ribonuclease
RNS	Reactive nitrogen species
ROS	Reactive oxygen species
RPA	Replication protein A
RQC	RecQ C-terminal domain
RT	Room temperature
RTS	Rothmund-Thomson syndrome
SCE	Sister-chromatid exchanges
SD	Standard deviation
SDS	Sodium dodecyl sulfate
SEM/s.e.m.	Standard error of the means
shRNA	Small hairpin RNA
siRNA	Small interfering RNA
SIRT1	Sirtuin 1
SNP	Single nucleotide polymorphism
SP/LP-BER	Short-patch/long-patch BER
SRI	Set2 Rpb1 interacting domain
ss	Single strand
SSA	Single-strand annealing
SSB	DNA single-strand break
SSBR	Single-strand break repair
SSC	Side scatter
SUMO	Small ubiquitin-like modifier
TALEN	Transcription activator-like effector nuclease
TBE	Tris-borate-EDTA buffer
TBST	Tris-buffered saline with Tween
TC/GG-NER	Transcription-coupled/global genome-NER
TCA	Trichloroacetic acid
TE	Tris-EDTA
Terc	RNA component of telomerase
TFIIH	Transcription factor II human
TLS	Translesion synthesis
TNKS1/2	Tankyrase 1/2
TNT	Tris-NaCl-Tween (≙TBST)
TOPO1/2	Topoisomerase 1/2
TRF1/2	Telomere repeat factor 1/2
U	Unit
U2OS	Cell line derived from human osteocarcoma cells
UCP	Uncoupling protein
UV	Ultraviolet
UV-DDB	UV-damaged DNA-binding protein complex (DDB1&2)
VCP	Valosin-containing protein
V_{max}	Maximum reaction rate

w/	With
w/o	Without
WGR	Tryptophan-glycine-arginine domain (of PARP1)
WRN	Werner syndrome protein (RECQL2)
WS	Werner Syndrome
WT	Wild-type
WWE	Tryptophan-tryptophan-glutamate domain (of PARP1)
X-WRN	WRN with impaired exonuclease function (E84A)
XC	Xylene cyanol
XP	Xeroderma pigmentosum
XPA/XPB/XPC/XPD/XPF/XPG	Xeroderma pigmentosum, complementation group A/B/C/D/F/G
XRCC1/4/5/6	X-ray repair cross-complementing protein 1/4/5/6
ZnI/II/III or Zn1/2/3	Zinc-finger I/II/III domain of PARP1
β-OHB	β-hydroxybutyrate
γH2A.X	Phosphorylated form of H2A

SI units and units derived thereof are not listed, as well as symbols for chemical elements.

DNA/RNA-bases:
A: Adenine; G: Guanine; T: Thymine; C: Cytosine; U: Uracile

Table of Figures

Figure 1: Overview of the different DNA damage lesions, their possible causes and their respective repair pathways. 20
Figure 2: Overview of the domain structures of RecQL helicases. 28
Figure 3: Biochemistry of poly(ADP-ribosyl)ation. 30
Figure 4: Biochemical consequences of poly(ADP-ribosyl)ation (PARylation). 32
Figure 5: The role of PARylatio in aging and cancer. 33
Figure 6: Interplay of RECQL1, PARP1, and PARylation. 35
Figure 7: Interplay of WRN, PARP1, and PARylation. 39
Figure 8: Interplay of BLM, PARP1, and PARylation. 46
Figure 9: Interplay of RECQL4, PARP1, and PARylation. 49
Figure 10: Interplay of RECQL5, PARP1 and PAR. 52
Figure 11: Patients suffering from WS and CS at different ages. 61
Figure 12: Flow chart for the LC-MS/MS quantification of WRN exonuclease activity. 70
Figure 13: Analysis of WRN exonuclease activity by isotope dilution mass spectrometry. 71
Figure 14: Analysis of WRN substrate and strand specificity. 72
Figure 15: Analysis of Exo I activity. 73
Figure 16: Graphical abstract, summarizing the main findings: PAR can bind to WRN non-covalently and thus inhibit WRN's ability to bind DNA and its enzymatic functions. 84
Figure 17: *In vitro* production and biotinylation of poly(ADP-ribose). 86
Figure 18: PAR binds to WRN in a non-covalent manner. 89
Figure 19: WRN exhibits a PAR-binding motif in its exonuclease domain. 91
Figure 20: PAR-overlay blot with mutant WRN peptides derived from peptide '166-188'. 92
Figure 21: WRN-PAR interaction inhibits binding of WRN to DNA. 94
Figure 22: WRN-PAR interaction inhibits WRN's helicase activity. 96
Figure 23: WRN-PAR interaction inhibits WRN's exonuclease activity. 97
Figure 24: Potential molecular mechanism for temporally controlled regulation of WRN activity by PAR and PARP1. 98
Figure 25: RECQL5 directly binds PAR and PARP1, but is not PARylated by PARP1. 110

Figure 26: Both RECQL5 and WRN's helicase activities are regulated by PARP1, PARylated PARP1 and PAR. 112
Figure 27: Activation of PARP1 alters the ATPase activities of both RECQL5 and WRN. 114
Figure 28: The effects of PARP1, PARylated PARP1 and PAR on single-strand annealing activities of RECQL5 and WRN..... 116
Figure 29: PARylation regulates the early recruitment of RECQL5 to laser induced DNA damage. 118
Figure 30: Cancer cell lines with loss of RECQL5 or WRN show increased sensitivity to PARP inhibitor. 120
Figure 31: RECQL5-GFP fragment's recruitment to laser induced DSBs depends on PARP1's PARylation activity. 121
Figure 32: The effects of PARP1 on WRN or RECQL5 mediated HR or NHEJ DSB repair *in vivo*. 123
Figure 33: WRN has a PAR-binding motif in its nucleolar targeting sequence. 145
Figure 34: WRN relocalizes from nucleolus to nucleoplasm upon oxidative stress. 147
Figure 35: Stress-dependent WRN relocalization is not restricted to oxidative stress. 149
Figure 36: WRN relocalization is dependent on PARP1. 151
Figure 37: WRN relocalization is partially dependent on PARP activity. 152
Figure 38: PBM4 is not relevant for WRN translocation. 153
Figure 39: WRN returns to nucleoli after stress release. 155
Figure 40: PARP1 relocalizes from nucleolus to nucleoplasm upon oxidative stress. 156
Figure 41: TALEN-mediated gene targeting of *PARP1* in HeLa cells and its consequences on PAR metabolism. 175
Figure 42: Functional consequences of *PARP1* deletion in HeLa cells. 177
Figure 43: Overview of PARP1 variants included in this study. 179
Figure 44: Cellular biochemistry of artificial PARP1 mutants. 181
Figure 45: Non-covalent PARP1-PAR interaction. 184
Figure 46: PARP1\E988K mutant affects nuclear architecture. 186
Figure 47: PARP1\E988K affects cell cycle regulation and induces DNA damage signaling. 188
Figure 48: PARP1 mutants influence cell viability and cell cycle progression upon CPT treatment. 189
Figure 49: Biochemical and cellular characteristics of natural PARP1 variants. 192
Figure 50: CSB interacts with PAR non-covalently and influences the cellular PARylation capacity. 216
Figure 51: CSB inhibits PARP1 activation *in vitro* and *in vivo* through displacement of PARylated PARP1 from DNA. 218

Table of Tables

Table 1: Summary of interacting partner's effect on human RecQL protein activities. 124

Table of Supplementary Figures

Supplementary Figure 1: Characterization of purified human His-tagged WRN..... 79
Supplementary Figure 2: Analyzing WRN exonuclease activity by detection of a biotin 5'-end-labeled oligonucleotide duplex via streptavidin-POD. 79
Supplementary Figure 3: LC-MS/MS quantification of WRN exonuclease activity. 80
Supplementary Figure 4: Method validation. 81
Supplementary Figure 5: Analytical HPLC fractionation of PAR and subsequent characterization of pooled fractions by sequencing gel analysis. 103
Supplementary Figure 6: XPA binds longer PAR chains with higher affinity than short ones. 104
Supplementary Figure 7: Confirmation of the inhibitory effect of PAR on WRN's exonuclease activity. 104
Supplementary Figure 8: EMSA with end-biotinylated PAR to examine WRN-PAR interaction in solution. 136
Supplementary Figure 9: Five putative PAR binding motifs are identified in RECQL5. 137
Supplementary Figure 10: The presence of single stranded DNA stimulates the helicase activity of RECQL5. 138
Supplementary Figure 11: PARylation regulates the recruitments of both RECQL5 and WRN to laser induced DNA damage. 138
Supplementary Figure 12: RECQL5 and WRN are recruited to sites of DSBs in *PARP1* knock-out cells. 139
Supplementary Figure 13: RECQL5 recruitment to DSBs is abrogated when cells are treated with both veliparib and PI3 kinase inhibitors. 140
Supplementary Figure 14: Medium change is a sufficient stressor to trigger WRN relocalization. 166
Supplementary Figure 15: Optimization of PFA fixation procedure..... 167
Supplementary Figure 16: Recovery of WRN nucleolar distribution. 168
Supplementary Figure 17: Time course analysis of cellular PARylation capacity of artificial PARP1 mutants. 210
Supplementary Figure 18: Overexpression of different PARP1 variants changes H327K methylation status. 211
Supplementary Figure 19: Biochemical and cellular characteristics of natural PARP1 variants. 212
Supplementary Figure 20: Recruitment of natural PARP1 variants to sites of laser-induced DNA damage. 213

Table of Supplementary Tables

Supplementary Table 1: WRN substrates used in this study. 81
Supplementary Table 2: Optimized settings for mass spectrometric analysis. 82
Supplementary Table 3: Concentrations of ^{14}N-dG, ^{15}N-dG and ^{14}N/^{12}C-dC, ^{15}N/^{13}C-dC used for acquisition of calibration curves. 82

References

Aamann, M.D., Hvitby, C., Popuri, V., Muftuoglu, M., Lemminger, L., Skeby, C.K., Keijzers, G., Ahn, B., Bjørås, M., Bohr, V.A., et al. (2014). Cockayne Syndrome group B protein stimulates NEIL2 DNA glycosylase activity. Mech. Ageing Dev. *135*, 1–14.

Aamann, M.D., Sorensen, M.M., Hvitby, C., Berquist, B.R., Muftuoglu, M., Tian, J., de Souza-Pinto, N.C., Scheibye-Knudsen, M., Wilson, D.M., Stevnsner, T., et al. (2010). Cockayne syndrome group B protein promotes mitochondrial DNA stability by supporting the DNA repair association with the mitochondrial membrane. Faseb J. *24*, 2334–2346.

Acharya, S., Kaul, Z., Gocha, A.S., Martinez, A.R., Harris, J., Parvin, J.D., and Groden, J. (2014). Association of BLM and BRCA1 during Telomere Maintenance in ALT Cells. PLoS ONE *9*, e103819.

Adelfalk, C., Kontou, M., Hirsch-Kauffmann, M., and Schweiger, M. (2003). Physical and functional interaction of the Werner syndrome protein with poly-ADP ribosyl transferase. FEBS Lett. *554*, 55–58.

Adey, A., Burton, J.N., Kitzman, J.O., Hiatt, J.B., Lewis, A.P., Martin, B.K., Qiu, R., Lee, C., and Shendure, J. (2013). The haplotype-resolved genome and epigenome of the aneuploid HeLa cancer cell line. Nature *500*, 207–211.

Aggarwal, M., Banerjee, T., Sommers, J.A., and Brosh, R.M. (2013). Targeting an Achilles' heel of cancer with a WRN helicase inhibitor. Cell Cycle *12*.

Aggarwal, M., Sommers, J.A., Morris, C., and Brosh, R.M. (2010). Delineation of WRN helicase function with EXO1 in the replicational stress response. DNA Repair (Amst.) *9*, 765–776.

Aggarwal, M., Sommers, J.A., Shoemaker, R.H., and Brosh, R.M. (2011). Inhibition of helicase activity by a small molecule impairs Werner syndrome helicase (WRN) function in the cellular response to DNA damage or replication stress. Proc. Natl. Acad. Sci. U.S.a. *108*, 1525–1530.

Agrelo, R., Cheng, W.-H., Setien, F., Ropero, S., Espada, J., Fraga, M.F., Herranz, M., Paz, M.F., Sanchez-Cespedes, M., Artiga, M.J., et al. (2006). Epigenetic inactivation of the premature aging Werner syndrome gene in human cancer. Proc. Natl. Acad. Sci. U.S.a. *103*, 8822–8827.

Aguilar-Quesada, R., Muñoz-Gámez, J.A., Martín-Oliva, D., Peralta, A., Valenzuela, M.T., Matínez-Romero, R., Quiles-Pérez, R., Ménissier-de Murcia, J., de Murcia, G., Ruiz de Almodóvar, M., et al. (2007). Interaction between ATM and PARP-1 in response to DNA damage and sensitization of ATM deficient cells through PARP inhibition. BMC Mol. Biol. *8*, 29.

Ahel, D., Horejsí, Z., Wiechens, N., Polo, S.E., Garcia-Wilson, E., Ahel, I., Flynn, H., Skehel, M., West, S.C., Jackson, S.P., et al. (2009). Poly(ADP-ribose)-dependent regulation of DNA repair by the chromatin remodeling enzyme ALC1. Science *325*, 1240–1243.

Ahel, I., Ahel, D., Matsusaka, T., Clark, A.J., Pines, J., Boulton, S.J., and West, S.C. (2008). Poly(ADP-ribose)-binding zinc finger motifs in DNA repair/checkpoint proteins. Nature *451*, 81–85.

Ahn, B., and Bohr, V.A. (2011). DNA secondary structure of the released strand stimulates WRN helicase action on forked duplexes without coordinate action of WRN exonuclease. Biochem. Biophys. Res. Commun. *411*, 684–689.

Ahn, B., Harrigan, J.A., Indig, F.E., Wilson, D.M., and Bohr, V.A. (2004). Regulation of WRN helicase activity in human base excision repair. J. Biol. Chem. *279*, 53465–53474.

Ali, A.A.E., Timinszky, G., Arribas-Bosacoma, R., Kozlowski, M., Hassa, P.O., Hassler, M., Ladurner, A.G., Pearl, L.H., and Oliver, A.W. (2012). The zinc-finger domains of PARP1 cooperate to recognize DNA strand breaks. Nat. Struct. Mol. Biol. *19*, 685–692.

Alshammari, A.H., Shalaby, M.A., Alanazi, M.S., and Saeed, H.M. (2014). Novel mutations of the PARP-1 gene associated with colorectal cancer in the Saudi population. Asian Pac. J. Cancer Prev. *15*, 3667–3673.

Althaus, F.R., Bachmann, S., Höfferer, L., Kleczkowska, H.E., Malanga, M., Panzeter, P.L., Realini, C., and Zweifel, B. (1995). Interactions of poly(ADP-ribose) with nuclear proteins. Biochimie *77*, 423–432.

Althaus, F.R., Kleczkowska, H.E., Malanga, M., Müntener, C.R., M, P.J., Ebner, M., and Auer, B. (1999). Poly

ADP-ribosylation: a DNA break signal mechanism. Mol. Cell. Biochem. *193*, 5–11.

Altmeyer, M., Neelsen, K.J., Teloni, F., Pozdnyakova, I., Pellegrino, S., Grøfte, M., Rask, M.-B.D., Streicher, W., Jungmichel, S., Nielsen, M.L., et al. (2015). Liquid demixing of intrinsically disordered proteins is seeded by poly(ADP-ribose). Nat Commun *6*, 8088.

Alvarez-Gonzalez, R., Spring, H., Müller, M., and Burkle, A. (1999). Selective loss of poly(ADP-ribose) and the 85-kDa fragment of poly(ADP-ribose) polymerase in nucleoli during alkylation-induced apoptosis of HeLa cells. Journal of Biological Chemistry *274*, 32122–32126.

Amé, J.C., Rolli, V., Schreiber, V., Niedergang, C., Apiou, F., Decker, P., Muller, S., Höger, T., Ménissier-De Murcia, J., and de Murcia, G. (1999). PARP-2, A novel mammalian DNA damage-dependent poly(ADP-ribose) polymerase. Journal of Biological Chemistry *274*, 17860–17868.

Anindya, R., Mari, P.-O., Kristensen, U., Kool, H., Giglia-Mari, G., Mullenders, L.H., Fousteri, M., Vermeulen, W., Egly, J.-M., and Svejstrup, J.Q. (2010). A ubiquitin-binding domain in Cockayne syndrome B required for transcription-coupled nucleotide excision repair. Mol. Cell *38*, 637–648.

Arora, H., Chacon, A.H., Choudhary, S., McLeod, M.P., Meshkov, L., Nouri, K., and Izakovic, J. (2014). Bloom syndrome. Int. J. Dermatol. *53*, 798–802.

Audas, T.E., Jacob, M.D., and Lee, S. (2012). Immobilization of proteins in the nucleolus by ribosomal intergenic spacer noncoding RNA. Mol. Cell *45*, 147–157.

Audebert, M., Salles, B., and Calsou, P. (2004). Involvement of poly(ADP-ribose) polymerase-1 and XRCC1/DNA ligase III in an alternative route for DNA double-strand breaks rejoining. Journal of Biological Chemistry *279*, 55117–55126.

Aygün, O., Svejstrup, J., and Liu, Y. (2008). A RECQ5-RNA polymerase II association identified by targeted proteomic analysis of human chromatin. Proc. Natl. Acad. Sci. U.S.a. *105*, 8580–8584.

Aygün, O., Xu, X., Liu, Y., Takahashi, H., Kong, S.E., Conaway, R.C., Conaway, J.W., and Svejstrup, J.Q. (2009). Direct inhibition of RNA polymerase II transcription by RECQL5. Journal of Biological Chemistry *284*, 23197–23203.

Bai, P. (2015). Biology of Poly(ADP-Ribose) Polymerases: The Factotums of Cell Maintenance. Mol. Cell *58*, 947–958.

Bai, P., and Cantó, C. (2012). The Role of PARP-1 and PARP-2 Enzymes in Metabolic Regulation and Disease. Cell Metab. –.

Barefield, C., and Karlseder, J. (2012). The BLM helicase contributes to telomere maintenance through processing of late-replicating intermediate structures. Nucleic Acids Res. *40*, 7358–7367.

Barkauskaite, E., Brassington, A., Tan, E.S., Warwicker, J., Dunstan, M.S., Banos, B., Lafite, P., Ahel, M., Mitchison, T.J., Ahel, I., et al. (2013a). Visualization of poly(ADP-ribose) bound to PARG reveals inherent balance between exo- and endo-glycohydrolase activities. Nat Commun *4*, 2164.

Barkauskaite, E., Jankevicius, G., and Ahel, I. (2015). Structures and Mechanisms of Enzymes Employed in the Synthesis and Degradation of PARP-Dependent Protein ADP-Ribosylation. Mol. Cell *58*, 935–946.

Barkauskaite, E., Jankevicius, G., Ladurner, A.G., Ahel, I., and Timinszky, G. (2013b). The recognition and removal of cellular poly(ADP-ribose) signals. Febs J. *280*, 3491–3507.

Batenburg, N.L., Thompson, E.L., Hendrickson, E.A., and Zhu, X.-D. (2015). Cockayne syndrome group B protein regulates DNA double-strand break repair and checkpoint activation. Embo J. *34*, 1399–1416.

Bauer, P.I., Chen, H.J., Kenesi, E., Kenessey, I., Buki, K.G., Kirsten, E., Hakam, A., Hwang, J.I., and Kun, E. (2001). Molecular interactions between poly(ADP-ribose) polymerase (PARP I) and topoisomerase I (Topo I): identification of topology of binding. FEBS Lett. *506*, 239–242.

Beck, C., Robert, I., Reina-San-Martin, B., Schreiber, V., and Dantzer, F. (2014). Poly(ADP-ribose) polymerases in double-strand break repair: focus on PARP1, PARP2 and PARP3. Exp. Cell Res. *329*, 18–25.

Beerens, N., Hoeijmakers, J.H.J., Kanaar, R., Vermeulen, W., and Wyman, C. (2005). The CSB protein actively wraps DNA. Journal of Biological Chemistry *280*, 4722–4729.

Bendtsen, K.M., Jensen, M.B., May, A., Rasmussen, L.J., Trusina, A., Bohr, V.A., and Jensen, M.H. (2014).

Dynamics of the DNA repair proteins WRN and BLM in the nucleoplasm and nucleoli. Eur. Biophys. J.

Beneke, S., Alvarez-Gonzalez, R., and Burkle, A. (2000). Comparative characterisation of poly(ADP-ribose) polymerase-1 from two mammalian species with different life span. Exp. Gerontol. *35*, 989–1002.

Beneke, S. (2012). Regulation of chromatin structure by poly(ADP-ribosyl)ation. Front Genet *3*, 169.

Beneke, S., and Bürkle, A. (2007). Poly(ADP-ribosyl)ation in mammalian ageing. Nucleic Acids Res. *35*, 7456–7465.

Beneke, S., Cohausz, O., Malanga, M., Boukamp, P., Althaus, F., and Bürkle, A. (2008). Rapid regulation of telomere length is mediated by poly(ADP-ribose) polymerase-1. Nucleic Acids Res. *36*, 6309–6317.

Beneke, S., Meyer, K., Holtz, A., Hüttner, K., and Bürkle, A. (2012). Chromatin composition is changed by poly(ADP-ribosyl)ation during chromatin immunoprecipitation. PLoS ONE *7*, e32914.

Beneke, S., Scherr, A.-L., Ponath, V., Popp, O., and Bürkle, A. (2010). Enzyme characteristics of recombinant poly(ADP-ribose) polymerases-1 of rat and human origin mirror the correlation between cellular poly(ADP-ribosyl)ation capacity and species-specific life span. Mech. Ageing Dev. *131*, 366–369.

Berger, F., Lau, C., and Ziegler, M. (2007). Regulation of poly(ADP-ribose) polymerase 1 activity by the phosphorylation state of the nuclear NAD biosynthetic enzyme NMN adenylyl transferase 1. Proc. Natl. Acad. Sci. U.S.a. *104*, 3765–3770.

Bernstein, C., and Bernstein, H. (1991). Aging and Sex, DNA Repair (Weinheim, Germany: Wiley-VCH Verlag GmbH & Co. KGaA).

Bernstein, K.A., Gangloff, S., and Rothstein, R. (2010). The RecQ DNA helicases in DNA repair. Annu. Rev. Genet. *44*, 393–417.

Berquist, B.R., and Wilson, D.M. (2009). Nucleic acid binding activity of human Cockayne syndrome B protein and identification of Ca(2+) as a novel metal cofactor. J. Mol. Biol. *391*, 820–832.

Berti, M., Chaudhuri, A.R., Thangavel, S., Gomathinayagam, S., Kenig, S., Vujanovic, M., Odreman, F., Glatter, T., Graziano, S., Mendoza-Maldonado, R., et al. (2013). Human RECQ1 promotes restart of replication forks reversed by DNA topoisomerase I inhibition. Nat. Struct. Mol. Biol. *20*, 347–354.

Biffi, G., Tannahill, D., McCafferty, J., and Balasubramanian, S. (2013). Quantitative visualization of DNA G-quadruplex structures in human cells. Nat Chem *5*, 182–186.

Blander, G., Zalle, N., Daniely, Y., Taplick, J., Gray, M.D., and Oren, M. (2002). DNA damage-induced translocation of the Werner helicase is regulated by acetylation. J. Biol. Chem. *277*, 50934–50940.

Blasco, M.A. (2007). Telomere length, stem cells and aging. Nat. Chem. Biol. *3*, 640–649.

Blenn, C., Wyrsch, P., and Althaus, F.R. (2012). The Sound of Silence: RNAi in Poly (ADP-Ribose) Research. Genes (Basel) *3*, 779–805.

Bloom, D. (1954). Congenital telangiectatic erythema resembling lupus erythematosus in dwarfs; probably a syndrome entity. AMA Am J Dis Child *88*, 754–758.

Boamah, E.K., Kotova, E., Garabedian, M., Jarnik, M., and Tulin, A.V. (2012). Poly(ADP-Ribose) polymerase 1 (PARP-1) regulates ribosomal biogenesis in Drosophila nucleoli. PLoS Genet. *8*, e1002442.

Boboila, C., Alt, F.W., and Schwer, B. (2012). Classical and alternative end-joining pathways for repair of lymphocyte-specific and general DNA double-strand breaks. Adv. Immunol. *116*, 1–49.

Bodnar, A.G., Ouellette, M., Frolkis, M., Holt, S.E., Chiu, C.P., Morin, G.B., Harley, C.B., Shay, J.W., Lichtsteiner, S., and Wright, W.E. (1998). Extension of life-span by introduction of telomerase into normal human cells. Science *279*, 349–352.

Bohr, V.A. (2008). Rising from the RecQ-age: the role of human RecQ helicases in genome maintenance. Trends Biochem. Sci. *33*, 609–620.

Boiteux, S., and Guillet, M. (2004). Abasic sites in DNA: repair and biological consequences in Saccharomyces cerevisiae. DNA Repair (Amst.) *3*, 1–12.

Boubriak, I., Mason, P.A., Clancy, D.J., Dockray, J., Saunders, R.D.C., and Cox, L.S. (2009). DmWRNexo is a

3“-5” exonuclease: phenotypic and biochemical characterization of mutants of the Drosophila orthologue of human WRN exonuclease. Biogerontology *10*, 267–277.

Bouwman, P., and Jonkers, J. (2012). The effects of deregulated DNA damage signalling on cancer chemotherapy response and resistance. Nat. Rev. Cancer *12*, 587–598.

Böhm, S., and Bernstein, K.A. (2014). The role of post-translational modifications in fine-tuning BLM helicase function during DNA repair. DNA Repair (Amst.) *22*, 123–132.

Brosh, R.M., Karmakar, P., Sommers, J.A., Yang, Q., Wang, X.W., Spillare, E.A., Harris, C.C., and Bohr, V.A. (2001a). p53 Modulates the exonuclease activity of Werner syndrome protein. J. Biol. Chem. *276*, 35093–35102.

Brosh, R.M., Kobbe, von, C., Sommers, J.A., Karmakar, P., Opresko, P.L., Piotrowski, J., Dianova, I., Dianov, G.L., and Bohr, V.A. (2001b). Werner syndrome protein interacts with human flap endonuclease 1 and stimulates its cleavage activity. Embo J. *20*, 5791–5801.

Brosh, R.M., Li, J.L., Kenny, M.K., Karow, J.K., Cooper, M.P., Kureekattil, R.P., Hickson, I.D., and Bohr, V.A. (2000). Replication protein A physically interacts with the Bloom's syndrome protein and stimulates its helicase activity. Journal of Biological Chemistry *275*, 23500–23508.

Brosh, R.M. (2013). DNA helicases involved in DNA repair and their roles in cancer. Nat. Rev. Cancer *13*, 542–558.

Brosh, R.M., Opresko, P.L., and Bohr, V.A. (2006). Enzymatic mechanism of the WRN helicase/nuclease. Meth. Enzymol. *409*, 52–85.

Bryant, H.E., Petermann, E., Schultz, N., Jemth, A.-S., Loseva, O., Issaeva, N., Johansson, F., Fernandez, S., McGlynn, P., and Helleday, T. (2009). PARP is activated at stalled forks to mediate Mre11-dependent replication restart and recombination. Embo J. *28*, 2601–2615.

Bryant, H.E., Schultz, N., Thomas, H.D., Parker, K.M., Flower, D., Lopez, E., Kyle, S., Meuth, M., Curtin, N.J., and Helleday, T. (2005). Specific killing of BRCA2-deficient tumours with inhibitors of poly(ADP-ribose) polymerase. Nature *434*, 913–917.

Bugreev, D.V., Brosh, R.M., and Mazin, A.V. (2008). RECQ1 possesses DNA branch migration activity. Journal of Biological Chemistry *283*, 20231–20242.

Bukowy, Z., Harrigan, J.A., Ramsden, D.A., Tudek, B., Bohr, V.A., and Stevnsner, T. (2008). WRN Exonuclease activity is blocked by specific oxidatively induced base lesions positioned in either DNA strand. Nucleic Acids Res. *36*, 4975–4987.

Campalans, A., Kortulewski, T., Amouroux, R., Menoni, H., Vermeulen, W., and Radicella, J.P. (2013). Distinct spatiotemporal patterns and PARP dependence of XRCC1 recruitment to single-strand break and base excision repair. Nucleic Acids Res. *41*, 3115–3129.

Campisi, J., and d'Adda di Fagagna, F. (2007). Cellular senescence: when bad things happen to good cells. Nat. Rev. Mol. Cell Biol. *8*, 729–740.

Cantó, C., Sauve, A.A., and Bai, P. (2013). Crosstalk between poly(ADP-ribose) polymerase and sirtuin enzymes. Mol. Aspects Med. *34*, 1168–1201.

Chaganti, R.S., Schonberg, S., and German, J. (1974). A manyfold increase in sister chromatid exchanges in Bloom's syndrome lymphocytes. Proc. Natl. Acad. Sci. U.S.a. *71*, 4508–4512.

Chang, S., Multani, A.S., Cabrera, N.G., Naylor, M.L., Laud, P., Lombard, D., Pathak, S., Guarente, L., and DePinho, R.A. (2004). Essential role of limiting telomeres in the pathogenesis of Werner syndrome. Nat. Genet. *36*, 877–882.

Chen, L., Huang, S., Lee, L., Davalos, A., Schiestl, R.H., Campisi, J., and Oshima, J. (2003). WRN, the protein deficient in Werner syndrome, plays a critical structural role in optimizing DNA repair. Aging Cell *2*, 191–199.

Cheng, W.-H., Kobbe, von, C., Opresko, P.L., Fields, K.M., Ren, J., Kufe, D., and Bohr, V.A. (2003). Werner syndrome protein phosphorylation by abl tyrosine kinase regulates its activity and distribution. Mol. Cell. Biol. *23*, 6385–6395.

Cheng, W.-H., Kusumoto, R., Opresko, P.L., Sui, X., Huang, S., Nicolette, M.L., Paull, T.T., Campisi, J., Seidman, M., and Bohr, V.A. (2006). Collaboration of Werner syndrome protein and BRCA1 in cellular

responses to DNA interstrand cross-links. Nucleic Acids Res. *34*, 2751–2760.

Chester, N., Kuo, F., Kozak, C., O'Hara, C.D., and Leder, P. (1998). Stage-specific apoptosis, developmental delay, and embryonic lethality in mice homozygous for a targeted disruption in the murine Bloom's syndrome gene. Genes Dev. *12*, 3382–3393.

Chevanne, M., Calia, C., Zampieri, M., Cecchinelli, B., Caldini, R., Monti, D., Bucci, L., Franceschi, C., and Caiafa, P. (2007). Oxidative DNA damage repair and parp 1 and parp 2 expression in Epstein-Barr virus-immortalized B lymphocyte cells from young subjects, old subjects, and centenarians. Rejuvenation Res *10*, 191–204.

Choudhary, S., Sommers, J.A., and Brosh, R.M. (2004). Biochemical and kinetic characterization of the DNA helicase and exonuclease activities of werner syndrome protein. J. Biol. Chem. *279*, 34603–34613.

Chu, W.K., and Hickson, I.D. (2009). RecQ helicases: multifunctional genome caretakers. Nat. Rev. Cancer *9*, 644–654.

Ciccia, A., and Elledge, S.J. (2010). The DNA damage response: making it safe to play with knives. Mol. Cell *40*, 179–204.

Citterio, E., Van Den Boom, V., Schnitzler, G., Kanaar, R., Bonte, E., Kingston, R.E., Hoeijmakers, J.H., and Vermeulen, W. (2000). ATP-dependent chromatin remodeling by the Cockayne syndrome B DNA repair-transcription-coupling factor. Mol. Cell. Biol. *20*, 7643–7653.

Cockayne, E.A. (1936). Dwarfism with retinal atrophy and deafness. Arch. Dis. Child. *11*, 1–8.

Cockayne, E.A. (1946). Dwarfism with Retinal Atrophy and Deafness. Arch. Dis. Child. *21*, 52–54.

Cohen-Armon, M., Visochek, L., Rozensal, D., Kalal, A., Geistrikh, I., Klein, R., Bendetz-Nezer, S., Yao, Z., and Seger, R. (2007). DNA-independent PARP-1 activation by phosphorylated ERK2 increases Elk1 activity: a link to histone acetylation. Mol. Cell *25*, 297–308.

Compton, S.A., Tolun, G., Kamath-Loeb, A.S., Loeb, L.A., and Griffith, J.D. (2008). The Werner syndrome protein binds replication fork and holliday junction DNAs as an oligomer. J. Biol. Chem. *283*, 24478–24483.

Constantinou, A., Tarsounas, M., Karow, J.K., Brosh, R.M., Bohr, V.A., Hickson, I.D., and West, S.C. (2000). Werner's syndrome protein (WRN) migrates Holliday junctions and co-localizes with RPA upon replication arrest. EMBO Rep. *1*, 80–84.

Cooper, M.P., Machwe, A., Orren, D.K., Brosh, R.M., Ramsden, D., and Bohr, V.A. (2000). Ku complex interacts with and stimulates the Werner protein. Genes Dev. *14*, 907–912.

Coquelle, N., and Glover, J.N.M. (2012). PARP pairs up to PARsylate. Nat. Struct. Mol. Biol. *19*, 660–661.

Cottet, F., Blanché, H., Verasdonck, P., Le Gall, I., Schächter, F., Burkle, A., and Muiras, M.L. (2000). New polymorphisms in the human poly(ADP-ribose) polymerase-1 coding sequence: lack of association with longevity or with increased cellular poly(ADP-ribosyl)ation capacity. J. Mol. Med. *78*, 431–440.

Croteau, D.L., Popuri, V., Opresko, P.L., and Bohr, V.A. (2014). Human RecQ Helicases in DNA Repair, Recombination, and Replication. Annu. Rev. Biochem.

Croteau, D.L., Rossi, M.L., Ross, J., Dawut, L., Dunn, C., Kulikowicz, T., and Bohr, V.A. (2012a). RAPADILINO RECQL4 mutant protein lacks helicase and ATPase activity. Biochim. Biophys. Acta *1822*, 1727–1734.

Croteau, D.L., Singh, D.K., Hoh Ferrarelli, L., Lu, H., and Bohr, V.A. (2012b). RECQL4 in genomic instability and aging. Trends Genet. *28*, 624–631.

Cui, S., Arosio, D., Doherty, K.M., Brosh, R.M., Falaschi, A., and Vindigni, A. (2004). Analysis of the unwinding activity of the dimeric RECQ1 helicase in the presence of human replication protein A. Nucleic Acids Res. *32*, 2158–2170.

Curtin, N.J., and Szabo, C. (2013). Therapeutic applications of PARP inhibitors: anticancer therapy and beyond. Mol. Aspects Med. *34*, 1217–1256.

d'Adda di Fagagna, F., Hande, M.P., Tong, W.M., Lansdorp, P.M., Wang, Z.Q., and Jackson, S.P. (1999). Functions of poly(ADP-ribose) polymerase in controlling telomere length and chromosomal stability. Nat. Genet. *23*, 76–80.

Dantzer, F., and Santoro, R. (2013). The expanding role of PARPs in the establishment and maintenance of heterochromatin. Febs J. *280*, 3508–3518.

Dantzer, F., Giraud-Panis, M.-J., Jaco, I., Amé, J.-C., Schultz, I., Blasco, M., Koering, C.-E., Gilson, E., Ménissier-de Murcia, J., de Murcia, G., et al. (2004). Functional interaction between poly(ADP-Ribose) polymerase 2 (PARP-2) and TRF2: PARP activity negatively regulates TRF2. Mol. Cell. Biol. *24*, 1595–1607.

DaRosa, P.A., Wang, Z., Jiang, X., Pruneda, J.N., Cong, F., Klevit, R.E., and Xu, W. (2015). Allosteric activation of the RNF146 ubiquitin ligase by a poly(ADP-ribosyl)ation signal. Nature *517*, 223–226.

Das, A., Boldogh, I., Lee, J.W., Harrigan, J.A., Hegde, M.L., Piotrowski, J., Pinto, N. de S., Ramos, W., Greenberg, M.M., Hazra, T.K., et al. (2007). The human Werner syndrome protein stimulates repair of oxidative DNA base damage by the DNA glycosylase NEIL1. Journal of Biological Chemistry *282*.

de Murcia, J.M., Niedergang, C., Trucco, C., Ricoul, M., Dutrillaux, B., Mark, M., Oliver, F.J., Masson, M., Dierich, A., LeMeur, M., et al. (1997). Requirement of poly(ADP-ribose) polymerase in recovery from DNA damage in mice and in cells. Proc. Natl. Acad. Sci. U.S.a. *94*, 7303–7307.

De Sandre-Giovannoli, A., Bernard, R., Cau, P., Navarro, C., Amiel, J., Boccaccio, I., Lyonnet, S., Stewart, C.L., Munnich, A., Le Merrer, M., et al. (2003). Lamin a truncation in Hutchinson-Gilford progeria. Science *300*, 2055.

De Vos, M., Schreiber, V., and Dantzer, F. (2012). The diverse roles and clinical relevance of PARPs in DNA damage repair: current state of the art. Biochem. Pharmacol. *84*, 137–146.

Deschênes, F., Massip, L., Garand, C., and Lebel, M. (2005). In vivo misregulation of genes involved in apoptosis, development and oxidative stress in mice lacking both functional Werner syndrome protein and poly(ADP-ribose) polymerase-1. Hum. Mol. Genet. *14*, 3293–3308.

Desmarais, Y., Ménard, L., Lagueux, J., and Poirier, G.G. (1991). Enzymological properties of poly(ADP-ribose)polymerase: characterization of automodification sites and NADase activity. Biochim. Biophys. Acta *1078*, 179–186.

Desnoyers, S., Kaufmann, S.H., and Poirier, G.G. (1996). Alteration of the nucleolar localization of poly(ADP-ribose) polymerase upon treatment with transcription inhibitors. Exp. Cell Res. *227*, 146–153.

Dexheimer, T.S. (2013). DNA Repair of Cancer Stem Cells (Dordrecht: Springer Netherlands).

Dietschy, T., Shevelev, I., and Stagljar, I. (2007). The molecular role of the Rothmund-Thomson-, RAPADILINO- and Baller-Gerold-gene product, RECQL4: recent progress. Cell. Mol. Life Sci. *64*, 796–802.

Doh, Y.J., Kim, H.K., Jung, E.D., Choi, S.H., Kim, J.G., Kim, B.W., and Lee, I.K. (2009). Novel LMNA gene mutation in a patient with Atypical Werner's Syndrome. Korean J. Intern. Med. *24*, 68–72.

El-Khamisy, S.F., Masutani, M., Suzuki, H., and Caldecott, K.W. (2003). A requirement for PARP-1 for the assembly or stability of XRCC1 nuclear foci at sites of oxidative DNA damage. Nucleic Acids Res. *31*, 5526–5533.

Ellis, N.A., Ciocci, S., Proytcheva, M., Lennon, D., Groden, J., and German, J. (1998). The Ashkenazic Jewish Bloom syndrome mutation blmAsh is present in non-Jewish Americans of Spanish ancestry. Am. J. Hum. Genet. *63*, 1685–1693.

Ellis, N.A., Groden, J., Ye, T.Z., Straughen, J., Lennon, D.J., Ciocci, S., Proytcheva, M., and German, J. (1995). The Bloom's syndrome gene product is homologous to RecQ helicases. Cell *83*, 655–666.

Epstein, C.J., Martin, G.M., Schultz, A.L., and Motulsky, A.G. (1966). Werner's syndrome a review of its symptomatology, natural history, pathologic features, genetics and relationship to the natural aging process. Medicine (Baltimore) *45*, 177–221.

Eriksson, M., Brown, W.T., Gordon, L.B., Glynn, M.W., Singer, J., Scott, L., Erdos, M.R., Robbins, C.M., Moses, T.Y., Berglund, P., et al. (2003). Recurrent de novo point mutations in lamin A cause Hutchinson-Gilford progeria syndrome. Nature *423*, 293–298.

Essen, L.O., and Klar, T. (2006). Light-driven DNA repair by photolyases. Cell. Mol. Life Sci. *63*, 1266–1277.

Ethier, C., Labelle, Y., and Poirier, G.G. (2007). PARP-1-induced cell death through inhibition of the MEK/ERK pathway in MNNG-treated HeLa cells. Apoptosis *12*, 2037–2049.

Fahrer, J., Kranaster, R., Altmeyer, M., Marx, A., and Burkle, A. (2007). Quantitative analysis of the binding affinity of poly(ADP-ribose) to specific binding proteins as a function of chain length. Nucleic Acids Res. *35*, e143–e143.

Fahrer, J., Popp, O., Malanga, M., Beneke, S., Markovitz, D.M., Ferrando-May, E., Bürkle, A., and Kappes, F. (2010). High-affinity interaction of poly(ADP-ribose) and the human DEK oncoprotein depends upon chain length. Biochemistry *49*, 7119–7130.

Fan, W., and Luo, J. (2008). RecQ4 facilitates UV light-induced DNA damage repair through interaction with nucleotide excision repair factor xeroderma pigmentosum group A (XPA). Journal of Biological Chemistry *283*, 29037–29044.

Farmer, H., McCabe, N., Lord, C.J., Tutt, A.N.J., Johnson, D.A., Richardson, T.B., Santarosa, M., Dillon, K.J., Hickson, I., Knights, C., et al. (2005). Targeting the DNA repair defect in BRCA mutant cells as a therapeutic strategy. Nature *434*, 917–921.

Fatokun, A.A., Dawson, V.L., and Dawson, T.M. (2014). Parthanatos: mitochondrial-linked mechanisms and therapeutic opportunities. Br. J. Pharmacol. *171*, 2000–2016.

Fischer, J.M.F., Popp, O., Gebhard, D., Veith, S., Fischbach, A., Beneke, S., Leitenstorfer, A., Bergemann, J., Scheffner, M., Ferrando-May, E., et al. (2014). Poly(ADP-ribose)-mediated interplay of XPA and PARP1 leads to reciprocal regulation of protein function. Febs J.

Fortini, P., and Dogliotti, E. (2007). Base damage and single-strand break repair: mechanisms and functional significance of short- and long-patch repair subpathways. DNA Repair (Amst.) *6*, 398–409.

Fouché, N., Ozgür, S., Roy, D., and Griffith, J.D. (2006). Replication fork regression in repetitive DNAs. Nucleic Acids Res. *34*, 6044–6050.

Fouquerel, E., and Sobol, R.W. (2014). ARTD1 (PARP1) activation and NAD(+) in DNA repair and cell death. DNA Repair (Amst.) *23*, 27–32.

Fousteri, M., Vermeulen, W., van Zeeland, A.A., and Mullenders, L.H.F. (2006). Cockayne syndrome A and B proteins differentially regulate recruitment of chromatin remodeling and repair factors to stalled RNA polymerase II in vivo. Mol. Cell *23*, 471–482.

Friedrich, K., Lee, L., Leistritz, D.F., Nürnberg, G., Saha, B., Hisama, F.M., Eyman, D.K., Lessel, D., Nürnberg, P., Li, C., et al. (2010). WRN mutations in Werner syndrome patients: genomic rearrangements, unusual intronic mutations and ethnic-specific alterations. Hum. Genet. *128*, 103–111.

Fukui, K. (2010). DNA mismatch repair in eukaryotes and bacteria. J Nucleic Acids *2010*.

Gagné, J.-P., Ethier, C., Defoy, D., Bourassa, S., Langelier, M.-F., Riccio, A.A., Pascal, J.M., Moon, K.-M., Foster, L.J., Ning, Z., et al. (2015). Quantitative site-specific ADP-ribosylation profiling of DNA-dependent PARPs. DNA Repair (Amst.) *30*, 68–79.

Gagné, J.-P., Hunter, J.M., Labrecque, B., Chabot, B., and Poirier, G.G. (2003). A proteomic approach to the identification of heterogeneous nuclear ribonucleoproteins as a new family of poly(ADP-ribose)-binding proteins. Biochem. J. *371*, 331–340.

Gagné, J.-P., Isabelle, M., Lo, K.S., Bourassa, S., Hendzel, M.J., Dawson, V.L., Dawson, T.M., and Poirier, G.G. (2008). Proteome-wide identification of poly(ADP-ribose) binding proteins and poly(ADP-ribose)-associated protein complexes. Nucleic Acids Res. *36*, 6959–6976.

Gagné, J.-P., Pic, E., Isabelle, M., Krietsch, J., Ethier, C., Paquet, E., Kelly, I., Boutin, M., Moon, K.-M., Foster, L.J., et al. (2012). Quantitative proteomics profiling of the poly(ADP-ribose)-related response to genotoxic stress. Nucleic Acids Res.

Garcia, P.L., Liu, Y., Jiricny, J., West, S.C., and Janscak, P. (2004). Human RECQ5beta, a protein with DNA helicase and strand-annealing activities in a single polypeptide. Embo J. *23*, 2882–2891.

Genois, M.-M., Paquet, E.R., Laffitte, M.-C.N., Maity, R., Rodrigue, A., Ouellette, M., and Masson, J.-Y. (2014). DNA repair pathways in trypanosomatids: from DNA repair to drug resistance. Microbiol. Mol. Biol. Rev. *78*, 40–73.

German, J., Sanz, M.M., Ciocci, S., Ye, T.Z., and Ellis, N.A. (2007). Syndrome-causing mutations of the BLM gene in persons in the Bloom's Syndrome Registry. Hum. Mutat. *28*, 743–753.

Gerold, M. (1959). [Healing of a Fracture in an Unusual Case of Congenital Anomaly of the Upper Extremities]. Zentralbl Chir *84*, 831–834.

Ghosh, A.K., Rossi, M.L., Singh, D.K., Dunn, C., Ramamoorthy, M., Croteau, D.L., Liu, Y., and Bohr, V.A. (2012). RECQL4, the protein mutated in Rothmund-Thomson syndrome, functions in telomere maintenance. J. Biol. Chem. *287*, 196–209.

Ghosh, S., and Zhou, Z. (2014). Genetics of aging, progeria and lamin disorders. Curr. Opin. Genet. Dev. *26*, 41–46.

Gibson, B.A., and Kraus, W.L. (2012). New insights into the molecular and cellular functions of poly(ADP-ribose) and PARPs. Nat. Rev. Mol. Cell Biol. *13*, 411–424.

Godon, C., Cordelières, F.P., Biard, D., Giocanti, N., Mégnin-Chanet, F., Hall, J., and Favaudon, V. (2008). PARP inhibition versus PARP-1 silencing: different outcomes in terms of single-strand break repair and radiation susceptibility. Nucleic Acids Res. *36*, 4454–4464.

Gomez, M., Wu, J., Schreiber, V., Dunlap, J., Dantzer, F., Wang, Y., and Liu, Y. (2006). PARP1 Is a TRF2-associated poly(ADP-ribose)polymerase and protects eroded telomeres. Mol. Biol. Cell *17*, 1686–1696.

Goss, K.H., Risinger, M.A., Kordich, J.J., Sanz, M.M., Straughen, J.E., Slovek, L.E., Capobianco, A.J., German, J., Boivin, G.P., and Groden, J. (2002). Enhanced tumor formation in mice heterozygous for Blm mutation. Science *297*, 2051–2053.

Goto, M. (1997). Hierarchical deterioration of body systems in Werner's syndrome: implications for normal ageing. Mech. Ageing Dev. *98*, 239–254.

Goto, M., Ishikawa, Y., Sugimoto, M., and Furuichi, Y. (2013). Werner syndrome: a changing pattern of clinical manifestations in Japan (1917~2008). Biosci Trends *7*, 13–22.

Goto, M., Tanimoto, K., Horiuchi, Y., and Sasazuki, T. (1981). Family analysis of Werner's syndrome: a survey of 42 Japanese families with a review of the literature. Clin. Genet. *19*, 8–15.

Goto, M., and Matsuura, M. (2008). Secular trends towards delayed onsets of pathologies and prolonged longevities in Japanese patients with Werner syndrome. Biosci Trends *2*, 81–87.

Gottipati, P., Vischioni, B., Schultz, N., Solomons, J., Bryant, H.E., Djureinovic, T., Issaeva, N., Sleeth, K., Sharma, R.A., and Helleday, T. (2010). Poly(ADP-ribose) polymerase is hyperactivated in homologous recombination-defective cells. Cancer Res. *70*, 5389–5398.

Gottschalk, A.J., Timinszky, G., Kong, S.E., Jin, J., Cai, Y., Swanson, S.K., Washburn, M.P., Florens, L., Ladurner, A.G., Conaway, J.W., et al. (2009). Poly(ADP-ribosyl)ation directs recruitment and activation of an ATP-dependent chromatin remodeler. Proc. Natl. Acad. Sci. U.S.a. *106*, 13770–13774.

Gray, M.D., Shen, J.C., Kamath-Loeb, A.S., Blank, A., Sopher, B.L., Martin, G.M., Oshima, J., and Loeb, L.A. (1997). The Werner syndrome protein is a DNA helicase. Nat. Genet. *17*, 100–103.

Gray, M.D., Wang, L., Youssoufian, H., Martin, G.M., and Oshima, J. (1998). Werner helicase is localized to transcriptionally active nucleoli of cycling cells. Exp. Cell Res. *242*, 487–494.

Groisman, R., Polanowska, J., Kuraoka, I., Sawada, J.-I., Saijo, M., Drapkin, R., Kisselev, A.F., Tanaka, K., and Nakatani, Y. (2003). The ubiquitin ligase activity in the DDB2 and CSA complexes is differentially regulated by the COP9 signalosome in response to DNA damage. Cell *113*, 357–367.

Grube, K., and Burkle, A. (1992). Poly(ADP-ribose) polymerase activity in mononuclear leukocytes of 13 mammalian species correlates with species-specific life span. Proc. Natl. Acad. Sci. U.S.a. *89*, 11759–11763.

Guarente, L. (2013). Introduction: sirtuins in aging and diseases. Methods Mol. Biol. *1077*, 3–10.

Guastafierro, T., Cecchinelli, B., Zampieri, M., Reale, A., Riggio, G., Sthandier, O., Zupi, G., Calabrese, L., and Caiafa, P. (2008). CCCTC-binding factor activates PARP-1 affecting DNA methylation machinery. Journal of Biological Chemistry *283*, 21873–21880.

Guetg, C., Scheifele, F., Rosenthal, F., Hottiger, M.O., and Santoro, R. (2012). Inheritance of silent rDNA chromatin is mediated by PARP1 via noncoding RNA. Mol. Cell *45*, 790–800.

Haince, J.-F., Kozlov, S., Dawson, V.L., Dawson, T.M., Hendzel, M.J., Lavin, M.F., and Poirier, G.G. (2007). Ataxia telangiectasia mutated (ATM) signaling network is modulated by a novel poly(ADP-ribose)-dependent

pathway in the early response to DNA-damaging agents. J. Biol. Chem. *282*, 16441–16453.

Haince, J.-F., McDonald, D., Rodrigue, A., Déry, U., Masson, J.-Y., Hendzel, M.J., and Poirier, G.G. (2008). PARP1-dependent kinetics of recruitment of MRE11 and NBS1 proteins to multiple DNA damage sites. Journal of Biological Chemistry *283*, 1197–1208.

Hanada, K., and Hickson, I.D. (2007). Molecular genetics of RecQ helicase disorders. Cell. Mol. Life Sci. *64*, 2306–2322.

Harley, C.B., Futcher, A.B., and Greider, C.W. (1990). Telomeres shorten during ageing of human fibroblasts. Nature *345*, 458–460.

Harrigan, J.A., and Bohr, V.A. (2003). Human diseases deficient in RecQ helicases. Biochimie *85*, 1185–1193.

Harrigan, J.A., Opresko, P.L., Kobbe, von, C., Kedar, P.S., Prasad, R., Wilson, S.H., and Bohr, V.A. (2003). The Werner syndrome protein stimulates DNA polymerase beta strand displacement synthesis via its helicase activity. J. Biol. Chem. *278*, 22686–22695.

Harrigan, J.A., Wilson, D.M., Prasad, R., Opresko, P.L., Beck, G., May, A., Wilson, S.H., and Bohr, V.A. (2006). The Werner syndrome protein operates in base excision repair and cooperates with DNA polymerase beta. Nucleic Acids Res. *34*, 745–754.

Hassa, P.O., Buerki, C., Lombardi, C., Imhof, R., and Hottiger, M.O. (2003). Transcriptional coactivation of nuclear factor-kappaB-dependent gene expression by p300 is regulated by poly(ADP)-ribose polymerase-1. Journal of Biological Chemistry *278*, 45145–45153.

Hassa, P.O., Haenni, S.S., Buerki, C., Meier, N.I., Lane, W.S., Owen, H., Gersbach, M., Imhof, R., and Hottiger, M.O. (2005). Acetylation of poly(ADP-ribose) polymerase-1 by p300/CREB-binding protein regulates coactivation of NF-kappaB-dependent transcription. Journal of Biological Chemistry *280*, 40450–40464.

Hayflick, L. (1965). THE LIMITED IN VITRO LIFETIME OF HUMAN DIPLOID CELL STRAINS. Exp. Cell Res. *37*, 614–636.

Henderson, A., Wu, Y., Huang, Y.C., Chavez, E.A., Platt, J., Johnson, F.B., Brosh, R.M., Sen, D., and Lansdorp, P.M. (2014). Detection of G-quadruplex DNA in mammalian cells. Nucleic Acids Res. *42*, 860–869.

Henson, J.D., Neumann, A.A., Yeager, T.R., and Reddel, R.R. (2002). Alternative lengthening of telomeres in mammalian cells. Oncogene *21*, 598–610.

Hochegger, H., Dejsuphong, D., Fukushima, T., Morrison, C., Sonoda, E., Schreiber, V., Zhao, G.Y., Saberi, A., Masutani, M., Adachi, N., et al. (2006). Parp-1 protects homologous recombination from interference by Ku and Ligase IV in vertebrate cells. Embo J. *25*, 1305–1314.

Hoeijmakers, J.H. (2001). Genome maintenance mechanisms for preventing cancer. Nature *411*, 366–374.

Hoischen, A., van Bon, B.W.M., Rodríguez-Santiago, B., Gilissen, C., Vissers, L.E.L.M., de Vries, P., Janssen, I., van Lier, B., Hastings, R., Smithson, S.F., et al. (2011). De novo nonsense mutations in ASXL1 cause Bohring-Opitz syndrome. Nat. Genet. *43*, 729–731.

Hoki, Y., Araki, R., Fujimori, A., Ohhata, T., Koseki, H., Fukumura, R., Nakamura, M., Takahashi, H., Noda, Y., Kito, S., et al. (2003). Growth retardation and skin abnormalities of the Recql4-deficient mouse. Hum. Mol. Genet. *12*, 2293–2299.

Honjo, T., Nishizuka, Y., and Hayaishi, O. (1968). Diphtheria toxin-dependent adenosine diphosphate ribosylation of aminoacyl transferase II and inhibition of protein synthesis. Journal of Biological Chemistry *243*, 3553–3555.

Hottiger, M.O. (2015). Nuclear ADP-Ribosylation and Its Role in Chromatin Plasticity, Cell Differentiation, and Epigenetics. Annu. Rev. Biochem. *84*, 227–263.

Hottiger, M.O., Hassa, P.O., Lüscher, B., Schüler, H., and Koch-Nolte, F. (2010). Toward a unified nomenclature for mammalian ADP-ribosyltransferases. Trends Biochem. Sci. *35*, 208–219.

Howlett, N.G., Taniguchi, T., Olson, S., Cox, B., Waisfisz, Q., De Die-Smulders, C., Persky, N., Grompe, M., Joenje, H., Pals, G., et al. (2002). Biallelic inactivation of BRCA2 in Fanconi anemia. Science *297*, 606–609.

Hu, Y., Lu, X., and Luo, G. (2010). Effect of Recql5 deficiency on the intestinal tumor susceptibility of Apc(min) mice. World J. Gastroenterol. *16*, 1482–1486.

Hu, Y., Lu, X., Barnes, E., Yan, M., Lou, H., and Luo, G. (2005). Recql5 and Blm RecQ DNA helicases have nonredundant roles in suppressing crossovers. Mol. Cell. Biol. *25*, 3431–3442.

Hu, Y., Lu, X., Zhou, G., Barnes, E.L., and Luo, G. (2009). Recq15 Plays an Important Role in DNA Replication and Cell Survival after Camptothecin Treatment. Mol. Biol. Cell *20*, 114–123.

Hu, Y., Petit, S.A., Ficarro, S.B., Toomire, K.J., Xie, A., Lim, E., Cao, S.A., Park, E., Eck, M.J., Scully, R., et al. (2014). PARP1-driven poly-ADP-ribosylation regulates BRCA1 function in homologous recombination-mediated DNA repair. Cancer Discov *4*, 1430–1447.

Hu, Y., Raynard, S., Sehorn, M.G., Lu, X., Bussen, W., Zheng, L., Stark, J.M., Barnes, E.L., Chi, P., Janscak, P., et al. (2007). RECQL5/Recql5 helicase regulates homologous recombination and suppresses tumor formation via disruption of Rad51 presynaptic filaments. Genes Dev. *21*, 3073–3084.

Hua, R.-X., Li, H.-P., Liang, Y.-B., Zhu, J.-H., Zhang, B., Ye, S., Dai, Q.-S., Xiong, S.-Q., Gu, Y., and Sun, X.-Z. (2014). Association between the PARP1 Val762Ala polymorphism and cancer risk: evidence from 43 studies. PLoS ONE *9*, e87057.

Huambachano, O., Herrera, F., Rancourt, A., and Satoh, M.S. (2011). Double-stranded DNA binding domain of poly(ADP-ribose) polymerase-1 and molecular insight into the regulation of its activity. J. Biol. Chem. *286*, 7149–7160.

Huang, S., Beresten, S., Li, B., Oshima, J., Ellis, N.A., and Campisi, J. (2000). Characterization of the human and mouse WRN 3“-->5” exonuclease. Nucleic Acids Res. *28*, 2396–2405.

Huang, S., Li, B., Gray, M.D., Oshima, J., Mian, I.S., and Campisi, J. (1998). The premature ageing syndrome protein, WRN, is a 3“-->5” exonuclease. Nat. Genet. *20*, 114–116.

Huang, S., Kennedy, B.K., and Oshima, J. (2005). LMNA mutations in progeroid syndromes. Novartis Found. Symp. *264*, 197–202; discussion202–discussion207, 227–230.

Huang, S., Lee, L., Hanson, N.B., Lenaerts, C., Hoehn, H., Poot, M., Rubin, C.D., Chen, D.-F., Yang, C.-C., Juch, H., et al. (2006). The spectrum of WRN mutations i.n Werner syndrome patients. Hum. Mutat. *27*, 558–567.

Illuzzi, G., Fouquerel, E., Amé, J.-C., Noll, A., Rehmet, K., Nasheuer, H.-P., Dantzer, F., and Schreiber, V. (2014). PARG is dispensable for recovery from transient replicative stress but required to prevent detrimental accumulation of poly(ADP-ribose) upon prolonged replicative stress. Nucleic Acids Res. *42*, 7776–7792.

Indig, F.E., Partridge, J.J., Kobbe, von, C., Aladjem, M.I., Latterich, M., and Bohr, V.A. (2004). Werner syndrome protein directly binds to the AAA ATPase p97/VCP in an ATP-dependent fashion. J. Struct. Biol. *146*, 251–259.

Islam, M.N., Fox, D., Guo, R., Enomoto, T., and Wang, W. (2010). RecQL5 promotes genome stabilization through two parallel mechanisms--interacting with RNA polymerase II and acting as a helicase. Mol. Cell. Biol. *30*, 2460–2472.

Islam, M.N., Paquet, N., Fox, D., Dray, E., Zheng, X.-F., Klein, H., Sung, P., and Wang, W. (2012). A variant of the breast cancer type 2 susceptibility protein (BRC) repeat is essential for the RECQL5 helicase to interact with RAD51 recombinase for genome stabilization. J. Biol. Chem. *287*, 23808–23818.

Jacobson, E.L., and Jacobson, M.K. (1976). Pyridine nucleotide levels as a function of growth in normal and transformed 3T3 cells. Arch. Biochem. Biophys. *175*, 627–634.

Jankevicius, G., Hassler, M., Golia, B., Rybin, V., Zacharias, M., Timinszky, G., and Ladurner, A.G. (2013). A family of macrodomain proteins reverses cellular mono-ADP-ribosylation. Nat. Struct. Mol. Biol.

Janscak, P., Garcia, P.L., Hamburger, F., Makuta, Y., Shiraishi, K., Imai, Y., Ikeda, H., and Bickle, T.A. (2003). Characterization and mutational analysis of the RecQ core of the bloom syndrome protein. J. Mol. Biol. *330*, 29–42.

Jeggo, P.A. (1998). DNA repair: PARP - another guardian angel? Curr. Biol. *8*, R49–R51.

Jin, W., Liu, H., Zhang, Y., Otta, S.K., Plon, S.E., and Wang, L.L. (2008). Sensitivity of RECQL4-deficient fibroblasts from Rothmund-Thomson syndrome patients to genotoxic agents. Hum. Genet. *123*, 643–653.

Ju, B.-G., Lunyak, V.V., Perissi, V., Garcia-Bassets, I., Rose, D.W., Glass, C.K., and Rosenfeld, M.G. (2006). A

topoisomerase IIbeta-mediated dsDNA break required for regulated transcription. Science *312*, 1798–1802.

Juarez-Salinas, H., Sims, J.L., and Jacobson, M.K. (1979). Poly(ADP-ribose) levels in carcinogen-treated cells. Nature *282*, 740–741.

Jungmichel, S., Rosenthal, F., Altmeyer, M., Lukas, J., Hottiger, M.O., and Nielsen, M.L. (2013). Proteome-wide Identification of Poly(ADP-Ribosyl)ation Targets in Different Genotoxic Stress Responses. Mol. Cell.

Kahyo, T., Mostoslavsky, R., Goto, M., and Setou, M. (2008). Sirtuin-mediated deacetylation pathway stabilizes Werner syndrome protein. FEBS Lett. *582*, 2479–2483.

Kamath-Loeb, A.S., Shen, J.C., Loeb, L.A., and Fry, M. (1998). Werner syndrome protein. II. Characterization of the integral 3“ --> 5” DNA exonuclease. J. Biol. Chem. *273*, 34145–34150.

Kamath-Loeb, A.S., Lan, L., Nakajima, S., Yasui, A., and Loeb, L.A. (2007). Werner syndrome protein interacts functionally with translesion DNA polymerases. Proc. Natl. Acad. Sci. U.S.a. *104*, 10394–10399.

Kamath-Loeb, A.S., Shen, J.C., Schmitt, M.W., and Loeb, L.A. (2012). The Werner syndrome exonuclease facilitates DNA degradation and high fidelity DNA polymerization by human DNA polymerase δ. J. Biol. Chem. *287*, 12480–12490.

Kanagaraj, R., Parasuraman, P., Mihaljevic, B., van Loon, B., Burdova, K., König, C., Furrer, A., Bohr, V.A., Hübscher, U., and Janscak, P. (2012). Involvement of Werner syndrome protein in MUTYH-mediated repair of oxidative DNA damage. Nucleic Acids Res.

Kanagaraj, R., Saydam, N., Garcia, P.L., Zheng, L., and Janscak, P. (2006). Human RECQ5beta helicase promotes strand exchange on synthetic DNA structures resembling a stalled replication fork. Nucleic Acids Res. *34*, 5217–5231.

Kappes, F., Fahrer, J., Khodadoust, M.S., Tabbert, A., Strasser, C., Mor-Vaknin, N., Moreno-Villanueva, M., Burkle, A., Markovitz, D.M., and Ferrando-May, E. (2008). DEK is a poly(ADP-ribose) acceptor in apoptosis and mediates resistance to genotoxic stress. Mol. Cell. Biol. *28*, 3245–3257.

Karmakar, P., and Bohr, V.A. (2005). Cellular dynamics and modulation of WRN protein is DNA damage specific. Mech. Ageing Dev. *126*, 1146–1158.

Karmakar, P., Piotrowski, J., Brosh, R.M., Sommers, J.A., Miller, S.P.L., Cheng, W.-H., Snowden, C.M., Ramsden, D.A., and Bohr, V.A. (2002). Werner protein is a target of DNA-dependent protein kinase in vivo and in vitro, and its catalytic activities are regulated by phosphorylation. J. Biol. Chem. *277*, 18291–18302.

Karow, J.K., Wu, L., and Hickson, I.D. (2000). RecQ family helicases: roles in cancer and aging. Curr. Opin. Genet. Dev. *10*, 32–38.

Kauppinen, T.M., Chan, W.Y., Suh, S.W., Wiggins, A.K., Huang, E.J., and Swanson, R.A. (2006). Direct phosphorylation and regulation of poly(ADP-ribose) polymerase-1 by extracellular signal-regulated kinases 1/2. Proc. Natl. Acad. Sci. U.S.a. *103*, 7136–7141.

Kawaichi, M., Ueda, K., and Hayaishi, O. (1981). Multiple autopoly(ADP-ribosyl)ation of rat liver poly(ADP-ribose) synthetase. Mode of modification and properties of automodified synthetase. J. Biol. Chem. *256*, 9483–9489.

Kawamitsu, H., Hoshino, H., Okada, H., Miwa, M., Momoi, H., and Sugimura, T. (1984). Monoclonal antibodies to poly(adenosine diphosphate ribose) recognize different structures. Biochemistry *23*, 3771–3777.

Kääriäinen, H., Ryöppy, S., and Norio, R. (1989). RAPADILINO syndrome with radial and patellar aplasia/hypoplasia as main manifestations. Am. J. Med. Genet. *33*, 346–351.

Khadka, P., Hsu, J.K., Veith, S., Tadokoro, T., Shamanna, R., Mangerich, A., Croteau, D.L., and Bohr, V.A. (2015). Differential and concordant roles for PARP1 and poly(ADP-ribose) in regulating WRN and RECQL5 activities. Mol. Cell. Biol.

Kiehlbauch, C.C., Aboul-Ela, N., Jacobson, E., Ringer, D., and Jacobson, M. (1993). High resolution fractionation and characterization of ADP-ribose polymers. Anal. Biochem. *208*, 26–34.

Kim, H., and Kim, J.-S. (2014). A guide to genome engineering with programmable nucleases. Nat. Rev. Genet. *15*, 321–334.

Kim, M.Y., Zhang, T., and Kraus, W.L. (2005). Poly(ADP-ribosyl)ation by PARP-1: “PAR-laying” NAD+ into

a nuclear signal. Genes Dev. *19*, 1951–1967.

King, B.S., Cooper, K.L., Liu, K.J., and Hudson, L.G. (2012). Poly(ADP-ribose) contributes to an association between Poly(ADP-ribose)polymerase-1 and Xeroderma pigmentosum complementation group A in nucleotide excision repair. J. Biol. Chem.

Kitano, K., Kim, S.-Y., and Hakoshima, T. (2010). Structural basis for DNA strand separation by the unconventional winged-helix domain of RecQ helicase WRN. Structure *18*, 177–187.

Kitao, S., Lindor, N.M., Shiratori, M., Furuichi, Y., and Shimamoto, A. (1999). Rothmund-thomson syndrome responsible gene, RECQL4: genomic structure and products. Genomics *61*, 268–276.

Kitao, S., Ohsugi, I., Ichikawa, K., Goto, M., Furuichi, Y., and Shimamoto, A. (1998). Cloning of two new human helicase genes of the RecQ family: biological significance of multiple species in higher eukaryotes. Genomics *54*, 443–452.

Kobbe, von, C., and Bohr, V.A. (2002). A nucleolar targeting sequence in the Werner syndrome protein resides within residues 949-1092. J. Cell. Sci. *115*, 3901–3907.

Kobbe, von, C., Harrigan, J.A., May, A., Opresko, P.L., Dawut, L., Cheng, W.-H., and Bohr, V.A. (2003a). Central role for the Werner syndrome protein/poly(ADP-ribose) polymerase 1 complex in the poly(ADP-ribosyl)ation pathway after DNA damage. Mol. Cell. Biol. *23*, 8601–8613.

Kobbe, von, C., Harrigan, J.A., Schreiber, V., Stiegler, P., Piotrowski, J., Dawut, L., and Bohr, V.A. (2004a). Poly(ADP-ribose) polymerase 1 regulates both the exonuclease and helicase activities of the Werner syndrome protein. Nucleic Acids Res. *32*, 4003–4014.

Kobbe, von, C., Karmakar, P., Dawut, L., Opresko, P., Zeng, X., Brosh, R.M., Hickson, I.D., and Bohr, V.A. (2002). Colocalization, physical, and functional interaction between Werner and Bloom syndrome proteins. Journal of Biological Chemistry *277*, 22035–22044.

Kobbe, von, C., May, A., Grandori, C., and Bohr, V.A. (2004b). Werner syndrome cells escape hydrogen peroxide-induced cell proliferation arrest. Faseb J. *18*, 1970–1972.

Kobbe, von, C., Thomä, N.H., Czyzewski, B.K., Pavletich, N.P., and Bohr, V.A. (2003b). Werner syndrome protein contains three structure-specific DNA binding domains. J. Biol. Chem. *278*, 52997–53006.

Kohzaki, M., Chiourea, M., Versini, G., Adachi, N., Takeda, S., Gagos, S., and Halazonetis, T.D. (2012). The helicase domain and C-terminus of human RecQL4 facilitate replication elongation on DNA templates damaged by ionizing radiation. Carcinogenesis *33*, 1203–1210.

Kraus, W.L., and Hottiger, M.O. (2013). PARP-1 and gene regulation: progress and puzzles. Mol. Aspects Med. *34*, 1109–1123.

Krietsch, J., Rouleau, M., Pic, E., Ethier, C., Dawson, T.M., Dawson, V.L., Masson, J.-Y., Poirier, G.G., and Gagné, J.-P. (2012). Reprogramming cellular events by poly(ADP-ribose)-binding proteins. Mol. Aspects Med.

Krukenberg, K.A., Jiang, R., Steen, J.A., and Mitchison, T.J. (2014). Basal activity of a PARP1-NuA4 complex varies dramatically across cancer cell lines. Cell Rep *8*, 1808–1818.

Krukenberg, K.A., Kim, S., Tan, E.S., Maliga, Z., and Mitchison, T.J. (2015). Extracellular Poly(ADP-Ribose) Is a Pro-inflammatory Signal for Macrophages. Chem. Biol. *22*, 446–452.

Kudlow, B.A., Kennedy, B.K., and Monnat, R.J. (2007). Werner and Hutchinson-Gilford progeria syndromes: mechanistic basis of human progeroid diseases. Nat. Rev. Mol. Cell Biol. *8*, 394–404.

Kunzmann, A., Dedoussis, G., Jajte, J., Malavolta, M., Mocchegiani, E., and Bürkle, A. (2008). Effect of zinc on cellular poly(ADP-ribosyl)ation capacity. Exp. Gerontol. *43*, 409–414.

Kusumoto, R., Dawut, L., Marchetti, C., Wan Lee, J., Vindigni, A., Ramsden, D., and Bohr, V.A. (2008). Werner protein cooperates with the XRCC4-DNA ligase IV complex in end-processing. Biochemistry *47*, 7548–7556.

Kusumoto, R., Muftuoglu, M., and Bohr, V.A. (2007). The role of WRN in DNA repair is affected by post-translational modifications. Mech. Ageing Dev. *128*, 50–57.

Labbé, A., Lafleur, V.N., Patten, D.A., Robitaille, G.A., Garand, C., Lamalice, L., Lebel, M., and Richard, D.E. (2012). The Werner syndrome gene product (WRN): a repressor of hypoxia-inducible factor-1 activity. Exp. Cell

Res. *318*, 1620–1632.

Lachapelle, S., Gagné, J.-P., Garand, C., Desbiens, M., Coulombe, Y., Bohr, V.A., Hendzel, M.J., Masson, J.-Y., Poirier, G.G., and Lebel, M. (2011). Proteome-wide Identification of WRN-Interacting Proteins in Untreated and Nuclease-Treated Samples. J Proteome Res *10*, 1216–1227.

Lam, E.Y.N., Beraldi, D., Tannahill, D., and Balasubramanian, S. (2013). G-quadruplex structures are stable and detectable in human genomic DNA. Nat Commun *4*, 1796.

Lam, Y.W., and Trinkle-Mulcahy, L. (2015). New insights into nucleolar structure and function. F1000Prime Rep *7*, 48.

Lan, L., Nakajima, S., Komatsu, K., Nussenzweig, A., Shimamoto, A., Oshima, J., and Yasui, A. (2005). Accumulation of Werner protein at DNA double-strand breaks in human cells. J. Cell. Sci. *118*, 4153–4162.

Landry, J.J.M., Pyl, P.T., Rausch, T., Zichner, T., Tekkedil, M.M., Stütz, A.M., Jauch, A., Aiyar, R.S., Pau, G., Delhomme, N., et al. (2013). The genomic and transcriptomic landscape of a HeLa cell line. G3 (Bethesda) *3*, 1213–1224.

Langelier, M.-F., and Pascal, J.M. (2013). PARP-1 mechanism for coupling DNA damage detection to poly(ADP-ribose) synthesis. Curr. Opin. Struct. Biol.

Langelier, M.-F., Planck, J.L., Roy, S., and Pascal, J.M. (2012). Structural basis for DNA damage-dependent poly(ADP-ribosyl)ation by human PARP-1. Science *336*, 728–732.

Langelier, M.-F., Riccio, A.A., and Pascal, J.M. (2014). PARP-2 and PARP-3 are selectively activated by 5' phosphorylated DNA breaks through an allosteric regulatory mechanism shared with PARP-1. Nucleic Acids Res. *42*, 7762–7775.

Langelier, M.-F., Servent, K.M., Rogers, E.E., and Pascal, J.M. (2008). A third zinc-binding domain of human poly(ADP-ribose) polymerase-1 coordinates DNA-dependent enzyme activation. J. Biol. Chem. *283*, 4105–4114.

Lao, V.V., Welcsh, P., Luo, Y., Carter, K.T., Dzieciatkowski, S., Dintzis, S., Meza, J., Sarvetnick, N.E., Monnat, R.J., Loeb, L.A., et al. (2013). Altered RECQ Helicase Expression in Sporadic Primary Colorectal Cancers. Transl Oncol *6*, 458–469.

Lauper, J.M., Krause, A., Vaughan, T.L., and Monnat, R.J. (2013). Spectrum and risk of neoplasia in Werner syndrome: a systematic review. PLoS ONE *8*, e59709.

Lavoie, J., Carter, R., Drouin, R., and Lebel, M. (2005). Increased frequency of multiradial chromosome structures in mouse embryonic fibroblasts lacking functional Werner syndrome protein and poly(ADP-ribose) polymerase-1. Cancer Genet. Cytogenet. *156*, 134–143.

Lebel, M., and Leder, P. (1998). A deletion within the murine Werner syndrome helicase induces sensitivity to inhibitors of topoisomerase and loss of cellular proliferative capacity. Proc. Natl. Acad. Sci. U.S.a. *95*, 13097–13102.

Lebel, M. (2002). Increased frequency of DNA deletions in pink-eyed unstable mice carrying a mutation in the Werner syndrome gene homologue. Carcinogenesis *23*, 213–216.

Lebel, M., Lavoie, J., Gaudreault, I., Bronsard, M., and Drouin, R. (2003). Genetic cooperation between the Werner syndrome protein and poly(ADP-ribose) polymerase-1 in preventing chromatid breaks, complex chromosomal rearrangements, and cancer in mice. Am. J. Pathol. *162*, 1559–1569.

Lee, J.W., Kusumoto, R., Doherty, K.M., Lin, G.-X., Zeng, W., Cheng, W.-H., Kobbe, von, C., Brosh, R.M., Hu, J.-S., and Bohr, V.A. (2005). Modulation of Werner syndrome protein function by a single mutation in the conserved RecQ domain. J. Biol. Chem. *280*, 39627–39636.

Lee, S.-Y., Lee, H., Kim, E.-S., Park, S., Lee, J., and Ahn, B. (2015). WRN translocation from nucleolus to nucleoplasm is regulated by SIRT1 and required for DNA repair and the development of chemoresistance. Mutat. Res. *774*, 40–48.

Leppard, J.B., Dong, Z., Mackey, Z.B., and Tomkinson, A.E. (2003). Physical and functional interaction between DNA ligase IIIalpha and poly(ADP-Ribose) polymerase 1 in DNA single-strand break repair. Mol. Cell. Biol. *23*, 5919–5927.

LeRoy, G., Carroll, R., Kyin, S., Seki, M., and Cole, M.D. (2005). Identification of RecQL1 as a Holliday

junction processing enzyme in human cell lines. Nucleic Acids Res. *33*, 6251–6257.

Léger, K., Bär, D., Savić, N., Santoro, R., and Hottiger, M.O. (2014). ARTD2 activity is stimulated by RNA. Nucleic Acids Res. *42*, 5072–5082.

Li, B., and Comai, L. (2000). Functional interaction between Ku and the werner syndrome protein in DNA end processing. Journal of Biological Chemistry *275*, 28349–28352.

Li, B., and Comai, L. (2001). Requirements for the nucleolytic processing of DNA ends by the Werner syndrome protein-Ku70/80 complex. Journal of Biological Chemistry *276*, 9896–9902.

Li, B., Navarro, S., Kasahara, N., and Comai, L. (2004). Identification and biochemical characterization of a Werner's syndrome protein complex with Ku70/80 and poly(ADP-ribose) polymerase-1. J. Biol. Chem. *279*, 13659–13667.

Li, D., Frazier, M., Evans, D.B., Hess, K.R., Crane, C.H., Jiao, L., and Abbruzzese, J.L. (2006a). Single nucleotide polymorphisms of RecQ1, RAD54L, and ATM genes are associated with reduced survival of pancreatic cancer. J. Clin. Oncol. *24*, 1720–1728.

Li, D., Liu, H., Jiao, L., Chang, D.Z., Beinart, G., Wolff, R.A., Evans, D.B., Hassan, M.M., and Abbruzzese, J.L. (2006b). Significant effect of homologous recombination DNA repair gene polymorphisms on pancreatic cancer survival. Cancer Res. *66*, 3323–3330.

Li, G.-M. (2008). Mechanisms and functions of DNA mismatch repair. Cell Res. *18*, 85–98.

Li, K., Casta, A., Wang, R., Lozada, E., Fan, W., Kane, S., Ge, Q., Gu, W., Orren, D., and Luo, J. (2008). Regulation of WRN protein cellular localization and enzymatic activities by SIRT1-mediated deacetylation. J. Biol. Chem. *283*, 7590–7598.

Li, K., Wang, R., Lozada, E., Fan, W., Orren, D.K., and Luo, J. (2010). Acetylation of WRN protein regulates its stability by inhibiting ubiquitination. PLoS ONE *5*, e10341.

Li, M., and Yu, X. (2013). Function of BRCA1 in the DNA damage response is mediated by ADP-ribosylation. Cancer Cell *23*, 693–704.

Li, M., Lu, L.-Y., Yang, C.-Y., Wang, S., and Yu, X. (2013). The FHA and BRCT domains recognize ADP-ribosylation during DNA damage response. Genes Dev. *27*, 1752–1768.

Li, X., and Heyer, W.-D. (2008). Homologous recombination in DNA repair and DNA damage tolerance. Cell Res. *18*, 99–113.

Liberti, S.E., Andersen, S.D., Wang, J., May, A., Miron, S., Perderiset, M., Keijzers, G., Nielsen, F.C., Charbonnier, J.-B., Bohr, V.A., et al. (2011). Bi-directional routing of DNA mismatch repair protein human exonuclease 1 to replication foci and DNA double strand breaks. DNA Repair (Amst.) *10*, 73–86.

Lieber, M.R. (2010). The mechanism of double-strand DNA break repair by the nonhomologous DNA end-joining pathway. Annu. Rev. Biochem. *79*, 181–211.

Lin, S.J., Defossez, P.A., and Guarente, L. (2000). Requirement of NAD and SIR2 for life-span extension by calorie restriction in Saccharomyces cerevisiae. Science *289*, 2126–2128.

Lindahl, T. (1993). Instability and decay of the primary structure of DNA. Nature *362*, 709–715.

Lindahl, T., and Nyberg, B. (1972). Rate of depurination of native deoxyribonucleic acid. Biochemistry *11*, 3610–3618.

Liu, Y., Kadyrov, F.A., and Modrich, P. (2011). PARP-1 enhances the mismatch-dependence of 5'-directed excision in human mismatch repair in vitro. DNA Repair (Amst.) *10*, 1145–1153.

Lockett, K.L., Hall, M.C., Xu, J., Zheng, S.L., Berwick, M., Chuang, S.-C., Clark, P.E., Cramer, S.D., Lohman, K., and Hu, J.J. (2004). The ADPRT V762A genetic variant contributes to prostate cancer susceptibility and deficient enzyme function. Cancer Res. *64*, 6344–6348.

Lombard, D.B., Beard, C., Johnson, B., Marciniak, R.A., Dausman, J., Bronson, R., Buhlmann, J.E., Lipman, R., Curry, R., Sharpe, A., et al. (2000). Mutations in the WRN gene in mice accelerate mortality in a p53-null background. Mol. Cell. Biol. *20*, 3286–3291.

Lord, C.J., and Ashworth, A. (2012). The DNA damage response and cancer therapy. Nature *481*, 287–294.

Lord, C.J., Tutt, A.N.J., and Ashworth, A. (2015). Synthetic lethality and cancer therapy: lessons learned from the development of PARP inhibitors. Annu. Rev. Med. *66*, 455–470.

Lozada, E., Yi, J., Luo, J., and Orren, D.K. (2014). Acetylation of Werner syndrome protein (WRN): relationships with DNA damage, DNA replication and DNA metabolic activities. Biogerontology.

López-Otín, C., Blasco, M.A., Partridge, L., Serrano, M., and Kroemer, G. (2013). The hallmarks of aging. Cell *153*, 1194–1217.

Lu, X., Lou, H., and Luo, G. (2011). A Blm-Recql5 partnership in replication stress response. J Mol Cell Biol *3*, 31–38.

Luo, G., Santoro, I.M., McDaniel, L.D., Nishijima, I., Mills, M., Youssoufian, H., Vogel, H., Schultz, R.A., and Bradley, A. (2000). Cancer predisposition caused by elevated mitotic recombination in Bloom mice. Nat. Genet. *26*, 424–429.

Machwe, A., Ganunis, R., Bohr, V.A., and Orren, D.K. (2000). Selective blockage of the 3"-->5" exonuclease activity of WRN protein by certain oxidative modifications and bulky lesions in DNA. Nucleic Acids Res. *28*, 2762–2770.

Machwe, A., Xiao, L., and Orren, D.K. (2004). TRF2 recruits the Werner syndrome (WRN) exonuclease for processing of telomeric DNA. Oncogene *23*, 149–156.

Machwe, A., Xiao, L., and Orren, D.K. (2006). Length-dependent degradation of single-stranded 3' ends by the Werner syndrome protein (WRN): implications for spatial orientation and coordinated 3‘ to 5’ movement of its ATPase/helicase and exonuclease domains. BMC Mol. Biol. *7*, 6.

Maddukuri, L., Ketkar, A., Eddy, S., Zafar, M.K., and Eoff, R.L. (2014). The Werner syndrome protein limits the error-prone 8-oxo-dG lesion bypass activity of human DNA polymerase kappa. Nucleic Acids Res.

Maddukuri, L., Ketkar, A., Eddy, S., Zafar, M.K., Griffin, W.C., and Eoff, R.L. (2012). Enhancement of human DNA polymerase η activity and fidelity is dependent upon a bipartite interaction with the Werner syndrome protein. J. Biol. Chem. *287*, 42312–42323.

Malanga, M., Atorino, L., Tramontano, F., Farina, B., and Quesada, P. (1998a). Poly(ADP-ribose) binding properties of histone H1 variants. Biochim. Biophys. Acta *1399*, 154–160.

Malanga, M., M, P.J., Kleczkowska, H.E., and Althaus, F.R. (1998b). Poly(ADP-ribose) binds to specific domains of p53 and alters its DNA binding functions. J. Biol. Chem. *273*, 11839–11843.

Malanga, M., and Althaus, F.R. (2004). Poly(ADP-ribose) reactivates stalled DNA topoisomerase I and Induces DNA strand break resealing. J. Biol. Chem. *279*, 5244–5248.

Malanga, M., and Althaus, F.R. (2011). Noncovalent protein interaction with poly(ADP-ribose). Methods Mol. Biol. *780*, 67–82.

Mangerich, A., and Bürkle, A. (2011). How to kill tumor cells with inhibitors of poly(ADP-ribosyl)ation. Int. J. Cancer *128*, 251–265.

Mangerich, A., and Bürkle, A. (2012). Pleiotropic cellular functions of PARP1 in longevity and aging: genome maintenance meets inflammation. Oxid Med Cell Longev *2012*, 321653.

Mangerich, A., Debiak, M., Birtel, M., Ponath, V., Balszuweit, F., Lex, K., Martello, R., Burckhardt-Boer, W., Strobelt, R., Siegert, M., et al. (2015). Sulfur and nitrogen mustards induce characteristic poly(ADP-ribosyl)ation responses in HaCaT keratinocytes with distinctive cellular consequences. Toxicol. Lett.

Mangerich, A., Veith, S., Popp, O., Fahrer, J., Martello, R., Bohr, V.A., and Bürkle, A. (2012). Quantitative analysis of WRN exonuclease activity by isotope dilution mass spectrometry. Mech. Ageing Dev. *133*, 575–579.

Manthei, K.A., and Keck, J.L. (2013). The BLM dissolvasome in DNA replication and repair. Cell. Mol. Life Sci. *70*, 4067–4084.

Mao, Z., Bozzella, M., Seluanov, A., and Gorbunova, V. (2008). DNA repair by nonhomologous end joining and homologous recombination during cell cycle in human cells. Cell Cycle *7*, 2902–2906.

Marsischky, G.T., Wilson, B.A., and Collier, R.J. (1995). Role of glutamic acid 988 of human poly-ADP-ribose polymerase in polymer formation. Evidence for active site similarities to the ADP-ribosylating toxins. Journal of Biological Chemistry *270*, 3247–3254.

Martello, R., Mangerich, A., Sass, S., Dedon, P.C., and Bürkle, A. (2013). Quantification of cellular poly(ADP-ribosyl)ation by stable isotope dilution mass spectrometry reveals tissue- and drug-dependent stress response dynamics. ACS Chem. Biol. *8*, 1567–1575.

Martin, K.A., Cesaroni, M., Denny, M.F., Lupey, L.N., and Tempera, I. (2015). Global Transcriptome Analysis Reveals That Poly(ADP-Ribose) Polymerase 1 Regulates Gene Expression through EZH2. Mol. Cell. Biol. *35*, 3934–3944.

Mason, P.A., and Cox, L.S. (2012). The role of DNA exonucleases in protecting genome stability and their impact on ageing. Age (Dordr) *34*, 1317–1340.

Masutani, M., Suzuki, H., Kamada, N., Watanabe, M., Ueda, O., Nozaki, T., Jishage, K., Watanabe, T., Sugimoto, T., Nakagama, H., et al. (1999). Poly(ADP-ribose) polymerase gene disruption conferred mice resistant to streptozotocin-induced diabetes. Proc. Natl. Acad. Sci. U.S.a. *96*, 2301–2304.

Mayne, L.V., and Lehmann, A.R. (1982). Failure of RNA synthesis to recover after UV irradiation: an early defect in cells from individuals with Cockayne's syndrome and xeroderma pigmentosum. Cancer Res. *42*, 1473–1478.

McNeill, D.R., Paramasivam, M., Baldwin, J., Huang, J., Vyjayanti, V.N., Seidman, M.M., and Wilson, D.M. (2013). NEIL1 responds and binds to psoralen-induced DNA interstrand crosslinks. J. Biol. Chem. *288*, 12426–12436.

Meder, V.S., Boeglin, M., de Murcia, G., and Schreiber, V. (2005). PARP-1 and PARP-2 interact with nucleophosmin/B23 and accumulate in transcriptionally active nucleoli. J. Cell. Sci. *118*, 211–222.

Mendoza-Alvarez, H., and Alvarez-Gonzalez, R. (1993). Poly(ADP-ribose) polymerase is a catalytic dimer and the automodification reaction is intermolecular. Journal of Biological Chemistry *268*, 22575–22580.

Merideth, M.A., Gordon, L.B., Clauss, S., Sachdev, V., Smith, A.C.M., Perry, M.B., Brewer, C.C., Zalewski, C., Kim, H.J., Solomon, B., et al. (2008). Phenotype and course of Hutchinson-Gilford progeria syndrome. N. Engl. J. Med. *358*, 592–604.

Messner, S., Schuermann, D., Altmeyer, M., Kassner, I., Schmidt, D., Schär, P., Müller, S., and Hottiger, M.O. (2009). Sumoylation of poly(ADP-ribose) polymerase 1 inhibits its acetylation and restrains transcriptional coactivator function. Faseb J. *23*, 3978–3989.

Meyer-Ficca, M.L., Meyer, R.G., Coyle, D.L., Jacobson, E.L., and Jacobson, M.K. (2004). Human poly(ADP-ribose) glycohydrolase is expressed in alternative splice variants yielding isoforms that localize to different cell compartments. Exp. Cell Res. *297*, 521–532.

Ménissier-de Murcia, J., Ricoul, M., Tartier, L., Niedergang, C., Huber, A., Dantzer, F., Schreiber, V., Amé, J.-C., Dierich, A., LeMeur, M., et al. (2003). Functional interaction between PARP-1 and PARP-2 in chromosome stability and embryonic development in mouse. Embo J. *22*, 2255–2263.

Midorikawa, R., Takei, Y., and Hirokawa, N. (2006). KIF4 motor regulates activity-dependent neuronal survival by suppressing PARP-1 enzymatic activity. Cell *125*, 371–383.

Min, W., Bruhn, C., Grigaravicius, P., Zhou, Z.-W., Li, F., Krüger, A., Siddeek, B., Greulich, K.-O., Popp, O., Meisezahl, C., et al. (2013). Poly(ADP-ribose) binding to Chk1 at stalled replication forks is required for S-phase checkpoint activation. Nat Commun *4*, 2993.

Min, W., Cortes, U., Herceg, Z., Tong, W.-M., and Wang, Z.-Q. (2010). Deletion of the nuclear isoform of poly(ADP-ribose) glycohydrolase (PARG) reveals its function in DNA repair, genomic stability and tumorigenesis. Carcinogenesis *31*, 2058–2065.

Miranda, E.A., Dantzer, F., O'Farrell, M., de Murcia, G., and de Murcia, J.M. (1995). Characterisation of a gain-of-function mutant of poly(ADP-ribose) polymerase. Biochem. Biophys. Res. Commun. *212*, 317–325.

Miwa, M., Hanai, S., Poltronieri, P., Uchida, M., and Uchida, K. (1999). Functional analysis of poly(ADP-ribose) polymerase in Drosophila melanogaster. Mol. Cell. Biochem. *193*, 103–107.

Mohaghegh, P., Karow, J.K., Brosh, R.M., Bohr, V.A., and Hickson, I.D. (2001). The Bloom“s and Werner”s syndrome proteins are DNA structure-specific helicases. Nucleic Acids Res. *29*, 2843–2849.

Mortusewicz, O., Amé, J.-C., Schreiber, V., and Leonhardt, H. (2007). Feedback-regulated poly(ADP-ribosyl)ation by PARP-1 is required for rapid response to DNA damage in living cells. Nucleic Acids Res. *35*,

7665–7675.

Moser, M.J., Bigbee, W.L., Grant, S.G., Emond, M.J., Langlois, R.G., Jensen, R.H., Oshima, J., and Monnat, R.J. (2000). Genetic instability and hematologic disease risk in Werner syndrome patients and heterozygotes. Cancer Res. *60*, 2492–2496.

Muftuoglu, M., de Souza-Pinto, N.C., Dogan, A., Aamann, M., Stevnsner, T., Rybanska, I., Kirkali, G., Dizdaroglu, M., and Bohr, V.A. (2009). Cockayne syndrome group B protein stimulates repair of formamidopyrimidines by NEIL1 DNA glycosylase. Journal of Biological Chemistry *284*, 9270–9279.

Muftuoglu, M., Kusumoto, R., Speina, E., Beck, G., Cheng, W.-H., and Bohr, V.A. (2008a). Acetylation regulates WRN catalytic activities and affects base excision DNA repair. PLoS ONE *3*, e1918.

Muftuoglu, M., Oshima, J., Kobbe, von, C., Cheng, W.-H., Leistritz, D.F., and Bohr, V.A. (2008b). The clinical characteristics of Werner syndrome: molecular and biochemical diagnosis. Hum. Genet. *124*, 369–377.

Muftuoglu, M., Sharma, S., Thorslund, T., Stevnsner, T., Soerensen, M.M., Brosh, R.M., and Bohr, V.A. (2006). Cockayne syndrome group B protein has novel strand annealing and exchange activities. Nucleic Acids Res. *34*, 295–304.

Muiras, M.L., Müller, M., Schächter, F., and Burkle, A. (1998). Increased poly(ADP-ribose) polymerase activity in lymphoblastoid cell lines from centenarians. J. Mol. Med. *76*, 346–354.

Murai, J., Huang, S.-Y.N., Das, B.B., Renaud, A., Zhang, Y., Doroshow, J.H., Ji, J., Takeda, S., and Pommier, Y. (2012). Trapping of PARP1 and PARP2 by Clinical PARP Inhibitors. Cancer Res. *72*, 5588–5599.

Na, Z., Peng, B., Ng, S., Pan, S., Lee, J.-S., Shen, H.-M., and Yao, S.Q. (2015). A small-molecule protein-protein interaction inhibitor of PARP1 that targets its BRCT domain. Angew. Chem. Int. Ed. Engl. *54*, 2515–2519.

Nakazawa, K., Ueda, K., Honjo, T., Yoshihara, K., Nishizuka, Y., and Hayaishi, O. (1968). Nicotinamide adenine dinucleotide glycohydrolases and poly adenosine diphosphate ribose synthesis in rat liver. Biochem. Biophys. Res. Commun. *32*, 143–149.

Natale, V. (2011). A comprehensive description of the severity groups in Cockayne syndrome. Am. J. Med. Genet. A *155A*, 1081–1095.

Nguyen, G.H., Dexheimer, T.S., Rosenthal, A.S., Chu, W.K., Singh, D.K., Mosedale, G., Bachrati, C.Z., Schultz, L., Sakurai, M., Savitsky, P., et al. (2013). A small molecule inhibitor of the BLM helicase modulates chromosome stability in human cells. Chem. Biol. *20*, 55–62.

Niere, M., Kernstock, S., Koch-Nolte, F., and Ziegler, M. (2008). Functional localization of two poly(ADP-ribose)-degrading enzymes to the mitochondrial matrix. Mol. Cell. Biol. *28*, 814–824.

Niere, M., Mashimo, M., Agledal, L., Dölle, C., Kasamatsu, A., Kato, J., Moss, J., and Ziegler, M. (2012). ADP-ribosylhydrolase 3 (ARH3), not poly(ADP-ribose) glycohydrolase (PARG) isoforms, is responsible for degradation of mitochondrial matrix-associated poly(ADP-ribose). J. Biol. Chem. *287*, 16088–16102.

Nimonkar, A.V., Ozsoy, A.Z., Genschel, J., Modrich, P., and Kowalczykowski, S.C. (2008). Human exonuclease 1 and BLM helicase interact to resect DNA and initiate DNA repair. Proc. Natl. Acad. Sci. U.S.a. *105*, 16906–16911.

Noren Hooten, N., Fitzpatrick, M., Kompaniez, K., Jacob, K.D., Moore, B.R., Nagle, J., Barnes, J., Lohani, A., and Evans, M.K. (2012). Coordination of DNA repair by NEIL1 and PARP-1: a possible link to aging. Aging (Albany NY) *4*, 674–685.

Nouspikel, T. (2009). DNA repair in mammalian cells : Nucleotide excision repair: variations on versatility. Cell. Mol. Life Sci. *66*, 994–1009.

Nouspikel, T. (2008). Nucleotide excision repair and neurological diseases. DNA Repair (Amst.) *7*, 1155–1167.

O'Connor, M.S., Safari, A., Liu, D., Qin, J., and Songyang, Z. (2004). The human Rap1 protein complex and modulation of telomere length. Journal of Biological Chemistry *279*, 28585–28591.

Ogata, N., Ueda, K., Kagamiyama, H., and Hayaishi, O. (1980). ADP-ribosylation of histone H1. Identification of glutamic acid residues 2, 14, and the COOH-terminal lysine residue as modification sites. Journal of Biological Chemistry *255*, 7616–7620.

Ogata, N., Ueda, K., Kawaichi, M., and Hayaishi, O. (1981). Poly(ADP-ribose) synthetase, a main acceptor of poly(ADP-ribose) in isolated nuclei. J. Biol. Chem. *256*, 4135–4137.

Oka, S., Kato, J., and Moss, J. (2006). Identification and characterization of a mammalian 39-kDa poly(ADP-ribose) glycohydrolase. J. Biol. Chem. *281*, 705–713.

Opresko, P.L., Kobbe, von, C., Laine, J.-P., Harrigan, J., Hickson, I.D., and Bohr, V.A. (2002). Telomere-binding protein TRF2 binds to and stimulates the Werner and Bloom syndrome helicases. J. Biol. Chem. *277*, 41110–41119.

Opresko, P.L., Mason, P.A., Podell, E.R., Lei, M., Hickson, I.D., Cech, T.R., and Bohr, V.A. (2005). POT1 stimulates RecQ helicases WRN and BLM to unwind telomeric DNA substrates. J. Biol. Chem. *280*, 32069–32080.

Opresko, P.L., Otterlei, M., Graakjaer, J., Bruheim, P., Dawut, L., Kølvraa, S., May, A., Seidman, M.M., and Bohr, V.A. (2004). The Werner syndrome helicase and exonuclease cooperate to resolve telomeric D loops in a manner regulated by TRF1 and TRF2. Mol. Cell *14*, 763–774.

Orren, D.K., Brosh, R.M., Nehlin, J.O., Machwe, A., Gray, M.D., and Bohr, V.A. (1999). Enzymatic and DNA binding properties of purified WRN protein: high affinity binding to single-stranded DNA but not to DNA damage induced by 4NQO. Nucleic Acids Res. *27*, 3557–3566.

Orren, D.K., Machwe, A., Karmakar, P., Piotrowski, J., Cooper, M.P., and Bohr, V.A. (2001). A functional interaction of Ku with Werner exonuclease facilitates digestion of damaged DNA. Nucleic Acids Res. *29*, 1926–1934.

Otsuki, M., Seki, M., Kawabe, Y.-I., Inoue, E., Dong, Y.P., Abe, T., Kato, G., Yoshimura, A., Tada, S., and Enomoto, T. (2007). WRN counteracts the NHEJ pathway upon camptothecin exposure. Biochem. Biophys. Res. Commun. *355*, 477–482.

Paliwal, S., Kanagaraj, R., Sturzenegger, A., Burdova, K., and Janscak, P. (2013). Human RECQ5 helicase promotes repair of DNA double-strand breaks by synthesis-dependent strand annealing. Nucleic Acids Res.

Panzeter, P.L., Realini, C.A., and Althaus, F.R. (1992). Noncovalent interactions of poly(adenosine diphosphate ribose) with histones. Biochemistry *31*, 1379–1385.

Partridge, J.J., Lopreiato, J.O., Latterich, M., and Indig, F.E. (2003). DNA damage modulates nucleolar interaction of the Werner protein with the AAA ATPase p97/VCP. Mol. Biol. Cell *14*, 4221–4229.

Parvathaneni, S., Stortchevoi, A., Sommers, J.A., Brosh, R.M., and Sharma, S. (2013). Human RECQ1 Interacts with Ku70/80 and Modulates DNA End-Joining of Double-Strand Breaks. PLoS ONE *8*, e62481.

Patel, A.G., Flatten, K.S., Schneider, P.A., Dai, N.T., McDonald, J.S., Poirier, G.G., and Kaufmann, S.H. (2012). Enhanced killing of cancer cells by poly(ADP-ribose) polymerase inhibitors and topoisomerase I inhibitors reflects poisoning of both enzymes. J. Biol. Chem. *287*, 4198–4210.

Patro, B.S., Frøhlich, R., Bohr, V.A., and Stevnsner, T. (2011). WRN helicase regulates the ATR-CHK1-induced S-phase checkpoint pathway in response to topoisomerase-I-DNA covalent complexes. J. Cell. Sci.

Pines, A., Mullenders, L.H., van Attikum, H., and Luijsterburg, M.S. (2013). Touching base with PARPs: moonlighting in the repair of UV lesions and double-strand breaks. Trends Biochem. Sci. *38*, 321–330.

Pines, A., Vrouwe, M.G., Marteijn, J.A., Typas, D., Luijsterburg, M.S., Cansoy, M., Hensbergen, P., Deelder, A., de Groot, A., Matsumoto, S., et al. (2012). PARP1 promotes nucleotide excision repair through DDB2 stabilization and recruitment of ALC1. J. Cell Biol. *199*, 235–249.

Piskunova, T.S., Yurova, M.N., Ovsyannikov, A.I., Semenchenko, A.V., Zabezhinski, M.A., Popovich, I.G., Wang, Z.-Q., and Anisimov, V.N. (2008). Deficiency in Poly(ADP-ribose) Polymerase-1 (PARP-1) Accelerates Aging and Spontaneous Carcinogenesis in Mice. Curr Gerontol Geriatr Res 754190.

Pleschke, J.M., Kleczkowska, H.E., Strohm, M., and Althaus, F.R. (2000). Poly(ADP-ribose) Binds to Specific Domains in DNA Damage Checkpoint Proteins. Journal of Biological Chemistry *275*, 40974–40980.

Poele, te, R.H., Okorokov, A.L., Jardine, L., Cummings, J., and Joel, S.P. (2002). DNA damage is able to induce senescence in tumor cells in vitro and in vivo. Cancer Res. *62*, 1876–1883.

Polo, S.E., and Jackson, S.P. (2011). Dynamics of DNA damage response proteins at DNA breaks: a focus on

protein modifications. Genes Dev. *25*, 409–433.

Poot, M., Hoehn, H., Rünger, T.M., and Martin, G.M. (1992). Impaired S-phase transit of Werner syndrome cells expressed in lymphoblastoid cell lines. Exp. Cell Res. *202*, 267–273.

Popp, O., Veith, S., Fahrer, J., Bohr, V.A., Bürkle, A., and Mangerich, A. (2012). Site-specific non-covalent interaction of the biopolymer poly(ADP-ribose) with the Werner syndrome protein regulates protein functions. ACS Chem. Biol.

Popuri, V., Hsu, J., Khadka, P., Horvath, K., Liu, Y., Croteau, D.L., and Bohr, V.A. (2014). Human RECQL1 participates in telomere maintenance. Nucleic Acids Res.

Popuri, V., Huang, J., Ramamoorthy, M., Tadokoro, T., Croteau, D.L., and Bohr, V.A. (2012a). RECQL5 plays co-operative and complementary roles with WRN syndrome helicase. Nucleic Acids Res.

Popuri, V., Ramamoorthy, M., Tadokoro, T., Singh, D.K., Karmakar, P., Croteau, D.L., and Bohr, V.A. (2012b). Recruitment and retention dynamics of RECQL5 at DNA double strand break sites. DNA Repair (Amst.) *11*, 624–635.

Popuri, V., Tadokoro, T., Croteau, D.L., and Bohr, V.A. (2013). Human RECQL5: Guarding the crossroads of DNA replication and transcription and providing backup capability. Crit. Rev. Biochem. Mol. Biol.

Qin, Q., Lu, J., Zhu, H., Xu, L., Cheng, H., Zhan, L., Yang, X., Zhang, C., and Sun, X. (2014). PARP-1 Val762Ala polymorphism and risk of cancer: a meta-analysis based on 39 case-control studies. PLoS ONE *9*, e98022.

Ramamoorthy, M., Tadokoro, T., Rybanska, I., Ghosh, A.K., Wersto, R., May, A., Kulikowicz, T., Sykora, P., Croteau, D.L., and Bohr, V.A. (2012). RECQL5 cooperates with Topoisomerase II alpha in DNA decatenation and cell cycle progression. Nucleic Acids Res. *40*, 1621–1635.

Rancourt, A., and Satoh, M.S. (2009). Delocalization of nucleolar poly(ADP-ribose) polymerase-1 to the nucleoplasm and its novel link to cellular sensitivity to DNA damage. DNA Repair (Amst.) *8*, 286–297.

Ray Chaudhuri, A., Hashimoto, Y., Herrador, R., Neelsen, K.J., Fachinetti, D., Bermejo, R., Cocito, A., Costanzo, V., and Lopes, M. (2012). Topoisomerase I poisoning results in PARP-mediated replication fork reversal. Nat. Struct. Mol. Biol. *19*, 417–423.

Reddy, S., Li, B., and Comai, L. (2010). Processing of human telomeres by the Werner syndrome protein. Cell Cycle *9*, 3137–3138.

Ren, X., Lim, S., Smith, M.T., and Zhang, L. (2009). Werner Syndrome Protein, WRN, Protects Cells from DNA Damage Induced by the Benzene Metabolite Hydroquinone. Toxicological Sciences *107*, 367–375.

Richter, C., Park, J.W., and Ames, B.N. (1988). Normal oxidative damage to mitochondrial and nuclear DNA is extensive. Proc. Natl. Acad. Sci. U.S.a. *85*, 6465–6467.

Robert, I., Karicheva, O., Reina-San-Martin, B., Schreiber, V., and Dantzer, F. (2013). Functional aspects of PARylation in induced and programmed DNA repair processes: preserving genome integrity and modulating physiological events. Mol. Aspects Med. *34*, 1138–1152.

Robu, M., Shah, R.G., Petitclerc, N., Brind'Amour, J., Kandan-Kulangara, F., and Shah, G.M. (2013). Role of poly(ADP-ribose) polymerase-1 in the removal of UV-induced DNA lesions by nucleotide excision repair. Proc. Natl. Acad. Sci. U.S.a. *110*, 1658–1663.

Rolli, V., O'Farrell, M., Ménissier-De Murcia, J., and de Murcia, G. (1997). Random mutagenesis of the poly(ADP-ribose) polymerase catalytic domain reveals amino acids involved in polymer branching. Biochemistry *36*, 12147–12154.

Rosenthal, F., Feijs, K.L.H., Frugier, E., Bonalli, M., Forst, A.H., Imhof, R., Winkler, H.C., Fischer, D., Caflisch, A., Hassa, P.O., et al. (2013). Macrodomain-containing proteins are new mono-ADP-ribosylhydrolases. Nat. Struct. Mol. Biol.

Rossi, M.L., Ghosh, A.K., and Bohr, V.A. (2010a). Roles of Werner syndrome protein in protection of genome integrity. DNA Repair (Amst.) *9*, 331–344.

Rossi, M.L., Ghosh, A.K., Kulikowicz, T., Croteau, D.L., and Bohr, V.A. (2010b). Conserved helicase domain of human RecQ4 is required for strand annealing-independent DNA unwinding. DNA Repair (Amst.) *9*, 796–

804.

Rouleau, M., Patel, A., Hendzel, M.J., Kaufmann, S.H., and Poirier, G.G. (2010). PARP inhibition: PARP1 and beyond. Nat. Rev. Cancer *10*, 293–301.

Rudolph, K.L., Chang, S., Lee, H.W., Blasco, M., Gottlieb, G.J., Greider, C., and DePinho, R.A. (1999). Longevity, stress response, and cancer in aging telomerase-deficient mice. Cell *96*, 701–712.

Sakai, A., Sakasai, R., Kakeji, Y., Kitao, H., and Maehara, Y. (2012). PARP and CSB modulate the processing of transcription-mediated DNA strand breaks. Genes Genet. Syst. *87*, 265–272.

Sallmyr, A., Tomkinson, A.E., and Rassool, F.V. (2008). Up-regulation of WRN and DNA ligase IIIalpha in chronic myeloid leukemia: consequences for the repair of DNA double-strand breaks. Blood *112*, 1413–1423.

Sami, F., and Sharma, S. (2013). Probing Genome Maintenance Functions of human RECQ1. Comput Struct Biotechnol J *6*, e201303014.

Sancar, A. (2003). Structure and function of DNA photolyase and cryptochrome blue-light photoreceptors. Chem. Rev. *103*, 2203–2237.

Sancar, A., Lindsey-Boltz, L.A., Unsal-Kaçmaz, K., and Linn, S. (2004). Molecular mechanisms of mammalian DNA repair and the DNA damage checkpoints. Annu. Rev. Biochem. *73*, 39–85.

Saponaro, M., Kantidakis, T., Mitter, R., Kelly, G.P., Heron, M., Williams, H., Söding, J., Stewart, A., and Svejstrup, J.Q. (2014). RECQL5 controls transcript elongation and suppresses genome instability associated with transcription stress. Cell *157*, 1037–1049.

Satoh, M., Imai, M., Sugimoto, M., Goto, M., and Furuichi, Y. (1999). Prevalence of Werner's syndrome heterozygotes in Japan. Lancet *353*, 1766.

Sauermann, G., and Wesierska-Gadek, J. (1986). Poly(ADP-ribose) effectively competes with DNA for histone H4 binding. Biochem. Biophys. Res. Commun. *139*, 523–529.

Savage, D.B., Agostini, M., Barroso, I., Gurnell, M., Luan, J., Meirhaeghe, A., Harding, A.-H., Ihrke, G., Rajanayagam, O., Soos, M.A., et al. (2002). Digenic inheritance of severe insulin resistance in a human pedigree. Nat. Genet. *31*, 379–384.

Scheibye-Knudsen, M., Croteau, D.L., and Bohr, V.A. (2013a). Mitochondrial deficiency in Cockayne syndrome. Mech. Ageing Dev. *134*, 275–283.

Scheibye-Knudsen, M., Mitchell, S.J., Fang, E.F., Iyama, T., Ward, T., Wang, J., Dunn, C.A., Singh, N., Veith, S., Hasan-Olive, M.M., et al. (2014). A High-Fat Diet and NAD(+) Activate Sirt1 to Rescue Premature Aging in Cockayne Syndrome. Cell Metab. *20*, 840–855.

Scheibye-Knudsen, M., Scheibye-Alsing, K., Canugovi, C., Croteau, D.L., and Bohr, V.A. (2013b). A novel diagnostic tool reveals mitochondrial pathology in human diseases and aging. Aging (Albany NY) *5*, 192–208.

Schurman, S.H., Hedayati, M., Wang, Z., Singh, D.K., Speina, E., Zhang, Y., Becker, K., Macris, M., Sung, P., Wilson, D.M., et al. (2009). Direct and indirect roles of RECQL4 in modulating base excision repair capacity. Hum. Mol. Genet. *18*, 3470–3483.

Seki, M., Yanagisawa, J., Kohda, T., Sonoyama, T., Ui, M., and Enomoto, T. (1994). Purification of two DNA-dependent adenosinetriphosphatases having DNA helicase activity from HeLa cells and comparison of the properties of the two enzymes. J. Biochem. *115*, 523–531.

Selby, C.P., and Sancar, A. (1997). Human transcription-repair coupling factor CSB/ERCC6 is a DNA-stimulated ATPase but is not a helicase and does not disrupt the ternary transcription complex of stalled RNA polymerase II. Journal of Biological Chemistry *272*, 1885–1890.

Shall, S., and de Murcia, G. (2000). Poly(ADP-ribose) polymerase-1: what have we learned from the deficient mouse model? Mutat. Res. *460*, 1–15.

Shamanna, R.A., Hoque, M., Lewis-Antes, A., Azzam, E.I., Lagunoff, D., Pe'ery, T., and Mathews, M.B. (2011). The NF90/NF45 complex participates in DNA break repair via nonhomologous end joining. Mol. Cell. Biol. *31*, 4832–4843.

Sharma, S., and Brosh, R.M. (2007). Human RECQ1 is a DNA damage responsive protein required for genotoxic stress resistance and suppression of sister chromatid exchanges. PLoS ONE *2*, e1297.

Sharma, S., Phatak, P., Stortchevoi, A., Jasin, M., and Larocque, J.R. (2012). RECQ1 plays a distinct role in cellular response to oxidative DNA damage. DNA Repair (Amst.).

Sharma, S., Sommers, J.A., Choudhary, S., Faulkner, J.K., Cui, S., Andreoli, L., Muzzolini, L., Vindigni, A., and Brosh, R.M. (2005). Biochemical analysis of the DNA unwinding and strand annealing activities catalyzed by human RECQ1. Journal of Biological Chemistry *280*, 28072–28084.

Sharma, S., Stumpo, D.J., Balajee, A.S., Bock, C.B., Lansdorp, P.M., Brosh, R.M., and Blackshear, P.J. (2007). RECQL, a member of the RecQ family of DNA helicases, suppresses chromosomal instability. Mol. Cell. Biol. *27*, 1784–1794.

Shay, J.W., and Bacchetti, S. (1997). A survey of telomerase activity in human cancer. Eur. J. Cancer *33*, 787–791.

Shen, J.C., and Loeb, L.A. (2000). Werner syndrome exonuclease catalyzes structure-dependent degradation of DNA. Nucleic Acids Res. *28*, 3260–3268.

Shieh, W.M., Amé, J.C., Wilson, M.V., Wang, Z.Q., Koh, D.W., Jacobson, M.K., and Jacobson, E.L. (1998). Poly(ADP-ribose) polymerase null mouse cells synthesize ADP-ribose polymers. J. Biol. Chem. *273*, 30069–30072.

Shilovsky, G.A., Khokhlov, A.N., and Shram, S.I. (2013). The protein poly(ADP-ribosyl)ation system: its role in genome stability and lifespan determination. Biochemistry Mosc. *78*, 433–444.

Shimamoto, A., Nishikawa, K., Kitao, S., and Furuichi, Y. (2000). Human RecQ5beta, a large isomer of RecQ5 DNA helicase, localizes in the nucleoplasm and interacts with topoisomerases 3alpha and 3beta. Nucleic Acids Res. *28*, 1647–1655.

Shiratori, M., Suzuki, T., Itoh, C., Goto, M., Furuichi, Y., and Matsumoto, T. (2002). WRN helicase accelerates the transcription of ribosomal RNA as a component of an RNA polymerase I-associated complex. Oncogene *21*, 2447–2454.

Shuck, S.C., Short, E.A., and Turchi, J.J. (2008). Eukaryotic nucleotide excision repair: from understanding mechanisms to influencing biology. Cell Res. *18*, 64–72.

Sidorova, J.M. (2008). Roles of the Werner syndrome RecQ helicase in DNA replication. DNA Repair (Amst.) *7*, 1776–1786.

Sidorova, J.M., Kehrli, K., Mao, F., and Monnat, R. (2013). Distinct functions of human RECQ helicases WRN and BLM in replication fork recovery and progression after hydroxyurea-induced stalling. DNA Repair (Amst.) *12*, 128–139.

Siitonen, H.A., Kopra, O., Kääriäinen, H., Haravuori, H., Winter, R.M., Säämänen, A.-M., Peltonen, L., and Kestilä, M. (2003). Molecular defect of RAPADILINO syndrome expands the phenotype spectrum of RECQL diseases. Hum. Mol. Genet. *12*, 2837–2844.

Silva, B.A., Stambaugh, J.R., Yokomori, K., Shah, J.V., and Berns, M.W. (2014). DNA damage to a single chromosome end delays anaphase onset. J. Biol. Chem. *289*, 22771–22784.

Singh, D.K., Ghosh, A.K., Croteau, D.L., and Bohr, V.A. (2012a). RecQ helicases in DNA double strand break repair and telomere maintenance. Mutat. Res. *736*, 15–24.

Singh, D.K., Karmakar, P., Aamann, M., Schurman, S.H., May, A., Croteau, D.L., Burks, L., Plon, S.E., and Bohr, V.A. (2010). The involvement of human RECQL4 in DNA double-strand break repair. Aging Cell *9*, 358–371.

Singh, D.K., Popuri, V., Kulikowicz, T., Shevelev, I., Ghosh, A.K., Ramamoorthy, M., Rossi, M.L., Janscak, P., Croteau, D.L., and Bohr, V.A. (2012b). The human RecQ helicases BLM and RECQL4 cooperate to preserve genome stability. Nucleic Acids Res. *40*, 6632–6648.

Singleton, M.R., Dillingham, M.S., and Wigley, D.B. (2007). Structure and mechanism of helicases and nucleic acid translocases. Annu. Rev. Biochem. *76*, 23–50.

Smith, S., Giriat, I., Schmitt, A., and de Lange, T. (1998). Tankyrase, a poly(ADP-ribose) polymerase at human telomeres. Science *282*, 1484–1487.

Sommers, J.A., Sharma, S., Doherty, K.M., Karmakar, P., Yang, Q., Kenny, M.K., Harris, C.C., and Brosh, R.M.

(2005). p53 modulates RPA-dependent and RPA-independent WRN helicase activity. Cancer Res. *65*, 1223–1233.

Sonnenblick, A., de Azambuja, E., Azim, H.A., and Piccart, M. (2015). An update on PARP inhibitors--moving to the adjuvant setting. Nat Rev Clin Oncol *12*, 27–41.

Spagnolo, L., Barbeau, J., Curtin, N.J., Morris, E.P., and Pearl, L.H. (2012). Visualization of a DNA-PK/PARP1 complex. Nucleic Acids Res. *40*, 4168–4177.

Speina, E., Dawut, L., Hedayati, M., Wang, Z., May, A., Schwendener, S., Janscak, P., Croteau, D.L., and Bohr, V.A. (2010). Human RECQL5 beta stimulates flap endonuclease 1. Nucleic Acids Res. *38*, 2904–2916.

Stark, J.M., Pierce, A.J., Oh, J., Pastink, A., and Jasin, M. (2004). Genetic steps of mammalian homologous repair with distinct mutagenic consequences. Mol. Cell. Biol. *24*, 9305–9316.

Stevnsner, T., Muftuoglu, M., Aamann, M.D., and Bohr, V.A. (2008). The role of Cockayne Syndrome group B (CSB) protein in base excision repair and aging. Mech. Ageing Dev. *129*, 441–448.

Sturzenegger, A., Burdova, K., Kanagaraj, R., Levikova, M., Pinto, C., Cejka, P., and Janscak, P. (2014). DNA2 cooperates with the WRN and BLM RecQ helicases to mediate long-range DNA-end resection in human cells. J. Biol. Chem.

Su, Y., Meador, J.A., Calaf, G.M., Proietti De-Santis, L., Zhao, Y., Bohr, V.A., and Balajee, A.S. (2010). Human RecQL4 helicase plays critical roles in prostate carcinogenesis. Cancer Res. *70*, 9207–9217.

Sugimura, K., Takebayashi, S.-I., Taguchi, H., Takeda, S., and Okumura, K. (2008). PARP-1 ensures regulation of replication fork progression by homologous recombination on damaged DNA. J. Cell Biol. *183*, 1203–1212.

Sukhanova, M.V., Khodyreva, S.N., Lebedeva, N.A., Prasad, R., Wilson, S.H., and Lavrik, O.I. (2005). Human base excision repair enzymes apurinic/apyrimidinic endonuclease1 (APE1), DNA polymerase beta and poly(ADP-ribose) polymerase 1: interplay between strand-displacement DNA synthesis and proofreading exonuclease activity. Nucleic Acids Res. *33*, 1222–1229.

Suzuki, N., Shimamoto, A., Imamura, O., Kuromitsu, J., Kitao, S., Goto, M., and Furuichi, Y. (1997). DNA helicase activity in Werner's syndrome gene product synthesized in a baculovirus system. Nucleic Acids Res. *25*, 2973–2978.

Tadokoro, T., Kulikowicz, T., Dawut, L., Croteau, D.L., and Bohr, V.A. (2012a). DNA binding residues in the RQC domain of Werner protein are critical for its catalytic activities. Aging (Albany NY) *4*, 417–430.

Tadokoro, T., Ramamoorthy, M., Popuri, V., May, A., Tian, J., Sykora, P., Rybanska, I., Wilson, D.M.I., Croteau, D.L., and Bohr, V.A. (2012b). Human RECQL5 participates in the removal of endogenous DNA damage. Mol. Biol. Cell *23*, 4273–4285.

Tadokoro, T., Rybanska-Spaeder, I., Kulikowicz, T., Dawut, L., Oshima, J., Croteau, D.L., and Bohr, V.A. (2013). Functional deficit associated with a missense Werner syndrome mutation. DNA Repair (Amst.) *12*, 414–421.

Tang, B., Xiong, H., Sun, P., Zhang, Y., Wang, D., Hu, Z., Zhu, Z., Ma, H., Pan, Q., Xia, J.-H., et al. (2006). Association of PINK1 and DJ-1 confers digenic inheritance of early-onset Parkinson's disease. Hum. Mol. Genet. *15*, 1816–1825.

Thangavel, S., Berti, M., Levikova, M., Pinto, C., Gomathinayagam, S., Vujanovic, M., Zellweger, R., Moore, H., Lee, E.H., Hendrickson, E.A., et al. (2015). DNA2 drives processing and restart of reversed replication forks in human cells. J. Cell Biol. *208*, 545–562.

Thangavel, S., Mendoza-Maldonado, R., Tissino, E., Sidorova, J.M., Yin, J., Wang, W., Monnat, R.J., Falaschi, A., and Vindigni, A. (2010). Human RECQ1 and RECQ4 helicases play distinct roles in DNA replication initiation. Mol. Cell. Biol. *30*, 1382–1396.

Thorslund, T., Kobbe, von, C., Harrigan, J.A., Indig, F.E., Christiansen, M., Stevnsner, T., and Bohr, V.A. (2005). Cooperation of the Cockayne syndrome group B protein and poly(ADP-ribose) polymerase 1 in the response to oxidative stress. Mol. Cell. Biol. *25*, 7625–7636.

Timinszky, G., Till, S., Hassa, P.O., Hothorn, M., Kustatscher, G., Nijmeijer, B., Colombelli, J., Altmeyer, M., Stelzer, E.H.K., Scheffzek, K., et al. (2009). A macrodomain-containing histone rearranges chromatin upon sensing PARP1 activation. Nat. Struct. Mol. Biol. *16*, 923–929.

Tomas, M., Blumhardt, P., Deutzmann, A., Schwarz, T., Kromm, D., Leitenstorfer, A., and Ferrando-May, E. (2013). Imaging of the DNA damage-induced dynamics of nuclear proteins via nonlinear photoperturbation. J Biophotonics *6*, 645–655.

Trego, K.S., Chernikova, S.B., Davalos, A.R., Perry, J.J.P., Finger, L.D., Ng, C., Tsai, M.-S., Yannone, S.M., Tainer, J.A., Campisi, J., et al. (2011). The DNA repair endonuclease XPG interacts directly and functionally with the WRN helicase defective in Werner syndrome. Cell Cycle *10*, 1998–2007.

Troelstra, C., van Gool, A., de Wit, J., Vermeulen, W., Bootsma, D., and Hoeijmakers, J.H. (1992). ERCC6, a member of a subfamily of putative helicases, is involved in Cockayne's syndrome and preferential repair of active genes. Cell *71*, 939–953.

Troen, B.R. (2003). The biology of aging. Mt. Sinai J. Med. *70*, 3–22.

Ueda, K., Oka, J., Naruniya, S., Miyakawa, N., and Hayaishi, O. (1972). Poly ADP-ribose glycohydrolase from rat liver nuclei, a novel enzyme degrading the polymer. Biochem. Biophys. Res. Commun. *46*, 516–523.

Umen, J.G. (2005). The elusive sizer. Curr. Opin. Cell Biol. *17*, 435–441.

Vaitiekunaite, R., Butkiewicz, D., Krześniak, M., Przybyłek, M., Gryc, A., Snietura, M., Benedyk, M., Harris, C.C., and Rusin, M. (2007). Expression and localization of Werner syndrome protein is modulated by SIRT1 and PML. Mech. Ageing Dev. *128*, 650–661.

Van Maldergem, L., Siitonen, H.A., Jalkh, N., Chouery, E., De Roy, M., Delague, V., Muenke, M., Jabs, E.W., Cai, J., Wang, L.L., et al. (2006). Revisiting the craniosynostosis-radial ray hypoplasia association: Baller-Gerold syndrome caused by mutations in the RECQL4 gene. J. Med. Genet. *43*, 148–152.

van Steeg, H. (2001). The role of nucleotide excision repair and loss of p53 in mutagenesis and carcinogenesis. Toxicol. Lett. *120*, 209–219.

Veith, S., and Mangerich, A. (2014). RecQ helicases and PARP1 team up in maintaining genome integrity. Ageing Res. Rev.

Vermeulen, W., and Fousteri, M. (2013). Mammalian transcription-coupled excision repair. Cold Spring Harb Perspect Biol *5*, a012625.

Vijg, J., and Suh, Y. (2013). Genome instability and aging. Annu. Rev. Physiol. *75*, 645–668.

Vissers, L.E.L.M., de Ligt, J., Gilissen, C., Janssen, I., Steehouwer, M., de Vries, P., van Lier, B., Arts, P., Wieskamp, N., del Rosario, M., et al. (2010). A de novo paradigm for mental retardation. Nat. Genet. *42*, 1109–1112.

Vodenicharov, M.D., Ghodgaonkar, M.M., Halappanavar, S.S., Shah, R.G., and Shah, G.M. (2005). Mechanism of early biphasic activation of poly(ADP-ribose) polymerase-1 in response to ultraviolet B radiation. J. Cell. Sci. *118*, 589–599.

Vyas, S., and Chang, P. (2014). New PARP targets for cancer therapy. Nat. Rev. Cancer *14*, 502–509.

Wacker, D.A., Ruhl, D.D., Balagamwala, E.H., Hope, K.M., Zhang, T., and Kraus, W.L. (2007). The DNA binding and catalytic domains of poly(ADP-ribose) polymerase 1 cooperate in the regulation of chromatin structure and transcription. Mol. Cell. Biol. *27*, 7475–7485.

Walker, J.W., Jijon, H.B., and Madsen, K.L. (2006). AMP-activated protein kinase is a positive regulator of poly(ADP-ribose) polymerase. Biochem. Biophys. Res. Commun. *342*, 336–341.

Wang, H.-T., Gao, Y., Zhao, Y.-X., Yu, H., Wang, T.-L., Bai, L., Chen, Y.-Z., Zhang, H.-B., Zhou, B.-S., Qu, Y.-L., et al. (2014). PARP-1 rs3219073 polymorphism may contribute to susceptibility to lung cancer. Genet Test Mol Biomarkers *18*, 736–740.

Wang, J., Chen, J., and Gong, Z. (2013). TopBP1 controls BLM protein level to maintain genome stability. Mol. Cell *52*, 667–678.

Wang, M., Wu, W., Wu, W., Rosidi, B., Zhang, L., Wang, H., and Iliakis, G. (2006). PARP-1 and Ku compete for repair of DNA double strand breaks by distinct NHEJ pathways. Nucleic Acids Res. *34*, 6170–6182.

Wang, W., and Bambara, R.A. (2005). Human Bloom protein stimulates flap endonuclease 1 activity by resolving DNA secondary structure. Journal of Biological Chemistry *280*, 5391–5399.

Wang, X.-G., Wang, Z.-Q., Tong, W.-M., and Shen, Y. (2007). PARP1 Val762Ala polymorphism reduces enzymatic activity. Biochem. Biophys. Res. Commun. *354*, 122–126.

Wang, Y., Kim, N.S., Haince, J.-F., Kang, H.C., David, K.K., Andrabi, S.A., Poirier, G.G., Dawson, V.L., and Dawson, T.M. (2011). Poly(ADP-ribose) (PAR) binding to apoptosis-inducing factor is critical for PAR polymerase-1-dependent cell death (parthanatos). Sci Signal *4*, ra20.

Wang, Z.Q., Auer, B., Stingl, L., Berghammer, H., Haidacher, D., Schweiger, M., and Wagner, E.F. (1995). Mice lacking ADPRT and poly(ADP-ribosyl)ation develop normally but are susceptible to skin disease. Genes Dev. *9*, 509–520.

Wang, Z., Michaud, G.A., Cheng, Z., Zhang, Y., Hinds, T.R., Fan, E., Cong, F., and Xu, W. (2012). Recognition of the iso-ADP-ribose moiety in poly(ADP-ribose) by WWE domains suggests a general mechanism for poly(ADP-ribosyl)ation-dependent ubiquitination. Genes Dev. *26*, 235–240.

Waters, L.S., Minesinger, B.K., Wiltrout, M.E., D'Souza, S., Woodruff, R.V., and Walker, G.C. (2009). Eukaryotic translesion polymerases and their roles and regulation in DNA damage tolerance. Microbiol. Mol. Biol. Rev. *73*, 134–154.

Weber, S. (2005). Light-driven enzymatic catalysis of DNA repair: a review of recent biophysical studies on photolyase. Biochim. Biophys. Acta *1707*, 1–23.

Werner, O. (1904). On cataract in conjunction with scleroderma. Doctoral dissertation by Otto Werner, Kiel. Doctoral Dissertation *190*, 1–14.

Werner, S.R., Prahalad, A.K., Yang, J., and Hock, J.M. (2006). RECQL4-deficient cells are hypersensitive to oxidative stress/damage: Insights for osteosarcoma prevalence and heterogeneity in Rothmund-Thomson syndrome. Biochem. Biophys. Res. Commun. *345*, 403–409.

Wong, H.-K., Muftuoglu, M., Beck, G., Imam, S.Z., Bohr, V.A., and Wilson, D.M. (2007). Cockayne syndrome B protein stimulates apurinic endonuclease 1 activity and protects against agents that introduce base excision repair intermediates. Nucleic Acids Res. *35*, 4103–4113.

Woo, L.L., Futami, K., Shimamoto, A., Furuichi, Y., and Frank, K.M. (2006). The Rothmund-Thomson gene product RECQL4 localizes to the nucleolus in response to oxidative stress. Exp. Cell Res. *312*, 3443–3457.

Wu, L., and Hickson, I.D. (2003). The Bloom's syndrome helicase suppresses crossing over during homologous recombination. Nature *426*, 870–874.

Xu, X., and Liu, Y. (2009). Dual DNA unwinding activities of the Rothmund-Thomson syndrome protein, RECQ4. Embo J. *28*, 568–577.

Xue, Y., Ratcliff, G.C., Wang, H., Davis-Searles, P.R., Gray, M.D., Erie, D.A., and Redinbo, M.R. (2002). A minimal exonuclease domain of WRN forms a hexamer on DNA and possesses both 3'- 5‘ exonuclease and 5’-protruding strand endonuclease activities. Biochemistry *41*, 2901–2912.

Yannone, S.M., Roy, S., Chan, D.W., Murphy, M.B., Huang, S., Campisi, J., and Chen, D.J. (2001). Werner syndrome protein is regulated and phosphorylated by DNA-dependent protein kinase. J. Biol. Chem. *276*, 38242–38248.

Ying, S., Hamdy, F.C., and Helleday, T. (2012). Mre11-dependent degradation of stalled DNA replication forks is prevented by BRCA2 and PARP1. Cancer Res. *72*, 2814–2821.

Young, M.D., Willson, T.A., Wakefield, M.J., Trounson, E., Hilton, D.J., Blewitt, M.E., Oshlack, A., and Majewski, I.J. (2011). ChIP-seq analysis reveals distinct H3K27me3 profiles that correlate with transcriptional activity. Nucleic Acids Res. *39*, 7415–7427.

Yu, C.E., Oshima, J., Fu, Y.H., Wijsman, E.M., Hisama, F., Alisch, R., Matthews, S., Nakura, J., Miki, T., Ouais, S., et al. (1996). Positional cloning of the Werner's syndrome gene. Science *272*, 258–262.

Yung, T.M.C., Sato, S., and Satoh, M.S. (2004). Poly(ADP-ribosyl)ation as a DNA damage-induced post-translational modification regulating poly(ADP-ribose) polymerase-1-topoisomerase I interaction. Journal of Biological Chemistry *279*, 39686–39696.

Zahradka, P., and Ebisuzaki, K. (1982). A shuttle mechanism for DNA-protein interactions. The regulation of poly(ADP-ribose) polymerase. Eur. J. Biochem. *127*, 579–585.

Zaremba, T., Ketzer, P., Cole, M., Coulthard, S., Plummer, E.R., and Curtin, N.J. (2009). Poly(ADP-ribose) polymerase-1 polymorphisms, expression and activity in selected human tumour cell lines. Br. J. Cancer *101*, 256–262.

Zeman, M.K., and Cimprich, K.A. (2014). Causes and consequences of replication stress. Nat. Cell Biol. *16*, 2–9.

Zglinicki, von, T., Saretzki, G., Döcke, W., and Lotze, C. (1995). Mild hyperoxia shortens telomeres and inhibits proliferation of fibroblasts: a model for senescence? Exp. Cell Res. *220*, 186–193.

Zhang, F., Chen, Y., Li, M., and Yu, X. (2014). The oligonucleotide/oligosaccharide-binding fold motif is a poly(ADP-ribose)-binding domain that mediates DNA damage response. Proc Natl Acad Sci USA.

Zhang, Y., Wang, J., Ding, M., and Yu, Y. (2013). Site-specific characterization of the Asp- and Glu-ADP-ribosylated proteome. Nat. Methods.

Zhang, Y., Liu, S., Mickanin, C., Feng, Y., Charlat, O., Michaud, G.A., Schirle, M., Shi, X., Hild, M., Bauer, A., et al. (2011). RNF146 is a poly(ADP-ribose)-directed E3 ligase that regulates axin degradation and Wnt signalling. Nat. Cell Biol. *13*, 623–629.

Zharkov, D.O. (2008). Base excision DNA repair. Cell. Mol. Life Sci. *65*, 1544–1565.

Zheng, L., Baumann, U., and Reymond, J.-L. (2004). An efficient one-step site-directed and site-saturation mutagenesis protocol. Nucleic Acids Res. *32*, e115.

Zheng, L., Kanagaraj, R., Mihaljevic, B., Schwendener, S., Sartori, A.A., Gerrits, B., Shevelev, I., and Janscak, P. (2009). MRE11 complex links RECQ5 helicase to sites of DNA damage. Nucleic Acids Res. *37*, 2645–2657.